# Resource Allocation Strategies and Linear Precoded OFDM Optimization for Ultra-Wideband Communications

Antoine Stephan

N$^o$ d'ordre : D08-29

**INSA**
RENNES

**IETR**
INSTITUT D'ÉLECTRONIQUE ET DE TÉLÉCOMMUNICATIONS DE RENNES

# Thèse

présentée devant

l'**Institut National des Sciences Appliquées de Rennes**

pour obtenir le titre de

**Docteur**

spécialité : *Électronique*

# Resource Allocation Strategies and Linear Precoded OFDM Optimization for Ultra-Wideband Communications

par

Antoine STEPHAN

Soutenue le 15 décembre 2008 devant la commission d'Examen

*Composition du jury*

### *Rapporteurs*
| | |
|---|---|
| Michel Jézéquel | Directeur des Etudes – HDR à TELECOM Bretagne |
| Dirk Slock | Professeur à EURECOM |

### *Examinateurs*
| | |
|---|---|
| Andrea Tonello | Professeur à l'Université de Udine, Italie |
| Luc Vandendorpe | Professeur à l'Université Catholique de Louvain, Belgique |
| Rodolphe Le Gouable | Docteur-Ingénieur à Orange Labs (France Télécom R&D) |
| Jean-Yves Baudais | Chargé de Recherches CNRS à l'IETR |
| Jean-François Hélard | Professeur à l'INSA de Rennes |

Institut d'Électronique et de Télécommunications de Rennes
Institut National des Sciences Appliquées de Rennes

*To my Parents*

# Abstract

Ultra-wideband (UWB) is a fast technology that has recently attracted considerable interest in the research and standardization communities, due to its ability to provide high data rate at low cost and low power consumption. The objective of this thesis is to propose a new UWB system for high data rate wireless personal area network (WPAN) applications, based on the well-known multiband orthogonal frequency-division multiplexing (MB-OFDM) solution supported by the WiMedia Alliance.

In a first step, we analytically investigate the use of a linear precoded OFDM (LP-OFDM) waveform for UWB systems. The resulting scheme reduces in practice to a simple addition of a precoding matrix, or equivalently spreading sequences, to the MB-OFDM transmission chain, which does not increase the system complexity significantly. The precoding function is then analytically optimized and different resource allocation strategies based on a classical target symbol-error-rate (SER) approach and on a new mean bit-error-rate (BER) approach are investigated. Efficient allocation algorithms maximizing the system range and throughput, and minimizing the system mean BER, are thus proposed for different application scenarios. The numerical results of simulations carried out on the different adaptive and non-adaptive schemes show that the LP-OFDM system outperforms the MB-OFDM system in terms of throughput and range. This is due to the spreading gain provided by the linear precoding component, and to the efficiency of the proposed algorithms.

In a second step, a global UWB system approach is carried out. This system study, complementary to the analytical one, points out the advantages of appropriately adding the linear precoding to the MB-OFDM solution. Furthermore, a MIMO component is added to the LP-OFDM system in order to improve the system robustness as well as to provide a data rate of 1 Gb/s. System simulation results show that the joint use of MIMO and LP-OFDM schemes in UWB leads to a significant system improvement compared to the MB-OFDM system. Thus, the proposed MIMO LP-OFDM system can be advantageously exploited for high data rate UWB applications at reasonable additional system complexity.

# Acknowledgments

I owe my gratitude to all the people who have made this thesis possible with their help, support and contributions.

First and foremost, I would like to thank my advisor, Prof. Jean-François Hélard, who has given me an invaluable opportunity to do research and work on challenging and extremely interesting subjects over the past three years, and my supervisor, Dr. Jean-Yves Baudais, for his special theoretical ideas and mathematical expertise. They have been great mentors throughout my Ph.D. by helping me establish a direction of research and providing valuable guidance and advice. I will never forget the fun moments and the dialogues we had on various subjects.

Many thanks go to Prof. Luc Vandendorpe, the jury president, Prof. Michel Jézéquel, Prof. Dirk Slock, Prof. Andrea Tonello, and Dr. Rodolphe Le Gouable, for coming from the different corners of France, Italy and Belgium to serve on my thesis committee, and for sparing their invaluable time reviewing the manuscript.

I want to thank Dr. Matthieu Crussière and Dr. Emeric Guéguen for letting me benefit from their exceptional previous work, which improved my research work significantly. Many thanks also go to all those who collaborated with me, particularly Fahad Syed Muhammad and Ayman Khalil.

I would like to express my sincere thanks to Orange Labs RESA/WIN/CREM (France Télécom R&D) and to the European ICT FP7 OMEGA project for supporting this work. Special thanks go to Isabelle Siaud for her helpful advice and interesting discussions.

All my colleagues at IETR have enriched my graduate life in many ways. I would like to thank my "Bocal" colleagues Minh, Christophe, Yvan, Patrice, Sylvie and Pierre, as well as Irène, Youssef and the rest of the staff. Special thanks go to Prof. Ghais El Zein and Hanna Farhat who have always made themselves available for help and advice.

I would like to thank Marielle for her love, support, and unlimited kindness. She has always been by my side, especially during the hardest moments of the Ph.D.

Last but not least, I owe my deepest thanks to my wonderful family, my parents, my sister and my brother, who are always there for me even though we are a thousand miles apart. I express my gratitude to my parents for having guided me through life, and supported and encouraged me to move to Sweden and France to pursue my Master's and Ph.D. studies.

# Contents

# Résumé étendu en Français

## Introduction

L'ultra large bande ou UWB (*ultra-wideband*) est une nouvelle technologie à fort potentiel pour les futurs réseaux personnels WPAN (*wireless personal area networks*) à très haut débit et faible portée. L'objectif de cette thèse est de proposer une nouvelle forme d'onde de type LP-OFDM (*linear precoded orthogonal frequency division multiplexing*) pour les applications WPAN, visant à améliorer la solution MB-OFDM (*multiband* OFDM) supportée par la WiMedia Alliance.

Dans un premier temps, une étude analytique est menée sur l'apport de la composante de précodage au système UWB, cette composante se réduisant en pratique à une simple addition d'une matrice d'étalement fréquentiel. La fonction de précodage est ensuite optimisée et différentes stratégies d'allocation dynamique des ressources sont étudiées. En considérant une approche classique tenant compte du taux d'erreur symbole (TES) ainsi qu'une nouvelle approche tenant compte du taux d'erreur binaire (TEB) moyen, différents algorithmes d'allocation dynamique visant à maximiser la portée ou le débit du système, ou à minimiser le TEB moyen du système, sont proposés. Les résultats analytiques montrent l'avantage d'utiliser une composante de précodage pour les applications UWB dont le canal est très sélectif en fréquence.

Dans un second temps, une étude système complémentaire à l'étude analytique est réalisée pour le système LP-OFDM UWB. Une composante MIMO est ajoutée au système, d'une part pour augmenter la portée du système à bas et moyen débit, et d'autre part pour augmenter le débit du système qui peut atteindre dans ce cas 1 Gb/s. Les résultats de simulation sur le système proposé montrent que ce système est plus performant que le système MB-OFDM pour les débits déjà offerts par la norme, et qu'il offre par ailleurs un débit double du débit maximal proposé par la norme conjointement avec de meilleures performances en terme de TEB.

# Chapitre 1

# Les communications ultra large bande

## Introduction

L'UWB se présente comme une technologie attractive pour les systèmes de communications radio à très hauts débits depuis l'an 2002 quand la FCC (*Federal Communications Commission*) a réglementé les systèmes UWB en imposant un masque spectral avec une densité spectrale de puissance (DSP) limitée à -41,3 dBm/MHz. Ce premier chapitre présente une introduction générale aux techniques UWB. Il décrit les origines et les motivations qui ont conduit au développement des systèmes UWB. Les problèmes de régularisation et de normalisation ainsi que les principales applications UWB sont présentés. De plus, les deux principales techniques de modulation considérées pour les applications WPAN UWB à très haut débit, l'IR-UWB (*impulse radio* UWB) et la MB-OFDM (*multiband orthogonal frequency-division multiplexing*) sont décrites, suivies d'une comparaison entre ces deux techniques. Enfin, le modèle de canal considéré par l'IEEE 802.15.3a pour des applications UWB et adopté dans cette thèse est présenté.

## Définition et régularisations

L'UWB est une technique de transmission radio qui consiste à utiliser des signaux s'étalant sur une large bande de fréquences, typiquement de l'ordre de 500 MHz à plusieurs GHz. Une définition aujourd'hui communément admise est que les signaux UWB ont un rapport largeur de bande sur fréquence centrale, ou *fractional bandwidth*, au moins égal à 20% ou bien une largeur de bande supérieure à 500 MHz.

Aux États-Unis, la FCC a alloué un spectre s'étalant de 3,1 à 10,6 GHz pour les applications UWB sans licence, avec une limite de DSP de -41,3 dBm/MHz sur tout le spectre, alors qu'en Europe l'ECC (*European Communications Commission*) a imposé une limite de DSP beaucoup plus faible, sauf sur la bande de 6–8,5 GHz. Des mesures similaires sur la puissance d'émission des systèmes UWB ont aussi été prises dans le reste du monde. Ces sévères limitations en puissance ont pour but principal de réduire les interférences avec les systèmes à bande étroite dont le spectre est masqué par celui de l'UWB, tels que l'UMTS, le GSM et le WLAN.

## Normalisation

En 2001, le groupe de normalisation des réseaux personnels WPAN IEEE 802.15 avait organisé le Task Group 3a visant à définir une couche physique très haut débit basée sur un système UWB. Le débat pour une solution unique s'articulait autour de deux propositions qui ont divisé les participants du groupe : l'étalement de spectre UWB (IR-UWB) et la modulation OFDM à bandes multiples (MB-OFDM). Malheureusement, les travaux du groupe IEEE 802.15.3a ont été stoppés en janvier 2006 faute d'un accord général sur une solution unique. Néanmoins, d'importants groupes industriels, comme l'UWB Forum et la WiMedia Alliance se sont engagés dans la conception d'équipements basés sur la technologie UWB en adoptant respectivement la solution IR-UWB et MB-OFDM. La solution WiMedia semble être aujourd'hui une solution dominante pour les applications UWB à très haut débit, et serait sans doute adoptée pour les futurs systèmes Bluetooth 3.0 et WUSB (*Wireless* USB). En outre, d'autres standards basés sur la technologie UWB existent également, tels que l'IEEE 802.15.4a qui définit une nouvelle couche physique pour les applications WPAN à bas débit.

## Applications

Les applications de l'UWB sont diverses. Comme pour la plupart des technologies de communications durant les dernières décennies, les applications militaires ont fortement contribué au développement de l'UWB. Depuis 2002, l'UWB est devenu l'un des candidats principaux pour les applications WPAN à bas et très haut débit. La technique UWB est aussi utilisée dans les applications radars, médicales, et de positionnement. Dans cette thèse, nous nous intéressons uniquement aux applications WPAN à très haut débit.

Enfin, le modèle de canal utilisé dans cette étude est celui adopté par la commission IEEE 802.15.3a, qui est une version modifiée du modèle de Saleh-Valenzuela pour les applications indoor.

# Chapitre 2

# Spécifications du système

### Introduction et motivations

Le deuxième chapitre présente les principales techniques de transmission exploitées dans cette thèse. Tout d'abord, le principe des modulations multiporteuses, en particulier le concept d'OFDM, est détaillé. Ensuite, le principe d'étalement de spectre est décrit, suivi par une présentation des principaux schémas de modulation résultant de la combinaison des techniques d'étalement de spectre et de modulation OFDM. La deuxième partie de ce chapitre est consacrée à la description du système WiMedia MB-OFDM qui est considéré comme le point de départ de nos études. Les performances du système MB-OFDM sur les canaux UWB sont présentées, suivies par une discussion des avantages et inconvénients de cette approche. Ensuite, nous proposons une nouvelle forme d'onde basée sur l'addition d'une technique d'étalement de spectre, ou d'une façon équivalente, des principes de précodage linéaire, à la modulation OFDM du système MB-OFDM. Puis, nous discutons des avantages de cette approche et des motivations qui ont conduit à ce choix. Ce système proposé sera nommé LP-OFDM (*linear precoded* OFDM) par la suite.

### La solution MB-OFDM

La solution MB-OFDM est basée sur une modulation OFDM et une technique multibande qui divise le spectre UWB en 14 sous-bandes de 528 MHz chacune. La plupart des études ont été réalisées sur les trois premières sous-bandes. Le système MB-OFDM est composé de 100 sous-porteuses de données et les constellations utilisées sont la MAQ-4 (modulation d'amplitude en quadrature) pour les faibles débits, et la DCM (*dual carrier modulation*) pour les hauts débits, ce qui conduit à une transmission de 200 bits par symbole OFDM. Les avantages de la solution MB-OFDM résident principalement dans sa faible complexité technique, la modulation OFDM présentant un grand degré de maturité et étant déjà adoptée par plusieurs standards (e.g., DVB-T, DVB-H, ADSL, 802.11a, etc.).

### Le système LP-OFDM proposé

Afin d'améliorer les performances du système, nous proposons une forme d'onde de type LP-OFDM en ajoutant une fonction d'étalement. La solution LP-OFDM, lorsqu'elle permet l'accès multiple entre les utilisateurs, consiste à attribuer à chaque utilisateur un bloc
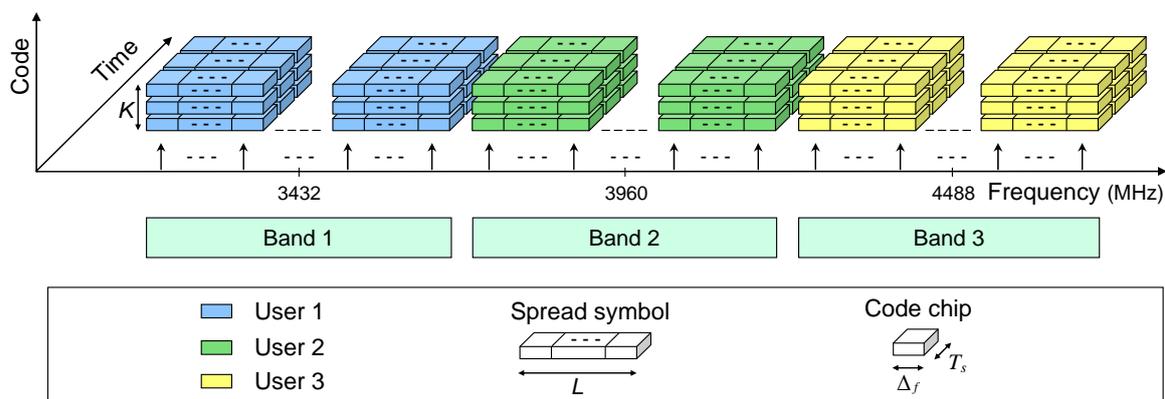
Figure 1 : Représentation schématique de la forme d'onde LP-OFDM.

de sous-porteuses qui lui est propre, en respectant un schéma de multiplexage fréquentiel. L'étalement est choisi selon l'axe fréquentiel afin d'améliorer la robustesse du signal vis-à-vis de la sélectivité fréquentielle des canaux UWB et des brouilleurs à bande étroite.

Une représentation schématique du signal LP-OFDM pour trois utilisateurs occupant les trois premières bandes MB-OFDM est donnée figure 1. La forme d'onde LP-OFDM est utilisée dans le contexte UWB en allouant à chaque utilisateur un groupe de 100 sous-porteuses utiles, occupant l'une des sous-bandes de largeur égale à 528 MHz. Chaque sous-bande propre à un utilisateur est ensuite divisée en différents blocs contenant un nombre de sous-porteuses égal à la longueur $L$ du code d'étalement. De plus, comme dans la solution MB-OFDM, la gestion multi-utilisateur est facilitée par l'utilisation de codes temps-fréquence (TFC) qui assurent des sauts en fréquence d'une sous-bande à une autre à la fin de chaque symbole OFDM.

## Avantages du LP-OFDM

Le système LP-OFDM est plus robuste que le système WiMedia vis-à-vis de la sélectivité fréquentielle des canaux UWB et des brouilleurs à bande étroite, grâce à la composante d'étalement. De plus, l'allocation des ressources est plus flexible puisque l'étalement apporte un degré de liberté supplémentaire. En outre, l'estimation de canal en réception est plus simple que celle d'un système MC-CDMA (*multicarrier code-division multiple-access*). En effet, une même sous-porteuse n'est affectée que par un seul canal relatif à un seul utilisateur, alors que dans un système MC-CDMA, une sous-porteuse est affectée par les différents canaux des différents utilisateurs. D'autre part, dans la solution WiMedia, des conflits entre utilisateurs augmentent considérablement dès que quatre utilisateurs sont considérés. En revanche, avec le système LP-OFDM, la dimension des codes peut être exploitée pour partager une même sous-bande entre 2 voire 3 utilisateurs si nécessaire. Le signal généré dans un bloc donné correspond alors à un signal MC-CDMA.

# Chapitre 3

# Principes d'allocation des ressources, approche du taux d'erreur symbole

## Introduction et motivations

L'allocation des ressources est un aspect fondamental dans la conception des systèmes à porteuses multiples. Ce chapitre est consacré à l'étude des principes d'allocation dynamique des ressources pour les applications OFDM et LP-OFDM. L'exploitation de cette allocation dynamique pour les systèmes UWB constitue un réel avantage du fait que le canal UWB indoor varie lentement dans le temps, ce qui réduit l'augmentation de la complexité des systèmes.

Une présentation générale des principes de gestion des ressources est d'abord donnée et les principales stratégies d'optimisation, à savoir la maximisation du débit et la maximisation de la marge, sont décrites. Les solutions classiques pour les systèmes OFDM sont présentées et les nouvelles solutions optimales pour les systèmes LP-OFDM sont dérivées. De nouveaux algorithmes d'allocation sont proposés et les performances du système LP-OFDM sont comparées à celles du système OFDM. Notons que dans ce chapitre, une approche classique basée sur un taux d'erreur symbole (TES ou SER) cible est considérée, alors que dans le chapitre 4, une étude basée sur une nouvelle approche du taux d'erreur binaire (TEB ou BER) moyen du système est exploitée. Enfin, une étude d'optimisation supplémentaire basée sur une distribution dynamique des codes temps-fréquence (TFC) entre les utilisateurs d'un système UWB est proposée. Les différents résultats d'optimisation présentés dans ce chapitre montrent que la composante de précodage linéaire peut être efficacement exploitée pour les applications UWB à très haut débit, et que le système LP-OFDM est plus performant que le système OFDM.

## Capacité du système LP-OFDM

Le système LP-OFDM est optimisé afin d'améliorer les performances en terme de portée ou de débit, grâce à l'ajout de la composante d'étalement. Pour mieux se concentrer sur l'étude de l'étalement, seules les fonctions de précodage et OFDM sont considérées. Les autres fonctions de la chaîne globale de transmission, comme le codage de canal, ne sont pas prises en compte dans l'étude présentée dans ce chapitre. Afin d'optimiser analytiquement le système LP-OFDM, une détection ZF (*zero-forcing*) est utilisée.

Le débit total en bit par symbole d'un système LP-OFDM utilisant une détection ZF est donné par

$$R_{LP-OFDM} = \sum_{b=1}^{B} \sum_{k=1}^{K_b} \log_2 \left( 1 + \frac{1}{\Gamma} \frac{L^2}{\sum_{n=1}^{L} \left( 1/|h_{n,b}|^2 \right)} \frac{E_{k,b}}{N_0} \right), \tag{1}$$

avec $B$ et $L$ le nombre et la longueur des blocs, $K_b$ le nombre de codes d'étalement dans le bloc $b$, $\Gamma$ la marge de bruit des constellations MAQ, $E_{k,b}$ l'énergie allouée au code $k$ du bloc $b$, avec la contrainte de DSP

$$\sum_{k=1}^{K_b} E_{k,b} \leq \tilde{E}, \quad \forall b, \tag{2}$$

où $\tilde{E}$ est la limite de DSP. Le système est ensuite optimisé en considérant deux cas : le cas où l'on se limite à une MAQ-4 fixe pour rester dans le cadre de la norme WiMedia, et le cas où l'on considère un ordre variable de constellation.

## Maximisation de la portée du système LP-OFDM à constellation fixe

Dans un premier temps, nous considérons uniquement la MAQ-4 et un nombre $N$ de sous-porteuses utiles par sous-bande. Nous cherchons le nombre optimal $B$ de blocs, et par suite la longueur optimale $L$ des codes d'étalement, qui maximise la marge de bruit, et par conséquence la portée du système LP-OFDM, en considérant un débit cible de $2N$ bits par symbole OFDM. Nous trouvons que pour maximiser la marge de bruit ou la portée du système LP-OFDM, un seul bloc LP-OFDM doit être utilisé, et par suite la longueur des codes doit être égale au nombre de sous-porteuses utiles. L'avantage de cette solution est qu'il n'est pas nécessaire de connaître les coefficients du canal à l'émission pour répartir les sous-porteuses entre les blocs.

## Optimisation du système LP-OFDM à constellations variables

Dans un second temps, nous considérons des constellations variables de type MAQ-4, MAQ-8 et MAQ-16, afin de mieux bénéficier de la capacité du canal. La réponse du canal UWB variant lentement dans le temps, nous pouvons considérer une connaissance parfaite du canal à l'émission. Le problème de maximisation du débit peut être donné par

$$\begin{cases} \max \sum_{b=1}^{B} \sum_{k=1}^{K} \log_2 \left( 1 + \frac{1}{\Gamma} \frac{L^2}{\sum_{n=1}^{L} \left( 1/|h_{n,b}|^2 \right)} \frac{E_{k,b}}{N_0} \right), \\ \text{avec} \quad \sum_{k=1}^{K} E_{k,b} \leq \tilde{E}, \quad \forall b. \end{cases} \tag{3}$$

Après résolution de l'équation (3), la répartition optimale des bits et énergies devient

$$\begin{cases} \overline{R}_{k,b} = \lfloor R_b / L \rfloor + 1, & \forall k \in [1:m_b], \forall b, \\[2mm] \overline{R}_{k,b} = \lfloor R_b / L \rfloor, & \forall k \in [m_b+1:L], \forall b, \\[2mm] \text{avec } m_b = \left\lfloor L\left(2^{R_b/L - \lfloor R_b/L \rfloor} - 1\right) \right\rfloor \quad \text{et} \quad R_b = L\log_2\left(1 + \frac{1}{\Gamma}\frac{L}{\sum_{n=1}^{L}\left(1/|h_{n,b}|^2\right)}\frac{\tilde{E}}{N_0}\right), \\[4mm] \overline{E}_{k,b} = \frac{\Gamma}{L^2}\sum_{n=1}^{L}\frac{N_0}{|h_{n,b}|^2}\left(2^{\overline{R}_{k,b}} - 1\right), \quad \forall k, \forall b. \end{cases} \quad (4)$$

De même, le problème de maximisation de la marge ou de la portée peut être donné par

$$\begin{cases} \max \dfrac{\tilde{E}}{\Gamma N_0}\dfrac{L^2}{\sum_{n=1}^{L}\left(1/|h_{n,b}|^2\right)}\dfrac{1}{\sum_{k=1}^{K}\left(2^{R_{k,b}} - 1\right)}, & \forall b, \\[4mm] \text{avec} \quad \sum_{b=1}^{B}\sum_{k=1}^{K}R_{k,b} = \sum_{b=1}^{B}R_b = \tilde{R}. \end{cases} \quad (5)$$

## Résultats analytiques

Les figures 2 et 3 présentent quelques résultats numériques obtenus en appliquant les algorithmes d'allocation dynamique des ressources aux systèmes OFDM et LP-OFDM. Nous trouvons que la forme d'onde LP-OFDM a un grand avantage sur celle proposée par la solution WiMedia. Avec les algorithmes proposés, nous pouvons transmettre des données à des niveaux d'atténuation supérieurs aux niveaux d'atténuation limites de la solution Wi-Media. En outre, cette composante d'étalement permet aux sous-porteuses d'un même bloc de grouper leurs énergies pour transmettre un ou plusieurs bits supplémentaires alors que le système OFDM est incapable d'exploiter toute l'énergie disponible sur chaque sous-porteuse.

## Exploitation du TFC dynamique

Finalement, nous proposons une étude supplémentaire qui choisit les TFC pour les différents utilisateurs d'une façon dynamique, afin de maximiser la portée du système LP-OFDM. En effet, la proposition décrite par la norme WiMedia consiste à choisir les TFC d'une façon régulière sans tenir compte de l'état de la réponse du canal de chaque utilisateur et de chaque sous-bande. Un algorithme qui maximise la portée du système LP-OFDM en choisissant les TFC d'une façon dynamique est proposé. Les résultats obtenus par cet

algorithme s'avèrent très avantageux par rapport à ceux obtenus par la solution WiMedia. D'où l'intérêt de cette exploitation du TFC qui nous permet de transmettre des données à des niveaux d'atténuation plus élevés que ceux de la solution WiMedia.
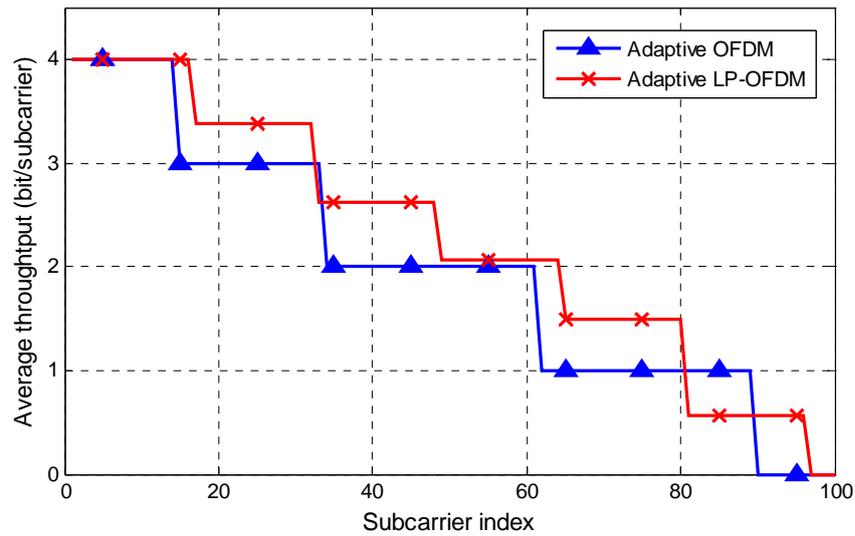


Figure 2 : Débit moyen par sous-porteuse pour les systèmes OFDM et LP-OFDM adaptatifs utilisant des ordres variables de constellation.
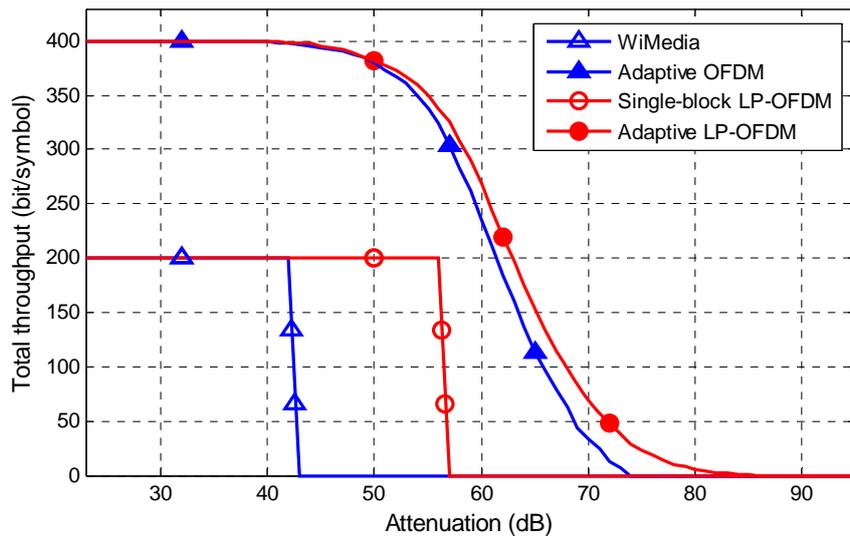


Figure 3 : Débit total des systèmes obtenu en utilisant l'algorithme de maximisation du débit avec des ordres variables de constellation, pour différents niveaux d'atténuation.

# Chapitre 4

# Minimisation du taux d'erreur binaire moyen

## Introduction et motivations

Après avoir présenté dans le chapitre précédent les différentes stratégies d'allocation des ressources qui peuvent être proposées pour le système LP-OFDM suivant une approche classique considérant une contrainte en TES, nous proposons dans ce chapitre différentes stratégies d'allocation pour l'UWB basées sur une nouvelle approche du TEB moyen. L'idée est d'optimiser les performances du système LP-OFDM en tenant compte de la valeur du TEB moyen du système. Ainsi, le problème d'optimisation peut être de minimiser le TEB moyen du système pour un débit cible donné afin d'améliorer sa robustesse, ou vice versa, de maximiser le débit du système sous une contrainte sur le TEB moyen. Cependant, dans ce chapitre nous présentons le problème de minimisation du TEB moyen (MBM ou *mean BER minimization*) pour un débit cible donné.

## Minimisation du TEB moyen à constellation fixe

Dans un premier temps, nous considérons uniquement la MAQ-4 (comme dans WiMedia) et un nombre $N$ de sous-porteuses utiles par sous-bande. Le problème de minimisation du TEB moyen d'un système LP-OFDM multibloc s'écrit

$$\begin{cases} \min_{B} \dfrac{1}{N} \sum_{b=1}^{B} \left( L_b\, Pb_b \right), \\[2mm] \text{avec} \quad \sum_{b=1}^{B} L_b = N, \end{cases} \tag{6}$$

avec $Pb_b$ le TEB moyen d'un bloc $b$ donné par

$$Pb_b = \frac{1}{2} erfc \left( \sqrt{\frac{L_b \tilde{E}}{2 N_0} \frac{1}{\sum_{n=1}^{L_b} \left( 1/ | h_{n,b} |^2 \right)}} \right). \tag{7}$$

L'étude analytique montre que les performances du système dépendent fortement du rapport SNR (*signal-to-noise ratio*) considéré. Ainsi, le système OFDM est plus performant en terme de TEB moyen pour les faibles valeurs du SNR et le système LP-OFDM est plus performant pour les moyennes et fortes valeurs du SNR. De plus, les valeurs limites du

SNR qui définissent quel système est plus performant sont déterminées analytiquement. Un algorithme qui minimise le TEB moyen du système en utilisant des longueurs variables de code d'étalement est ensuite proposé. Les résultats de simulation, présentés dans la figure 4, montrent que le système LP-OFDM utilisant cet algorithme (MBM) est toujours plus performant que le système OFDM et le système LP-OFDM utilisant une longueur de codes d'étalement constante.
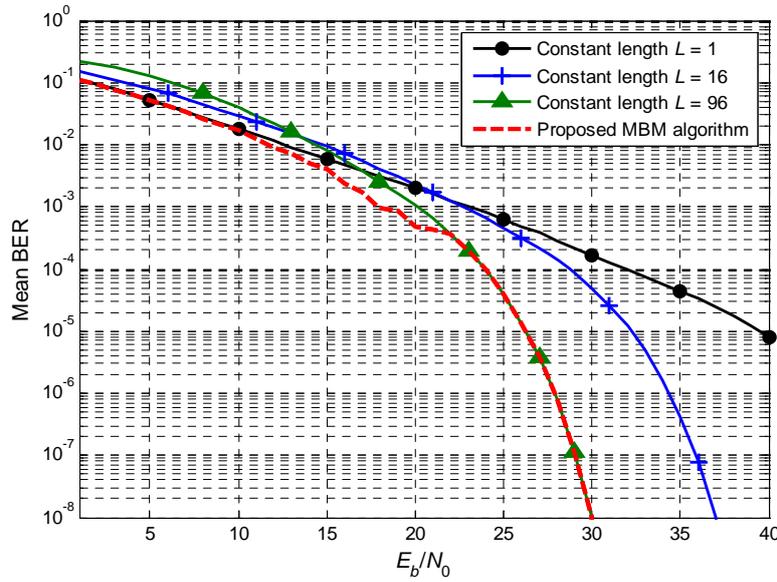


Figure 4: Performances de l'algorithme de minimisation du TEB moyen avec des longueurs variables de code d'étalement à constellation fixe.

## Minimisation du TEB moyen à constellations variables

Dans un second temps, nous considérons des constellations variables de type MAQ-4, MAQ-8 et MAQ-16, afin de mieux bénéficier de la capacité du canal. La réponse du canal UWB variant lentement dans le temps, nous pouvons considérer une connaissance parfaite du canal à l'émission. Le problème de minimisation du TEB moyen d'un système LP-OFDM monobloc est donné par

$$
\begin{cases}
\min \dfrac{\sum_{k=1}^{K} \left( R_k Pb_k \right)}{\sum_{k=1}^{K} R_k}, \\
\\
\text{avec} \quad \sum_{k=1}^{K} E_k \leq \tilde{E} \quad \text{et} \quad \sum_{k=1}^{K} R_k = \tilde{R},
\end{cases}
\tag{8}
$$

avec $Pb_k$ le TEB moyen du code $k$ donné par

$$Pb_k \approx \frac{1}{R_k} 2erfc\left(\sqrt{\frac{3}{2} \frac{L^2}{\sum_{n=1}^{L}\left(1/\left|h_n\right|^2\right)} \frac{E_k}{N_0} \frac{1}{2^{R_k}-1}}\right).\qquad(9)$$

La répartition optimale des bits dans le cas d'un système LP-OFDM multibloc est ainsi donnée par

$$\begin{cases} \overline{R}_{k,b} = \left\lfloor \overline{R}_b / K_b^* \right\rfloor + 1, & \forall b, \; \forall k \in \left[1:m_b\right], \\[2mm] \overline{R}_{k,b} = \left\lfloor \overline{R}_b / K_b^* \right\rfloor, & \forall b, \; \forall k \in \left[m_b+1:K_b^*\right], \\[2mm] \text{avec} \quad m_b = \overline{R}_b - K_b^* \left\lfloor \overline{R}_b / K_b^* \right\rfloor, \\[2mm] K_b^* \approx \text{Round}\left[\frac{2}{3} \frac{\alpha_b \tilde{E}}{2^{\overline{R}_b}-1} e^{\left(\overline{R}_b - 0.415\right)/1.4427 - 1}\right], \\[2mm] \overline{R}_b \text{ déterminé par un algorithme de type greedy.} \end{cases} \qquad (10)$$

Les performances de l'algorithme de minimisation du TEB moyen (MBM) utilisant des ordres variables de constellation et une longueur d'étalement constante $L = 16$ sont présentées dans la figure 5. Nous remarquons que cet algorithme minimise considérablement le TEB moyen du système par comparaison aux systèmes OFDM et LP-OFDM avec une constellation fixe MAQ-4.
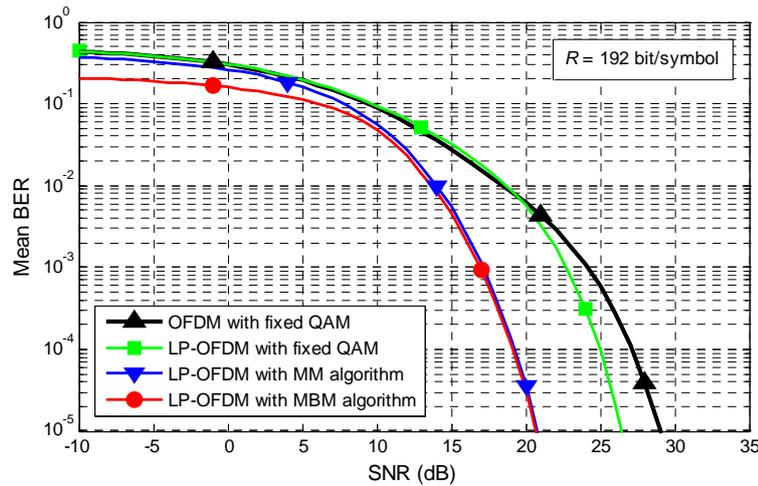


Figure 5: Performances de l'algorithme de minimisation du TEB moyen utilisant des ordres variables de constellation et une longueur constante de code d'étalement.

# Chapitre 5

# Optimisation du système MIMO LP-OFDM UWB global

### Introduction et motivations

Après avoir étudié analytiquement le schéma de précodage linéaire proposé dans les chapitres précédents et présenté ses avantages quand il est combiné avec une modulation OFDM, nous considérons ici une étude globale du système LP-OFDM UWB qui tient compte des différentes fonctions de la chaîne de transmission. Ce chapitre est divisé en deux parties. La première partie présente les performances du système LP-OFDM proposé dans un contexte SISO (*single-input single-output*). Après une discussion sur les principales stratégies de choix des paramètres qui améliorent les performances du système, la longueur du code d'étalement est optimisée, et les résultats de simulation obtenus vérifient les résultats analytiques obtenus dans le chapitre 4. La deuxième partie du chapitre est consacrée à l'étude des techniques MIMO (*multiple-input multiple-output*) pour les applications UWB. Après une présentation générale des techniques MIMO, un nouveau modèle de canal MIMO UWB réaliste, développé au sein de l'IETR, est décrit. Un schéma temps-espace de type Alamouti est proposé pour le système LP-OFDM dans le but d'améliorer la portée du système en considérant une constellation MAQ-4, et puis d'offrir un débit double grâce à la combinaison de la composante MIMO avec une constellation de type MAQ-16.

### Système LP-OFDM dans un contexte SISO

Dans le système SISO LP-OFDM proposé, les différents blocs de la chaîne de transmission ainsi que les paramètres OFDM sont quasiment les mêmes que ceux du système WiMedia, dans le but de ne pas trop augmenter la complexité du système par comparaison à WiMedia. De plus, la composante d'étalement se réduit à une simple addition d'une matrice orthogonale de Walsh-Hadamard. Les sous-porteuses adjacentes sont ensuite réparties sur les différents blocs LP-OFDM, ce qui réduit la SI (*self-interference*). L'un des principaux avantages du système LP-OFDM est qu'il offre un grand choix de débits grâce aux différentes sélections possibles du rendement de codage du canal et du nombre de codes d'étalement. Les résultats de simulation du système LP-OFDM global pour différentes valeurs de longueur d'étalement vérifient les résultats analytiques obtenus dans le chapitre 4 et montrent que l'ajout d'une composante d'étalement optimisée offre un gain variant

entre 0.5 et 1 dB environ par rapport au système WiMedia, comme on le constate à la figure 6.
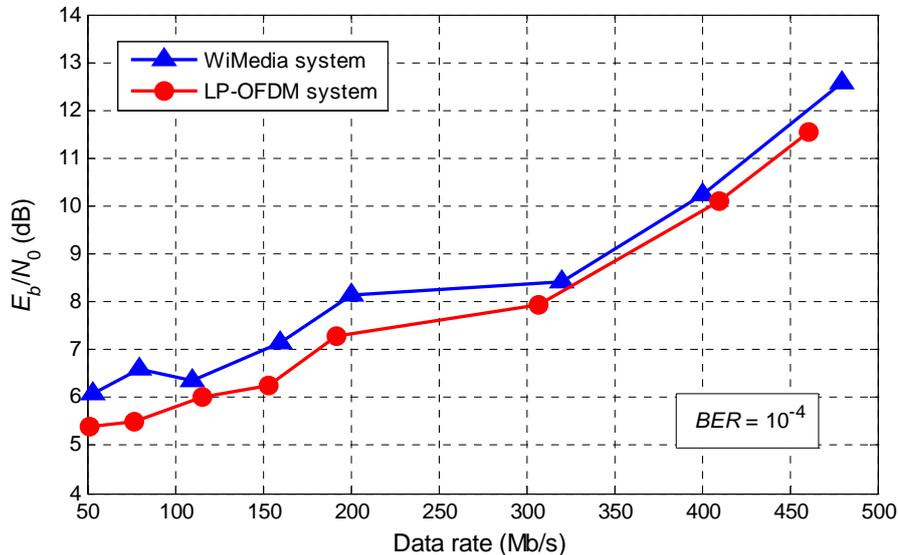


Figure 6 : Performances du système SISO LP-OFDM pour les différents débits proposés : rapport $E_b / N_0$ nécessaire pour obtenir un taux d'erreur binaire cible de $10^{-4}$.

## Système LP-OFDM dans un contexte MIMO

Dans cette étude, nous proposons d'ajouter un schéma temps-espace de type Alamouti au système LP-OFDM, avec deux antennes à l'émission et deux antennes à la réception. Grâce à ses caractéristiques orthogonales, le décodage ML (*maximum likelihood*) de ce schéma se résume à un simple décodage linéaire, ce qui réduit le coût du récepteur. En considérant une seule constellation MAQ-4 comme dans WiMedia, l'ajout de la composante MIMO améliore la portée du système pour des débits proches de ceux proposés par WiMedia. D'autre part, en augmentant l'ordre de la constellation jusqu'à la MAQ-16, le système LP-OFDM résultant offre de très hauts débits variant de 614 Mb/s à environ 1 Gb/s.

Le modèle de canal MIMO utilisé dans cette étude est un nouveau modèle géométrique statistique, développé au sein de l'IETR. Il est basé sur le principe du modèle 3GPP/3GPP2, utilisant les paramètres géométriques du modèle IEEE 802.11n avec une réponse impulsionnelle SISO du modèle IEEE 802.15.3a.

## Résultats analytiques

Les performances des systèmes SISO et MIMO LP-OFDM pour les différents débits proposés sont présentées figure 7. Pour les bas et moyens débits (de 51,2 à 460 Mb/s), le sys-

tème MIMO LP-OFDM proposé est plus performant que le système WiMedia en terme de robustesse, et par conséquence, en terme de portée. Ainsi, le système MIMO LP-OFDM offre un débit de 460 Mb/s avec un gain de 5,2 dB comparé au système WiMedia. D'autre part, le système MIMO LP-OFDM offre un débit très proche de 1 Gb/s, qui est le double du débit maximal offert par WiMedia, conjointement avec de meilleures performances en terme de TEB. Notons que ces résultats sont obtenus avec un espacement d'antennes réaliste de 5 cm entres les deux antennes à la fois à l'émission et à la réception. En conclusion, le système MIMO LP-OFDM proposé peut être avantageusement exploité pour les applications UWB à très haut débit.
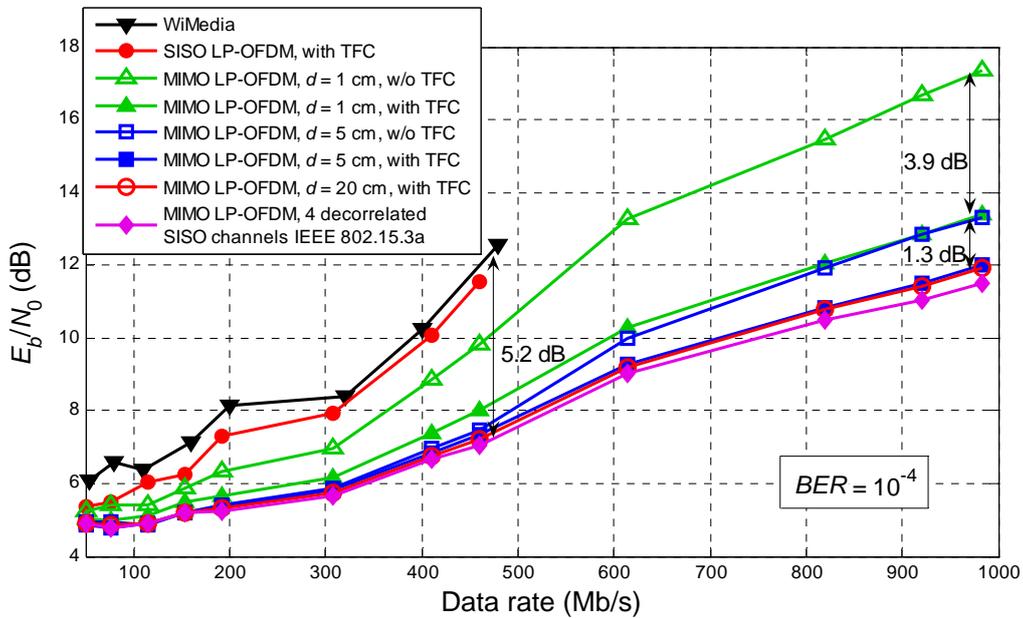


Figure 7 : Performances des systèmes SISO et MIMO LP-OFDM pour les différents débits proposés, à un taux d'erreur binaire cible de $10^{-4}$.

# Conclusion

Dans cette thèse, nous avons proposé un système LP-OFDM pour les applications UWB très haut débit. Tout d'abord, nous avons montré analytiquement que la forme d'onde LP-OFDM a un grand avantage sur l'OFDM classique proposé par la solution WiMedia. L'ajout d'une composante d'étalement selon l'axe fréquentiel s'avère une bonne solution qui offre une meilleure robustesse vis-à-vis de la sélectivité fréquentielle du canal UWB. En outre, cette composante d'étalement permet aux sous-porteuses d'un même bloc de grouper leurs énergies pour transmettre un ou plusieurs bits supplémentaires alors que le système OFDM est incapable d'exploiter toute l'énergie disponible sur chaque sous-porteuse. De plus, des algorithmes d'allocation dynamique des ressources on été proposés dans le but de maximiser le débit ou la portée, ou de minimiser le TEB moyen du système.

D'autre part, complémentairement à l'étude analytique, une étude du système global LP-OFDM a été effectuée, prenant en compte les différents blocs de la chaîne de transmission. Dans un premier temps, les résultats de simulation obtenus dans un contexte SISO vérifient les résultats analytiques trouvés précédemment, et montrent que le système LP-OFDM est plus performant que le système WiMedia. Dans un second temps, une composante MIMO a été ajoutée dans le but d'améliorer la portée du système en considérant une constellation MAQ-4, et d'offrir un très haut débit grâce à une combinaison des techniques MIMO avec une constellation MAQ-16. Le système MIMO LP-OFDM résultant offre un débit avoisinant 1 Gb/s, ce qui est le double du débit maximal offert par WiMedia, avec même de meilleures performances en terme de TEB.

Les résultats théoriques et pratiques dans cette thèse ont conduit à des contributions dans le cadre du projet Européen FP7 OMEGA et dans le cadre d'un contrat de recherche externe avec Orange Labs RESA/WIN/CREM (France Télécom R&D). Les solutions obtenues ont abouti à la publication de deux revues et sept communications internationales, et à la soumission d'un article de revue et de deux articles de conférence supplémentaires.

# List of Figures

# List of Tables

# Acronyms

| | |
|---|---|
| **ADC** | Analog-to-Digital Converter |
| **ADSL** | Asymmetric Digital Subscriber Line |
| **AoA** | Angle Of Arrival |
| **AoD** | Angle Of Departure |
| **BER** | Bit-Error-Rate |
| **BPSK** | Binary Phase-Shift Keying |
| **CDM** | Code-Division Multiplexing |
| **CDMA** | Code-Division Multiple Access |
| **CP** | Cyclic Prefix |
| **CSI** | Channel State Information |
| **DAA** | Detect And Avoid |
| **DAB** | Digital Audio Broadcasting |
| **DAC** | Digital-to-Analog Converter |
| **DCM** | Dual-Carrier Modulation |
| **DFT / IDFT** | Discrete Fourier Transform / Inverse Discrete Fourier Transform |
| **DS** | Direct-Sequence |
| **DTFC** | Dynamic Time-Frequency Code |
| **DVB** | Digital Video Broadcasting |
| **ECMA** | European Computer Manufacturers Association |
| **ETSI** | European Telecommunications Standards Institute |
| **FCC** | Federal Communications Commission |
| **FDM** | Frequency-Division Multiplexing |
| **FDMA** | Frequency-Division Multiple Access |
| **FDS** | Frequency-Domain Spreading |
| **FEC** | Forward Error Correction |
| **FFT / IFFT** | Fast Fourier Transform / Inverse Fast Fourier Transform |
| **FH** | Frequency-Hopping |

| | |
|---|---|
| **GI** | Guard Interval |
| **GPS** | Global Positioning System |
| **GSC** | Geometric Statistic Channel |
| **GSM** | Global System for Mobile communications |
| **ICI** | Inter-Carrier Interference |
| **IR** | Impulse Radio |
| **ISI** | Inter-Symbol Interference |
| **LLR** | Log-Likelihood Ratio |
| **LNA** | Low-Noise Amplifier |
| **LOS** | Line-Of-Sight |
| **LP** | Linear Precoding / Linear Precoded |
| **LST** | Layered Space-Time |
| **MAI** | Multiple Access Interference |
| **MBM** | Mean BER Minimization |
| **MBOA** | MultiBand OFDM Alliance |
| **MB-OFDM** | MultiBand OFDM |
| **MC-CDMA** | MultiCarrier CDMA |
| **MC-SS** | MultiCarrier Spread Spectrum |
| **ML** | Maximum Likelihood |
| **MIMO** | Multiple-Input Multiple-Output |
| **MM** | Margin Maximization |
| **MMSE** | Minimum Mean-Square Error |
| **NLOS** | Non-Line-Of-Sight |
| **OFDM** | Orthogonal Frequency-Division Multiplexing |
| **OMEGA** | European FP7 "hOME Gigabit Access" project |
| **OOK** | On-Off Keying |
| **OSTBC** | Orthogonal Space-Time Block Code |
| **PAM** | Pulse Amplitude Modulation |
| **PAPR** | Peak-to-Average Power Ratio |
| **PLC** | Power Line Communication |
| **PN** | Pseudorandom Noise |
| **PPM** | Pulse Position Modulation |
| **PSD** | Power Spectral Density |
| **PSM** | Pulse Shape Modulation |
| **QAM** | Quadrature Amplitude Modulation |

| | |
|---|---|
| **QoS** | Quality Of Service |
| **QPSK** | Quadrature Phase-Shift Keying |
| **RF** | Radio-Frequency |
| **RM** | Rate Maximization |
| **SER** | Symbol-Error-Rate |
| **SISO** | Single-Input Single-Output |
| **SNR** | Signal-to-Noise Ratio |
| **SS** | Spread Spectrum |
| **SS-MC-MA** | Spread Spectrum MultiCarrier Multiple Access |
| **STBC** | Space-Time Block Code |
| **STTC** | Space-Time Treillis Code |
| **SV** | Saleh-Valenzuela |
| **TDM** | Time-Division Multiplexing |
| **TDMA** | Time-Division Multiple Access |
| **TDS** | Time-Domain Spreading |
| **TFC** | Time-Frequency Code |
| **TH** | Time-Hopping |
| **UMTS** | Universal Mobile Telecommunications System |
| **UWB** | Ultra-WideBand |
| **WLAN** | Wireless Local Area Network |
| **WPAN** | Wireless Personal Area Network |
| **ZF** | Zero Forcing |
| **ZPS** | Zero-Padded Suffix |

# Introduction

W IRELESS home networks at gigabit speed are a pivotal technology for realizing the world vision of the future internet. The demand for gigabit home networks is driven by the emerging future internet services running over new high-speed wireless access networks and the rapidly growing number of communicating devices in the home. Current home networks suffer from the fact that many devices are limited to transmission rates of 54 Mb/s in case of wireless links, or require troublesome wiring to achieve higher rates. Thus, the existing home networks are at risk of becoming a bottleneck when fed by higher speed networks.

The future internet will offer extremely high bandwidth in core and access networks. Home area networks play a key role in realizing the benefits of this high bandwidth and making it tangible for the users by providing critical access to this infrastructure for end devices within the home. Future home area networks must enrich the lives of users, for example by allowing visual communications with their friends or relatives and by enabling interactive experiences through entertainment. In short, users must have the ability to control their virtual as well as their physical environment via home networks, and will require such networks to be simple to install without any new wiring. For instance, mobility and freedom of movement in viewing documents, pictures and videos with high throughput wireless transmissions are a prerequisite.

One of the most promising radio communications candidates for the future high data rate home networks is the ultra-wideband (UWB) technology. UWB radio has received great attention in both academia and industry for applications in wireless communications since 2002 when the Federal Communications Commission (FCC) of the USA reserved an unlicensed frequency band between 3.1 and 10.6 GHz for indoor UWB applications. This FCC decision led to the introduction of many UWB-based industrial standardization groups, such as IEEE 802.15.3a (high data rate) and IEEE 802.15.4a (very low data rate).

The idea behind UWB is to transmit a signal on a very large frequency band with a very low transmit power, which provides very high data rates at low cost. The large UWB spectrum overlays several existing and future spectrums allocated for other systems, e.g. WLAN and WiMAX, which led to significant difficulties to define a worldwide regulation

for UWB systems. The spectral mask defined by the FCC for the USA raised controversy in other countries as many studies showed that this mask does not guarantee that UWB systems will not interfere with other systems. In Europe for instance, after intensive discussions within the European regulation bodies, a much constrained spectral mask was proposed for UWB applications, which significantly reduces the potentials of UWB systems. Thus, the objective of this thesis is to propose a new UWB system that can cope with the different UWB constraints, including the stringent power limitations. In short, different enhancements on the physical layer of the existing UWB systems, including the addition and optimization of linear precoded OFDM, MIMO and resource allocation schemes, are considered to improve the system performance in terms of throughput, robustness and range.

## Thesis overview and contributions

This work was carried out at the Institute of Electronics and Telecommunications of Rennes (IETR) – National Institute of Applied Sciences (INSA). It was sponsored by Orange Labs RESA/WIN/CREM (France Télécom R&D) within an external research contract (no. 46 136 582) of three years. This research was also part of the OMEGA project [1], which is an Integrated Project in the ICT area funded by the European Commission under the Seventh Research Framework Programme (FP7). It consists of 20 European partners from industry and academia, including France Télécom R&D, Siemens AG, Thomson, Infineon, Telefonica, IETR, University of Oxford and University of Udine.

The objective of the OMEGA project is to set a global standard for ultra broadband home area networks. The new standard will enable transmission speeds of 1 Gb/s via heterogeneous communication technologies, including power line communications and wireless connections. Thus, OMEGA aims to make home area networks as easy to use as electricity from the socket, putting an end to the coverage limitations as well as the wiring clutter in the home. With OMEGA's gigabit home network, users will get easy access to high-bandwidth information and communication services such as 3D gaming, enhanced interactivity, virtual reality, high-definition video as well as e-health applications and services for the exchange of user-generated business or multimedia content.

This dissertation is organized as follows. In **Chapter 1**, we present a state of the art of the UWB technology. The first part of this chapter provides a historical overview of UWB, discusses the regulatory and standardization issues, and lists the main UWB applications. Next, we describe the two main modulation techniques considered for WPAN high data rate UWB applications, based on impulse radio and multiband orthogonal frequency-division multiplexing (MB-OFDM), followed by a comparison of these two techniques.

Finally, we present the indoor channel model that we will use for the UWB system simulations.

In **Chapter 2**, we first describe the main transmission techniques that are exploited in this thesis, mainly the multicarrier modulation and spread spectrum techniques. Then, we present the main modulation schemes resulting from the combination of these two techniques. The second part of this chapter describes the MB-OFDM system, which is the starting point of our studies, and discusses its performance, advantages and drawbacks. Afterwards, we present the proposed linear precoded OFDM (LP-OFDM) system for UWB applications, which can be seen as an evolution of the MB-OFDM approach. We discuss the main advantages and motivations that led to this system choice.

In **Chapter 3**, we first present the resource allocation principles and optimization strategies, namely, the rate maximization and margin maximization. These principles can be efficiently applied for indoor UWB communications without significantly increasing the implementation complexity, thanks to the slow time variation of the UWB channel. Classical solutions for OFDM systems and new optimal solutions for LP-OFDM systems are then detailed, taking into account the UWB characteristics. Note that in this chapter, a classical target symbol-error-rate (SER) approach is considered. Finally, an additional optimization study based on a dynamic distribution of the time-frequency codes between users of an UWB system is proposed. The different optimization results show that the linear precoding component can be efficiently exploited for high data rate UWB applications, and that the LP-OFDM system outperforms the OFDM system of the WiMedia solution. The proposed new allocation algorithms and the results presented in this chapter have led to publications [C1]–[C6], listed at the end of this section.

In **Chapter 4**, we propose different allocation strategies for UWB, based on a new mean BER approach. The idea is to optimize the LP-OFDM system performance taking into account the system mean BER value instead of the SER value. First, we present an efficient resource allocation algorithm that reduces the mean BER of a LP-OFDM UWB system using only a single QPSK constellation. Then, in order to further improve the system performance, we consider variable constellation orders and we propose a study that minimizes the mean BER of OFDM and LP-OFDM systems for a given target throughput. The simulation results show that the proposed algorithms reduce the system mean BER significantly, compared to the MB-OFDM system. This work has led to publications [J3], [C8] and [C9].

**Chapter 5** presents the global UWB system study taking into account the different functions of the transmission chain. The first part of the chapter discusses the performance of the proposed LP-OFDM system in a single-input single-output (SISO) context. Analyti-

cal results obtained in previous chapters are verified here through system simulations. In the second part, after a brief overview on multiple-input multiple-output (MIMO) technology, we study the efficiency of MIMO for UWB applications. A new realistic MIMO UWB channel model developed at IETR, which will be used for the system simulations, is described. Then, a low complexity Alamouti space-time scheme is combined with the LP-OFDM scheme. The objective is first to improve the system range while maintaining a QPSK constellation, and second to provide very high data rates of around 1 Gb/s through a joint combination of MIMO with a 16-QAM constellation. Simulation results of the global MIMO LP-OFDM system show the advantage of combining MIMO and LP techniques in UWB, in terms of performance and flexibility. Besides, this work has led to publications [J1], [J2] and [C7].

Finally, in the **Conclusion and perspectives** section, we summarize this thesis and give some concluding remarks as well as suggestions for future research directions.

## List of Publications

### Journal Papers

[J3]   F-S. Muhammad, A. Stephan, J-Y. Baudais and J-F. Hélard, "Optimization of linear precoded OFDM systems based on a mean BER approach," submitted to *IEEE Transactions on Wireless Communications*, 2008.

[J2]   A. Stephan, J-Y. Baudais and J-F. Hélard, "Range improvement of UWB systems using adaptive multicarrier spread-spectrum and MIMO techniques," *European Transactions on Telecommunications (ETT), Special Issue on Multi-Carrier Spread Spectrum*, vol. 19, no. 5, pp. 589–599, 2008.

[J1]   A. Stephan, E. Guéguen, M. Crussière, J-Y. Baudais and J-F. Hélard, "Optimization of linear precoded OFDM for high-data-rate UWB systems," *EURASIP Journal on Wireless Communications and Networking*, vol. 2008, Article ID 317257, 2008.

### International Conferences

[C9]   F-S. Muhammad, A. Stephan, J-Y. Baudais and J-F. Hélard, "Mean BER minimization loading algorithm for linear precoded OFDM," submitted to *IEEE Sarnoff Symposium (Sarnoff'09)*, Princeton, USA, March, April 2009.

[C8]   F-S. Muhammad, A. Stephan, J-Y. Baudais and J-F. Hélard, "Bit rate maximization loading algorithm with mean BER-constraint for linear precoded OFDM," submit-

ted to *IEEE International Conference on Telecommunications (ICT'09)*, Morocco, May 2009.

[C7]  A. Stephan, J-F. Hélard and B. Uguen, "MIMO UWB systems based on linear pre-coded OFDM for home gigabit applications," in *Proc. IEEE Global Communications Conference (GLOBECOM'08)*, pp. 1–6, USA, Dec. 2008.

[C6]  A. Khalil, A. Stephan, M. Crussière and J-F. Hélard, "Multi-user cross-layer allocation design for LP-OFDM high data rate UWB systems," in *Proc. IEEE International Symposium on Wireless Communication Systems (ISWCS'08)*, pp. 6–10, Iceland, Oct. 2008.

[C5]  A. Stephan, J-Y. Baudais and J-F. Hélard, "Efficient allocation algorithms for multicarrier spread-spectrum schemes in UWB applications," in *Proc. IEEE International Conference on Ultra-Wideband (ICUWB'07)*, pp. 551–555, Singapore, Sept. 2007.

[C4]  A. Stephan, J-Y. Baudais and J-F. Hélard, "Adaptive multi-carrier spread-spectrum with dynamic time-frequency codes for UWB applications," in *Proc. IEEE Workshop on Multi-Carrier Spread Spectrum (MC-SS'07)*, pp. 197–206, Germany, May 2007.

[C3]  A. Stephan, J-Y. Baudais and J-F. Hélard, "Adaptive spread spectrum multicarrier multiple-access for UWB systems," in *Proc. IEEE 65th Vehicular Technology Conference (VTC'07 Spring)*, pp. 2926–2930, Dublin, Ireland, April 2007.

[C2]  A. Stephan, J-Y. Baudais and J-F. Hélard, "Optimisation des systèmes MIMO SS-MC-MA dans le contexte UWB," in *21st Colloque GRETSI*, pp. 297–300, Troyes, France, Sept. 2007.

[C1]  A. Stephan, J-Y. Baudais and J-F. Hélard, "Resource allocation for multicarrier CDMA systems in ultra-wideband communications," in *Proc. IEEE International Telecommunications Symposium (ITS'06)*, pp. 135–140, Fortaleza, Brazil, Sept. 2006.

# Chapter 1

# Ultra-wideband communications

ULTRA-WIDEBAND (UWB) is a fast emerging technology that has attracted considerable interest in the research and standardization communities for wireless communications. This first chapter presents a general introduction to UWB communications. It describes the origins and motivations that led to the development of UWB systems. The regulatory and standardization issues are then discussed and the main UWB applications briefly presented. In addition, the two main modulation techniques considered for high data rate WPAN UWB applications, based on impulse radio and multiband orthogonal frequency-division multiplexing (MB-OFDM) respectively, are described, followed by a comparison between these two techniques. Besides, the indoor channel model considered by the Institute of Electrical and Electronics Engineers (IEEE) 802.15.3a standardization group for UWB applications and adopted in this thesis is presented. Finally, after having presented a general overview of UWB communications, this chapter is concluded with a listing of the main UWB specifications and objectives that will be considered in our studies, including the modulation and applications choices.

## 1.1 Historical overview

Although considered as a recent breakdown in wireless technology, UWB has experienced over 45 years of technological developments, traveling from the lab, to the military, and recently into commercial prototyping and implementation. The term "ultra-wideband" was used for the first time in the late 1980s, by the U.S. Department of Defense [2]. The UWB technology has been known by many other names, including impulse radio, short-pulse, baseband communication, carrier free communication, nonsinusoidal, super wideband, fast frequency chirp, monopulse and Walsh waves communication [3], [4].

The spark-gap transmission experiments of Marconi and Hertz in the late 1890s represent some of the first experiments in a crude form of impulse radio. In other words, the first wireless communication system was based on UWB. However, owing to the technical

limitations, narrowband communication was preferred to UWB. Besides, spark gaps and arc discharges between carbon electrodes were the dominant wave generators about 20 years after Hertz first experiments.

The modern era of UWB radio started in the early 1960s with some work in time-domain electromagnetics, and was led by Harmuth at Catholic University of America, Ross and Robins at Sperry Rand Corporation, and Van Etten at the United States Air Force Rome Air Development Center. The development of the sampling oscilloscope by both Tektronix and Hewlett-Packard in the 1960s and the corresponding techniques for generating sub-nanosecond baseband pulses sped up the development of UWB.

By the early 1970s, the main focus moved to develop radar and communications devices. The first ground penetrating radar based on UWB was commercialized in 1974 by Morey at the Geophysical Survey Systems. In 1973, the first U.S. patent on UWB communications was awarded [5]. During the 1970s and 1980s, practical development work continued and pioneering contributions were made by Bennett and Ross [6] and Harmuth [7]. Bennett and Ross presented many examples of radar and communications applications based on UWB technology. Other applications, such as positioning systems, liquid-level sensing, and automobile collision avoidance, were also developed. Most of the applications and development occurred in the military or in work performed under classified U.S. government programs. However, the late 1990s saw the move to commercialize UWB communication devices and systems. Thus, different companies pursuing commercial opportunities, such as XtremeSpectrum, were formed.

A substantial change occurred in February 2002 when the U.S. Federal Communications Commission (FCC) issued a Report & Order that authorizes the commercial and unlicensed deployment of UWB in the USA [8]. A 7.5 GHz spectrum was allocated for UWB applications, with a given spectral mask for both indoor and outdoor applications. This spectral allocation has initiated an extremely productive activity for industry and academia.

## 1.2   UWB principles and characteristics

When UWB technology was proposed for commercial applications, there were no definitions for the signal. The Defense Advanced Research Projects Agency provided the first definition for UWB signals based on the fractional bandwidth $B_f$ of the signal which is defined as [4]

$$B_f = 2\frac{f_H - f_L}{f_H + f_L},\qquad(1.1)$$

where $f_H$ and $f_L$ are respectively the higher and lower -3 dB point in the spectrum. This first definition provided that a signal can be classified as an UWB signal if $B_f$ is greater than 0.25. In February 2002, the FCC approved that any signal having a -10 dB fractional bandwidth larger than 0.20, or a bandwidth greater than 500 MHz, is characterized as an UWB signal.

UWB technology has a number of features that make it attractive for consumer communications applications. In particular, UWB systems

- Provide high data rates.

- Have potentially small size, low complexity and low cost.

- Are resistant to multipath and interference.

- Allow ranging and communication at the same time.

The advantages of UWB systems in terms of data rate compared to narrow bandwidth systems can be understood by examining the Shannon famous capacity equation which is expressed as [9]

$$C = W \log_2 \left( 1 + \frac{S}{N} \right), \tag{1.2}$$

where $C$ is the maximum channel capacity in b/s, $W$ the channel bandwidth in Hz, and $S/N$ the signal-to-noise ratio (SNR). From this equation, we notice that to improve the channel capacity, we can increase either the system bandwidth or the SNR. However, the capacity grows linearly with the bandwidth, but only logarithmically with the signal power. For this reason, communication engineers in general prefer to increase the system bandwidth rather than the power, to achieve higher data rates. Consequently, systems using the UWB spectrum can be designed to achieve high bit rate better than narrow bandwidth systems.

UWB systems can be implemented in low cost, low-power integrated circuit processes thanks to the baseband nature of the signal transmission. Unlike conventional radio systems, the UWB transmitter produces a very short time-domain pulse, which is able to propagate without the need of an additional radio-frequency (RF) mixing stage [10]. The UWB signal spans frequencies commonly used as carrier frequencies due to its very wideband nature. Consequently, the signal will propagate well without using additional upconversion and down-conversion stages. Besides, single chip complementary metal-oxide-semiconductor (CMOS) integration of UWB transceiver contributes directly to low cost, low power and small size devices.

Because of the large bandwidth of the transmitted signal, UWB transmissions can resolve many paths, and consequently very high multipath resolution is achieved. For instance, a Gaussian monocycle UWB transceiver experiences only a 1.5 dB fading margin in dense multipath, which is very low compared to deep fades experienced in narrowband systems [11].

Finally, the ultra-short duration of UWB waveforms offers the ability to provide high precision ranging and high-speed data communication. For instance, UWB radios offer timing precisions much better than the global positioning system (GPS) and other radio systems [12], as well as opportunities for short-range radar applications.

## 1.3    Regulatory bodies

### 1.3.1    UWB regulations in the USA

In the FCC Report & Order of 2002 [8], a 3.1–10.6 GHz spectrum was allocated for unlicensed use of UWB devices in the USA. As depicted in Figure 1.1, this very wide spectrum overlays several existing allocated spectrums (UMTS, GSM, WLAN, fixed satellite services…), as well as many spectrums that will be allocated for future services (WiMAX, future mobile systems). Thus, the problem is twofold. First, UWB must mitigate or be able to operate in the presence of these strong interferers. Second, reciprocally, UWB must not provide substantial interference to the users of these narrowband services. In order to opti-
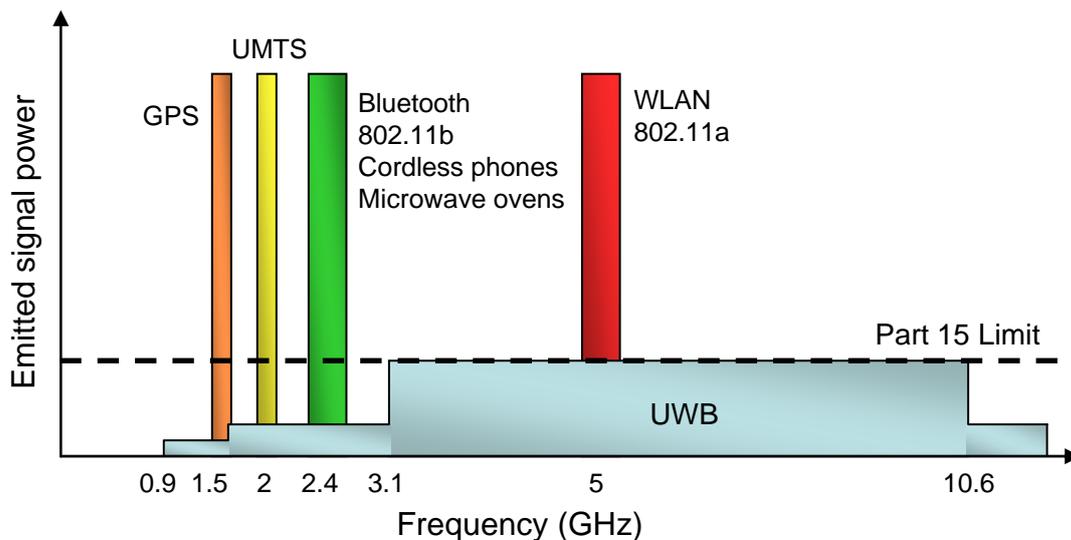


Figure 1.1: UWB spectrum overlaying existing narrowband systems.

mize spectrum use and reduce this interference, the FCC imposed very restrictive rulings and a power spectral density (PSD) spectral mask that must be respected by the UWB signal. Besides, a large number of studies on interference and coexistence of UWB with other systems have been carried out since the FCC decision [13]–[16].

According to the FCC spectral mask, illustrated in Figure 1.2, the PSD of an UWB signal measured in 1 MHz bandwidth must not exceed -41.3 dBm, which complies with the FCC Part 15 general emission limits to successfully control radio interference. We also notice in this figure that the PSD limit is even much lower for particularly sensitive bands, such as the GPS band (0.96–1.61 GHz).

On the other hand, the FCC decision has generated studies and considerations of radio spectrum implications within many administrations around the world. As a result, the International Telecommunication Union-Radiocommunication Sector (ITU-R) created Task Group 1/8 (TG 1/8) to study UWB radio coexistence issues.

### 1.3.2 UWB regulations in Europe

In Europe, the process of regulation has been ongoing for a considerable time and has experienced repeated delays after the FCC decision in 2002. The two main organizations involved in the European UWB regulations are the European Conference of Postal and Telecommunications Administrations (CEPT) focused on the harmonization of telecommunications regulations across its member countries, and the European Telecommunications Standards Institute (ETSI) working on developing a European standard for UWB.

The deployment of the first UWB chipsets in the USA has put pressure on the European regulation bodies to issue a first decision, in order to avoid the invasion of unauthorized and potentially interfering systems on the European market. Consequently, in March 2006, the European Communications Commission (ECC) published its first decision on UWB regulations in Europe [17]. Figure 1.2 summarizes the spectral mask defined by the ECC. In the frequency band 6–8.5 GHz, the ECC decided that high and low data rate UWB applications can be implemented, with an emission mask of -41.3 dBm/MHz. However, in the other frequency bands, the PSD limits were much lower than the ones defined by the FCC. Besides, another decision was reached in December 2006 settling the case of the 3.1–4.8 GHz band [18]. In the 3.1–4.2 GHz band, by using appropriate mitigation techniques such as detect and avoid (DAA) technique, the PSD limit can be raised to -41.3 dBm/MHz. In the 4.2–4.8 GHz band, the emission mask is equal to -41.3 dBm/MHz without mitigation techniques until December 2010, since this band is considered for future mobile applications.
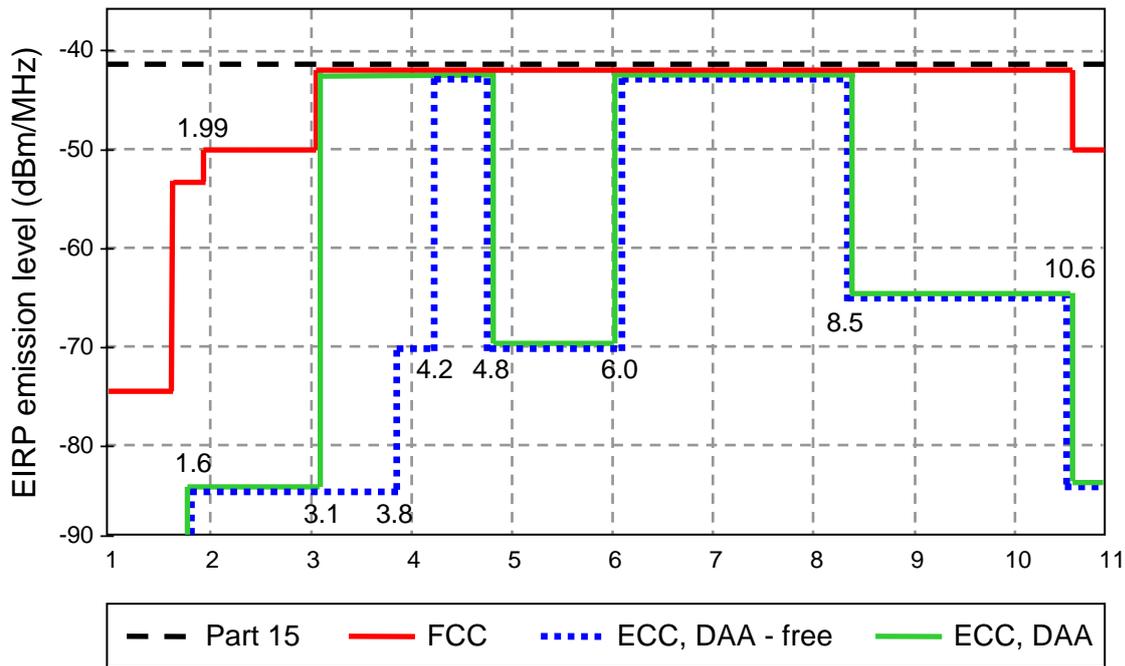
Figure 1.2: UWB spectrum mask for indoor communication systems.

Similar decisions have been taken or are under process by regulation bodies in other countries. Japan regulation authority (MIC) for instance issued a regulation that is close to the European one.

## 1.4   Standardization

### 1.4.1   IEEE 802.15.3a

The standardizations activity of wireless personal area networks (WPANs) takes place in the IEEE international standards working group 802.15. In late 2001, the IEEE established the 802.15.3a study group to define a new physical layer concept for short range high data rate WPAN applications. This was to serve the requirements of companies wishing to deploy very high data rate applications, such as video transmission, with data rates greater than 110 Mb/s at a distance of 10 m. The technical requirements, including high data rate, short range, system scalability, low cost and low power, led to the adoption of UWB technology by the standardization group.

The IEEE 802.15.3a task group considered two primary waveform approaches. The first approach is based on a multiband orthogonal frequency-division multiplexing (MB-OFDM) technique supported by the Multiband OFDM Alliance (MBOA) and the WiMedia forum, which merged in March 2005 and are today known as the WiMedia Alliance [19].

WiMedia board members include Alereon, HP, Intel, Kodak, Microsoft, Nokia, Philips, Samsung Electronics, Sony, STMicroelectronics, Staccato Communications, Texas Instruments and Wisair. The second approach considers an impulse radio spread spectrum technique (IR-UWB) supported by the UWB Forum (mainly, XtremeSpectrum and Motorola). The IEEE 802.15.3a was trying to reach a consensus between these two leading industry groups for more than three years without success, until January 2006 when the task group was withdrawn. More information on the standard efforts of IEEE 802.15.3a can be found in [20].

However, many forums are still engaged in international standardization efforts for high data rate UWB WPAN applications, including the European Computer Manufacturers Association (ECMA). For instance, shared members of WiMedia Alliance and ECMA submitted new WiMedia UWB platform specifications to ECMA in early 2005. These specifications led ECMA International to release two international ISO-based standards, ECMA-368 [21] and ECMA-369 [22], for high data rate UWB applications in December 2005.

### 1.4.2 IEEE 802.15.4a

In March 2004, the IEEE established the 802.15.4a to define a new physical layer for low data rate WPAN applications [23]. The primary interest in developing this alternate physical layer is to provide communications and high-precision ranging and location capability, ultra low power, and very low complexity systems. Potential applications are sensors, interactive toys, smart badges, remote controls, and home automation. In March 2005, two optional physical layers consisting of an UWB impulse radio and a chirp spread spectrum (C-SS) were selected.

### 1.4.3 Other standards

UWB technology is also a serious candidate for many other standardization groups, like IEEE 802.15.3c [24] for example, which is developing a millimeter-wave-based alternative physical layer for WPAN applications with over 2 Gb/s data rate, such as high speed internet access, streaming content download (video on demand, HDTV, etc.).

Another communication protocol using the UWB technology is the wireless universal serial bus (WUSB). Wireless USB is based on WiMedia Alliance UWB common radio platform which is capable of sending 480 Mb/s at distances up to 3 meters. In addition, the next generation of Bluetooth (Bluetooth 3.0) is also planning to adopt an UWB radio based on WiMedia Alliance platform.

## 1.5   Main applications

As with many wireless communication technologies, the military has been the major driving force behind the development of UWB. In particular, UWB radar applications have been developed by the U.S. military for many years. Using the location and communications characteristics of UWB, one very interesting military application is the asset location system developed by Multispectral Solutions and the U.S. Navy [25].

Since the UWB spectrum allocation in 2002, UWB has become a serious candidate for a huge number of wireless applications. Due to its very wide bandwidth, UWB can be efficiently used for radar imaging systems, including ground penetration radars, wall radar imaging, surveillance systems, and medical imaging [26]. The excellent time resolution and accurate ranging capability of UWB can be used for vehicular radar systems for collision avoidance for example.

One of the most promising commercial application areas for UWB technology is the WPAN environment. This is due to the UWB performance, particularly in terms of data rate, which exceeds the performance of all the current wireless local area network (WLAN) and WPAN standards. Many manufacturers and research projects, including the ICT FP7 European project OMEGA [1], are actually investigating UWB as the primary wireless means to connect devices, such as televisions, DVD players, camcorders, and audio sys-



Figure 1.3: An example of a home networking setup using UWB technology.

tems, together to remove some of the wiring clutter inside the house. Figure 1.3 presents an example of home devices that can be wirelessly connected together using UWB technology. Besides, UWB WPAN applications can be divided into high data rate and low data rate applications. High data rate mode is particularly important when we consider high-definition televisions or rapid file sharing and video downloading applications, whereas low data rate mode is used for home network systems not so demanding in terms of speed, such as a wireless mouse for instance.

## 1.6 Modulation techniques

UWB systems have historically been based on impulse radio concepts. However, since the FCC decision, different modulation techniques have been proposed for UWB applications. In this section, we describe the two main modulation techniques considered by the IEEE 802.15.3a study group for high data rate WPAN applications: the IR-UWB and the MB-OFDM techniques.

### 1.6.1 Impulse radio

The impulse radio scheme is based on the generation of a series of very short duration pulses so-called monocycles (of the order of hundreds of picoseconds). Each pulse has a very wide spectrum that must adhere to the spectral mask requirements. This type of transmission does not require the use of additional carrier modulation since the pulse propagates very well in the channel. A pioneering contribution in this field is the time hopping pulse position modulation (TH-PPM) proposed in 1993 by Scholtz [27]. Note that the main impulse radio approach considers a single frequency band for UWB signals, contrarily to the MB-OFDM technique, which divides the UWB spectrum into several sub-bands as will be detailed later on.

One transmitted symbol is spread over many monocycles to achieve a processing gain used to combat noise and interference. Commonly used pulse shapes are the derivatives of Gaussian functions. The first-order Gaussian monocycle can be expressed as

$$w(t) = \frac{A}{\sigma}\left(c - \frac{t}{\sigma}\right)e^{-0.5\left(\frac{t}{\sigma}-c\right)^2} , \qquad (1.3)$$

where $A$ is an amplitude normalization constant, $\sigma$ related to the pulse width, and $c$ a time-shifting term. A typical example of a Gaussian monocycle in the time and frequency domains is presented in Figure 1.4, with $2\pi\sigma = 1\,\text{ns}$. It can be seen from Figure 1.4 (b) that the Gaussian pulse spreads its power over a wide range of frequencies, and it has virtually

(a) Time domain           (b) Frequency domain
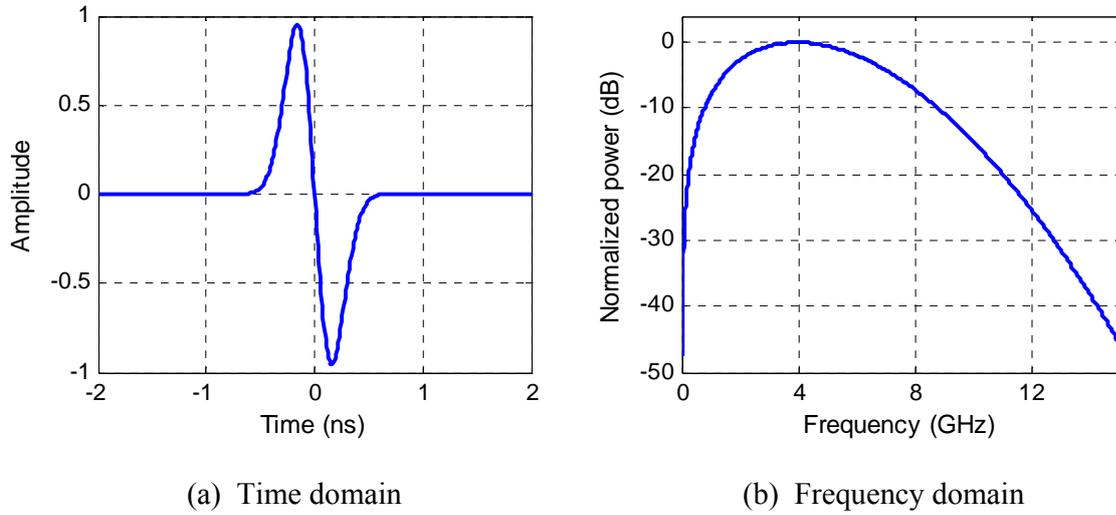
Figure 1.4: First-order Gaussian monocycle.

no DC and low-frequency components, which makes it suitable for UWB communications [28].

### 1.6.1.1    Data modulation techniques

A number of modulation techniques, classified as time-based or shape-based, may be used with the UWB impulse radio systems. The most commonly used modulations are described below.

**Pulse amplitude modulation**

The pulse amplitude modulation (PAM) is a technique where the amplitude of the pulse varies to carry digital information. The classic binary PAM can be implemented using two antipodal Gaussian pulses. The transmitted binary baseband PAM signal is presented as

$$s(t) = d_j \, w(t), \tag{1.4}$$

where $w(t)$ is the UWB pulse waveform, $j$ the transmitted bit ("0" or "1"), and $d_j$ an integer number given by

$$d_j = \begin{cases} -1, & j = 0, \\ +1, & j = 1. \end{cases} \tag{1.5}$$

The commonly used transmitted pulse is the first derivative of the Gaussian pulse given in (1.3).

## On-off keying

The on-off keying (OOK) is a modulation scheme where the presence or absence of a pulse means that the transmitted digital information is "1" or "0", respectively. The transmitted signal is defined as in (1.4), with

$$d_j = \begin{cases} 0, & j = 0, \\ 1, & j = 1. \end{cases} \tag{1.6}$$

Thus, the difference between OOK and PAM is that nothing is transmitted in OOK when a "0" bit arrives.

## Pulse position modulation

PPM is the most common modulation scheme in the literature. With this modulation, each pulse is delayed or sent in advance by a certain value $\delta$ of a regular time scale. The signal can be presented as

$$s(t) = w(t - \delta d_j), \tag{1.7}$$

where $d_j$ is given by (1.6), and $\delta$ may be chosen according to the autocorrelation characteristics of the pulse [29].

## Pulse shape modulation

Pulse shape modulation (PSM) is an alternative to PAM and PPM for UWB impulse radio systems, where different pulse shapes are used to represent different information bits. Many pulse sets have been proposed in the literature for PSM systems, such as modified hermite polynomial functions (MHPF) [30] and wavelets [31], and all exhibit orthogonal properties.

### 1.6.1.2   Multiple access schemes

In order to reduce interference from UWB transmissions, a randomizing technique is applied to the transmitted signal, which makes the UWB transmission spectrum more noise-like. The two main approaches that randomize the pulse train and provide multiple access schemes for impulse radio systems are the time-hopping (TH) and direct-sequence (DS) techniques.

## Time-hopping UWB

In the TH technique, the position of each impulse is defined by a pseudorandom code. When the pseudorandom code is used within a large time frame, the spectrums of the

transmitted pulses become much more noise-like. In addition, the pseudorandom TH scheme minimizes collisions between users in multiple access systems, where each user has a distinct pulse shift pattern [32]. Besides, this scheme can be considered as a time-hopping spread spectrum (TH-SS) technique, since a processing gain can be achieved by increasing the number of pulses used to carry a single data bit.

The TH technique can be combined with PAM, PPM and PSM. However, OOK can not take advantage of the TH because of the blank transmission of bit "0". The transmitted signal for user $m$ can be analytically expressed for PAM modulation as [33]

$$s^{(m)}(t) = \sum_{j} \sum_{n=1}^{N} w\left(t - jT_s - nT_f - c_n^{(m)}T_c\right) d_j^{(m)} , \qquad (1.8)$$

and for PPM modulation as

$$s^{(m)}(t) = \sum_{j} \sum_{n=1}^{N} w\left(t - jT_s - nT_f - c_n^{(m)}T_c - \delta d_j^{(m)}\right), \qquad (1.9)$$

where $j$ is the bit index, $N$ the number of transmitted impulses per data bit and $T_s$ the total symbol duration. $T_s$ is divided into $N$ frames of duration $T_f$, thus $T_s = NT_f$, and each frame is also divided into slots of duration $T_c$. Each impulse is transmitted in one of the $N$ frames, and its position inside the frame is determined by the pseudorandom code sequence $c_n^{(m)}$ that can have the values $\{-1, +1\}$.

### Direct-sequence UWB

In the DS technique, each user is assigned a pseudorandom sequence which controls pseudorandom inversions of the UWB pulse train. A bit is then used to modulate this sequence of pulses. The DS technique can be combined with PAM, OOK and PSM schemes, but not with PPM which is intrinsically a TH technique. The transmitted signal for user $m$ using PAM or OOK is given by

$$s^{(m)}(t) = \sum_{j} \sum_{n=1}^{N} w\left(t - jT_s - nT_c\right) c_n^{(m)} d_j^{(m)} , \qquad (1.10)$$

where $T_c$ is the UWB pulse length and $T_s$ the total symbol duration given by $T_s = NT_c$.

The DS-UWB system uses a RAKE receiver that benefits from multipath to improve the reception. However, the complexity of the system increases linearly with the number of RAKE fingers and the receiver sampling rate. For instance, a $m$-RAKE receiver requires $m$ complex multiply operations for every chip processed.

## 1.6.2 Multiband OFDM

### 1.6.2.1 Multiband technique

Many companies have proposed a multiband technique for UWB applications in order to solve common problems encountered when working on a single-band impulse radio technology. These problems include [20]

- Inflexible spectrum mask because the occupied spectrum can not be easily altered since it is dictated in large part by the pulse-shaping filter.
- Implementation difficulties and active circuits design giving rise to increased cost and power consumption.
- High sample rates in digital-to-analog (DAC) and analog-to-digital (ADC) converters.
- Vulnerability to strong interferers.
- Single-band UWB not well suited to low cost RF-CMOS implementations.

A multiband UWB signaling can be seen as a simple division of a single UWB signal into multiple sub-bands in the frequency domain. These sub-bands may be transmitted in parallel or sequentially and may be received by separate receive paths or one single receiver. Multiband schemes can be classified between two main approaches: pulsed multiband and multiband OFDM.

### 1.6.2.2 Pulsed multiband

A pulsed multiband approach dividing the UWB spectrum into several bands of around 500 MHz bandwidth was proposed in the literature. Pulsed transmissions use a constant pulse shape to obtain the frequency-domain properties for each sub-band. The information is modulated using PPM or binary phase-shift keying (BPSK) and transmitted on each band using narrow time-domain pulses, on the order of 2 to 4 ns [34]. Receiver detection schemes applicable to single-band UWB pulses can also be used.

### 1.6.2.3 Multiband OFDM approach

Multiband OFDM (MB-OFDM) is the main approach considered by UWB standardization committees. It was first proposed by Anuj Batra *et al.* from Texas Instruments for the IEEE 802.15.3a task group [35], [36]. This approach is based on the combination of an OFDM modulation with a multiband technique that divides the UWB spectrum into multiple sub-bands. The OFDM modulation can be separately applied in each sub-band, and consequently a further frequency division of each sub-band into a further parallel multiband
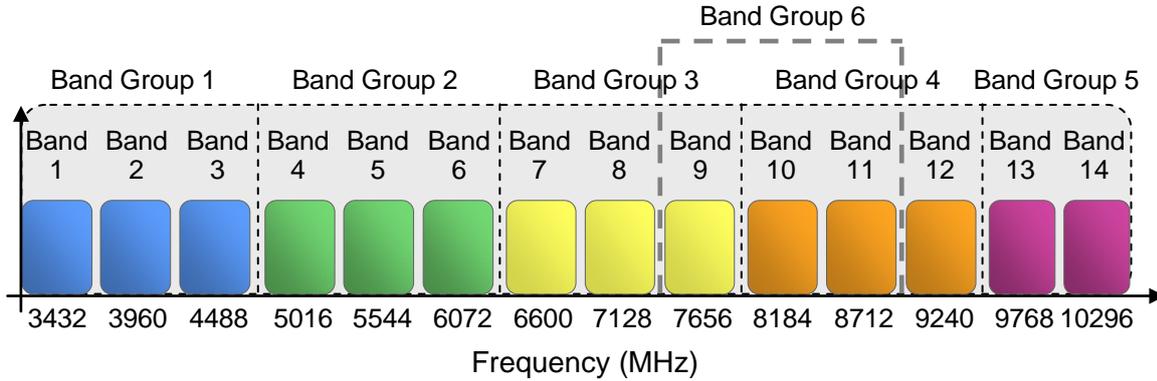
Figure 1.5: UWB spectrum bands in the MB-OFDM system.

scheme is obtained, which provides a much finer degree of granularity in the frequency domain.

The multiband technique proposed in the WiMedia Alliance MB-OFDM scheme divides the UWB spectrum into 14 bands of 528 MHz each, as illustrated in Figure 1.5. The first 12 bands are then grouped into four band groups consisting of three bands each. The last two bands are grouped into a fifth band group. In addition, in the ECMA-368 specification [21], a sixth band group is also defined within the spectrum of the first four, consistent with usage within worldwide regulatory regulations. Initially, most of the studies in the literature have been performed on the first band group from 3.1 to 4.8 GHz.

Since this thesis is mainly focused on the MB-OFDM approach, the description and performance evaluation of the MB-OFDM system will be detailed in Chapter 2.

### 1.6.3   Impulse radio and MB-OFDM comparison

One of the main advantages of single-band impulse radio modulations is that the transmitted signal can be easily generated in the analog domain using analog circuits. However, the analog circuits and mixed-signal circuits, such as the ADCs, in the receiver are difficult to design when the signal bandwidth is very large. In addition, these circuits will likely consume a large amount of current in order to process the signal at a high data rate and maintain a sufficiently low noise figure. Moreover, a large number of RAKE fingers are required in order to capture sufficient energy in a dense multipath environment, which significantly increases the digital baseband complexity [20].

The pulsed multiband approach solves the single-band impulse radio problems related to the very large occupied bandwidth, since it uses sub-bands of approximately 500 MHz bandwidth. Consequently, the information is processed over a much smaller bandwidth,

reducing the design complexity and power consumption, and improving spectral flexibility. However, the main disadvantage of this approach is that it is difficult to collect significant multipath energy using a single RF chain. The multipath energy collection can be improved by adding several RF chains, but this will increase power consumption and devices cost. Another disadvantage of the pulsed multiband system is that when employing a small number of RAKE fingers, its performance is very sensitive to group delay variations introduced by the analog front-end components [20].

On the other hand, the MB-OFDM approach benefits from the same multiband advantages as the pulsed multiband approach, as well as from the well-known OFDM advantages. For instance, the MB-OFDM system is able to capture multipath energy efficiently with a single RF chain. In addition, it offers relaxed frequency-switching time requirements and increases the spectral flexibility. One particularly important issue for UWB systems is to minimize interference with other existing services. The MB-OFDM system is well suited for interference avoidance, since the OFDM subcarriers can be precisely chosen to reduce interference to and from narrowband systems, without having to sacrifice a whole band. In addition, MB-OFDM technology was designed specifically to be built in low cost CMOS processes [20], which makes it easier to integrate into a single-chip solution. One of the few drawbacks of MB-OFDM is that the transmitter is slightly more complex because it requires inverse discrete Fourier transform (IDFT), and the peak-to-average power ratio (PAPR) may be slightly higher than that of the pulse-based multiband system.

These numerous advantages of the MB-OFDM system over the impulse radio system made us choose the MB-OFDM system as the starting point of this thesis studies. Note also that these advantages led to the adoption of the MB-OFDM technique in different international standards and applications, e.g. ECMA WiMedia, Wireless USB, and Bluetooth.

## 1.7 UWB indoor channel model

With the fast evolution of UWB technology, understanding the UWB channel has become very important for designing, testing and comparing different UWB systems. Thus, an accurate channel model is required to design efficient modulation and coding schemes, and to develop associated signal processing algorithms. Since the late 1990s, a number of propagation studies for UWB signals have been carried out and led to some notable publications by Cassioli, Win, Molisch, Scholtz, and Foerster [37]–[42]. However, UWB channel models are still far less comprehensive than narrowband models since more than thirty years of studies have been spent on narrowband wireless channels. Besides, narrowband models can not be easily generalized to UWB channels due to some basic differences in the propa-

Table 1.1: Multipath channel characteristics.

|                          | CM1  | CM2   | CM3   | CM4  |
|--------------------------|------|-------|-------|------|
| Mean excess delay (ns)   | 5.05 | 10.38 | 14.18 | —    |
| Delay spread (ns)        | 5.28 | 8.03  | 14.28 | 25   |
| Distance (m)             | < 4  | < 4   | 4–10  | 10   |
| LOS/NLOS                 | LOS  | NLOS  | NLOS  | NLOS |

gation process and resulting models. In fact, in UWB channels, each multipath component can lead to delay dispersion, due to the frequency-selective nature of reflection and diffraction coefficients [33]. In addition, the UWB signals are received with excellent delay resolution. Therefore, only a few multipath components can often make up one resolvable multipath component whose amplitude statistics is not complex Gaussian anymore. Particularly, due to the very fine resolution of UWB waveforms, different objects or walls in a room could contribute to different clusters of multipath components.

In early 2003, the IEEE 802.15.3a committee adopted a new UWB channel model for the evaluation of UWB physical layer proposals [43]. This model is based on the well-known Saleh-Valenzuela (SV) model for indoor channels [44], but with modified fading statistics to fit the properties of measured UWB channels.

The impulse response of the multipath model is described as

$$h_i(t) = G_i \sum_{z=0}^{Z_i} \sum_{p=0}^{P_i} \alpha_i(z, p) \delta\left(t - T_i(z) - \tau_i(z, p)\right), \tag{1.11}$$

where $G_i$ is the log-normal shadowing of channel realization $i$, $T_i(z)$ the delay of cluster $z$, $\alpha_i(z, p)$ and $\tau_i(z, p)$ represent the gain and the delay of multipath $p$ within cluster $z$, respectively. Independent fading is assumed for each cluster and each ray within the cluster. The cluster and path arrival times can be modeled as Poisson random variables. The path amplitude follows a log-normal distribution, whereas the path phase is a uniform random variable over $[0, 2\pi]$.

The IEEE 802.15.3a also defined four different channel models (CM1 to CM4) for the UWB system modeling, each with arrival rates and decay factors chosen to match different usage scenarios and to fit line-of-sight (LOS) and non-line-of-sight (NLOS) cases. The main characteristics of the proposed channel models are listed in Table 1.1, and typical realizations of the UWB channel in the time and frequency domains are presented in

Figure 1.6. The frequency diversity of model CM4 is clearly much higher than the frequency diversity of model CM1.

## 1.8  Conclusion

In this first chapter, we have presented a general overview on UWB technology which makes the reader familiar with the UWB environment. In brief, UWB has emerged as an exciting technology for wireless communications since 2002 when the FCC allocated a 7.5 GHz spectrum for unlicensed use of UWB devices. As described in Section 1.5, UWB holds enormous potential for wireless applications, which can be divided into high data rate and low data rate communications. This thesis focuses on the very high data rate WPAN applications. Besides, we have seen that there are two main modulation schemes considered for WPAN environment: the MB-OFDM and IR-UWB techniques. Since MB-OFDM seems to be the most promising candidate for high data rate WPAN applications, due to its numerous advantages over IR-UWB and its wide support by the standardization and industrial groups, this thesis will focus on the MB-OFDM approach. Different modifications will be proposed in the following chapters to improve the performance of the MB-OFDM system. On the other hand, the primary regulations and PSD constraints that will be taken into account are the ones imposed by the FCC, but some simulation results considering the European regulations will also be presented. Finally, the channel model that will be used for the single-input single-output (SISO) UWB applications is the one adopted by the IEEE 802.15.3a committee.
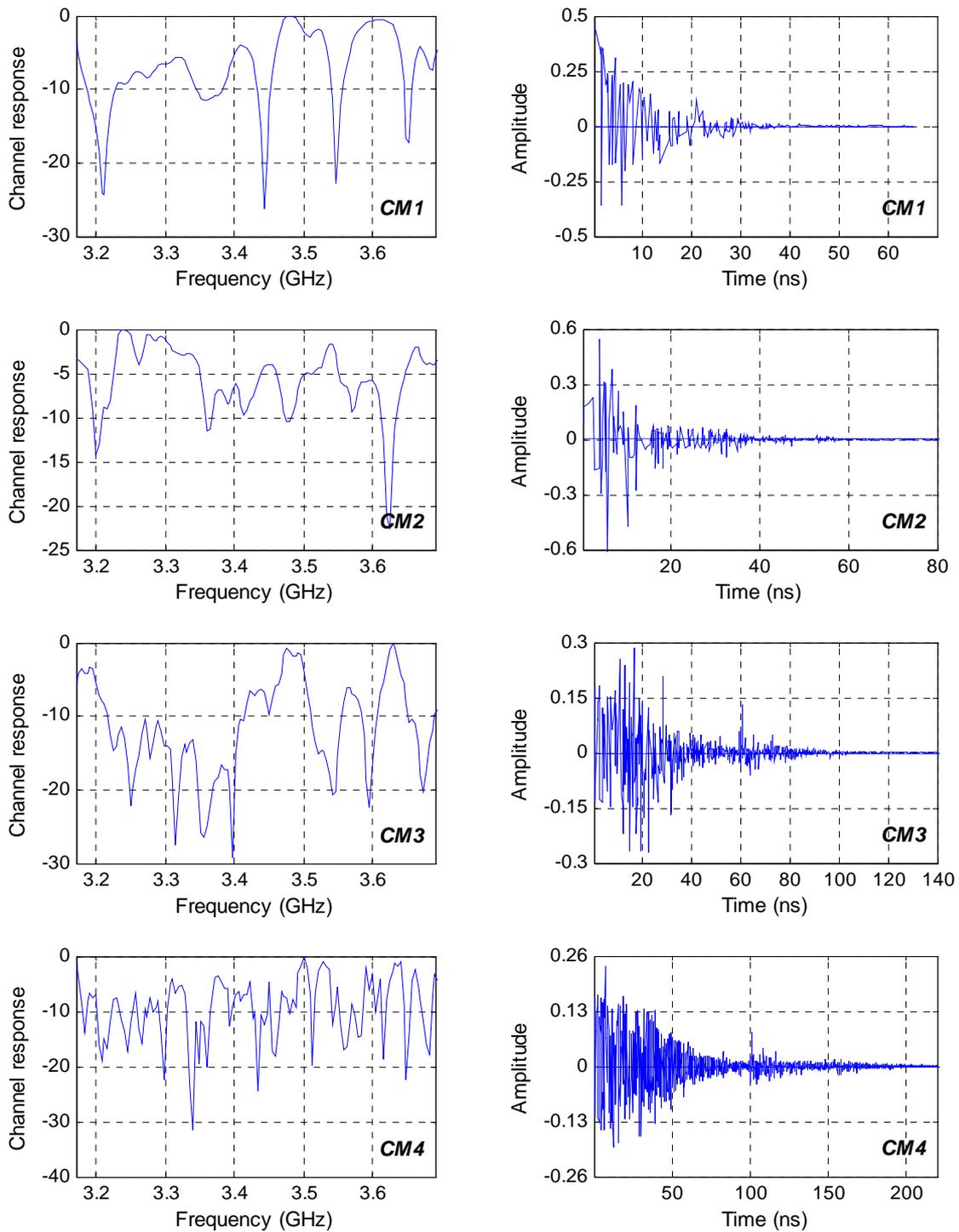
Figure 1.6: An example of UWB channel realizations for models CM1, CM2, CM3 and CM4, on the first MB-OFDM band, in the time and frequency domains.

# Chapter 2

# System specifications

T HE second chapter presents the main transmission techniques exploited in this thesis. First, the principle of multicarrier modulations, and particularly the concept of OFDM, is detailed. Then, the spread spectrum technique is described followed by a presentation of the main modulation schemes resulting from the combination of spread spectrum techniques with OFDM modulation.

The second part of this chapter is dedicated to the description of the MB-OFDM system which can be considered as the starting point of our studies. The MB-OFDM system performance with UWB channels is presented, followed by a discussion of the advantages and drawbacks of this approach. Afterwards, a new scheme based on the addition of a spread spectrum technique, or equivalently linear precoding principles, to the OFDM modulation of the MB-OFDM approach is proposed and the main advantages and motivations that led to this system choice are presented. This proposed system, which can be seen as an evolution of the MB-OFDM approach, will be referred to as linear precoded OFDM (LP-OFDM) system in the sequel.

## 2.1 Transmission techniques

### 2.1.1 Multicarrier modulations

#### 2.1.1.1 Principle

The multicarrier modulation is a concept that helps in reducing the detrimental effects of multi-path fading in communication systems. It was proposed for the first time by Doelz *et al.* for the U.S. military HF communication applications in the late 1950s [45]. Today, the multicarrier modulation is of increasing interest since it can now be implemented using powerful integrated circuits optimized for performing discrete Fourier transforms (DFT). Because of its increasingly widespread acceptance as the modulation scheme of wireless

networks of the future, it attracts a lot of research attention, in areas like time-domain equalization, PAPR reduction, phase noise mitigation and pulse shaping.

The delay spread of a multipath channel, like the UWB indoor channel for instance, can cause inter-symbol interference (ISI) when adjacent data symbols overlap and interfere with each other due to different delays on different propagation paths. The number of interfering symbols in a single-carrier modulated system is expressed as

$$N_{ISI}^{'} = \left\lceil \frac{\tau_{\max}}{T_d} \right\rceil, \tag{2.1}$$

where $\lceil . \rceil$ is the ceiling function which returns the smallest integer value bigger than or equal to its argument value, $\tau_{\max}$ the maximum delay spread of the channel and $T_d$ the symbol duration. From (2.1), we notice that for high data applications with very short symbol duration ($T_d < \tau_{\max}$), the effect of ISI increases. Consequently a higher complexity receiver is required. Thus, a compromise between the ISI effect and the system data rate that depends on the symbol duration value has to be achieved.

The principle of multicarrier modulation is to convert a serial high-rate data stream into multiple low-rate sub-streams which are then modulated on different frequency sub-channels, called subcarriers. If we consider $N$ serial data symbols with a symbol duration $T_d$, these symbols will be simultaneously transmitted on $N$ different subcarriers, with a new symbol duration $T_s = N T_d$, but with a same total data rate as with single-carrier modulation. Hence, the duration of the transmitted symbol is multiplied by a factor of $N$ which reduces the ISI, and consequently the number of interfering symbols in a multicarrier modulated system becomes

$$N_{ISI}^{''} = \left\lceil \frac{\tau_{\max}}{N T_d} \right\rceil. \tag{2.2}$$

Increasing the number $N$ of subcarriers reduces not only ISI, but also the signal distortions introduced by the channel since each subcarrier becomes very narrow and can be considered as flat.

However, this ISI reduction is subject to a second kind of interference: the inter-carrier interference (ICI). The first frequency-division multiplexing (FDM) systems proposed to reduce overlapping between subcarriers by increasing the frequency spacing $\Delta_f$ between them. However, this ICI minimization approach is not interesting in terms of spectral efficiency. In fact, a spectral band two times larger than the one of a single-carrier system is often required. A smarter approach for FDM consists in overlapping the subcarriers while

respecting orthogonal conditions in time and frequency, which optimizes the spectral efficiency. This combination of orthogonality concepts with FDM techniques gave rise in the 1960s to the first orthogonal frequency-division multiplexing (OFDM) system [46].

The orthogonality properties of OFDM symbols are related to the used pulse shaping functions. From the several functions proposed in the literature [47], the rectangular function is the most widely used. This function corresponds to a rectangular window over the symbols, with a duration $T_s$, equivalent to the duration of one OFDM symbol. In the frequency domain, it generates a sinc (sinus cardinal) function for each subcarrier of the generated signal. In order to achieve frequency orthogonality between the signals on the $N$ subcarriers, a minimum spacing between each two adjacent subcarriers is required. Presuming rectangular pulse shaping, the minimum subcarriers spacing is given by

$$\Delta_f = \frac{1}{T_s}.$$ 
(2.3)

Figure 2.1 represents an OFDM signal in the time and frequency domains. In the time domain, the OFDM signal can be seen as a superposition of different sinusoidal functions with a period equal to the inverse of the corresponding subcarrier frequency. In the frequency domain, the OFDM signal is represented by adjacent sinc functions separated by $\Delta_f$. Note that for large values of $N$, the OFDM spectrum becomes flatter in the occupied frequency band.



(a) Time domain          (b) Frequency domain
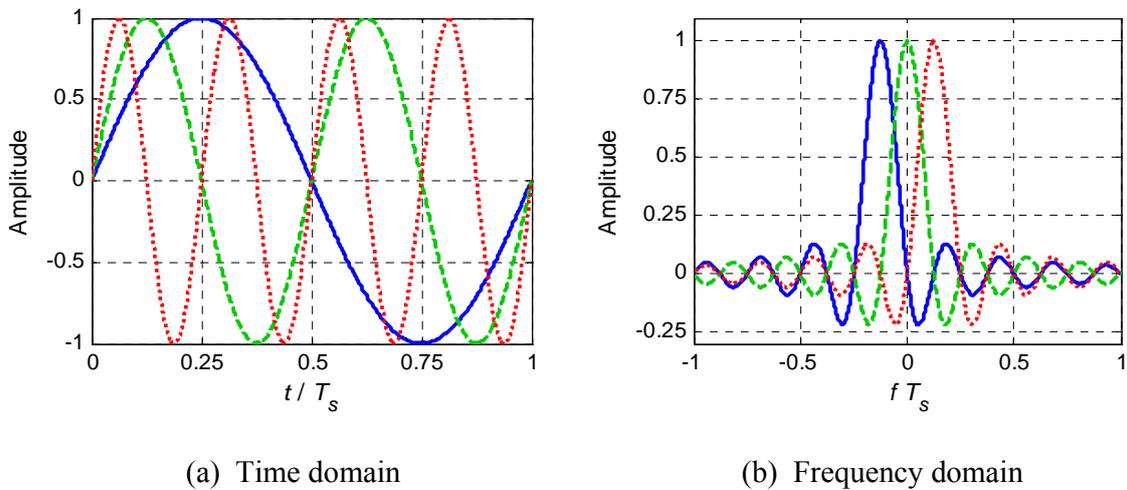
Figure 2.1: Example of three subcarriers within an OFDM symbol.

### 2.1.1.2 Guard interval and guard subcarriers

As described previously, the ISI effects can be considerably reduced by increasing the duration $T_s$ of the OFDM symbols, and consequently by increasing the number $N$ of subcarriers. However, $T_s$ can not be indefinitely extended due to the limitations imposed by the coherence time of the channel. To completely avoid the effects of ISI, a guard interval (GI) has to be inserted between adjacent OFDM symbols.

The guard interval is a cyclic extension of each OFDM symbol which is obtained by extending the duration of the symbol to

$$T_s' = T_g + T_s,\qquad(2.4)$$

where $T_g$ is the duration of the GI, such that $T_g \geq \tau_{\max}$. Note that the spacing between subcarriers is still equal to $1/T_s$, which leads to a loss of orthogonality between subcarriers at the transmitter, and thus to an ICI increase. However, this can be restored at the receiver if during the rectangular window on which the fast Fourier transform (FFT) is applied, each of the sinusoidal signals constituting the OFDM symbol includes an integer number of periods. This integer number of periods is usually obtained by making the GI a repeat of the symbol end. One disadvantage of this method is that it leads to a loss in spectral efficiency equivalent to $T_s / (T_s + T_g)$.

On the other hand, since the rectangular function generates a sinc function for each subcarrier, the OFDM signal spectrum has an infinite band even if there is a strong amplitude reduction on the borders of the band. Thus, a filter is often needed to limit the spectral occupation, which introduces a distortion on the subcarriers present on the borders. One solution consists in transmitting no information data on a certain number of subcarriers at both extremities of the spectrum. These reserved subcarriers are so-called guard subcarriers. Note that here also a loss in spectral efficiency has to be taken into account.

### 2.1.1.3 OFDM signal

The OFDM symbol is composed of $N$ subcarriers having a frequency $f_n = f_0 + n\Delta_f$, with $n = 0,\ldots,N-1$ and $f_0$ the first subcarrier frequency, used for the parallel transmission of $N$ symbols, noted $x_n$. Symbols $x_n$ are complex elements whose values depend on the type of the used constellation. By applying a rectangular function $\Pi(t)$ and without taking the GI into account, the normalized expression of the OFDM signal generated over $[0:T_s[$ can be expressed as

$$s(t) = \frac{1}{\sqrt{N}} \sum_{n=0}^{N-1} \mathrm{Re}\left\{ x_n \, \Pi(t) \, e^{j2\pi\left(f_0 + \frac{n}{T_s}\right)t} \right\}.\qquad(2.5)$$

Let $f_c = f_0 + N / 2T_s$ represent the center frequency of the signal, thus the signal during the useful part of the OFDM symbol becomes

$$s(t) = \text{Re}\left\{ \Pi(t)\, e^{j2\pi f_c t} \sum_{n=0}^{N-1} \frac{x_n}{\sqrt{N}}\, e^{j2\pi\left(n-\frac{N}{2}\right)\frac{t}{T_s}} \right\}, \tag{2.6}$$

which can also be written as

$$s(t) = \text{Re}\left\{ \tilde{s}(t)\, \Pi(t)\, e^{j2\pi f_c t} \right\}, \tag{2.7}$$

where $\tilde{s}(t)$ is the complex envelope of the signal $s(t)$ before rectangular windowing, having a spectrum interval of $[-N / 2T_s : N / 2T_s]$. $\tilde{s}(t)$ can then be sampled at a frequency $f_s = N / T_s$ and the resulting samples at the moments $mT_s / N$ are given by

$$\tilde{s}[m] = \sum_{n=0}^{N-1} \frac{x_n}{\sqrt{N}}\, e^{j2\pi\left(n-\frac{N}{2}\right)\frac{m}{N}}$$

$$= (-1)^m \sum_{n=0}^{N-1} \frac{x_n}{\sqrt{N}}\, e^{j2\pi\frac{nm}{N}}. \tag{2.8}$$

This result shows that the signal can be easily generated using an IDFT. Similarly, a DFT can be applied at the receiver to retrieve the transmitted symbols. Note that direct and inverse fast Fourier transforms (FFT and IFFT, respectively) provide an efficient implementation of the DFT. Also note that multiplying by $(-1)^m$ in (2.8) yields to a frequency centering around the null frequency in order to obtain a baseband representation of the transmitted signal.

The sampled sequence obtained after the GI addition is passed through a DAC whose output would be the signal waveform $s(t)$ with a duration $T_s'$ given in (2.4). The signal is then up-converted and the RF signal is transmitted through the channel. Afterwards, the received signal waveform $r(t)$ is obtained from the convolution of $s(t)$ with the channel impulse response $h(\tau,t)$ and the addition of a noise signal $n(t)$. $r(t)$ is passed through an ADC, followed by a GI removal. The resulting sequence is then multicarrier demodulated by inverse OFDM exploiting a DFT (or FFT). Finally, assuming that the fading on each subcarrier is flat and that ISI is removed and ICI avoided, the received symbol can be expressed in the frequency domain as

$$y_n = h_n\, x_n + \bar{n}_n, \quad n = 0,\ldots, N-1, \tag{2.9}$$
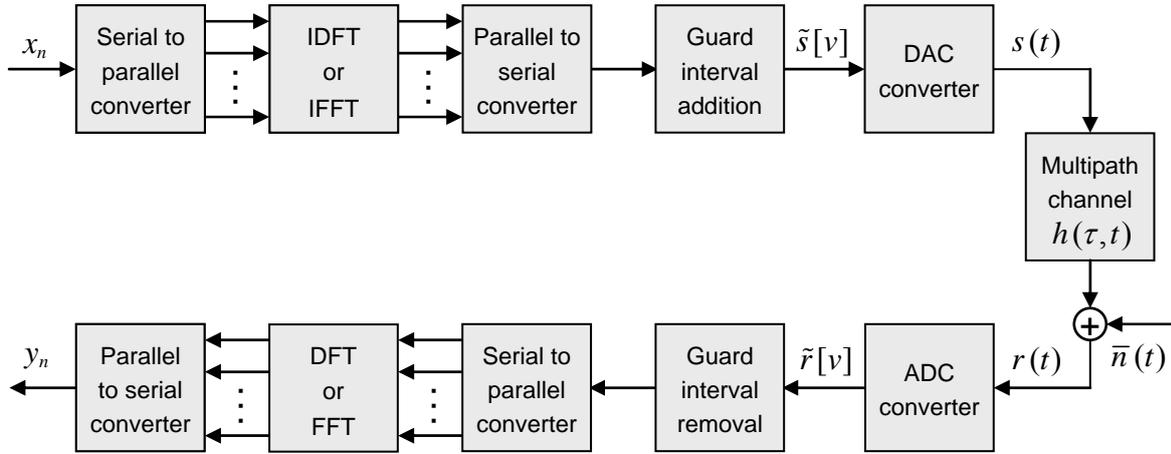
Figure 2.2: OFDM transmission system.

where $h_n$ and $\bar{n}_n$ are the flat fading frequency response and the noise of the $n^{\text{th}}$ subcarrier. Figure 2.2 summarizes the different steps of a digital OFDM transmission.

### 2.1.1.4   Advantages and drawbacks

Today, the OFDM modulation is the primary technology adopted by a large number of standards and products, for wired and wireless communications. These standards and applications include asymmetric digital subscriber line (ADSL), power line communication (PLC), WLAN (IEEE 802.11 a, g, n, HIPERLAN/2), digital audio broadcasting (DAB), digital video broadcasting (DVB-T, DVB-H), beyond 3G mobile communication (3GPP LTE), Wireless MAN (IEEE 802.16, WiMAX), and UWB (WiMedia, ECMA).

This wide interest in OFDM technique is due the numerous advantages that OFDM offers. The main OFDM advantages include

- High spectral efficiency.
- Efficient implementation using FFT.
- Robustness against ISI.
- Robustness against narrowband interference.
- Flexible spectrum adaptation can be realized (notch filtering).
- Different constellations can be applied on individual subcarriers, which allows numerous resource allocation strategies as will be seen in Chapter 3.

However, OFDM suffers from some drawbacks such as

- High PAPR, which requires high linear amplifiers.
- Sensitive to Doppler spread.

- Sensitive to time and frequency synchronization problems.

- Loss in spectral efficiency due to the guard interval insertion.

## 2.1.2 Spread spectrum concepts and combination with multicarrier schemes

### 2.1.2.1 Spread spectrum principle

Spread spectrum (SS) techniques have been implemented since the 1950s when they were first applied for military applications. Originally, the two main motivations for SS adoption were the anti-jamming tactical communications and the low probability of intercept [48]. With the fast evolution of mobile radio communications in the last two decades, spread spectrum techniques have found important commercial applications in cellular networks and wireless personal communication networks. The numerous application fields for spread spectrum techniques include interference rejection, multiple access, multipath reception, diversity reception, high resolution ranging, and accurate universal timing. Today, SS principles are adopted by many communication standards, such as the cellular mobile radio IS-95 standard [49], the 3$^{rd}$ generation universal mobile telecommunications system (UMTS) that adopts a wideband code-division multiple access (W-CDMA) scheme [50], IEEE 802.11, IEEE 802.15.4 (ZigBee), and the GPS systems.

Spread spectrum techniques consist in spreading a transmitted signal over a wide frequency band, much larger than the minimum bandwidth required to transmit the information. Same as with UWB technique, the advantage of spreading the spectrum can be understood by observing the Shannon equation given in (1.2). Hence, to transmit a certain amount $C$ of information without error, we can use either a narrow bandwidth $W$ with a high SNR, or a large bandwidth $W$ with a low SNR, which is the case of spread spectrum systems.

Different techniques based on spread spectrum principles can be implemented. Some examples include the following techniques and combinations of these techniques [51]

- Direct-sequence spread spectrum (DS-SS), which consists in spreading the signal over a continuous bandwidth by mixing it with a continuous string of pseudorandom codes made up of chips, each chips having a much shorter duration than the information bits. Since this technique is used in systems combining multicarrier and SS techniques, it will be detailed in the sequel.

- Frequency-hopping spread spectrum (FH-SS), which is similar to DS-SS where pseudorandom sequences are used to spread the signal. However, instead of spreading the signal over a continuous bandwidth, the signal is hopped over a

number of frequency channels each having the same bandwidth as the transmitted signal. FH-SS signals are highly resistant to narrowband interference and difficult to intercept. One application example is the Bluetooth 1.2 which uses adaptive FH-SS to avoid crowded frequencies.

- Time-hopping spread spectrum (TH-SS), in which the carrier is turned on and off by the pseudorandom code sequence. One application example is the TH-UWB based on an impulse radio modulation (see Section 1.6.1.2).

- Chirp spread spectrum (C-SS), which uses linear frequency modulated chirp pulses to encode information. A chirp signal is a sinusoidal signal whose frequency increases or decreases over a certain amount of time. Contrarily to the previous techniques, C-SS does not add any pseudorandom elements to the signal. One of the two physical layer proposals chosen by the IEEE 802.15.4a for low data rate WPAN application is based on C-SS, the second being the UWB impulse radio.

The DS-SS technique is the most commonly used, in particular for systems combining multicarrier and SS techniques. In DS-SS transmissions, the transmitted data is multiplied by a pseudorandom noise (PN) code or chip whose values are generally in $\{-1, +1\}$. Let $T_d$ represent the data symbol duration and $T_c$ the chip duration. Thus, the bandwidth $B_c = 1/T_c$ of the transmitted DS-SS signal is much larger than the bandwidth $B_d = 1/T_d$ of the message data to transmit. Consequently, the processing gain $P_G$ can be derived from the ratio of these two bandwidths as

$$P_G = \frac{B_c}{B_d} = \frac{T_d}{T_c} = L,$$                                    (2.10)

where $L$ is the length of the PN codes sequence, i.e. the number of used chips per sequence. The PSD of the transmitted signal is thus attenuated by a factor of $P_G$. At the receiver side, the original data can be exactly reconstructed by multiplying it by the same PN sequence. This process, known as "despreading", mathematically constitutes a correlation of the transmitted PN sequence with the PN sequence that the receiver believes the transmitter is using. The despreading works correctly if the transmit and receive sequences are well synchronized. A judicious selection of PN codes with good cross and autocorrelation facilitates the synchronization process [48].

The spread spectrum techniques are widely used in different communication systems and standards due to the numerous advantages they offer. Since the transmitted signal PSD is attenuated by a factor of $P_G$, other communication systems can use the same frequency bands. In addition, these techniques offer a low probability of intercept since the signal can be seen as noise-like by other users, and only users having the correct synchronous PN

sequence can intercept the communication. Moreover, the transmitted signal is robust against narrowband interference because these interfering signals are spread by the de-spreading process at the receiver. Finally, one of the main advantages of spread spectrum techniques is their ability to provide multiple access. In fact, multiple users can transmit simultaneously on the same frequency bands as long as they use different spreading codes.

### 2.1.2.2   Multiple access schemes

In order to efficiently share the available resources between different users in a communication system, several multiple access techniques can be used. The main techniques commonly implemented are frequency-division multiple access (FDMA), time-division multiple access (TDMA) and code-division multiple access (CDMA).

FDMA consists in dividing the spectrum into individual channels that will be allocated to the different users. FDMA technique can be easily implemented since users can be separated at the receiver using a simple filter. However, one disadvantage is the maximum number of users having to share a given band. In fact, increasing the number of users leads to reducing the bandwidth of the individual bands allocated to each user, which should be kept large enough in order to avoid strong signal attenuations.

TDMA allows several users to share the same frequency channel by dividing the signal into different short time slots. The users transmit in rapid succession, one after the other, each using its own time slot. TDMA is generally more difficult to implement than FDMA since it requires perfect synchronization between all transmitters and receivers. Systems adopting TDMA include the $2^{nd}$ generation cellular systems (GSM) and the digital enhanced cordless telecommunications (DECT) systems.

With the CDMA technique, several users are able to transmit data simultaneously over the same frequency band. The users signals are distinguished by different PN codes that have to be known at the receiver. The combination of direct-sequence principle and CDMA technique is referred to as DS-CDMA. A judicious selection of PN codes with good cross and autocorrelation is necessary for DS-CDMA systems. In the case of synchronous communications, optimal performance can be obtained using orthogonal codes, such as orthogonal variable spreading factor (OVSF) codes, Walsh-Hadamard codes [52], and the complementary series of Golay [53]. For asynchronous communications, non-orthogonal codes offering good cross and autocorrelation properties, such as Gold [54], Kasami [55], and Zadoff-Chu codes [56], can be used.

DS-CDMA systems offer several advantages including easy frequency planning, high immunity against interference, and flexible data rate adaptation. However, these systems suffer from many problems in a multi-user context with limited available bandwidth:

- Multiple access interference (MAI), when the number of simultaneously active users increases.

- High receiver complexity with adaptive receiver filter and considerable signaling overhead.

- Single-tone and multitone interference. If the interference suppression by the spreading operation is not sufficient, additional operations such as Notch filtering have to be done at the receiver, which leads to additional receiver complexity.

Note also that accurate power control is an inherent part of any DS-CDMA system. In fact, when multiple users access the same spectrum, it is possible that one user could mask all other users at the receiver side if its power level is too high.

**DS-CDMA signal**

If we want to transmit a number $K$ of data symbols streams simultaneously, we consider $K$ codes spreading sequences $c_k = [c_{1,k} \dots c_{l,k} \dots c_{L,k}]^T$ of length $L$, which constitute the vectors of the spreading codes matrix of size $L \times K$, given by $C = [c_1 \dots c_k \dots c_K]$. The symbol $[.]^T$ denotes the transposition of a vector or a matrix. Let $x = [x_1 \dots x_k \dots x_K]^T$ represent the vector of symbols to transmit, then each symbol $x_k$ from data stream $k$ is multiplied by its specific code $c_k$. The resulting baseband signal $s = [s_1 \dots s_l \dots s_L]^T$ after the spreading process can be expressed as

$$s = \frac{1}{\sqrt{L}} C x \,, \tag{2.11}$$

with

$$s_l = \frac{1}{\sqrt{L}} \sum_{k=1}^{K} c_{l,k} x_k \,. \tag{2.12}$$

Note that the normalization factor $1/\sqrt{L}$ in (2.11) maintains the power of the signal after the spreading process. Note also that (2.11) represents the baseband signal of a general DS-SS system. Besides, when the codes are used to multiplex the data of different users, and consequently when the $K$ data streams correspond to $K$ different users, this equation represents the baseband signal of a DS-CDMA signal.

### 2.1.2.3   Multicarrier spread spectrum systems

The large number of advantages offered by spread spectrum and multicarrier techniques, and their success for the second generation mobile radio and for digital broadcasting and WLAN respectively, motivated many researchers to investigate the combination of these

two techniques. Hence, different schemes combining DS-CDMA and multicarrier modulation were proposed in 1993 [57]–[61]. In the resulting multicarrier spread-spectrum (MC-SS) systems, the spread spectrum technique can be implemented before or after the OFDM scheme.

In this thesis, we consider MC-SS systems with OFDM schemes applied after the spreading function, which can be simply implemented. The resulting signal inherits the characteristics of multicarrier signals, and in particular the OFDM advantages such as the robustness against multipath channels, the low complexity receivers, and the ISI reduction. Contrarily to the OFDM system where the data symbols are simply distributed on the different subcarriers during one OFDM symbol period, the MC-SS system consists in allocating several subcarriers or several symbol periods to chips of CDMA symbols. The idea behind this procedure, also known as chip mapping, is to obtain a diversity gain and consequently improve the system performance by transmitting the same data over a whole code, which provides a time or frequency diversity gain depending on the chip mapping configuration.

Furthermore, the spreading component offers an additional degree of freedom which is the code dimension. In the MC-SS system, the CDMA component allows several users to transmit information simultaneously and over the whole frequency spectrum, which is not possible in OFDM systems without a loss in time or spectrum efficiency. In addition, this code dimension increases the resource allocation flexibility and more optimization strategies than with OFDM systems can be considered, as will be seen in Chapter 3, which improves the MC-SS system performance.

On the other hand, different MC-SS schemes can be obtained depending on how the codes are distributed, and specifically how the multiple access between users and the data multiplexing of each user are implemented. The multiple access can be applied in the time, frequency or code dimension, referred to as TDMA, FDMA and CDMA, respectively. In addition, the data multiplexing of a same user can also be applied in these three dimensions, referred to as TDM, FDM and CDM, respectively. When the spreading is carried out in the frequency direction, the code-division multiplexing is noted as F-CDM or F-CDMA, and when the spreading is carried out in the time direction, it is noted as T-CDM or T-CDMA. Furthermore, the subcarriers can be grouped in several smaller blocks, each of them having a specific multiplexing scheme. In this case, we talk about multiple-block systems, contrarily to the mono-block systems where all the subcarriers are grouped together in one single block.

## A.  Mono-block systems

First, we consider that the spreading code length $L$ is equal to the number $N$ of subcarriers present in the OFDM symbol, and that all the subcarriers are grouped in a single block. The multiple access can be carried out in the three dimensions mentioned previously.

In the code dimension multiple access schemes, the different users are assigned a number of specific codes for each generated CDMA symbol. The frequency and time dimensions can then be used by each user for data multiplexing and chips transmission. Different chip mapping techniques can be implemented. The most common scheme is the one that carries out the spreading in the frequency direction, referred to as F-CDMA. The signal is generated by a serial concatenation of classical DS-CDMA and OFDM. The chips of a spread data symbol are transmitted in parallel on different subcarriers, as represented in



(a)  TDM / F-CDMA (MC-CDMA)          (b)  FDM / T-CDMA (MC-DS-CDMA)

(c)  F-CDM / TDMA                    (d)  T-CDM / FDMA
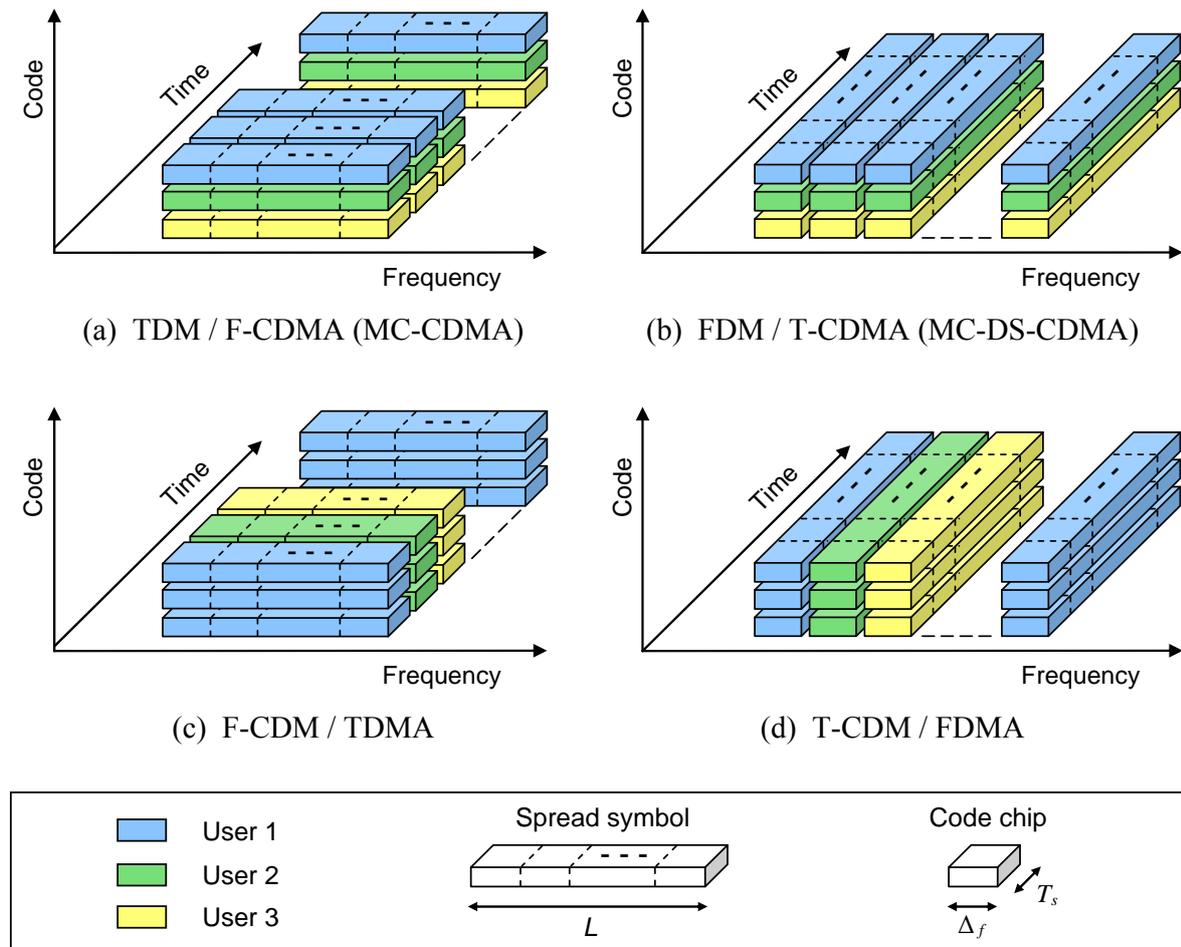
Figure 2.3: Graphical representation of an OFDM frame for different mono-block MC-SS configurations.

Figure 2.3 (a). This technique is also known as multicarrier code-division multiple access (MC-CDMA) in mobile radio communications. The main advantages are the high spectral efficiency, the high frequency diversity due to the spreading in the frequency direction and the low complexity receivers. Thus, MC-CDMA is considered as a good candidate for the downlink of a cellular system [62].

Furthermore, the spreading in these schemes using code dimension multiple access can also be carried out in the time direction, referred to as T-CDMA, as shown in Figure 2.3 (b). This technique is also known as multicarrier direct-sequence code-division multiple access (MC-DS-CDMA) in mobile radio communications, which is presented here as it was in the first publications in the literature, with $L$ equal to the number $N$ of subcarriers. The MC-DS-CDMA signal is generated by a serial-to-parallel conversion of the data symbols into $N$ sub-streams, followed by a DS-CDMA applied on each individual sub-stream. Thus all the chips of one CDMA symbol are transmitted on the same subcarrier but on different OFDM symbols. The main advantage is the high time diversity gain due to the spreading in the time direction and to the small number of subcarriers usually used with these schemes. In the MC-CDMA and MC-DS-CDMA schemes described above, the spreading is carried out in either the frequency or time direction. However, two-dimensional spreading code schemes where the chips are distributed in both the frequency and the time directions can also be implemented [63].

In the time dimension multiple access schemes, each user is allocated a number of OFDM symbols, and during one symbol duration only one user is able to transmit information, as depicted in Figure 2.3 (c). In this case, the chip mapping is only applied in the frequency direction, and the code dimension is used for data multiplexing of the same user. This scheme is referred to as F-CDM / TDMA.

In the frequency dimension multiple access, each user is allocated a number of subcarriers, and on each subcarrier only one user is able to transmit information, as depicted in Figure 2.3 (d). In this case, the chip mapping is only applied in the time direction, and the code dimension is used for data multiplexing of the same user. This scheme is referred to as T-CDM / FDMA.

## B.   Multiple-block systems

In the previous section, the spreading code length $L$ was assumed to be equal to the number $N$ of subcarriers, whereas in general $L$ has not to be necessarily equal to $N$. Besides, in order to better adapt the MC-SS signal to the channel characteristics, different system parameters have to be modified. For instance, reducing the code length $L$ enables a flexible system design and can further reduce the complexity of the receiver. Thus, different multi-

ple-block MC-SS configurations can be obtained by grouping the $N$ subcarriers into $B$ smaller blocks of length $L = N / B$, each of them having a specific multiplexing scheme.

When the multiple access is carried out in the code dimension, the spreading can be performed in the frequency direction, as with the previous versions of the MC-CDMA scheme. However, the data multiplexing of each user is performed in both time and frequency dimensions, as shown in Figure 2.4 (a). Here, we can also speak of MC-CDMA but with $L$ not equal to $N$ anymore. Note that all the users can transmit information simultaneously on all the subcarriers, and the number of multiplexed data per user in the frequency dimension is equal to the number $B$ of blocks. This configuration is referred to as FDM & TDM / F-CDMA. In addition, the spreading can also be performed in the time direction. In this case, we have a multiple-block FDM / T-CDMA scheme.

When the multiple access is in the frequency direction, different configurations can be obtained. One method consists in allocating each block of subcarriers to one user. In addition, when the spreading is in the time direction, we have a T-CDM & FDM / FDMA scheme, and when it is in the frequency direction, we have a F-CDM & TDM / FDMA scheme, represented in Figure 2.4 (b) and Figure 2.4 (c), respectively. The F-CDM & TDM / FDMA scheme is also known as spread spectrum multicarrier multiple access (SS-MC-MA), proposed for the first time by Kaiser and Fazel for mobile radio communications [64]. The SS-MC-MA scheme can be seen as an extension of orthogonal frequency-division multiple access (OFDMA) by a CDM that multiplexes the data symbols belonging to the same user.

In the different MC-SS configurations we have already presented, the spreading is carried out either in the frequency direction or in the time direction, and thus it is known as one-dimensional spreading. Spreading can also exploit both time and frequency diversity using one single MC-SS configuration. This spreading, known as two-dimensional spreading, can be performed by a two-dimensional code or by two cascaded one-dimensional codes. An efficient realization of two-dimensional spreading is to use one-dimensional code followed by a two-dimensional interleaver [62].

As will be explained in Section 2.3, the modulation scheme proposed in this thesis for UWB systems is based on a modified version of the SS-MC-MA scheme, referred to as linear precoded orthogonal frequency-division multiplexing (LP-OFDM). It consists in applying SS-MC-MA principles with a frequency-hopping technique. The main advantages of SS-MC-MA and LP-OFDM that led to this modulation choice for UWB applications will also be detailed in Section 2.3.
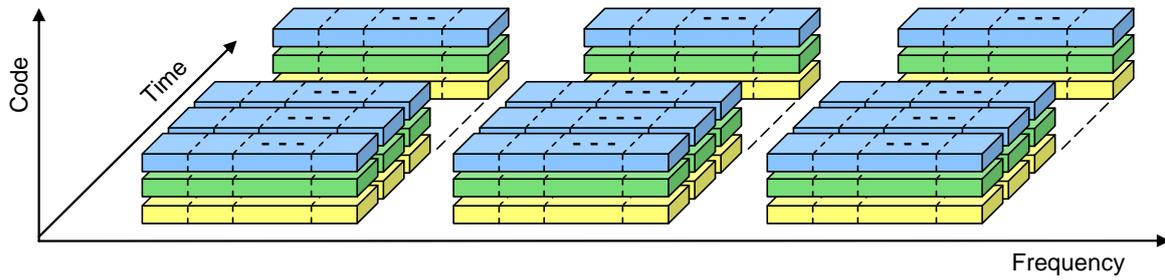
(a) FDM & TDM / F-CDMA
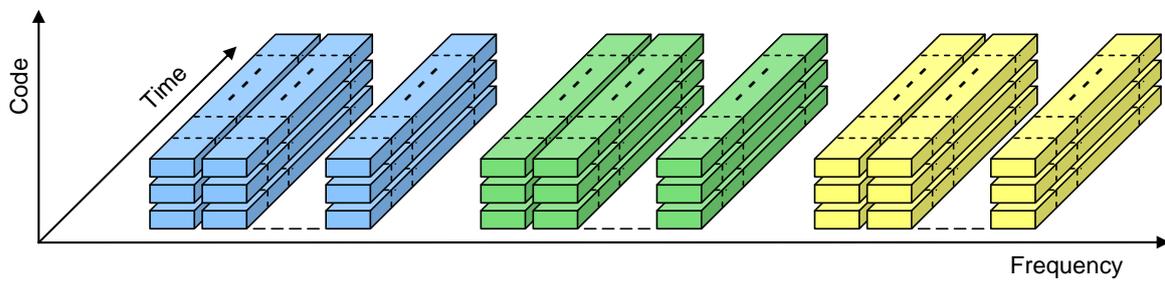
(b) T-CDM & FDM / FDMA
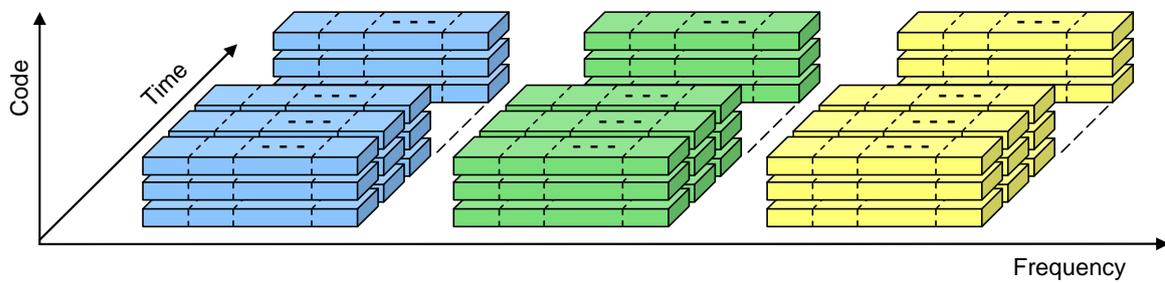
(c) F-CDM & TDM / FDMA (SS-MC-MA)
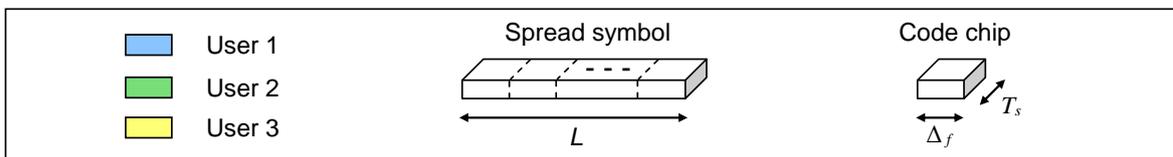
Figure 2.4: Graphical representation of an OFDM frame for different multiple-block MC-SS configurations.

## 2.2 Multiband OFDM

This section provides a description of the Multiband OFDM (MB-OFDM) technique which is the primary candidate for high data rate UWB applications. Proposed for the first time in 2003 by Batra *et al.* for the IEEE 802.15.3a WPAN standardization group [35], this approach is today supported by the WiMedia Alliance and adopted by the ECMA-368 standard [21]. Since this thesis research started in 2005, our studies will be mainly based on the MB-OFDM proposal of September 2004 for the IEEE 802.15.3a task group [65]. Note that some modifications have been made on the physical layer of the MB-OFDM approach by the standardization committees since 2004. These modifications will be mentioned in the sequel.

The MB-OFDM approach consists in dividing the UWB spectrum into 14 bands of 528 MHz each, as depicted in Figure 1.5, and applying an OFDM modulation on each band separately. The bandwidth of these bands was judiciously chosen in order not to increase the complexity of the low-noise amplifiers (LNA), the mixers, as well as the high-speed DACs and ADCs. In addition, limiting the upper frequency of the first three bands to 4.8 GHz has several advantages, including shortening the time to market, simplifying the design of RF and analog front-end circuits, as well as avoiding interference with systems allocating bands falling in the MB-OFDM bands, such as U-NII band in the USA which occupies the bandwidth from 5.15 to 5.85 GHz. Thus, a good choice of operating bands could remove the need to implement complicated notch filters to suppress the interference.

The MB-OFDM system is capable of transmitting information at different data rates varying from 53.3 to 480 Mb/s, listed in Table 2.1. These data rates are obtained through the use of different convolutional coding rates, frequency-domain spreading (FDS) and time-domain spreading (TDS) techniques.

### 2.2.1 Transmitter architecture

The architecture of the MB-OFDM transmitter is shown in Figure 2.5. At the transmitter, the input bit stream is first scrambled to make data more random which eliminates long runs of ones and zeros as well as repetitive patterns. A forward error correction (FEC) code is then applied to provide resilience against transmission errors. The encoded sequence is interleaved in three consecutive stages as will be explained later on, followed by a mapping into frequency bins of an OFDM symbol. An IFFT is used to transform the frequency-domain information into time-domain OFDM symbols, and a zero-padding is added to each symbol. The symbols are then converted via a DAC into continuous time-domain

analog waveforms, up-converted to the appropriate center frequency and ready to be transmitted.

### 2.2.1.1   Channel encoding

The scrambled data stream is encoded with a convolutional code. The convolutional encoder uses the industry-standard rate $\bar{r} = 1/3$ code, with generator polynomials $g_0 = 133_8$, $g_1 = 165_8$ and $g_2 = 171_8$, where $(.)_8$ refers to the octal representation of the polynomial. Additional coding rates are derived from the mother rate $\bar{r} = 1/3$ code by employing a puncturing procedure that omits some of the encoded bits at the transmitter, which reduces the number of transmitted bits and increases the coding rate, and inserts a dummy zero metric into the decoder at the receiver in place of the omitted bits. The proposed coding rates are listed in Table 2.1.

Table 2.1: WiMedia-based MB-OFDM data rates.

| Data rate (Mb/s) | Constellation | Coding rate ($r$) | FDS | TDS | Coded bits / OFDM symbol ($N_{CBPS}$) |
|---|---|---|---|---|---|
| 53.3 | QPSK | 1/3 | Yes | Yes | 100 |
| 80 | QPSK | 1/2 | Yes | Yes | 100 |
| 106.7 [1] | QPSK | 1/3 | No | Yes | 200 |
| 160 | QPSK | 1/2 | No | Yes | 200 |
| 200 | QPSK | 5/8 | No | Yes | 200 |
| 320 | DCM [2] | 1/2 | No | No | 200 |
| 400 | DCM [2] | 5/8 | No | No | 200 |
| 480 | DCM [2] | 3/4 | No | No | 200 |

[1] A data rate of 110 Mb/s ($r = 11/32$) is used instead in the IEEE 802.15.3a proposal of Sept. 2004 [65].

[2] A QPSK constellation is used instead of the DCM in [65].
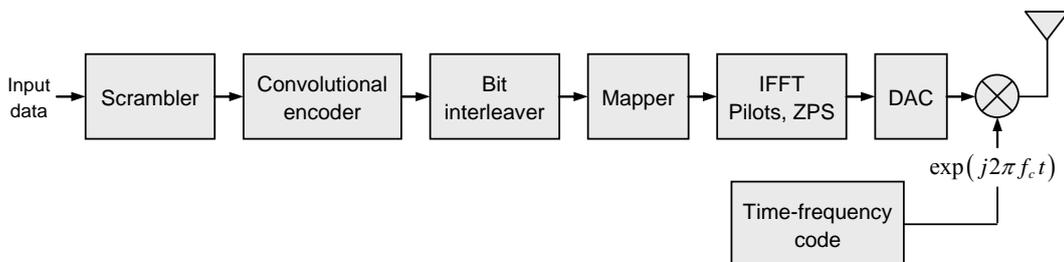


Figure 2.5: Transmitter architecture for the MB-OFDM system.

### 2.2.1.2 Bit interleaving

The encoded bit stream is interleaved to provide more diversity for transmissions over multipath fading channels, and consequently more robustness against burst errors. The bit interleaving process is performed in three distinct stages:

- *Symbol interleaving*, which permutes the bits across six consecutive OFDM symbols to exploit frequency diversity across the three bands within one band group.

- *Intra-symbol tone interleaving*, which permutes the bits across the data subcarriers within an OFDM symbol to exploit frequency diversity across subcarriers and provide robustness against narrowband interferers.

- *Intra-symbol cyclic shifts*, which cyclically shifts the bits in successive OFDM symbols by deterministic amounts to obtain a better exploitation of the frequency diversity.

The symbol interleaving operation is performed using a block interleaver of size $N_{CBPS} \times 6 / N_{TDS}$, where $N_{CBPS}$ is the number of coded bits per OFDM symbol and $N_{TDS}$ the TDS factor equal to 1 when there is no spreading in time, and to 2 when the time spreading is applied. Let the sequence $a[i]$, with $i = 0,\ldots,(6 / N_{TDS})N_{CBPS} - 1$, represent the input bits of the block interleaver. Thus, the symbol interleaver output $a_S[i]$ is given by

$$a_S[i] = a\left[\left\lfloor \frac{i}{N_{CBPS}} \right\rfloor + \left(\frac{6}{N_{TDS}}\right) \times \mathrm{mod}(i, N_{CBPS})\right], \qquad (2.13)$$

where $\lfloor . \rfloor$ is the floor function which returns the largest integer value less than or equal to its argument value, and $\mathrm{mod}(x, y)$ the modulus operator which returns the integer remainder after division of $x$ by $y$.

The output $a_S[i]$ of the symbol interleaver is then permuted using a block intra-symbol interleaver of size $N_{Tint} \times 10$, with $N_{Tint} = N_{CBPS} / 10$. The tone interleaver output $a_T[i]$, with $i = 0,\ldots,N_{CBPS} - 1$, is given by

$$a_T[i] = a_S\left[\left\lfloor \frac{i}{N_{Tint}} \right\rfloor + 10 \times \mathrm{mod}(i, N_{Tint})\right]. \qquad (2.14)$$

The sequence $a_T[i]$ is then passed through an intra-cyclic shifter whose output is expressed by

$$b[i] = a_T\left[m(i) \times N_{CBPS} + \mathrm{mod}(i + m(i) \times N_{cyc}, N_{CBPS})\right], \qquad (2.15)$$

where $i = 0,\ldots,(6 / N_{TDS})N_{CBPS} - 1$, $m(i) = \lfloor i / N_{CBPS} \rfloor$, and $N_{cyc}$ is a shift factor that can be equal to 33 or 66 depending on the selected data rate.

### 2.2.1.3 Constellation mapping

For data rates of 200 Mb/s and lower, the interleaved binary data is mapped onto a quadrature phase-shift keying (QPSK) constellation. For data rates of 320 Mb/s and higher, the binary data is mapped onto a multi-dimensional constellation using a dual-carrier modulation (DCM) technique. Note that the first MB-OFDM proposals for IEEE 802.15.3a, including the September 2004 proposal, considered only a QPSK constellation for all the data rates [65].

By switching from a QPSK constellation to a DCM scheme, an additional form of diversity can be obtained, which results in an improvement in the overall range of the system. This diversity is introduced by mapping four bits onto two 16-point constellations. The resulting symbols are then mapped onto tones that are separated by at least 200 MHz of bandwidth, which is equivalent approximately to 50 subcarriers. The DCM technique is not applied for low data rates (200 Mb/s and below) since the frequency diversity is better exploited through the use of low rate FEC codes, TDS and FDS techniques. Therefore, the expected DCM diversity gain for these data rates is minimal and the added complexity for DCM is not justified.

### 2.2.1.4 OFDM modulation

The MB-OFDM system uses an OFDM modulation on each 528 MHz band with a total of 128 subcarriers, divided into 100 data tones, 12 pilot tones, 10 guard tones and 6 null tones. The resulting 122 energy-carrying tones are modulated using QPSK or DCM. 5 guard tones are placed on each edge of the occupied frequency band, and the information carried by these tones is generated by replicating the information from the five outermost data-bearing tones [65]. The 12 pilot tones are distributed regularly over the whole frequency band with a spacing of 10 subcarriers between them, and are dedicated to pilot signals in order to allow for coherent detection and provide robustness against frequency offsets and phase noise. The different parameters of the OFDM scheme are listed in Table 2.2.

An IFFT of size $N_{IFFT} = N_{FFT} = 128$ is used to transform the frequency-domain information into a time-domain OFDM symbol, with a sampling frequency $f_s = 528$ MHz. The resulting symbol duration at the output of the IFFT is given by $T_{FFT} = 1/\Delta_f = 242.42$ ns, with $\Delta_f = 4.125$ MHz the spacing between subcarriers. The discrete-time signal during the useful part of the OFDM symbol can be expressed as

$$\tilde{s}_n[m] = \frac{1}{\sqrt{N_{FFT}}} \left[ \sum_{l=0}^{N_d-1} C_d(l) e^{j2\pi \frac{M_d(l)m}{N_{FFT}}} + \sum_{l=0}^{N_g-1} C_g(l) e^{j2\pi \frac{M_g(l)m}{N_{FFT}}} + \sum_{l=0}^{N_p-1} C_p(l) e^{j2\pi \frac{M_p(l)m}{N_{FFT}}} \right], \quad (2.16)$$

where $m = 0, \ldots, N_{FFT} - 1$, $n$ is the OFDM symbol index, $N_d$, $N_g$ and $N_p$ are the number of data, guard and pilot subcarriers respectively, $C_d$, $C_g$ and $C_p$ are the complex numbers placed on the $l^{th}$ data, guard and pilot subcarriers, respectively. The functions $M_d$, $M_g$ and $M_p$ define a mapping from the indices $[0, \ldots, N_d - 1]$, $[0, \ldots, N_g - 1]$ and $[0, \ldots, N_p - 1]$ to the logical frequency subcarriers $[-N_t/2, \ldots, N_t/2]$ excluding 0, with $N_t = 122$ the total number of used subcarriers.

In addition, a zero-padded suffix (ZPS) is appended to the IFFT output. The ZPS provides the same multipath robustness as with the traditional cyclic prefix (CP) considered in most conventional wireless OFDM systems [66], and offers a guard interval that allows sufficient time for the transmitter and receiver to switch between the different center frequencies. The main advantage of using ZPS instead of CP is that the transmit power can be maximized. In fact, when a CP is used, redundancy is introduced into the transmitted signal, which leads to ripples in the average PSD, and consequently a reduction in the transmitted power since the maximum radiated transmit power is limited by the FCC [20]. When a ZPS is used, the ripples in the PSD can be reduced to zero since the transmitted signal becomes random [20].

In [21] and [65], a ZPS of length 37 and duration $T_{ZPS} = 70.08$ ns is used to generate an output with the desired length of 165 samples. The length of the ZPS was smartly chosen to minimize the impact due to ISI, and thus ICI, and to maximize the collected multi-

Table 2.2: OFDM parameters of the MB-OFDM system.

| Parameter | Value |
| --- | :---: |
| Total number of subcarriers ($N_{FFT}$) | 128 |
| Number of data subcarriers ($N_d$) | 100 |
| Number of pilot subcarriers ($N_p$) | 12 |
| Number of guard subcarriers ($N_g$) | 10 |
| Total number of used subcarriers ($N_t$) | 122 |
| Sampling frequency ($f_s$) | 528 MHz |
| Subcarrier frequency spacing ($\Delta_f$) | 4.125 MHz |
| IFFT / FFT period ($T_{FFT}$) | 242.42 ns |
| Number of samples in ZPS ($N_{ZPS}$) | 37 |
| ZPS duration ($T_{ZPS}$) | 70.08 ns |
| Symbol interval ($T_s$) | 312.5 ns |

path energy, while limiting the overhead. Thus, the total symbol duration becomes $T_s = T_{FFT} + T_{ZPS} = 312.5$ ns .

On the other hand, within the OFDM modulation process, FDS and TDS techniques are used to provide additional diversity gain. FDS entails transmitting the same information on two separate subcarriers within the same OFDM symbol by forcing the input data into the IFFT to be conjugate symmetrical. The advantage is that the IFFT output is always real, implying that only the transmitter real part needs to be implemented or turned on [20]. TDS is obtained by transmitting the same information across two consecutive OFDM symbols. This technique is used to maximize frequency-diversity and improve the performance for low data rates (200 Mb/s and lower).

### 2.2.1.5   Time-frequency codes

In the MB-OFDM system, time-frequency codes (TFC) provide a frequency-hopping from a frequency band to another within a given band group, at the end of each OFDM symbol. Different TFC sequences of length 6 are used to define this hopping scheme [65]. The ECMA-368 standard specifies three types of TFC: one where the information is interleaved over three bands, one where it is interleaved over two bands, and one where it is transmitted on a single band, referred to as time-frequency interleaving (TFI), two-band TFI (TFI2), and fixed frequency interleaving (FFI). Figure 2.6 shows one TFC realization in the first band group (3168–4752 MHz), using the TFC sequence $\{1, 3, 2, 1, 3, 2\}$ . In this figure, the first OFDM symbol is transmitted on band 1 since the first element of the TFC sequence is 1, the second symbol is transmitted on band 2, the third symbol is transmitted on band 3, and so on.
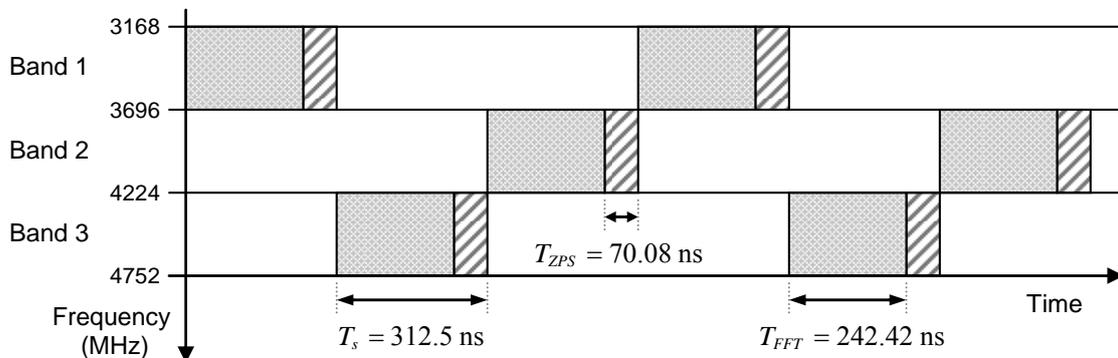


Figure 2.6: Example of time-frequency coding for the MB-OFDM system in the first band group, using the TFC sequence $\{1, 3, 2, 1, 3, 2\}$ .

The TFC technique offers a frequency diversity gain that can be added to the gain provided by the FEC coding and the FDS technique. This is due to the fact that TFC systems are using a frequency band that is three times larger than the band of 528 MHz allocated to a system not applying TFC. Another advantage of frequency hopping between the bands is that the effective total average transmit power is equal to the average power transmitted per band times the number $B$ of bands, which is equal to 3 in our case. Note that this advantage has been a very controversial issue due to the possible implication that the transmit power may have to be reduced by a factor of $B$ [20].

One of the main advantages of TFC technique is that it provides multiple access between users by assigning a unique TFC to each user. Thus, if we consider a 3-user system, at a given OFDM symbol duration, each user can occupy one of the three bands of a given band group, and during the next symbol duration, each of the users is allocated another band by following the used TFC sequence. However, collisions can not be avoided, especially when more than three users are transmitting simultaneously. Hence, the TFCs were designed to ensure that the average number of collisions between any two TFCs is 1/3, and that the distribution of collisions should be as uniform as possible for all asynchronous shifts of the codes.

On the other hand, the TFC can be implemented using simple synthesizer architectures that can rapidly switch between the three bands within a given band group. A low complexity architecture where all the center frequencies of the bands can be generated from a single phase-locked loop (PLL) is proposed in [20]. In addition, switching between the different bands can be accomplished within a few nanoseconds (approximately 2 ns).

The transmitted RF signal can be written in terms of the complex baseband signal as

$$s_{RF}(t) = \text{Re}\left\{ \sum_{n=0}^{N_{sym}-1} s_n(t - nT_s) e^{j2\pi f_c(M(n))t} \right\}, \tag{2.17}$$

where $N_{sym}$ is the number of symbols in the packet, $s_n(t)$ represents the complex baseband signal of the $n^{th}$ symbol, with $s_n(t) = 0$ for $t \notin [0:T_s]$, $M(n)$ the mapping TFC function of the $n^{th}$ symbol to the appropriate frequency band, and $f_c$ the center frequency of the corresponding frequency band.

### 2.2.2   Receiver architecture

After having detailed the transmission design of the MB-OFDM system, we move to a brief description of the corresponding receiver. The architecture of the MB-OFDM receiver is shown in Figure 2.7 [36]. First, the received signal is passed through a pre-select
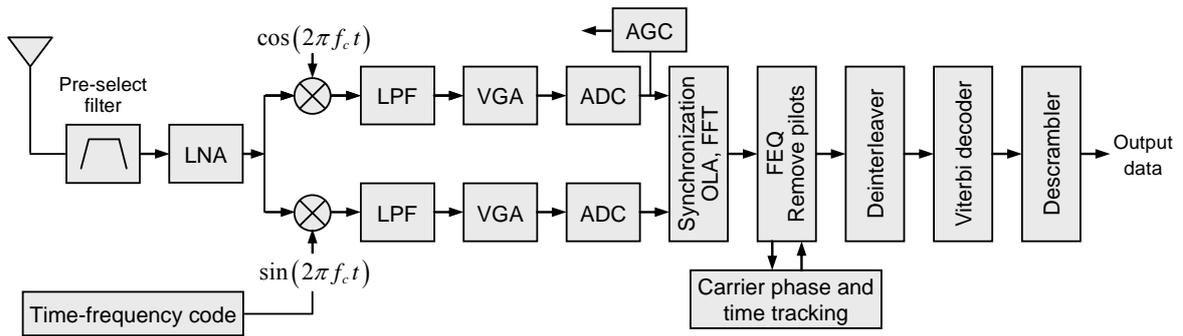
Figure 2.7: Receiver architecture for the MB-OFDM system.

filter, amplified with a LNA and down-converted to the complex baseband using in-phase and quadrature mixers. The sequence of center frequencies of the different bands is obtained through the knowledge of the appropriate TFC. The out-of-band interferers of the complex baseband signal are then rejected using a low-pass filter (LPF). The signal is then sampled and quantized using a 528 MHz ADC to obtain the complex digital baseband signal. The automatic gain control (AGC) loop controls the settings of the variable gain amplifier (VGA), and when a packet is detected, the receiver determines the optimal FFT placement window for each frequency band. The samples corresponding to the ZPS are added to the start of the OFDM symbol using an overlap-and-add (OLA) technique. A 128-point FFT is then carried out and the output is equalized using a frequency-domain equalizer (FEQ). The effect of carrier and timing mismatch between transmitter and receiver is removed using a phase correction. The signal is then demapped, deinterleaved, followed by a maximum likelihood decoding using a Viterbi decoder. Finally, the output is descrambled and the estimated sequence of binary data is collected.

### 2.2.3  System performance

In this section, we present some results of simulations carried out on the MB-OFDM system described previously, in order to analyze its performance. In these simulations, we consider an indoor environment, and we use the channel model adopted by the IEEE 802.15.3a task group, whose characteristics are listed in Table 1.1. In what follows, simulations are applied on channel model CM1 where a LOS case is considered and the transceiver spacing is less than 4 meters. Frames of 150 OFDM symbols are used, and each frame is transmitted on a different channel realization, from a total of 100 available realizations [43].

Figure 2.8 shows the simulation results performed on band 1 (3168–3696 MHz) where no TFC frequency hopping is applied. Consequently, all the OFDM symbols are transmit-

ted on the same band. On the other hand, Figure 2.9 shows the simulation results performed on the band group 1 (3168–4752 MHz) using a TFC sequence of $\{1,3,2,1,3,2\}$ which provides a frequency hopping between the three bands at the end of each OFDM symbol.

In Figure 2.8 and Figure 2.9, the average bit-error-rate (BER) is presented as a function of $E_b / N_0$, where $E_b$ is the average energy per useful bit and $N_0$ is the AWGN power density, and the ideal case of perfect channel estimation is considered. The performance of the MB-OFDM system is presented for the different MB-OFDM data rates listed in Table 2.1. Note that the parameters considered here are the ones adopted in [65]. Thus, a data rate of 110 Mb/s is presented instead of the data rate of 106.7 Mb/s, and a QPSK is used instead of a DCM for data rates 320, 400 and 480 Mb/s. Note that replacing QPSK by DCM would slightly improve the system performance at the expense of higher system complexity.

By comparing Figure 2.8 and Figure 2.9, we notice that the frequency hopping from a band to another using TFC offers a system gain varying between 0.5 and 1 dB at $BER = 10^{-5}$, depending on the selected data rate. This gain is due to the frequency diversity achieved by the use of a three times larger frequency band. As expected, the MB-OFDM system with a data rate of 55 Mb/s has the lowest BER, since it uses the lowest coding rate with FDS and TDS techniques. Similarly, the system with the highest data rate of 480 Mb/s has the worst performance in terms of BER due to its high coding rate of $r = 3/4$. Besides, in Figure 2.9, if we compare data rates 53.3 and 110 Mb/s, as well as data rates 80 and 160 Mb/s, we notice that the difference in $E_b / N_0$ at $BER = 10^{-5}$ is less than 0.5 dB. This means that applying the FDS reduces the data rate by half without offering a considerable $E_b / N_0$ gain. In addition, if we compare systems with data rates of 80 and 110 Mb/s, we notice that the system with a data rate of 110 Mb/s offers better BER performance even if it provides higher data rate. This is due to the fact that the FDS applied to the system with a data rate of 80 Mb/s is not efficiently exploited.

Similar simulations have been performed on channel models CM2, CM3 and CM4, and similar results, not presented here, have been obtained, leading to the same conclusions. However, we should note that a performance limitation can appear at high SNR levels for high data rates, when the channel model CM4 is used. This performance degradation can be understood by noticing that the guard interval length is smaller than the delay spread of channel CM4 [67].
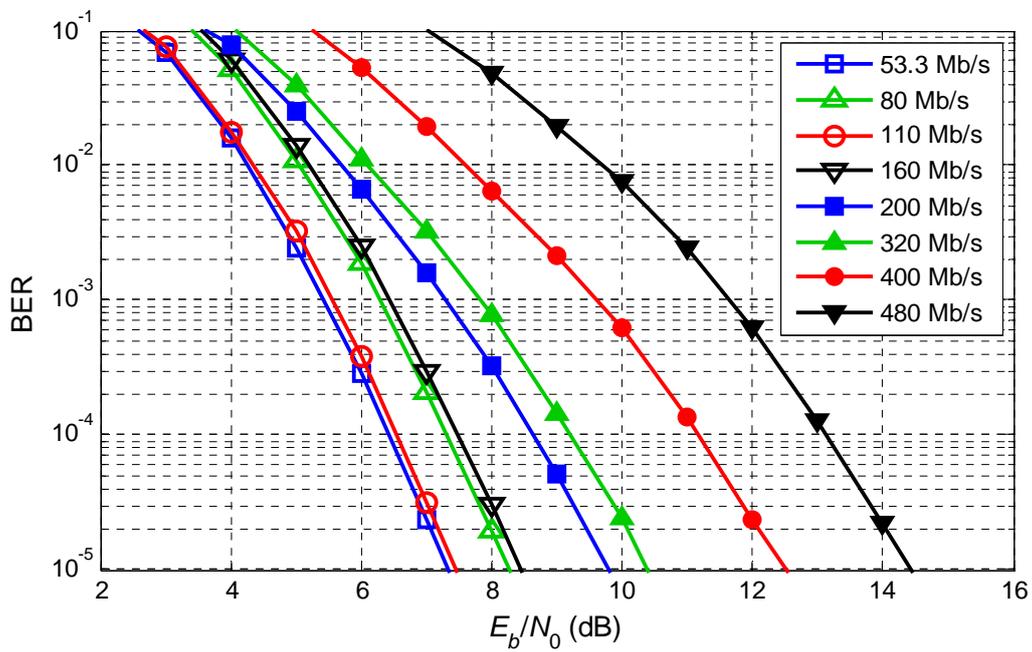
Figure 2.8: MB-OFDM system performance on band 1, using channel model CM1 and without applying the TFC frequency hopping technique.
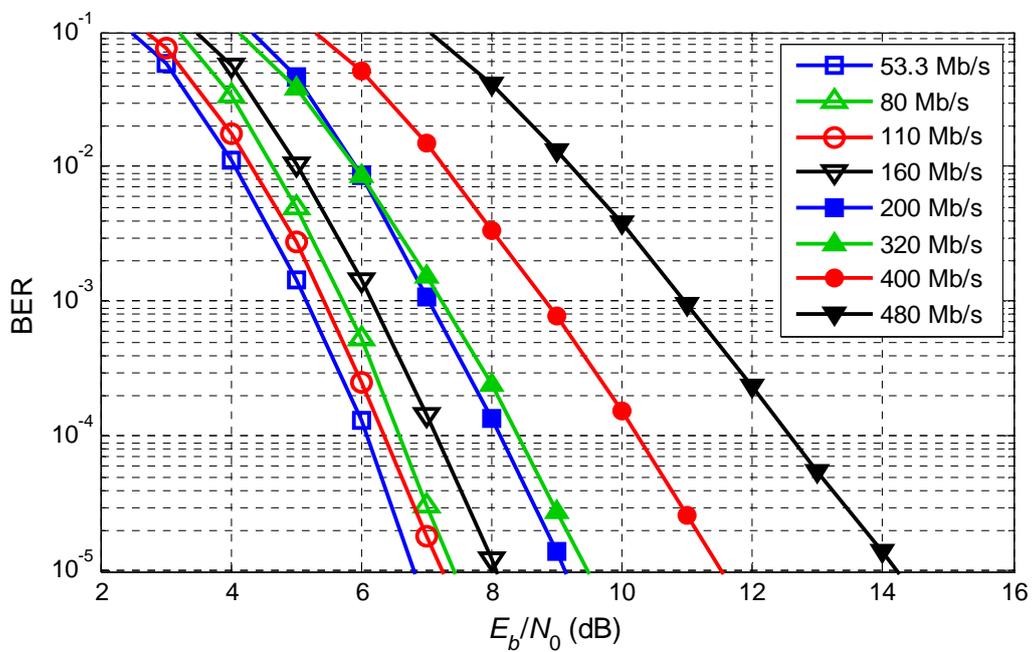


Figure 2.9: MB-OFDM system performance on bands 1, 2 and 3, using channel model CM1 and considering a TFC frequency hopping between the three bands.

## 2.3   Proposed LP-OFDM UWB system

### 2.3.1   MB-OFDM drawbacks

The MB-OFDM approach offers potential advantages for high data rate UWB applications, including the spectral flexibility and the ability to capture multipath energy efficiently and to deal with narrowband interferers. The numerous advantages make it the primary choice for high data UWB systems, compared to the IR-UWB approach. However, the MB-OFDM approach has some limitations that can be reduced using efficient techniques such as linear precoding, MIMO techniques and dynamic resource allocation.

The main MB-OFDM limitations occur when we consider a multi-user context. In fact, in the MB-OFDM solution, the multiple access is obtained by the use of specific TFC sequences that provide a frequency hopping between users from a band to another. Collisions between the TFCs, and thus interference between users, can occur due to the asynchronous shifts of the codes. These collisions can not be avoided especially when more than three users are transmitting simultaneously, since all the users are allocated one of the only three bands in a given band group. The only proposed solution in the MB-OFDM standards [65] consists in designing the TFCs in a way that the distribution of collisions would be as uniform as possible for all asynchronous shifts of the codes, and that the average number of collisions between any two TFCs would be equal to 1/3. Consequently, interference between users is not reduced significantly.

In addition, the TFCs are randomly distributed between the users. This strategy lacks in the ability to allocate bands optimally since the available bands are not assigned to each user according to its channel condition. Moreover, the transmit power of each user is equally distributed among the assigned band without any power adaptation to the channel variations. If adaptive resource allocation was considered, the performance of MB-OFDM systems would be improved significantly, as will be seen in Chapter 3 and Chapter 4.

On the other hand, the FCC limitation on the spectral mask leads to a significant reduction in terms of UWB systems performance. For instance, high data rate applications are limited to very short ranges. Currently, the coverage of UWB systems is at most 10 meters at the data rate of 110 Mb/s and only 3 meters at the data rate of 480 Mb/s [36]. However, different applications may require larger coverage, i.e. applications in warehouse or even residential environments. Consequently, more research and improvements on the existing UWB systems are required to increase the systems range, transmission rate, and robustness.

### 2.3.2   Previous works on MC-SS systems in an UWB context

In order to improve the performance of UWB systems, and particularly the performance of the MB-OFDM system, some studies have proposed to add a spread spectrum scheme to the MB-OFDM approach. Most of these studies consider a scheme based on the well-known MC-CDMA technique [68]–[73], with a spreading in the frequency direction, as described in Figure 2.3 (a). In the MC-CDMA systems proposed in [68]–[73], the different users transmit information on all the subcarriers simultaneously, and the multiple access is carried out in the code dimension where each user is allocated a specific code sequence.

The MC-CDMA frequency spreading improves the signal robustness against the frequency selectivity of UWB channels, as explained in [68]. The authors in [68] also describe how the transmitter range can be significantly improved using MC-CDMA compared to the range of TH-PPM UWB systems. In [69], a performance comparison between DS-CDMA, OFDM and MC-CDMA UWB systems is presented. This study shows that an OFDM system and a DS-CDMA system using 16 RAKE fingers have comparable performance in terms of BER, and that a MC-CDMA system can have better BER performance. However, the authors suggest using a MC-CDMA signal bandwidth of 1.584 GHz, equivalent to a total of three MB-OFDM bands, which increases the required sampling frequency of the ADCs, and thus increases the system complexity significantly.

One main advantage of MC-CDMA compared to MB-OFDM systems is the signal robustness against narrowband interference, since the MC-CDMA signal bandwidth becomes much larger than the interfering signal bandwidth due to the spreading in the frequency direction. In [70], the performance of MC-CDMA UWB systems is studied in the presence of narrowband interference. This paper shows that when the number of subcarriers jammed by narrowband interferers is small, the MC-CDMA scheme is efficient without using notch filters. This is due to the frequency diversity gain collected from the non-jammed subcarriers. However, when the number of jammed subcarriers is relatively large, using notch filters can improve the multicarrier system performance significantly. A complementary study showing that minimum mean-square error (MMSE) receivers in MC-CDMA UWB systems are robust to combat strong narrowband interference is given in [71]. Another interesting study on interference problems with MC-CDMA UWB systems is carried out in [72]. The authors propose a simple-hardware interference mitigation technique for two systems sharing the same frequency bands, both based on UWB technology. The first system considers a pulse-based UWB signal, whereas the second system is based on a MC-CDMA scheme using the same OFDM parameters as in the MB-OFDM solution.

Similarly to any multicarrier system using OFDM modulation, the MB-OFDM system is subject to high PAPR which leads to severe clipping effects. The spreading techniques

can be efficiently exploited to reduce the PAPR of the OFDM signal. Thus, the authors in [73] propose a MC-CDMA system for UWB applications, using spreading sequences smartly constructed in order to reduce the PAPR of the signal, while providing a good spread spectrum gain and bandwidth efficiency. However, this leads to a decrease in the transmission rate, and thus a trade-off between system robustness and transmission rate is required.

In addition, only few authors have recently proposed multicarrier spread spectrum schemes different than the classical MC-CDMA scheme. In [74], the author proposes a TH/MC-CDMA scheme based on time-hopping, multicarrier modulation and CDMA techniques. The main advantages are that the signals have a flat Gaussian noise-like PSD over a very wide bandwidth, and that the nonlinear fluctuations caused by the high PAPR in MC systems can be significantly mitigated due to the TH characteristics. Another scheme applying a spread spectrum technique to the MB-OFDM system is given in [75]. It employs an interleaving technique that places the modulated signal samples of different subcarriers at different instants instead of superposing them together. The main advantages of this scheme are that the frequency hopping technique would not be needed and the transmitted signal bandwidth can be flexibly selected to meet different system requirements.

### 2.3.3   LP-OFDM system description

In this thesis, we propose a new UWB scheme based on the combination of spread spectrum techniques, or equivalently linear precoding (LP) principles, with the OFDM waveform of the MB-OFDM system [76]. The objectives of this scheme are to make the MB-OFDM system more flexible, to reduce its limitations and to improve the overall system performance, without increasing the system complexity significantly. Although originally proposed for multi-user access schemes, the concept of combining spread spectrum techniques with multicarrier modulation can be extended to all single-user OFDM systems. In this case, the resulting scheme is also known as linear precoded OFDM (LP-OFDM). The LP process consists in applying precoding matrices to various blocks of subcarriers of the multicarrier spectrum [77], [78]. Thus, the system evolution reduces in practice to a simple addition of a precoding block in the transmission chain, which leads to a complexity equivalent to the one of a Hadamard matrix multiplication.

The proposed scheme, referred to as LP-OFDM in the sequel, can be seen as a modified version of the SS-MC-MA waveform proposed by Kaiser and Fazel for mobile radio communications [64] and described in Section 2.1.2.3. Taking into account the frequency selectivity and the slow-time variations of the UWB channel in an indoor WPAN environment, the spreading sequences of the LP-OFDM scheme are carried out in the frequency

dimension, same as in SS-MC-MA and MC-CDMA systems. This spreading component improves the signal robustness against frequency selectivity and narrowband interference, since the signal bandwidth becomes much larger than the coherence and interference bandwidths. Besides, the multiple access is carried out in the frequency dimension as in SS-MC-MA, and not in the code dimension as in MC-CDMA systems. However, the difference between SS-MC-MA and LP-OFDM is that, instead of distributing the blocks of subcarriers within one OFDM symbol to the different users, all these subcarriers blocks are allocated to only one user. The remaining users are then given other sets of blocks of subcarriers on different frequency bands, and each user is then able to transmit its own OFDM symbol simultaneously. Note that the OFDM parameters of the LP-OFDM scheme are the same as the OFDM parameters of the MB-OFDM technique, listed in Table 2.2, to present a fair systems comparison.

In order not to modify the ADCs design and increase the LP-OFDM system complexity compared to the MB-OFDM system, the same multiband technique with the same subbands bandwidth of 528 MHz is considered. Besides, the same TFC technique is applied to LP-OFDM systems in order to provide frequency hopping between the users from a band to another, and thus to benefit from an additional frequency diversity.

A schematic representation of the LP-OFDM signal for three users occupying the first three 528 MHz bands of the MB-OFDM scheme is depicted in Figure 2.10. At a given time, each user is allocated one of the three bands, depending on the used TFC sequence. Each band is divided into several blocks, each of them including a number of subcarriers equal to the spreading code length $L$. Thus, the total number of blocks per user is given by $B = N / L$, where $N$ is the number of data subcarriers per OFDM symbol. Note that in Figure 2.10, the subcarriers linked by a same spreading code are depicted adjacent to each other to simplify the schematic representation. However, in reality these subcarriers are not necessarily adjacent, and a smart subcarriers distribution on the different blocks of an OFDM symbol can improve the system performance in terms of range and throughput, as we will see in Chapter 3. In addition, a number $K$ of data symbols, equivalent to the number $K$ of used spreading sequences, are simultaneously transmitted by the same user on a specific subset of subcarriers and undergo the same distortions.

In brief, same as the MC-CDMA technique, the proposed LP-OFDM scheme exploits the advantages of combining spread spectrum techniques and multicarrier modulation. The spreading in the frequency direction improves the signal robustness against frequency selectivity. In addition, UWB systems are subject to strong narrowband interferers due to the large frequency band that overlays numerous existing spectral allocations. Thus, the frequency spreading can be considered as a potential solution to combat narrowband interfer-
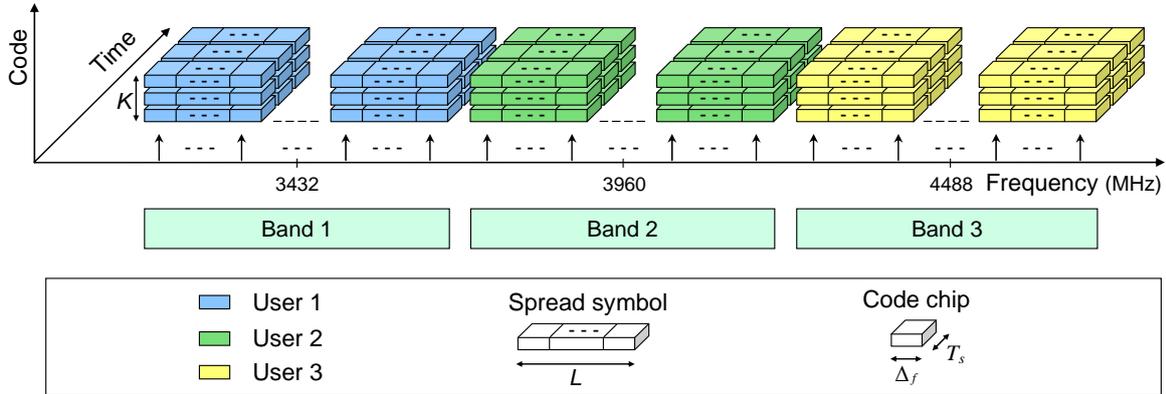
Figure 2.10: LP-OFDM schematic representation for three users occupying the first three bands of the MB-OFDM scheme.

ence. Furthermore, ISI and ICI can be avoided in both MC-CDMA and LP-OFDM systems, resulting in simple data detection techniques. Another advantage of both systems is the ability to reduce the PAPR of the OFDM modulation by a judicious exploitation of the LP component.

On the other hand, the proposed LP-OFDM scheme has numerous advantages over MC-CDMA. In fact, it is well known that the spreading operation introduces some interference between the spreading sequences when orthogonality is not maintained. Thus, MC-CDMA systems have to cope with multiple access interference (MAI) which is not present in the LP-OFDM system. Instead of MAI, the LP-OFDM system has to cope with self-interference caused by the superposition of signals from the same user. This self-interference can be easily compensated for by a simple detection with only one complex coefficient per subcarrier. Besides, different studies including judicious distributions of subcarriers and spreading codes can be carried out to reduce the effect of self-interference on LP-OFDM systems [76], [79]. In addition, in the LP-OFDM system, each subcarrier is exclusively used by one user at a given time, enabling low complexity channel estimation. In MC-CDMA systems on the other hand, the channel estimation has to cope with the superposition of signals from different users, which are faded independently on the same subcarriers if the signals have been transmitted from different places as in the uplink applications, which increases the complexity of the channel estimation [62].

Furthermore, the LP-OFDM scheme increases the resource allocation flexibility compared to the MB-OFDM system, as the spreading technique offers additional degrees of freedom, including the spreading code length, the number of codes, and the subcarriers distribution between the blocks [80]. Another advantage of LP-OFDM over MB-OFDM is

that it provides a wide range of possible data rates due to the high flexibility brought by the joint assignment of the coding rates and the number of used spreading codes.

In addition, as explained previously, when we consider more than three users transmitting simultaneously in the MB-OFDM system, collisions between them can not be avoided. In Figure 2.10, we have presented an example of three users transmitting information in the LP-OFDM system. This schematic representation is for LP-OFDM systems with one to three simultaneous users. However, the LP-OFDM scheme can be easily modified to fit the case of more than three users transmitting simultaneously. Different solutions avoiding collisions between users are possible. One solution consists in dividing each of the three MB-OFDM bands between two or three users in the code dimension, which corresponds to a MC-CDMA signal in each band. Consequently, a number of six to nine users will be able to send information without collision in the modified LP-OFDM scheme.

### 2.3.4 LP-OFDM signal

The architecture of the LP-OFDM transmitter of each user is depicted in Figure 2.11. Let $L$ represent the spreading code length which is considered the same for all the blocks, $B$ the number of blocks within a single band allocated to one single user, and $K$ the number of used codes. Thus, each user is able to transmit simultaneously a number $K$ of data symbols streams per block, using a CDM technique. The resulting $K$ parallel converted data symbols of a given block $b$ can be written as a vector
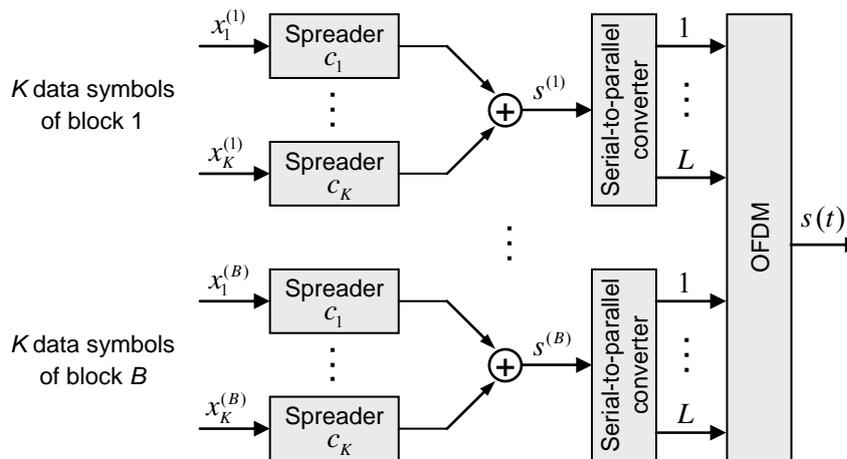


Figure 2.11: LP-OFDM transmitter for a single user.

$$x^{(b)} = \left[ x_1^{(b)}, \ldots, x_k^{(b)}, \ldots, x_K^{(b)} \right]^T. \tag{2.18}$$

Each data symbol is then multiplied by an orthogonal spreading code of length $L$, written as $c_k = [c_{1,k} \ldots c_{l,k} \ldots c_{L,k}]^T$. Codes $c_k$ constitute the vectors of the spreading codes matrix of size $L \times K$, given by

$$C = [c_1 \ldots c_k \ldots c_K]. \tag{2.19}$$

The spreading matrix $C$ can be the same for all the blocks. The modulated spreading codes are then synchronously added, resulting in the transmission vector per block

$$s^{(b)} = C\,x^{(b)}, \tag{2.20}$$

with $s^{(b)} = \left[ s_1^{(b)}, \ldots, s_l^{(b)}, \ldots, s_L^{(b)} \right]^T$. The transmission vectors of the different blocks are then inserted at the input of the OFDM modulation.

## 2.4 Conclusion

In this chapter, we have started by presenting the principles of the main transmission techniques we are dealing with in this thesis. Then, we have described the MB-OFDM system that can be considered as the starting point of our studies. The MB-OFDM approach offers potential advantages for high data rate UWB applications, which make it the main candidate for high data rate WPAN standardizations. These advantages include the spectral flexibility and the ability to capture multipath energy efficiently and to deal with narrowband interferers. However, the MB-OFDM approach is subject to some limitations notably in terms of system range and robustness, and in terms of multiple access between users.

In order to reduce the MB-OFDM limitations and to improve the total system performance, we have proposed a new UWB scheme based on the combination of spread spectrum techniques, or equivalently linear precoding principles, with the OFDM waveform of the MB-OFDM system. The system evolution reduces in practice to a simple addition of a precoding block in the transmission chain, which does not significantly increase the system complexity considerably. Taking into account the frequency selectivity and the slow-time variations of the UWB channel in an indoor WPAN environment, as well as the strong narrowband interferers in the UWB spectrum, the LP-OFDM spreading sequences are carried out in the frequency dimension. In order not to significantly increase the LP-OFDM system complexity compared to the MB-OFDM system, the same OFDM parameters and the same multiband technique as with the MB-OFDM technique are applied.

Furthermore, the LP-OFDM scheme is very flexible compared to the MB-OFDM system, since the spreading technique offers additional degrees of freedom, including the spreading code length, the number of codes, and the subcarriers distribution between the blocks. Chapter 3 and Chapter 4 present an analytical study of the LP-OFDM system, whose objective is to improve the system performance in terms of throughput, range and robustness. Thus, different resource allocation strategies optimizing the LP-OFDM system parameters are proposed. Besides, this analytical study shows that the spreading component of the LP-OFDM scheme can be advantageously exploited in terms of flexibility and performance.

Finally, Chapter 5 is dedicated to the global LP-OFDM system study taking into account all the blocks of the transmission chain. This study shows that the LP-OFDM system performance outperforms the MB-OFDM system performance, thanks to the spreading component. In addition, a MIMO scheme is added to the global LP-OFDM system in order to improve the total range.

# Chapter 3

# Resource allocation principles, target symbol-error-rate approach

RESOURCE allocation is a fundamental aspect in the design of multicarrier systems. This chapter is dedicated to the study of resource allocation principles and its exploitation in OFDM and LP-OFDM systems, considering an UWB context. Due to the slow time variations of the UWB channel, resource allocation can be efficiently implemented in UWB systems without significantly increasing the systems complexity. A general overview on resource management principles is first presented and the different optimization strategies, namely, rate maximization and margin maximization, are described. Classical solutions for OFDM systems and new optimal solutions for LP-OFDM systems are then detailed, taking into account the UWB characteristics. Besides, the performance of the proposed allocation algorithms is discussed and the simulation results obtained with the LP-OFDM scheme of the proposed system are compared to the results obtained with the OFDM scheme of the WiMedia approach. Note that in this chapter, a classical target symbol-error-rate (SER) approach is considered, whereas in Chapter 4, a study based on a new system mean bit-error-rate (BER) approach is carried out. Finally, an additional optimization study based on a dynamic distribution of the time-frequency codes between the users of an UWB system is proposed. The different optimization results presented in this chapter show that the linear precoding component can be efficiently exploited for high data rate UWB applications, and that the LP-OFDM system outperforms the OFDM system of the WiMedia solution.

## 3.1   Resource management principles

### 3.1.1   General overview

The management of the available resources of a communication system is of major importance when we want to optimize its performance. Every system is subject to physical and

technical limitations, and to some constraints imposed by the quality of service (QoS). Alternatively, different degrees of freedom provided by the system can be configured to deal with these limitations and constraints. For instance, when the channel state information (CSI) is partially or perfectly known at the transmitter side, these degrees of freedom can be adapted to the state of the channel in order to respect the system constraints and desired QoS. Note that when the channel response varies slowly in time, as in the case of indoor UWB applications, this response can be considered as quasi-static during one frame. Consequently, the CSI can be sent by a simple feedback to the transmitter at the beginning of each frame, which does not significantly increase the implementation complexity of the resource management process.

The main limitations in a communication system are the allocated frequencies and the transmit power. The frequency constraint is due to the fact that all the systems are assigned limited frequency bands, which reduces interference with each other, and the power constraint is imposed by the system standards mainly to respect medical regulations and reduce interference. In the case of UWB communications, the system benefits from a very large frequency band, contrarily to most of the communication systems. However, a strong power limitation in terms of power spectral density (PSD) is imposed. On the other hand, the system degrees of freedom strongly depend on the considered system. In an OFDM system for instance, a different number of bits and a different power level can be allocated to each subcarrier depending on its channel state. The LP-OFDM system on the other hand benefits from additional degrees of freedom related to the linear precoding scheme, such as the number of spreading codes being used and their distribution on the different subcarriers.

Theoretically, different studies have been recently carried out to determine the capacity of broadcast and multiple access channels [81], [82]. These studies focus on the capacity regions of these channels. Different allocation strategies aiming to reach the borders of these regions and thus to maximize the total system throughput have been proposed [83], [84]. The existing solutions are based on the use of optimal receivers with interference cancellation which are not considered in our study because of their implementation complexity. In the proposed LP-OFDM system, the transmitter and receiver have a specific scheme using orthogonal codes with a spreading operation carried out in the frequency direction. This kind of schemes is considered suboptimal in terms of information theory since the borders of the capacity regions can not be reachable. However, they offer receiver schemes with low complexity, and thus, they are widely used in practical systems. Consequently, we will be talking about resource allocation within system capacity regions instead of channel capacity regions.

## 3.1.2   Channel capacity and SNR gap

For a non-dispersive channel having an attenuation factor α and affected by the presence of an AWGN with a power density $N_0$, the maximum reachable throughput depends on the frequency band $W$ and the transmit power density $E_s$, and can be expressed as explained earlier by

$$C = W \log_2 \left( 1 + \frac{\alpha E_s}{N_0} \right),$$
(3.1)

where $C$ is given in b/s and $\alpha E_s / N_0$ is equivalent to the SNR. This throughput limit is only reachable if a theoretical code of infinite complexity and infinite coding/decoding delay is used, whereas in real systems, practical suboptimal codes are considered. Consequently, the binary throughput that can be transmitted by the channel is always lower than this theoretical capacity $C$. Thus, a parameter Γ, known as SNR gap, is introduced to measure the relative performance of a system using a given coding scheme versus the theoretical capacity of the channel.

For a given margin Γ, defined by a fixed SER probability $Ps$ and a given coding scheme, the total number $R$ of bits per symbol that can be transmitted is given by [85]

$$R = \log_2 \left( 1 + \frac{1}{\Gamma} \frac{\alpha E_s}{N_0} \right).$$
(3.2)

This practical capacity is clearly lower than the theoretical capacity. In addition, the SNR gap is also known as normalized SNR since from (3.2) it can be written as

$$\Gamma = \frac{SNR}{2^R - 1}.$$
(3.3)

Thus, by knowing the channel state information at the transmitter and the SNR gap of the chosen coding scheme, we can find the number of information, in bit per symbol, that can be transmitted on the channel for a given transmit power density $E_s$.

The constellation types that are considered in the proposed LP-OFDM system are quadrature amplitude modulations (QAM). The SNR gap which determines the efficiency of the QAM transmission schemes can be obtained from the error rate curves for a given operating point that can be for example a target BER or a target SER. Figure 3.1 presents the practical capacity of the different QAM constellations for a given BER probability $Pb = 10^{-5}$ and a given SER probability $Ps = 10^{-5}$. Note that the capacity curves depicted in this figure are derived from classical capacity approximations given in [86]. The SNR gap Γ is equivalent to the distance between the different QAM operating points and the

Shannon limit. We notice that for a fixed SER value, taking into account the capacity approximations, $\Gamma$ remains constant when the constellation order is changed, which offers a real advantage for the implementation of resource allocation algorithms. This advantage is one of the main reasons why most of the allocation studies in the literature consider a target constant SER approach. On the other hand, for a fixed BER value, $\Gamma$ is not constant anymore, and it slightly decreases when the constellation order increases. For instance, at $Pb = 10^{-5}$, $\Gamma = 8.42 \text{ dB}$ for 2-QAM constellations and $\Gamma = 7.45 \text{ dB}$ for 512-QAM constellations, whereas at $Ps = 10^{-5}$, $\Gamma = 8.42 \text{ dB}$ for all the constellations. Note that the SNR gap variation in the case of fixed BER is reduced when the BER value is low ($Pb = 10^{-5}$). Although it is not commonly used, considering a constant BER approach has several advantages that will be detailed in Chapter 4.

The SNR gap of QAM constellations can be theoretically obtained from the SER probability expression which can be approximated, in the case of a Gray code, by [86]

$$Ps \approx 2erfc\left(\sqrt{\frac{3R}{2\left(2^R-1\right)}\frac{E_b}{N_0}}\right),\tag{3.4}$$

with $E_b / N_0 \gg 1$, where $E_b$ is the bit energy. Besides, the SNR can be expressed as
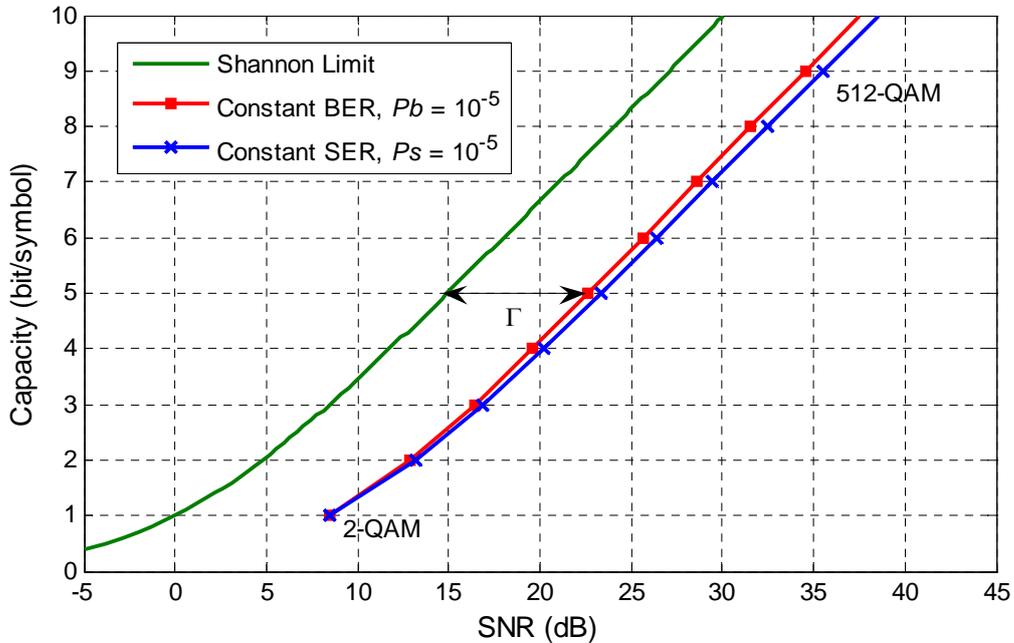


Figure 3.1: SNR gap for different QAM constellations, considering a constant BER and a constant SER.

$$SNR = \frac{E_s}{N_0} = \frac{RE_b}{N_0}.$$

(3.5)

Thus, by comparing with (3.2), we find that

$$Ps \approx 2erfc\left(\sqrt{\frac{3}{2}\Gamma}\right).$$

(3.6)

This equation shows that the SER probability is independent of the QAM constellation order, and consequently $\Gamma$ is constant for a given SER, which explains the results obtained in Figure 3.1.

On the other hand, in classical resource allocation problems, an additional margin $\gamma$, known as noise margin, is added to the SNR gap $\Gamma$. This margin ensures that the target error rate is reached even if the noise level is increased by a factor of $\gamma$. The total throughput in bit per symbol can then be written as

$$R = \log_2\left(1 + \frac{1}{\gamma\Gamma}\frac{\alpha E_s}{N_0}\right).$$

(3.7)

Thus, increasing the value of $\gamma$ improves the system robustness against noise, and hence the new operating point of the QAM constellations becomes at a distance of $(\Gamma + \gamma)$ dB from the Shannon limit.

### 3.1.3 Optimization strategies

When the CSI is known at the transmitter, adaptive bit and power loading algorithms can be proposed to distribute the available bits and power over the channels in an optimal way that maximizes performance and preserves a target QoS. The most common optimization problems are the maximization of the overall throughput for a given power constraint, known as rate maximization (RM), and the minimization of the energy for a given target throughput, known as margin maximization (MM). Note that the MM problem is equivalent to maximizing the system range.

Several loading algorithms have been proposed for multicarrier systems in the literature. These algorithms, which consider either RM or MM problem, can be classified in two types. The first type employs discrete greedy-type methods that incrementally allocate an integer number of bits at the expense of high computational complexity [87]. The second type treats the allocation problem using numerical methods, i.e. bit loading based on channel capacity approximations and bit error probability expressions, which in general results in real numbers for optimum bit allocation [88]–[91]. However, for practical applications,

the number of bits per subcarrier is restricted to integer values, and thus, this type of algorithms includes a final suboptimum bit-rounding step, which may sometimes lead to allocations that are far from the optimum. Therefore, the implementation of loading algorithms is usually a tradeoff between how close they come to the optimum allocation and how quickly they reach their final allocation. In this thesis, both types of algorithms are proposed for different resource allocation problems.

### 3.1.4 Resource allocation for UWB systems

In UWB systems, the channel response, described in Section 1.7, varies slowly in time and can be considered as quasi-static during one frame. Hence, the CSI can be sent to the transmitter by a simple feedback at the beginning of each frame, which does not increase the system complexity significantly. Thus, assuming the CSI knowledge at the transmitter, different adaptive loading algorithms can be proposed. However, to this date, research work on resource management for UWB communications is still limited. Some of the related existing work is summarized as follows.

In [92], a power allocation technique for clustered MB-OFDM is proposed. Each subband is divided into several groups of subcarriers, called clusters, and then each cluster is dynamically assigned a unique power in order to maximize the total system throughput. Results show that the proposed algorithm has a performance close to the one of a standard water-filling scheme, but with low complexity. In [93], a new scheme that efficiently allocates the sub-bands as well as the transmit power among all users and consequently reduces power consumption without compromising performance, is described. The sub-band assignment and power allocation strategy can be seen as an optimization problem whose goal is to minimize the overall transmit power provided that all users achieve their requested transmission rates and desired packet error rate, under a power spectral density constraint defined by the FCC regulations. The authors in [94] propose two power allocation schemes for single-band OFDM UWB transmissions with space-time codes, under the assumption of perfect and partial CSI at the transmitter. The results show that the water-filling scheme provides the smallest outage probability while the scheme with limited CSI feedback has lower feedback overhead and slight performance loss.

In [95], the radio resource sharing problem is formulated as a joint rate and power assignment problem that is central in multiuser UWB networks. The authors also propose suboptimal algorithms that dynamically assign the transmission rate and transmitted power of each node. The proposed radio resource sharing mechanism performs a handshaking procedure to establish a communication link. Specifically, the mechanism relies on two handshakes between the sender and its neighbors to obtain the required information for

link rate and power assignments. In [96], a radio resource allocation problem is also formulated to allocate transmitted power and data rate of each node such that the system throughput is maximized, while always reserving a specific amount of channel capacity for best effort traffic. In [97], the authors propose an algorithm which optimizes transmission efficiency of mobile UWB users by adapting the error protection to both channel status and QoS constraints. Performance in the case of a slowly time varying UWB channel is discussed.

## 3.2 OFDM system with a target symbol-error-rate

In this section, we present the classical rate and margin maximization principles that can be generally applied for OFDM systems, assuming knowledge of CSI at the transmitter. This study constitutes a reference to the next sections where a linear precoding component is added to the OFDM scheme. In this optimization study, we consider that the different subcarriers of the OFDM scheme have the same target SER.

### 3.2.1 System capacity

Let us first start by deriving the mathematical expression of the OFDM system capacity. As presented in Chapter 2, the received OFDM signal at the output of the FFT can be written as a vector

$$Y = HX + \bar{N} , \tag{3.8}$$

where $Y = [y_1 \dots y_n \dots y_N]^T$, $X = [x_1 \dots x_n \dots x_N]^T$, $\bar{N} = [\bar{n}_1 \dots \bar{n}_n \dots \bar{n}_N]^T$, with $n$ the subcarrier index and $N$ the total number of subcarriers in the system, and $H$ the channel matrix which contains the eigenvalues $h_n$ of the channel, i.e. the channel coefficients.

The system capacity can be derived from the mutual information between the transmitted and received signal, which can be expressed in the case of Gaussian signals with perfect CSI at the transmitter and receiver sides as

$$I(X \mid H, Y \mid H) = \log_2 \det \left[ I_N + \frac{1}{N_0} H R_X H^H \right], \tag{3.9}$$

with $I_N$ the identity matrix and $R_X$ the covariance matrix of $X$. The symbol $[.]^H$ denotes the Hermitian transpose of a vector or a matrix. By considering that the symbols transmitted on the different subcarriers are decorrelated, the covariance matrix $R_X$ becomes diagonal, with $E[x_n x_n^H] = E_n$, $\forall n$, with $E_n$ the energy of subcarrier $n$. The mutual information of the OFDM scheme, in bit per symbol, becomes

$$I = \log_2 \prod_{n=1}^{N} \left( 1 + |h_n|^2 \frac{E_n}{N_0} \right) = \sum_{n=1}^{N} \log_2 \left( 1 + |h_n|^2 \frac{E_n}{N_0} \right). \tag{3.10}$$

Thus, the total transmitted throughput, which is equivalent to the mutual information, is equal to the sum of the throughputs carried by the different subcarriers.

Taking into account the SNR gap of the real order QAM constellations and the noise margin described previously, the reachable OFDM throughput can then be derived from (3.10) as

$$R_{OFDM} = \sum_{n=1}^{N} R_n = \sum_{n=1}^{N} \log_2 \left( 1 + \frac{1}{\gamma\Gamma} |h_n|^2 \frac{E_n}{N_0} \right), \tag{3.11}$$

where $R_n$ is the reachable throughput of subcarrier $n$. The power constraint can be generally defined as a total power $E_T$ limitation, i.e. $\sum_n E_n \leq E_T$, or as a PSD constraint, i.e. $E_n \leq \tilde{E}_n, \forall n$, with $\tilde{E}_n$ the maximum authorized power on subcarrier $n$. Since the power limitations imposed by the FCC for UWB applications is in terms of PSD, we will only consider a PSD constraint in the sequel.

### 3.2.2   Rate maximization

In this section, the optimization strategy we start with is the maximization of the OFDM system throughput for a given target SER. The RM problem is defined as

$$\begin{cases} \max \sum_{n=1}^{N} \log_2 \left( 1 + \frac{1}{\gamma\Gamma} |h_n|^2 \frac{E_n}{N_0} \right), \\ \text{subject to} \quad E_n \leq \tilde{E}_n, \quad \forall n. \end{cases} \tag{3.12}$$

The throughput is maximized by judiciously distributing the energy $E_n$ on the different subcarriers. However, we notice that in this RM case, bit loading strategies are not useful since each subcarrier throughput only depends on its energy $E_n$, as we can see from (3.7).

The optimization study is carried out in two complementary steps. The first step finds out the optimal solution when the bits can have real values, and the second step considers the practical cases where the number of bits per subcarrier is restricted to integer values, and thus, a bit-rounding operation is carried out.

### 3.2.2.1    Real bit optimization

When the number of bits per subcarrier can have real values, it is obvious that the RM solution consists in allocating the maximum available energy to each subcarrier. Thus, the real bit and power allocation solution can be written as

$$
\begin{cases}
R_n = \log_2\left(1 + \dfrac{1}{\gamma\Gamma}|h_n|^2\,\dfrac{E_n}{N_0}\right), & \forall n, \\[2mm]
E_n = \tilde{E}_n, & \forall n.
\end{cases}
\tag{3.13}
$$

In this case, the practical capacity of the QAM constellations depicted in Figure 3.1 is reached. Note that if a total power constraint was considered instead of a PSD constraint, the solution would have been completely different, as described in [87].

### 3.2.2.2    Integer bit optimization

The solution is also straightforward in the case of integer bit optimization. In fact, the throughput of each subcarrier can be obtained by a simple rounding of the real number of bits per subcarrier. Note that the floor operation should be considered in order to respect the power limit and the SER probability. Thus, from (3.11) and (3.13) the integer bit and power allocation solution becomes

$$
\begin{cases}
\bar{R}_n = \lfloor R_n \rfloor, & \forall n, \\[2mm]
\bar{E}_n = \gamma\Gamma\dfrac{N_0}{|h_n|^2}\left(2^{\bar{R}_n} - 1\right), & \forall n,
\end{cases}
\tag{3.14}
$$

where $\bar{x}$ means that $x$ results from the integer bit optimization. Note that $\bar{E}_n$ given in (3.14) is always lower that the PSD limit $\tilde{E}_n$. However, in order to simplify calculations, each subcarrier is allocated the whole available energy, which also provides an additional noise margin.

As we will see from the numerical results later on, in the case of a PSD constraint, the OFDM scheme is not able to exploit all the available energy due to the bit rounding operation. In addition, the subcarriers with strong attenuations can even be unable to transmit a single bit if the PSD limit is too low. Thus, we will see that adding a linear precoding component to the OFDM scheme allows the system to benefit more from the available energy.

### 3.2.3   Margin maximization

The second allocation strategy that is described here is the maximization of the OFDM system noise margin $\gamma$ for a given target throughput $\tilde{R}$. From (3.11), we notice that $\gamma$ can not be directly expressed as a function of the throughput, thus we define for each subcarrier $n$ a noise margin $\gamma_n$ given by

$$\gamma_n = \frac{1}{\Gamma N_0} \frac{E_n |h_n|^2}{2^{R_n} - 1}. \tag{3.15}$$

It is clear that to maximize the noise margin, the whole available energy $E_n$ on subcarrier $n$ should be used, thus $E_n = \tilde{E}_n, \forall n$. The MM problem becomes

$$\begin{cases} \max \dfrac{1}{\Gamma N_0} \dfrac{\tilde{E}_n |h_n|^2}{2^{R_n} - 1}, & \forall n, \\[4mm] \text{subject to} \quad \displaystyle\sum_{n=1}^{N} R_n = \tilde{R}. \end{cases} \tag{3.16}$$

Hence, the objective is to maximize the noise margin of each subcarrier by efficiently distributing the $\tilde{R}$ bits on the different subcarriers.

### 3.2.3.1   Real bit optimization

As with the RM problem, we start with a real bit optimization study and then we move to a practical integer bit optimization. Maximizing $\gamma_n$ is equivalent to minimizing $1/\gamma_n$, and thus, the problem can be solved using Lagrange multipliers as follows

$$\mathrm{L}(R_n, \lambda) = \Gamma N_0 \frac{2^{R_n} - 1}{\tilde{E}_n |h_n|^2} + \lambda \sum_{n=1}^{N} R_n - \lambda \tilde{R}, \quad \forall n, \tag{3.17}$$

where $\mathrm{L}(.)$ is the Lagrangian function and $\lambda$ the Lagrange multiplier. After solving the derivative equation $d\mathrm{L}/dR_n = 0$, the subcarrier throughput $R_n$ can be written as a function of $\lambda$, we find

$$R_n = \log_2\left(-\frac{\lambda}{\ln 2} \frac{\tilde{E}_n |h_n|^2}{\Gamma N_0}\right). \tag{3.18}$$

The Lagrange multiplier $\lambda$ is then derived from the constraint equation in (3.16). We find

$$\lambda = -\ln 2 \frac{\Gamma N_0}{\tilde{E}_n} \frac{2^{\tilde{R}/N}}{\left(\prod_{n=1}^{N} |h_n|^2\right)^{1/N}}. \qquad (3.19)$$

Finally, the real bit and power allocation solution can be written as

$$\begin{cases} R_n = \dfrac{\tilde{R}}{N} + \log_2\left(|h_n|^2\right) - \dfrac{1}{N}\sum_{n=1}^{N}\log_2\left(|h_n|^2\right), \quad \forall n, \\[2mm] E_n = \tilde{E}_n, \quad \forall n. \end{cases} \qquad (3.20)$$

Note that when real bit allocation under a throughput constraint is considered, the noise margin maximization is equivalent to the total power minimization.

### 3.2.3.2 Integer bit optimization

In the MM case, the integer bit solution can not be simply obtained as in the RM case by rounding the real number $R_n$ of bits per subcarrier, since this procedure leads to a total throughput lower than the requested target throughput $\tilde{R}$. If $\overline{R}_n$ is the integer number of bits transmitted on subcarrier $n$, the noise margin $\overline{\gamma}_n$ of this subcarrier is given by

$$\overline{\gamma}_n = \frac{1}{\Gamma N_0} \frac{E_n |h_n|^2}{2^{\overline{R}_n} - 1}. \qquad (3.21)$$

Thus, the MM problem with integer bit optimization is expressed as

$$\begin{cases} \max \overline{\gamma}_n, \quad \forall n, \\[2mm] \text{subject to} \quad \sum_{n=1}^{N} \overline{R}_n = \tilde{R}. \end{cases} \qquad (3.22)$$

This problem can be solved using discrete greedy methods that incrementally allocate the bits to maximize the noise margin. Thus, bits can be distributed one by one on the different subcarriers, each new bit being allocated to the subcarrier with the strongest margin $\overline{\gamma}_n$. Note that the resulting noise margins $\overline{\gamma}_n$ are different from a subcarrier to another.

The MM algorithm that is proposed in this study is presented in Figure 3.2. This algorithm is derived from Hughes-Hartogs algorithm [87], and adapted to the case of a PSD constraint. In Figure 3.2, the algorithm starts with zero bits on each subcarrier, but can also start by allocating the maximum number of available bits to each subcarrier, which can be derived from (3.14). Note that the final number of bits per subcarrier should not exceed the

**1. Initialization**

Set $\bar{R}_n = 0, \quad \forall n$

**2. While** $\sum_{n=1}^{N} \bar{R}_n < \tilde{R}$

$\hat{n} = \arg\left[\max_{n,\,\bar{R}_n < R_{\max QAM}} \bar{\gamma}_n\left(\bar{R}_n + 1\right)\right]$

$\bar{R}_{\hat{n}} = \bar{R}_{\hat{n}} + 1$

**3. Output**

Return $\bar{R}_1 \cdots \bar{R}_N$
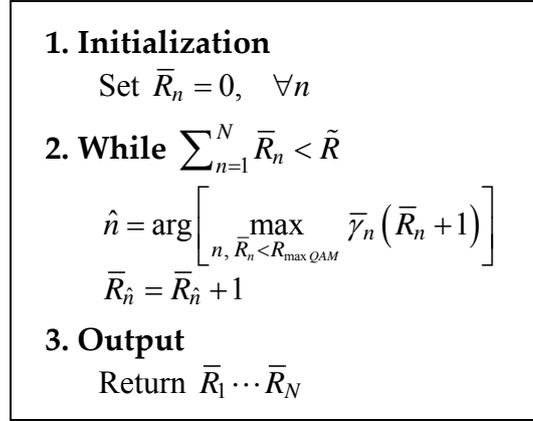
Figure 3.2: Margin maximization algorithm with integer bit allocation for OFDM systems.

maximum allowed constellation order $R_{\max QAM}$ in the system. Finally, the integer bit and power allocation solution becomes

$$\begin{cases} \bar{R}_n \text{ given by the greedy algorithm,} \quad \forall n, \\ \bar{E}_n = \tilde{E}_n, \quad \forall n. \end{cases} \tag{3.23}$$

The resulting noise margin $\gamma_n$ in the case of real bit optimization is constant on the whole frequency band. However, when we consider integer bit optimization, $\bar{\gamma}_n$ is not constant anymore. Thus, some subcarriers having a low noise margin will be weak against noise. Consequently, the OFDM scheme is not very efficient for noise margin maximization under a PSD constraint.

The numerical results of the allocation study for OFDM systems will be presented later on in comparison with the results of the allocation study carried out on LP-OFDM systems. These results show the advantage of adding a linear precoding component to the OFDM scheme.

## 3.3 LP-OFDM system with a target symbol-error-rate

After having presented the different resource allocation strategies applied to the OFDM system, we describe the different allocation algorithms that can be carried out on the proposed LP-OFDM scheme for high data rate UWB applications. In the LP-OFDM system described in Chapter 2, each user is allocated a whole MB-OFDM band of 528 MHz. Besides, one OFDM symbol consisting of $N = 100$ data subcarriers is transmitted on each band. Each band is then divided into $B$ blocks, each of them including a number of subcar-

riers equal to the spreading code length $L$. In addition, a number $K$ of spreading code sequences are used by each user to simultaneously transmit $K$ data symbols on a specific subset of subcarriers.

The LP-OFDM resource allocation study is divided in two parts. The first part considers a single QPSK constellation for all the subcarriers, as in the MB-OFDM solution. Different new resource allocation algorithms that optimize the system parameters, including the number $B$ of blocks and the number $K$ of codes, are proposed. In order to further improve the LP-OFDM system, the second part considers additional variable constellation orders. In this part, some of the algorithms have already been proposed for PLC applications [98]. Note that a perfect CSI is always considered available at the transmitter. Also note that this allocation study is applied on each MB-OFDM band, and consequently on each user, separately, and can be easily extended to the multi-user case.

### 3.3.1 System capacity

The capacity of a LP-OFDM system can be derived from the expression of the mutual information between the transmitted and received signals, before and after the spreading and despreading components. The received LP-OFDM signal at the output of the despreading component can be written as a vector

$$Y = \frac{1}{\sqrt{L}} C^H GHX + \frac{1}{\sqrt{L}} C^H G\overline{N} , \qquad (3.24)$$

where $C$ is the spreading matrix of dimension $L \times K$, defined in (2.19), and $G$ the equalizer matrix.

In our study, we consider simple equalization schemes in order not to increase the receiver complexity. The detection techniques that are used are zero forcing (ZF) and minimum mean-square error (MMSE). The ZF technique applies channel inversion and can eliminate multiple access interference by restoring the orthogonality between the spread data with an equalization coefficient chosen as

$$g_n = \frac{h_n^H}{|h_n|^2}, \quad \forall n . \qquad (3.25)$$

The drawback of ZF is that for small amplitudes of $h_n$ the equalizer enhances noise. On the other hand, the MMSE technique minimizes the mean square value of the error between the transmitted signal and the output of the equalizer. The resulting MMSE equalization coefficient can be expressed as

$$g_n = \frac{h_n{}^H}{|h_n|^2 + \dfrac{N_0}{E_n}}, \quad \forall n \,. \tag{3.26}$$

The MMSE detection offers better performance than the ZF technique, but for very high SNR, the performance of both techniques is quite similar. However, using MMSE leads to a very complex expression of the mutual information, which significantly increases the complexity of the allocation algorithms and sometimes the optimization problem can not be tractable theoretically. Thus, in the analytical study in Chapter 3 and Chapter 4, a ZF detection is considered instead of the MMSE. However, in the global LP-OFDM system study in Chapter 5, a MMSE detection will be used since it gives better performance.

Let us start by considering a single-block LP-OFDM system where all the subcarriers are linked together with a spreading code of length $L$. By using a ZF equalizer at the output of the OFDM demodulation, i.e. $G = H^{-1}$, the received signal becomes

$$Y = X + \frac{1}{\sqrt{L}} C^H H^{-1} \overline{N} \,. \tag{3.27}$$

Since vectors $X$ and $Y$ of size $C$ are Gaussians, the mutual information between them is given by [98]

$$I = \log_2 \det\left[ I_C - R_{X,Y} R_Y^{-1} \right], \tag{3.28}$$

with $I_C$ the identity matrix, $R_{X,Y}$ the covariance matrix of $X$ and $Y$, and $R_Y$ the autocovariance matrix of $Y$. Solving (3.28), we obtain

$$I_{single\text{-}block} = \sum_{k=1}^{K} \log_2\left( 1 + \frac{L^2}{\sum_{n=1}^{N}\left( 1/|h_n|^2 \right)} \frac{E_k}{N_0} \right), \tag{3.29}$$

with $E_k$ the energy of code $k$, which respects the PSD limit $\tilde{E}$ as follows

$$\sum_{k=1}^{K} E_k \le \tilde{E} \,. \tag{3.30}$$

As we can see, in the LP-OFDM system we talk about energy $E_k$ per code instead of the classical energy $E_n$ per subcarrier used in the OFDM system.

When we consider a multiple-block system, the mutual information can be expressed as the sum of the mutual informations corresponding to the different blocks, thus

$$I_{multiple-block} = \sum_{b=1}^{B} \sum_{k=1}^{K_b} \log_2 \left( 1 + \frac{L_b{}^2}{\sum_{n=1}^{L_b} \left( 1/|h_{n,b}|^2 \right)} \frac{E_{k,b}}{N_0} \right), \qquad (3.31)$$

where $K_b$ and $L_b$ are the number of codes and the spreading code length of block $b$, $h_{n,b}$ the frequency channel response of the $n^{th}$ subcarrier within block $b$, and $E_{k,b}$ the energy of code $k$ within block $b$, with

$$\sum_{k=1}^{K_b} E_{k,b} \le \tilde{E}, \quad \forall b. \qquad (3.32)$$

Note that if we choose $L = K = 1$ and $B = N$, the resulting mutual information becomes equal to the one of an OFDM system.

### 3.3.2 Fixed QPSK constellation order

In this optimization study, we only consider a single QPSK constellation for all the subcarriers in order not to increase the system complexity compared to the MB-OFDM solution. The proposed LP-OFDM system offers additional degrees of freedom that can be optimized even if a single constellation order is used [99]. In the sequel, the system parameters are optimized under fixed target throughput and variable throughput conditions.

The total throughput in bit per symbol of a LP-OFDM system using a ZF detection can be derived from (3.31) as

$$R_{LP-OFDM} = \sum_{b=1}^{B} \sum_{k=1}^{K_b} \log_2 \left( 1 + \frac{1}{\Gamma} \frac{L^2}{\sum_{n=1}^{L} \left( 1/|h_{n,b}|^2 \right)} \frac{E_{k,b}}{N_0} \right). \qquad (3.33)$$

Note that a unique spreading code length $L$ is used for the different blocks of the LP-OFDM system to reduce the system complexity.

### 3.3.2.1 Range improvement with fixed target throughput

In this paragraph, the objective is to maximize the noise margin and thus the total range of the LP-OFDM system when we have a fixed target throughput per OFDM symbol and a unique QPSK constellation as in the MB-OFDM solution. Hence, the objective is to find the optimal spreading code length *L*, and consequently the optimal number *B* of blocks, which maximizes the system range for a target throughput of 2*N* bits per OFDM symbol, where *N* is the total number of used subcarriers. Note that CSI is assumed available at the transmitter.

Using Lagrange multipliers in (3.32) and (3.33), we find that the optimal solution that maximizes the system throughput, or equivalently the system range when this throughput is fixed, is given by

$$\begin{cases} E_{k,b} = \tilde{E} / K, & \forall b, \\ K_b = K = L, & \forall b. \end{cases} \tag{3.34}$$

Then, the integer target throughput of the LP-OFDM system in bit per symbol should respect the following condition

$$\tilde{R} = 2N \le \sum_{b=1}^{B} L \log_2 \left( 1 + \frac{1}{\Gamma} \frac{L}{\sum_{n=1}^{L} \left( 1 / |h_{n,b}|^2 \right)} \frac{\tilde{E}}{N_0} \right). \tag{3.35}$$

Maximizing the system range is equivalent to maximizing the system noise margin. Thus, let us consider $\gamma_b$ the noise margin of block $b$, which can be seen as an amount of extra performance in the presence of unforeseen channel impairments. Introducing $\gamma_b$ in (3.35) gives

$$\tilde{R} = \sum_{b=1}^{B} L \log_2 \left( 1 + \frac{1}{\gamma_b} \frac{L}{\sum_{n=1}^{L} \left( 1 / |\hat{h}_{n,b}|^2 \right)} \right), \tag{3.36}$$

with
$$| \hat{h}_{n,b} |^2 = | h_{n,b} |^2 \frac{\tilde{E}}{\Gamma N_0}, \quad \forall n, \forall b. \tag{3.37}$$

Consequently, the noise margin per block is given by

$$\gamma_b = \frac{1}{3} \frac{L}{\sum_{n=1}^{L} \left( 1 / |\hat{h}_{n,b}|^2 \right)}, \quad \forall b. \tag{3.38}$$

**Theorem 3.1.** *To maximize the noise margin of a LP-OFDM system, and consequently the system range, a code length equal to the total number of useful subcarriers should be used.*

*Proof.* We want to maximize the minimum value of the noise margin $\gamma_b$. Let $\alpha$ and $\alpha_b$ be two variables such that

$$\gamma_b = \frac{1}{3} \frac{L}{(L/N)\alpha + \alpha_b}, \tag{3.39}$$

then we can write

$$\sum_{n=1}^{L}\frac{1}{|\hat{h}_{n,b}|^2} = \frac{L}{N}\sum_{b=1}^{B}\sum_{n=1}^{L}\frac{1}{|\hat{h}_{n,b}|^2} + \alpha_b = \frac{L}{N}\alpha + \alpha_b. \tag{3.40}$$

We have

$$\alpha = \sum_{b=1}^{B}\sum_{n=1}^{L}\frac{1}{|\hat{h}_{n,b}|^2} = \sum_{b=1}^{B}\left(\frac{L}{N}\alpha + \alpha_b\right) = \alpha + \sum_{b=1}^{B}\alpha_b. \tag{3.41}$$

Thus, we find that

$$\sum_{b=1}^{B}\alpha_b = 0. \tag{3.42}$$

Let $\gamma$ be the noise margin of the LP-OFDM system with one block. It can be written as

$$\gamma = \frac{1}{3}\frac{L}{\alpha}. \tag{3.43}$$

Let $b'$ be such that $\gamma_{b'} > \gamma$, then $\alpha_{b'} < 0$. Hence, $\exists b''$ such that $\alpha_{b''} > 0$, that is $\gamma_{b''} < \gamma$, and $\min_b \gamma_b < \gamma$.

Thus, in order to maximize the system noise margin and consequently the system range for a given fixed throughput, the spreading code length should be equal to the total number $N$ of useful subcarriers, i.e. one single block should be used.

Consequently, an interesting result of this analytical study is that, although it was assumed available at the transmitter, the CSI is not needed in the case of range improvement with fixed target throughput and single QPSK constellation. This is due to the fact that in the optimal solution, the subcarriers are used within the same single block, independently of the channel condition. Furthermore, Theorem 3.1 shows that the LP-OFDM noise margin can never be lower than the OFDM noise margin. The LP-OFDM system range is therefore larger than the OFDM system range.

### 3.3.2.2 Range improvement with variable throughput

In this paragraph, we consider the case where the throughput of $2N$ bits per OFDM symbol of the MB-OFDM solution is not reachable at very high attenuation levels. The MB-OFDM constraints are then relaxed and lower throughputs are authorized.

In a general approach with variable throughput, the number $C$ of codes can be lower than the code length $L$ and Theorem 3.1 is not applicable anymore. In this case, a multiple-block configuration has to be considered and each block can exploit its own code length. But finding the optimal block sizes amounts to resolving a complex combinational optimi-

zation problem that can not be reduced to an equivalent convex problem. Then, no analytical solution exists and the optimal solution can only be obtained following exhaustive search [100]. In order to avoid prohibitive computations, we assume a single-block configuration system.

**Theorem 3.2.** *The optimal number of codes that should be used to maximize the range of a LP-OFDM system using a QPSK constellation is equal to $K = \lfloor L(2^{R/L} - 1)/3 \rfloor$, with L the spreading code length and R the single-block optimal non-integer throughput given by*

$$R = L \log_2 \left( 1 + \frac{L}{\sum_{n=1}^{L} \left( 1/|\hat{h}_n|^2 \right)} \right), \tag{3.44}$$

*with* 
$$|\hat{h}_n|^2 = |h_n|^2 \frac{\tilde{E}}{\Gamma N_0}, \quad \forall n. \tag{3.45}$$

*Proof.* When the optimal number $K$ of codes is used, the LP-OFDM system should benefit the most from the available energy. In addition, $K$ is always smaller or equal to $L$ and the total system energy can never exceed the PSD limit defined by the regulation authorities. Hence, respecting these conditions, and considering a QPSK constellation, the optimal value of $K$ should satisfy the following two equations

$$\begin{cases} \tilde{E} - \sum_{k=1}^{K} E_k = \frac{L}{\alpha} \left( 2^{R/L} - 1 \right) - \frac{K}{\alpha} \left( 2^2 - 1 \right) \geq 0, \\[3mm] \tilde{E} - \sum_{k=1}^{K+1} E_k = \frac{L}{\alpha} \left( 2^{R/L} - 1 \right) - \frac{K+1}{\alpha} \left( 2^2 - 1 \right) < 0, \end{cases} \tag{3.46}$$

with 
$$\alpha = \frac{L^2}{\sum_{n=1}^{L} \left( \tilde{E}/|\hat{h}_n|^2 \right)}. \tag{3.47}$$

Solving (3.46), we find that the optimal number of codes that maximizes the LP-OFDM system range is equal to

$$K = \left\lfloor L \left( 2^{R/L} - 1 \right)/3 \right\rfloor. \tag{3.48}$$

Since $K \leq L$, the maximum reachable throughput for a given code length L is written as

$$R(L) = 2 \times \min\left\{\left\lfloor \frac{L}{3}\left(2^{R/L} - 1\right)\right\rfloor, L\right\}$$

$$= 2 \times \min\left\{\left\lfloor \frac{L^2}{3\sum_{n=1}^{L}\left(1/\mid \hat{h}_n \mid^2\right)}\right\rfloor, L\right\}.$$

(3.49)

Thus, the maximum reachable throughput of the LP-OFDM system using the optimal code length and number of codes can be obtained from

$$R_{\max} = \max_{1 \leq L \leq N}\left\{R(L)\right\}.$$

(3.50)

Consequently, a low complexity algorithm that derives the optimal code length and number of codes can be proposed for the LP-OFDM system. This algorithm can be advantageously exploited for high attenuation levels since it significantly increases the system range when the channel response is critical. In addition, these improvements can be obtained without changing the radio-frequency front end of the MB-OFDM solution.

### 3.3.2.3 Numerical results

After having described the different allocation strategies that can be carried out on the LP-OFDM system using a single QPSK constellation order and under a target SER approach, we present the simulations performed on the first three bands (3.1–4.7 GHz) of the MB-OFDM solution using the UWB channel model CM1. The transmitted PSD is $\tilde{E} = -41.3$ dBm/MHz and the noise density is $N_0 = -114$ dBm/MHz. In addition, for both systems we consider $N = 100$ data subcarriers per band, as in the MB-OFDM solution.

Figure 3.3 represents the total throughput per OFDM symbol of a single-user OFDM system and a single-user LP-OFDM system using the TFC distribution of the MB-OFDM solution, for different channel attenuation levels. The curve "Single-block LP-OFDM" is obtained by applying (3.35) and Theorem 3.1, and consequently by using a single-block LP-OFDM system with a code length $L = 100$. The curve "Adaptive LP-OFDM" is obtained by using (3.49) and (3.50) for different attenuation levels. With the OFDM scheme of the WiMedia solution, presented here as reference, the total throughput of 200 bit/symbol (100 data subcarriers with a QPSK constellation) is not reachable at attenuation levels higher than 46 dB, whereas the proposed LP-OFDM system using a single block of length $L = 100$ is able to transmit 200 bit/symbol until a 61 dB level. Consequently, a range gain of 15 dB is obtained. Moreover, when we optimize *L* and *K* of the LP-OFDM system, we are able to transmit data at much higher attenuation levels (until 84 dB), and the reachable range and throughput with adaptive LP-OFDM are always larger than the

adaptive OFDM system ones. With the called adaptive OFDM scheme, the number of QPSK modulated subcarriers can vary from 100 to 0, contrarily to the WiMedia solution where the number of active subcarriers is always equal to 100.
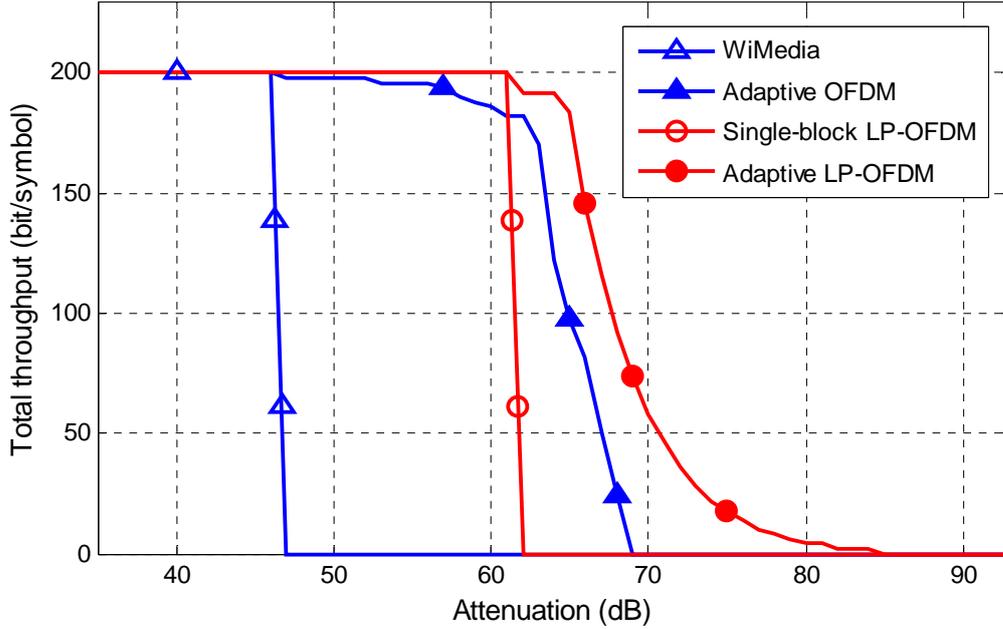


Figure 3.3: Total throughput per OFDM symbol of a single-user system with a unique QPSK constellation.

Figure 3.4 gives the optimal values of $L$ and $K$ obtained by applying the low complexity algorithm that maximizes the LP-OFDM system range for high attenuation levels. We notice that at attenuation levels lower than 62 dB, the optimal configuration is $K = L = 100$, and consequently, a single block should be used as explained before. However, at high attenuation levels when the target throughput of the WiMedia solution is not reachable, $K$ is not necessarily equal to $L$ in order to maximize the system range.

Through this analytical study on LP-OFDM with fixed constellation order, we have highlighted the fact that the LP-OFDM waveform has the capability to offer larger range than the non-precoded waveform of the WiMedia solution. To achieve such improvement, specific algorithms derived in this section have to be applied to get an adequate configuration of the precoding process, namely, in terms of spreading code length and number of codes.
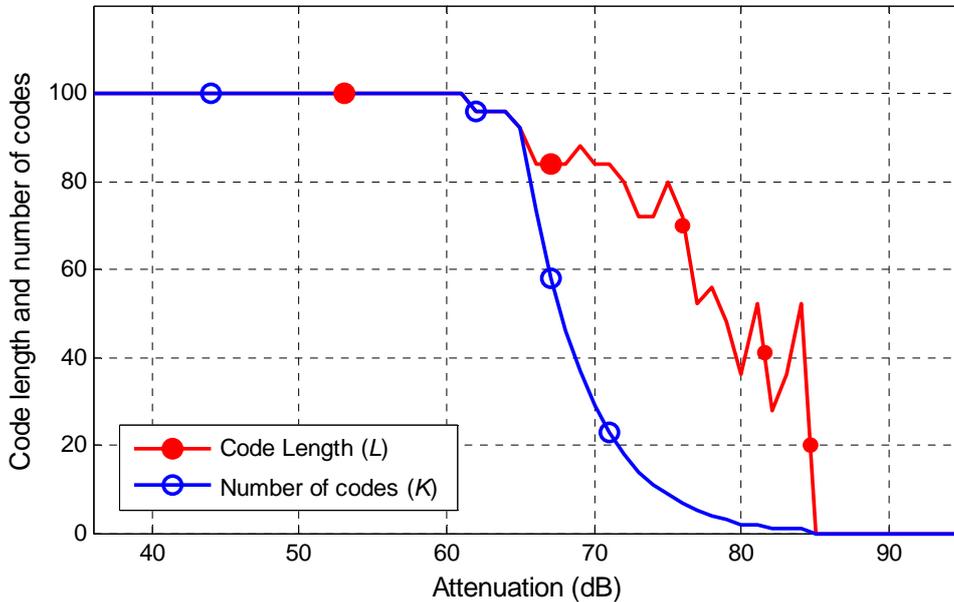
Figure 3.4: Optimal length *L* and number *K* of spreading codes that maximize the range of a single-user LP-OFDM system with a unique QPSK constellation.

The main result to keep in mind for the global system study in Chapter 5 is that the optimal solution to maximize the system range for a given throughput is to choose a code length equal to the number of used subcarriers ($L = N$). Note that this result strictly holds when a target SER approach is considered with a unique SNR gap $\Gamma$ for the whole system. However, even if a high range gain of about 15 dB has been intrinsically obtained without channel coding by the addition of the LP component, the performance of the two systems will be closer when considering the global chain with channel coding in Chapter 5.

### 3.3.3 Variable constellation orders

To further improve the LP-OFDM system, we move away from the MB-OFDM proposal and we consider variable constellations (BPSK, QPSK, 8-QAM and 16-QAM) [101]. Constellation orders higher than 16-QAM are not used in order not to significantly increase the system complexity compared to the complexity of the MB-OFDM system. Note that when a 16-QAM constellation is used, which is also the case in the MB-OFDM proposal for data rates using a DCM, one or two additional bits are needed for the analog-to-digital conversion. Besides, CSI is assumed available at the transmitter. As in the allocation study for OFDM systems in Section 3.2, we consider the RM and MM problems under a target SER approach.

### 3.3.3.1   Rate maximization

The maximization of the LP-OFDM system throughput is carried out in two steps. First, we consider a single-block LP-OFDM system, and then we move to a global multiple-block study.

### Single-block LP-OFDM system

The RM problem for a LP-OFDM system composed of a single block of length $L$ is defined as

$$\begin{cases} \max \sum_{k=1}^{K} \log_2 \left( 1 + \dfrac{1}{\Gamma} \dfrac{L^2}{\sum_{n=1}^{L} \left( 1/|h_n|^2 \right)} \dfrac{E_k}{N_0} \right), \\ \text{subject to} \quad \sum_{k=1}^{K} E_k \leq \tilde{E}. \end{cases} \tag{3.51}$$

Note that the target SER is represented by its equivalent SNR gap $\Gamma$. From (3.51), we notice that the throughput is maximized when $\sum_{n=1}^{L} \left( 1/|h_n|^2 \right)$ is minimized, and thus when large values of $h_n$ are considered. Consequently, the $L$ channel responses $h_n$ having the largest amplitudes have to be selected out of the $N$ available responses. The RM problem can be solved using Lagrange multipliers as follows

$$\mathrm{L}\left( E_k, \lambda \right) = \sum_{k=1}^{K} \log_2 \left( 1 + \dfrac{1}{\Gamma} \dfrac{L^2}{\sum_{n=1}^{L} \left( 1/|h_n|^2 \right)} \dfrac{E_k}{N_0} \right) + \lambda \sum_{k=1}^{K} E_k - \lambda \tilde{E}, \quad \forall k, \tag{3.52}$$

where $\lambda$ is the Lagrange multiplier. After solving the derivative equation $d\mathrm{L}/dE_k = 0$, the optimal energy per code becomes

$$E_k = \frac{\tilde{E}}{K}, \quad \forall k. \tag{3.53}$$

Thus, the total energy should be equally distributed on the different codes. The total real throughput of the single-block system is then given by

$$R = K \log_2 \left( 1 + \frac{1}{\Gamma} \frac{L^2}{\sum_{n=1}^{L} \left( 1/|h_n|^2 \right)} \frac{\tilde{E}}{KN_0} \right). \tag{3.54}$$

Equation (3.54) is strictly increasing with the variable $K$, when $K > 0$, i.e. $R$ is maximized when $K$ is maximal. Thus, the optimal number of codes is equal to $K = L$. Consequently, the total real throughput of the single-block system becomes

$$R = L \log_2 \left( 1 + \frac{1}{\Gamma} \frac{L}{\sum_{n=1}^{L} \left( 1/|h_n|^2 \right)} \frac{\tilde{E}}{N_0} \right). \tag{3.55}$$

Hence, the real bit and power allocation solution can be written as

$$\begin{cases} R_k = R/L, & \forall k, \\ E_k = \tilde{E}/L, & \forall k. \end{cases} \tag{3.56}$$

In the case of integer bit optimization, one solution would be to simply round the real number $R_k$ of bits per subcarrier, and thus to consider an integer number of bits per code equal to $\bar{R}_k = \lfloor R/L \rfloor, \forall k$. This solution clearly respects the PSD limitations but several bits might be lost due to this rounding operation, as the energy constraint is per block and not per code. An optimal solution for this problem is given in [102]. It shows that the optimal bits distribution would be to allocate $\lfloor R/L \rfloor + 1$ bits to $m$ codes and $\lfloor R/L \rfloor$ bits to the remaining $L - m$ codes, where $m$ is an integer number given by

$$m = \left\lfloor L \left( 2^{R/L - \lfloor R/L \rfloor} - 1 \right) \right\rfloor. \tag{3.57}$$

Finally, the integer bit and power allocation solution for a single-block system becomes

$$\begin{cases} \bar{R}_k = \lfloor R/L \rfloor + 1, & \forall k \in [1:m], \\ \bar{R}_k = \lfloor R/L \rfloor, & \forall k \in [m+1:L], \\ \bar{E}_k = \frac{\Gamma}{L^2} \sum_{n=1}^{L} \frac{N_0}{|h_n|^2} \left( 2^{\bar{R}_k} - 1 \right), & \forall k, \end{cases} \tag{3.58}$$

with $R$ the total real throughput given by (3.55) and $m$ given by (3.57). The total system integer throughput becomes

$$\bar{R} = \left\lfloor L(2^{R/L - \lfloor R/L \rfloor} - 1) \right\rfloor + L \lfloor R/L \rfloor. \tag{3.59}$$

**Multiple-block LP-OFDM system**

In the case of a LP-OFDM system composed of $B$ blocks having the same length $L$, the RM problem can be written as

$$
\begin{cases}
\max \sum_{b=1}^{B} \sum_{k=1}^{K} \log_2 \left( 1 + \frac{1}{\Gamma} \frac{L^2}{\sum_{n=1}^{L} \left( 1/|h_{n,b}|^2 \right)} \frac{E_{k,b}}{N_0} \right), \\
\\
\text{subject to} \quad \sum_{k=1}^{K} E_{k,b} \leq \tilde{E}, \quad \forall b.
\end{cases}
\tag{3.60}
$$

Before solving the RM problem, let us first distribute the system subcarriers on the different $B$ blocks. The optimal subcarriers distribution that maximizes the system throughput would be to sort the subcarriers according to the amplitude of their frequency responses, before distributing them on the different blocks [102]. Maximizing the total multiple-block system throughput is equivalent to maximizing the individual throughputs of the different blocks. Thus, from (3.56), the real bit and power allocation solution can be written as

$$
\begin{cases}
R_{k,b} = R_b / L, & \forall k, \forall b, \\
\\
E_{k,b} = \tilde{E} / L, & \forall k, \forall b,
\end{cases}
\tag{3.61}
$$

where $R_b$ is the optimal real throughput of block $b$, which can be derived from (3.55) as

$$
R_b = L \log_2 \left( 1 + \frac{1}{\Gamma} \frac{L}{\sum_{n=1}^{L} \left( 1/|h_{n,b}|^2 \right)} \frac{\tilde{E}}{N_0} \right).
\tag{3.62}
$$

The integer bit optimization solution can also be derived from the single-block study. Thus, the integer bit and power allocation solution of a multiple-block system becomes

$$
\begin{cases}
\overline{R}_{k,b} = \lfloor R_b / L \rfloor + 1, & \forall k \in [1 : m_b], \forall b, \\
\\
\overline{R}_{k,b} = \lfloor R_b / L \rfloor, & \forall k \in [m_b + 1 : L], \forall b, \\
\\
\overline{E}_{k,b} = \frac{\Gamma}{L^2} \sum_{n=1}^{L} \frac{N_0}{|h_{n,b}|^2} \left( 2^{\overline{R}_{k,b}} - 1 \right), & \forall k, \forall b,
\end{cases}
\tag{3.63}
$$

where $m_b$ is given by

$$m_b = \left\lfloor L\left(2^{R_b/L - \lfloor R_b/L \rfloor} - 1\right)\right\rfloor .$$

(3.64)

We notice that for $L = 1$, similar results as the ones of an OFDM system, presented in Section 3.2, are obtained.

A resource allocation algorithm based on this study can be proposed for LP-OFDM systems. This algorithm increases the system throughput considerably when applied to a LP-OFDM scheme with variable constellations as we will see later on in the numerical results section. In addition, the LP-OFDM system range is indirectly improved compared to the OFDM system range and the adaptive system is able to transmit data at very low attenuation levels.

### 3.3.3.2 Margin maximization

As with the RM problem, the maximization of the LP-OFDM system noise margin, and consequently the system range, is carried out in two steps. First we consider a single-block LP-OFDM system, and then we move to a global multiple-block study.

**Single-block LP-OFDM system**

To maximize the noise margin γ of the LP-OFDM system composed of a single block of length $L$, the whole available power should be used, thus $\sum_{k=1}^{K} E_k = \tilde{E}_k, \forall k$. This noise margin can be derived from (3.51) as

$$\gamma = \frac{\tilde{E}}{\Gamma N_0} \frac{L^2}{\sum_{n=1}^{L}\left(1/|h_n|^2\right)} \frac{1}{\sum_{k=1}^{K}\left(2^{R_k} - 1\right)} .$$

(3.65)

The MM problem is then defined as

$$\begin{cases} \max \gamma, \\ \text{subject to} \quad \sum_{k=1}^{K} R_k = \tilde{R}. \end{cases}$$

(3.66)

Maximizing γ is equivalent to minimizing $1/\gamma$, and thus, the problem can be solved using Lagrange multipliers. The real bit and power allocation solution becomes

$$\begin{cases} R_k = \tilde{R}/L, & \forall k, \\ E_k = \tilde{E}/L, & \forall k. \end{cases}$$

(3.67)

Thus, the noise margin of the single-block system is written as

$$\gamma = \frac{\tilde{E}}{\Gamma N_0} \frac{L}{\sum_{n=1}^{L} \left(1/|h_n|^2\right)} \frac{1}{2^{\tilde{R}/L} - 1}. \tag{3.68}$$

In the case of integer bit optimization, we have seen in the previous section that the optimal bits distribution would be to allocate $\lfloor \tilde{R}/L \rfloor + 1$ bits to $m$ codes and $\lfloor \tilde{R}/L \rfloor$ bits to the remaining $L-m$ codes. Since we have a target throughput $\tilde{R}$, $m$ should respect the equation $m\left(\lfloor \tilde{R}/L \rfloor + 1\right) + (L-m)\lfloor \tilde{R}/L \rfloor = \tilde{R}$, and we find

$$m = \tilde{R} - L\lfloor \tilde{R}/L \rfloor. \tag{3.69}$$

Thus, the integer bit and power allocation solution for a single-block system becomes

$$\begin{cases} \overline{R}_k = \lfloor \tilde{R}/L \rfloor + 1, & \forall k \in [1:m], \\[2mm] \overline{R}_k = \lfloor \tilde{R}/L \rfloor, & \forall k \in [m+1:L], \\[2mm] \overline{E}_k = \dfrac{2^{\overline{R}_k} - 1}{\sum_{k=1}^{L}\left(2^{\overline{R}_k} - 1\right)} \tilde{E}, & \forall k. \end{cases} \tag{3.70}$$

Consequently, the noise margin of the single-block system is given by

$$\overline{\gamma} = \frac{\tilde{E}}{\Gamma N_0} \frac{L}{\sum_{n=1}^{L}\left(1/|h_n|^2\right)} \frac{1}{2^{\lfloor \tilde{R}/L \rfloor}\left(\tilde{R}/L - \lfloor \tilde{R}/L \rfloor + 1\right) - 1}. \tag{3.71}$$

## Multiple-block LP-OFDM system

The noise margin $\gamma_b$ of each block $b$ of the multiple-block system can be derived from (3.68) as

$$\gamma_b = \frac{\tilde{E}}{\Gamma N_0} \frac{L^2}{\sum_{n=1}^{L}\left(1/|h_{n,b}|^2\right) \sum_{k=1}^{K}\left(2^{R_{k,b}} - 1\right)}. \tag{3.72}$$

The RM problem is then written as

$$\begin{cases} \max \gamma_b, & \forall b, \\[2mm] \text{subject to} \quad \sum_{b=1}^{B}\sum_{k=1}^{K} R_{k,b} = \sum_{b=1}^{B} R_b = \tilde{R}. \end{cases} \tag{3.73}$$

Using Lagrange multipliers, the real throughput of each block is found equal to

$$R_b = \frac{\tilde{R}}{B} - \log_2\left(\sum_{n=1}^{L}\frac{1}{|h_{n,b}|^2}\right) + \frac{1}{B}\sum_{b=1}^{B}\log_2\left(\sum_{n=1}^{L}\frac{1}{|h_{n,b}|^2}\right), \quad \forall b. \tag{3.74}$$

The real bit and power allocation solution becomes

$$\begin{cases} R_{k,b} = R_b / L, & \forall k, \forall b, \\ E_{k,b} = \tilde{E} / L, & \forall k, \forall b. \end{cases} \tag{3.75}$$

The MM problem with integer bit optimization is expressed as

$$\begin{cases} \max \overline{\gamma}_b, & \forall b, \\ \text{subject to} \quad \sum_{b=1}^{B} R_b = \tilde{R}. \end{cases} \tag{3.76}$$

As for the MM problem with OFDM systems, this problem can be solved using discrete greedy methods that incrementally allocate the bits to maximize the noise margin. A MM algorithm similar to the one proposed in Figure 3.2 but applied to multiple-block LP-OFDM can be used.

Finally, the integer bit and power allocation solution becomes

$$\begin{cases} \overline{R}_{k,b} = \lfloor \overline{R}_b / L \rfloor + 1, & \forall k \in [1:m_b], \forall b, \\ \overline{R}_{k,b} = \lfloor \overline{R}_b / L \rfloor, & \forall k \in [m_b+1:L], \forall b, \\ \overline{E}_{k,b} = \frac{2^{\overline{R}_{k,b}} - 1}{\sum_{k=1}^{L}\left(2^{\overline{R}_{k,b}} - 1\right)}\tilde{E}, & \forall k, \forall b, \end{cases} \tag{3.77}$$

where $\overline{R}_b$ is the integer throughput of block $b$ given by the greedy algorithm, and $m_b$ an integer variable equal to

$$m_b = \overline{R}_b - L\lfloor \overline{R}_b / L \rfloor. \tag{3.78}$$

The resulting LP-OFDM system noise margin is significantly larger than the noise margin of the OFDM system. This is due to the linear precoding component that groups weak subcarriers with stronger ones, which increases their robustness against noise.

### 3.3.3.3    Numerical results

After having described the different allocation strategies that can be carried out on the OFDM and LP-OFDM systems using variable constellation orders and under a target SER approach, we present the simulations performed on MB-OFDM bands 1, 2 and 3 (3.1–4.7 GHz) and bands 7, 8 and 9 (6.33–7.92 GHz). Bands 1, 2 and 3 represent the American UWB context whereas bands 7, 8 and 9 represent both the American and European contexts, as seen in Section 1.3. From Figure 1.2, we can see that the maximum transmitted PSD on these bands is $\tilde{E} = -41.3$ dBm/MHz for both contexts. Besides, we consider in these simulations $N = 100$ data subcarriers per band as with the MB-OFDM solution.

Figure 3.5 presents the average throughput per subcarrier of the adaptive OFDM and LP-OFDM systems. Here, the adaptive OFDM corresponds to a classical OFDM system with variable constellation orders and the adaptive LP-OFDM corresponds to a multiple-block LP-OFDM system using a code length $L = 16$ which is found to be the optimal code length in terms of throughput maximization. Note that the code length optimization is detailed later on in Chapter 4 and Chapter 5. Thus, 6 blocks of 16 subcarriers each can be used, and the remaining 4 subcarriers can be put together in an additional block of length 4. In addition, the subcarriers are ordered from the one having the highest channel response amplitude to the one having the lowest amplitude.

Complementarily to Figure 3.5, Figure 3.6 represents the effective PSD, i.e. the effective energy, which is used by the different subcarriers in the case of an OFDM system, or by the different codes in the case of a LP-OFDM system, to transmit the maximum number of bits. This PSD value can be derived from (3.14) for OFDM and from (3.63) for LP-OFDM. In the OFDM and LP-OFDM systems, a maximum number of four bits, equivalent to the highest possible constellation order of 16-QAM, are allocated to the subcarrier with the highest channel response amplitude. When the subcarrier index increases, i.e. the channel response amplitude decreases, the PSD required to transmit four bits is increased. If this PSD is lower than the FCC limit, these bits can be transmitted on this subcarrier, otherwise, the number of bits that can be transmitted is reduced until the effective PSD is lower than the FCC limit. For instance, if we take a look at the 14th subcarrier of the OFDM system, the PSD required to transmit four bits is -41.4 dBm/MHz, which is lower than the FCC mask. Thus, the four bits can be transmitted, contrarily to the 15th subcarrier that allows only three bits to be transmitted, which reduces the effective PSD to -44.4 dBm/MHz. Note that the last twelve subcarriers have critical channel response amplitudes that do not let them transmit any bit.
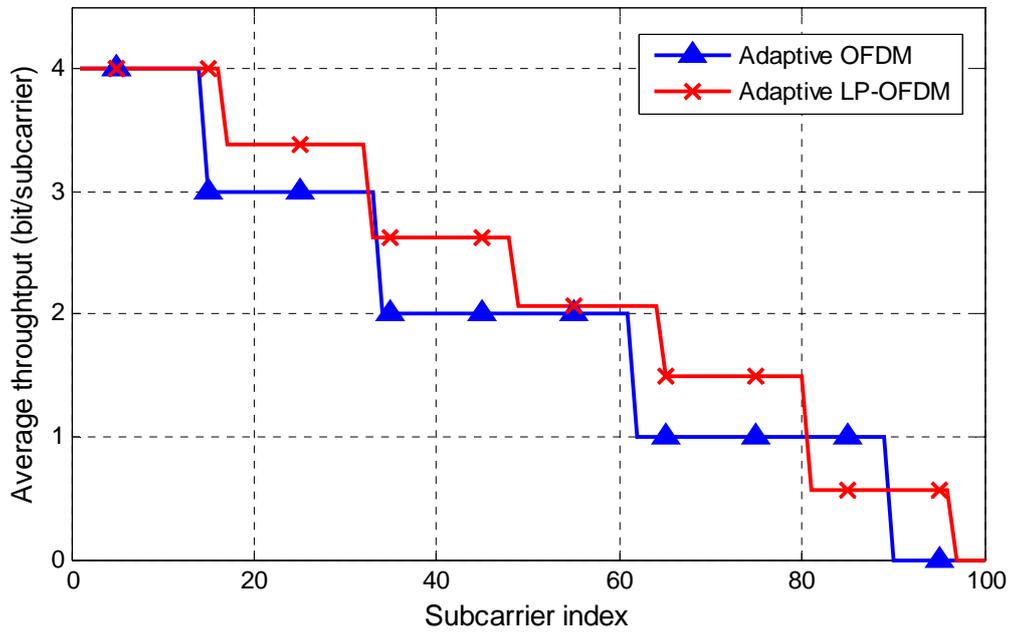
Figure 3.5: Average throughput per subcarrier for the adaptive OFDM and LP-OFDM systems using variable constellation orders.
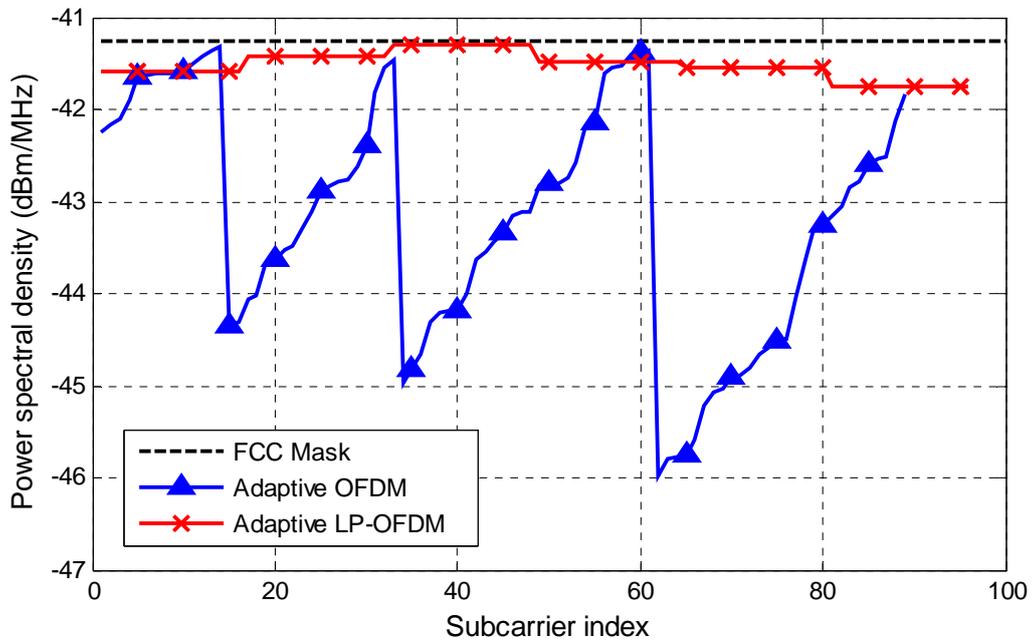


Figure 3.6: Effective transmitted power spectral density for the adaptive OFDM and LP-OFDM systems using variable constellation orders.

On the other hand, we can see that the LP-OFDM system provides an average subcarrier throughput that is most of the times higher than the one of an OFDM system. Note that the OFDM average throughput has an integer value whereas the LP-OFDM average throughput can have real values, since with LP-OFDM the integer bits are allocated to the codes and not to the subcarriers. For instance, subcarriers with indexes from 17 to 32 have the same average throughput of 3.375. This means that they are grouped in the same block of length $L=16$, where 6 codes are allocated 4 bits each and the remaining 10 codes are allocated 3 bits each, and thus a total of 54 bits are allocated to this block, which is equivalent to 3.375 bits per subcarrier. In addition, we notice from Figure 3.6 that the PSD of the adaptive LP-OFDM system is almost flat and very close to the FCC limit -41.3 dBm/MHz, whereas the PSD of the OFDM system varies significantly and is sometimes much lower than the FCC limit. This means that the LP-OFDM system benefits from the available PSD better than the OFDM system.

Figure 3.7 and Figure 3.8 represent the total throughput of a single user when the RM algorithm is applied with variable constellation orders (QPSK, 8-QAM and 16-QAM), taking into account the American and European contexts, respectively. When the resource allocation algorithm is applied to the LP-OFDM scheme, the throughput is equal to 400 bit/symbol at low attenuation levels. At high attenuation levels, the adaptive LP-OFDM range is always larger than the adaptive OFDM range (around 10 dB at critical attenuation levels). This is due to the energy gathering capability of the LP-OFDM scheme which can exploit, contrarily to OFDM, the residual energy conveyed by each subcarrier. Similar results are obtained for the different channel models (CM1 to CM4). In addition, using adaptive schemes for both OFDM and LP-OFDM systems improves the system throughput significantly compared to non-adaptive systems. For instance, we notice that the throughput of 200 bit/symbol is reachable until an attenuation level of 42 dB with WiMedia, which is limited to QPSK constellations, whereas with the adaptive OFDM system it is reachable at a 61 dB attenuation level, i.e. a 19 dB gain.

These results show that using adaptive schemes improves the systems performance significantly. In addition, the adaptive LP-OFDM system always outperforms the adaptive OFDM system in terms of total throughput. We should also note that since the highest possible constellation order is 16-QAM, only one or two additional bits are needed for the analog-to-digital conversion. Hence, the radio-frequency front-end complexity is not increased significantly compared to the MB-OFDM system using a unique QPSK constellation.
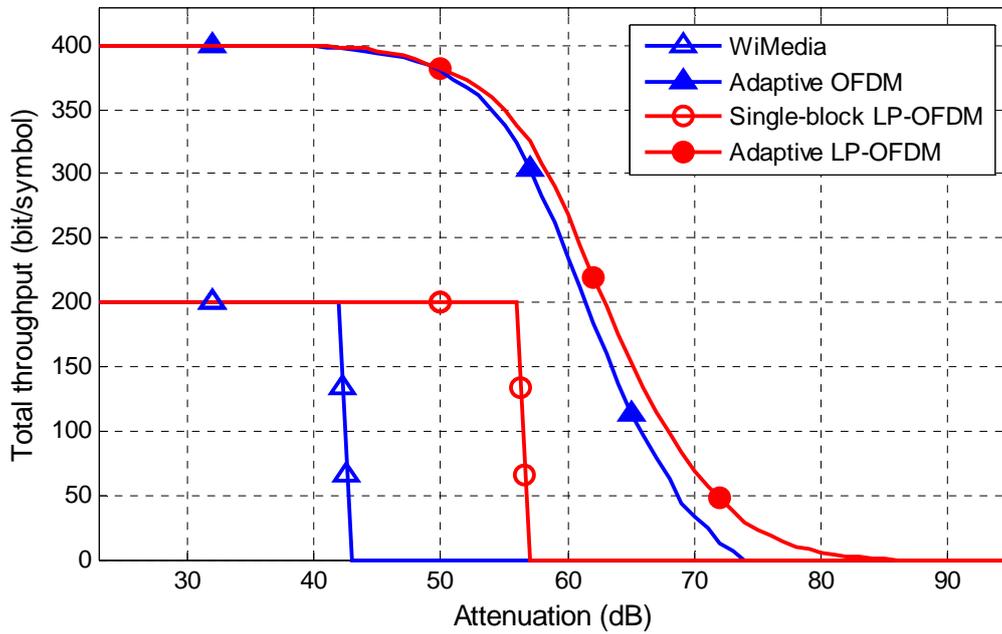
Figure 3.7: System throughput provided by the rate maximization algorithm with variable constellation orders, using channel model CM2 on MB-OFDM band 1 (American context).
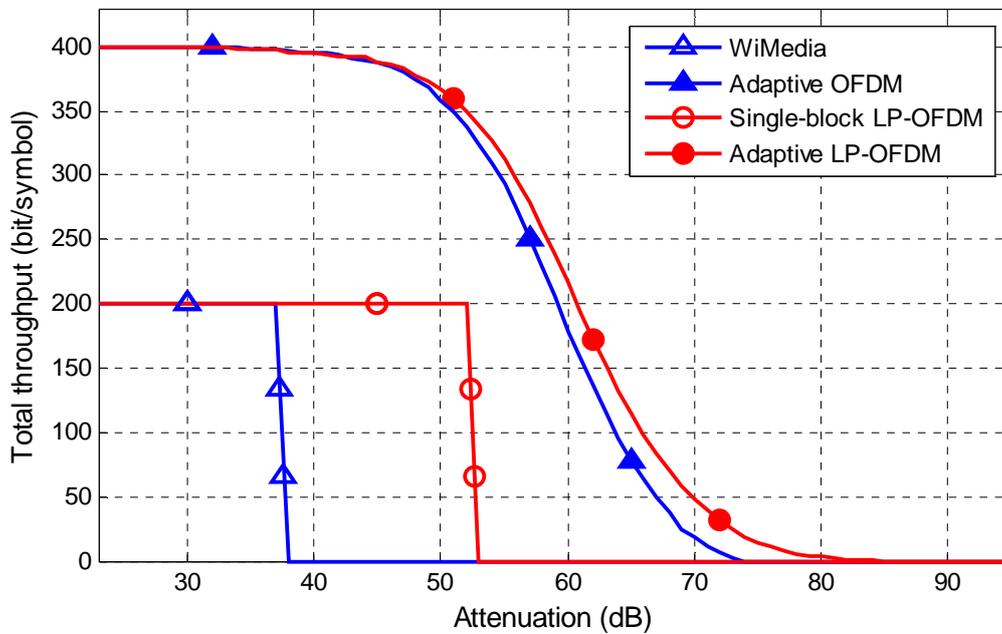


Figure 3.8: System throughput provided by the rate maximization algorithm with variable constellation orders, using channel model CM3 on MB-OFDM band 7 (European context).

## 3.4    Time-frequency codes optimization

### 3.4.1    Principle

In this section, an optional MB-OFDM system optimization study based on the time-frequency codes (TFC) allocation is proposed. In the MB-OFDM system of the WiMedia solution, unique logical channels corresponding to different users are defined by using a different TFC sequence for each user, as presented in Section 2.2.1.5. These codes provide frequency hopping from a MB-OFDM band to another at the end of each OFDM symbol. The configuration proposed in the WiMedia standard consists in choosing the TFC regularly without taking into account the channel response state of each user, as previously presented in Figure 2.6. Thus, this strategy lacks of the ability to optimally allocate the MB-OFDM bands.

The LP-OFDM system range can be efficiently increased by performing a dynamic TFC (DTFC) distribution which, contrarily to the WiMedia distribution, assigns the available bands to each user according to its channel condition [103]. Hence, different allocation strategies, such as total system margin maximization or equivalently total range maximization, can be proposed. Note that the DTFC distribution can be efficiently exploited whether the TFCs are assigned synchronously or asynchronously.

For instance, we consider three users transmitting simultaneously on the first three MB-OFDM bands, using three synchronous TFC sequences. In order to reduce interference, for every OFDM symbol, each band is occupied by only one of the three users. Thus, the number of unique possible distributions of the TFC sequences during three consecutive OFDM symbols can be found by solving a combinational problem: over one symbol duration, we have a permutation with order and without repetition of three users on three bands. The number of distributions per symbol duration is then equal to

$$d = \frac{Z!}{(Z-U)!} = 6 \,, \tag{3.79}$$

where $(.)!$ denotes the factorial function which returns the product result of all positive integers less than or equal to its argument value, $Z = 3$ is the number of bands and $U = 3$ the number of users. Consequently, a number of $6 \times 6 \times 6 = 216$ distributions are possible during three symbol durations. However, for each band, the order of users in time does not matter. Thus, the total number of unique TFC distributions is reduced from 216 to 55. A low complexity algorithm that selects, from the 55 possible TFC distributions, the optimal distribution that maximizes the total system range for example, can then be proposed.

On the other hand, some studies showing the advantage of using DTFC in the cross-layer design are presented in [104]. This paper exploits the use of DTFC combined with the QoS requirements provided by the MAC layer. This combination of the PHY and MAC layers improves the system performance, and ensures an efficient use of the spectrum in a multiple medium access demand, while respecting each user requirements. For instance, this cross-layer approach used with the adaptive TFC gives advantage to QoS users on best effort users in terms of error rate and quantity of resources.

### 3.4.2 Dynamic TFC and rate maximization algorithm

The dynamic TFC distribution study can be easily combined with the previous resource allocation strategies, with fixed and variable constellation orders, to constitute a global bit loading algorithm for OFDM and LP-OFDM systems. Thus, an algorithm combining dynamic TFC and RM with variable constellation orders is proposed in Figure 3.9.

### 3.4.3 Numerical results

Figure 3.10 and Figure 3.11 represent the total throughput over three consecutive OFDM symbols of a 3-user OFDM system and a 3-user LP-OFDM system, using channel model CM1. In Figure 3.10, non-adaptive systems with a unique QPSK constellation are considered. With the WiMedia system using the TFC distribution defined by the WiMedia solution, the three users are able to transmit $3 \times 3 \times 200 = 1800$ bits during the consecutive symbols until an attenuation level of 40 dB. At attenuation levels between 41 and 43 dB, only two users are able to transmit (1200 bit/3×symbol), at levels between 44 and 49 dB only one user is able to transmit, and at levels higher than 49 dB none of them is able to transmit. When applying the dynamic TFC (DTFC) algorithm to the WiMedia system, a range increase of more than 5 dB is obtained, and when applying DTFC to the LP-OFDM system, the system range becomes around 20 dB larger than the WiMedia initial system range.

In Figure 3.11, the same DTFC algorithm is applied to the adaptive OFDM and LP-OFDM systems. With the called adaptive OFDM scheme, the number of QPSK modulated subcarriers can vary from 100 to 0, contrarily to the WiMedia solution where the number of active subcarriers is always equal to 100. The adaptive LP-OFDM system in this figure is the system optimized using a fixed QPSK constellation order, i.e. by applying (3.49) and (3.50). We notice that the adaptive LP-OFDM system is able to reach an attenuation level of 89 dB. Moreover, when the DTFC is applied to the LP-OFDM system, the reachable range is increased, and for a given attenuation level, the throughput is also improved. Note that DTFC is more effective for the medium attenuation levels (levels be-

**1. Initialization**

   Set $\bar{R}_{k,b} = 0$ and $\bar{E}_{k,b} = 0$, $\forall k, \forall b$,

   $N = 100$ subcarriers,

   $S_b = \varphi$, $\forall b$,

   $H_{i,j} = $ channel response vector of user $i$ on band $j$,

   $Combin = \{Comb_1 \dots Comb_{55}\} = $ TFC combinations.

**2. For** $i = 1$ to 3 and $j = 1$ to 3,

   For $b = 1$ to $\lfloor N/L \rfloor$,

      find $S_b = $ best $L$ subcarriers in $H_{i,j}$,

      update $H_{i,j}$ : $H_{i,j} = H_{i,j} - S_b$,

      find the block throughput $R_b$ from (3.62),

      compute the code throughput,

         for $k = 1$ to $m_b$,

            $\bar{R}_{k,b} = \lfloor R_b / L \rfloor + 1$,

         for $k = m_b + 1$ to $L$,

            $\bar{R}_{k,b} = \lfloor R_b / L \rfloor$,

         with $m_b$ given in (3.64),

      $\bar{R}_{symbol} = \sum \bar{R}_{k,b}$.

**3. For** $Combin = Comb_1$ to $Comb_{55}$,

   Compute the system throughput over 3 symbols with 3 users,

      $\bar{R}_{system}(Combin) = \sum \bar{R}_{symbol}(Combin)$,

   $OptThroughput = \max(\bar{R}_{system})$,

   $OptTFC = Combin(OptThroughput)$.

**4. Output**

   Return *OptThroughput* and *OptTFC*.

Figure 3.9: Dynamic TFC and rate maximization algorithm with variable constellation orders for LP-OFDM systems.

tween 50 and 72 dB for adaptive OFDM, and levels between 58 and 77 dB for adaptive LP-OFDM). Similar results are obtained with CM2, CM3 and CM4 channel models.
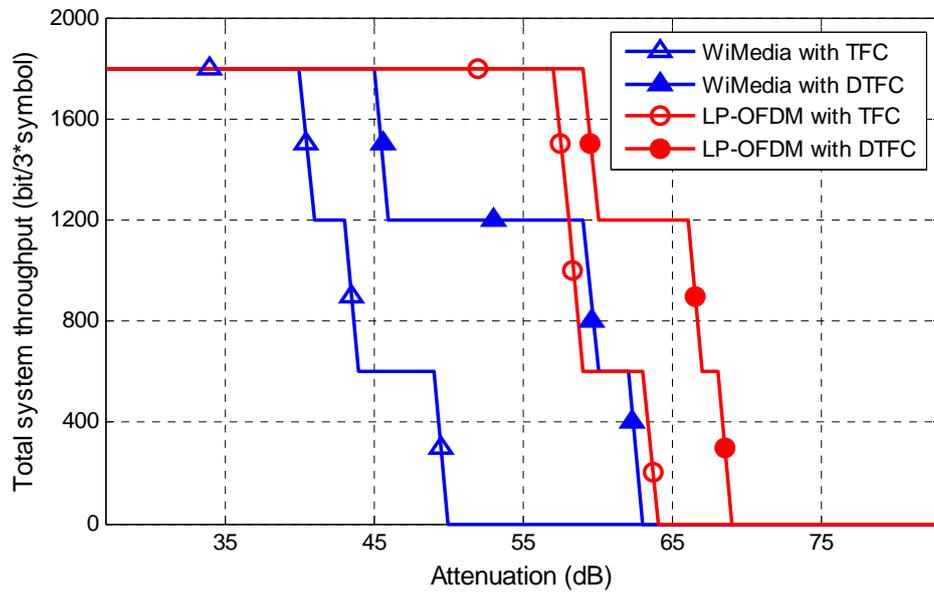
Figure 3.10: Total throughput of 3-user non-adaptive OFDM and LP-OFDM systems with classical TFC and dynamic TFC.
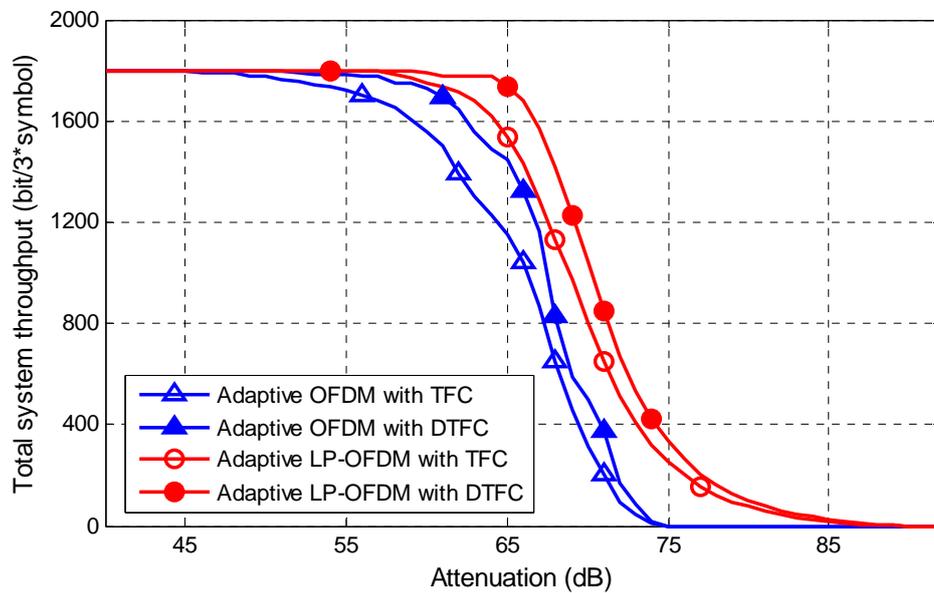


Figure 3.11: Total throughput of 3-user adaptive OFDM and LP-OFDM systems with classical TFC and dynamic TFC.

## 3.5 Conclusion

In this chapter, we have described the main adaptive resource allocation strategies that can be carried out on multicarrier systems, focusing on a classical target SER approach. Due to the slow time variations of the UWB channel, resource allocation can be efficiently exploited for UWB systems without significantly increasing the systems complexity. In fact, the UWB channel response can be considered as quasi-static during one frame and the CSI can be sent by a simple feedback to the transmitter at the beginning of each frame.

After having presented the classical rate and margin maximization solutions for OFDM systems, we moved to a new optimization study for LP-OFDM systems. First, we considered the case of a single constellation order as with the WiMedia solution, and then in order to further improve the LP-OFDM system, we considered variable constellation orders (BPSK, QPSK, 8-QAM and 16-QAM). Different low complexity resource allocation algorithms based on rate and margin maximization problems have been proposed. Furthermore, an additional system optimization study based on a dynamic TFC allocation was proposed. The numerical results of simulations carried out on the different adaptive and non-adaptive systems show that the LP-OFDM system outperforms the MB-OFDM system in terms of throughput and range. This is due to the spreading gain and the resource allocation flexibility provided by the linear precoding component.

On the other hand, the optimizations strategies carried out in this chapter did not take into account the channel coding scheme. However, the performance comparison of the global systems with channel coding, presented in Chapter 5, shows that the same tendency on the system behavior is obtained. Besides, a smart approach that modifies the proposed allocation algorithms to accommodate the coding gains relative to the channel coding schemes, at the expense of higher complexity, can be considered. This approach has been considered in [105] in the case of linear precoded discrete multitone modulation for power line communication. In fact, the SNR gap value for a given target SER or BER can be modified to carry the desired margin of the system as well as the coding gain of the channel coding scheme.

# Chapter 4

# Mean bit-error-rate minimization study

$\mathbf{A}$FTER having presented in the previous chapter the different resource allocation strategies that can be proposed for the LP-OFDM system following a classical SER approach, we propose here different allocation strategies for UWB based on a new mean BER approach. The idea is to optimize the LP-OFDM system performance taking into account the system mean BER value. For instance, the LP-OFDM system mean BER can be minimized to improve the system robustness for a given target throughput, or vice versa the system throughput can be maximized under a mean BER constraint. However, in this chapter we only present the case of mean BER minimization (MBM) for a given throughput. More information on the rate maximization strategies that can be considered under a fixed target mean BER can be found in [106].

In the sequel, we first describe the mean BER approach for resource allocation and we show its advantages. Then, we present an efficient resource allocation algorithm that reduces the mean BER of a LP-OFDM UWB system using only a single QPSK constellation. Besides, in order to further improve the system performance, we consider variable constellation orders and we propose a study that minimizes the mean BER of OFDM and LP-OFDM systems for a given target throughput. The simulation results show that the proposed algorithms reduce the system mean BER significantly.

## 4.1   Overview

In multicarrier systems, the resource allocation is generally formulated under a constant SER on every subcarrier as described in Chapter 3. One of the main reasons behind considering a target SER approach is that the approximated SNR gap $\Gamma$ remains constant when the QAM constellation order is changed. Consequently, the target system SER becomes equal to every subcarrier SER value. In general, the error rate limit is imposed by

the upper layers of the network and is given in terms of BER and not SER, since the symbols defined in the physical layer are different from the ones defined in upper layers. Thus, in this study, we propose new resource allocation strategies that take into account the system mean BER instead of the system SER.

Some authors have proposed bit loading algorithms that maximize the OFDM system throughput under a mean BER constraint on the OFDM symbol [107], [108]. The authors in [107] show that the target BER is rarely achieved when the SER is fixed on each subcarrier, and that target BER violations of up to 99% of the channel realizations can occur. This is the case of the SER approach proposed in [89]. In this chapter, we propose mean BER minimization (MBM) algorithms that reduce the system mean BER under a target throughput. This optimization problem, similarly to the margin maximization problem, improves the system robustness.

Figure 4.1 depicts the capacity of the different QAM constellations for different BER and SER operating points. Note that these capacity curves are derived from classical capacity approximations given in [86]. In this figure, we can see that for a given BER value, the approximated SNR gap $\Gamma$ varies with the constellation order, whereas for a given SER value, $\Gamma$ does not change. In addition, the SNR gap variation of the constellation orders we are considering in the proposed algorithms, mainly 2-QAM, 4-QAM, 8-QAM and 16-QAM, is not very large, and decreasing the BER operating point value reduces this variation. For instance, at a BER level of $Pb = 10^{-3}$, the SNR gap difference between the
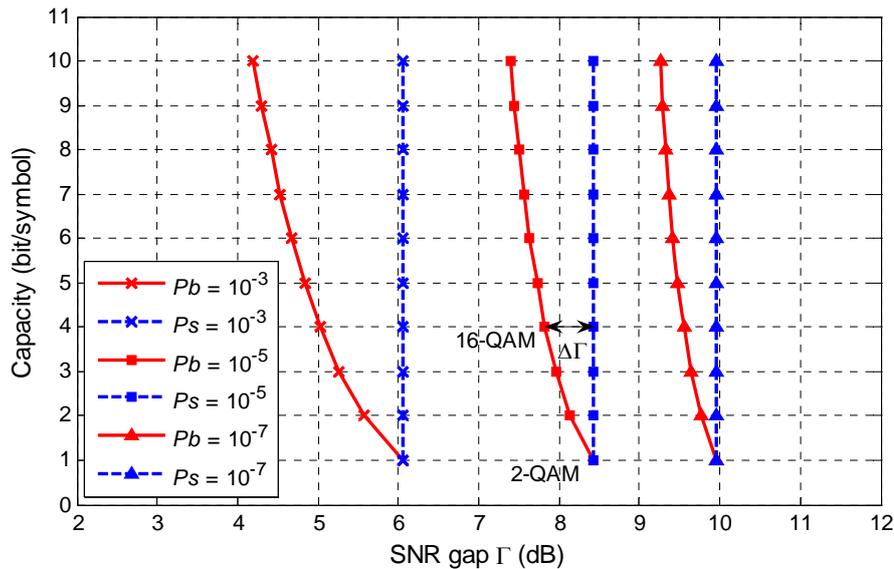


Figure 4.1: SNR gap variation for different QAM constellations and different BER and SER operating points.

2-QAM and 16-QAM constellations is $\Delta\Gamma = 1.05\,\text{dB}$, and at $Pb = 10^{-5}$, this difference is reduced to $\Delta\Gamma = 0.59\,\text{dB}$.

Although the SNR gap variation is not very large at low BER values, we consider in this study a practical approach using a variable SNR gap per subcarrier. Consequently, the allocation algorithms proposed in Chapter 3, which assume a constant SNR gap on all the subcarriers, are not applicable here.

Let us first give some analytical equations of the mean BER for different system configurations. The mean BER of a single-carrier system can be obtained using the following approximation [86]

$$Pb \approx \frac{Ps}{\log_2(M)}, \tag{4.1}$$

where $Ps$ and $M$ are the SER and order of the QAM constellation using Gray coding, respectively. In the case of multicarrier systems, the mean BER becomes [107]

$$Pb = \frac{\sum_{n=1}^{N} Ps_n}{\sum_{n=1}^{N} R_n} = \frac{\sum_{n=1}^{N}(R_n Pb_n)}{\sum_{n=1}^{N} R_n}, \tag{4.2}$$

where $N$ is the number of subcarriers, $R_n = \log_2(M_n)$ the number of bits allocated to subcarrier $n$ using a QAM constellation order $M_n$, and $Ps_n$ and $Pb_n$ the SER and BER for subcarrier $n$, respectively. When we consider a LP-OFDM system, the bits are allocated to the codes and not to the subcarriers as with OFDM systems. Thus, the mean BER of a single-block LP-OFDM system can be derived from (4.2) as

$$Pb = \frac{\sum_{k=1}^{K} Ps_k}{\sum_{k=1}^{K} R_k} = \frac{\sum_{k=1}^{K}(R_k Pb_k)}{\sum_{k=1}^{K} R_k}, \tag{4.3}$$

with $K$ the total number of codes in the block, $R_k$ the number of bits allocated to code $k$, and $Ps_k$ and $Pb_k$ the SER and BER for code $k$, respectively.

## 4.2 Fixed QPSK constellation order

In the new mean BER optimization approach, we first consider a single QPSK constellation for all the subcarriers in order not to increase the system complexity compared to the

MB-OFDM solution. In this case, the objective is to minimize the mean BER of the LP-OFDM system for a constant target throughput. As seen previously, the proposed LP-OFDM system offers additional degrees of freedom that can be optimized even if a single constellation order is used. In fact, the spreading code length $L$ and the number $B$ of blocks can be efficiently selected to minimize the system mean BER. In the sequel, this optimization study is carried out by first considering a simple single-block LP-OFDM system, and then moving to the case of a general multiple-block LP-OFDM system.

### 4.2.1  Single-block system

The throughput of a single-block LP-OFDM system in bit per symbol using a ZF detection can be derived from (3.33) as

$$R = \sum_{k=1}^{K} R_k = \sum_{k=1}^{K} \log_2 \left( 1 + \frac{1}{\Gamma_k} \frac{L^2}{\sum_{n=1}^{L} \left( 1/|h_n|^2 \right)} \frac{E_k}{N_0} \right), \tag{4.4}$$

where $R_k$ is the number of bits allocated to code $k$, $\Gamma_k$ the variable SNR gap relative to the QAM constellation order of code $k$, and $L$ the length of the single block, which is equal to the total number $N$ of subcarriers in this case. The MBM problem can be written as

$$\begin{cases} \min \dfrac{\sum_{k=1}^{K} \left( R_k P b_k \right)}{\sum_{k=1}^{K} R_k}, \\[2em] \text{subject to} \quad \sum_{k=1}^{K} E_k \leq \tilde{E} \\[2em] \text{and} \quad \sum_{k=1}^{K} R_k = \tilde{R}, \end{cases} \tag{4.5}$$

where $\tilde{E}$ is the PSD limit of the single block and $\tilde{R}$ the given target throughput. In this optimization study, we consider the maximum possible value of the throughput for a given QPSK constellation, which is obtained when the number $K$ of codes is equal to $L$. Consequently, we have $R_k = 2, \forall k$, and $\tilde{R} = 2N$ bits per OFDM symbol.

The BER for code $k$ using a single QPSK constellation can be derived from [86] and (4.4) as

$$Pb_k \approx \frac{1}{R_k} 2\left(1 - \frac{1}{\sqrt{2^{R_k}}}\right) erfc\left(\sqrt{\frac{3SNR}{2\left(2^{R_k}-1\right)}}\right),$$ (4.6)

$$Pb_k \approx \frac{1}{2} erfc\left(\sqrt{\frac{L^2 E_k}{2N_0} \frac{1}{\sum_{n=1}^{L}\left(1/|h_n|^2\right)}}\right).$$ (4.7)

The optimization problem can be solved using Lagrange multipliers in (4.5) as follows

$$L\left(E_k,\lambda\right) = \sum_{k=1}^{K} erfc\left(\sqrt{\alpha E_k}\right) + \lambda\left(\tilde{E} - \sum_{k=1}^{K} E_k\right),$$ (4.8)

with $$\alpha = \frac{L^2}{2N_0} \frac{1}{\sum_{n=1}^{L}\left(1/|h_n|^2\right)}.$$ (4.9)

After differentiating with respect to $E_k$, the Lagrange multiplier becomes

$$\lambda = -\sqrt{\frac{\alpha}{\pi}} \frac{e^{-\alpha E_k}}{\sqrt{E_k}}.$$ (4.10)

Equation (4.10) can be solved using the Lambert W function [110], which is defined as the inverse function of

$$f\left(w\right) = w e^{w},$$ (4.11)

where $e^{w}$ is the natural exponential function and $w$ a complex number. Thus, we find

$$\begin{cases} E_k = \dfrac{\tilde{E}}{L}, \quad \forall k, \\[3mm] \Gamma_k = \dfrac{L\tilde{E}}{3N_0} \dfrac{1}{\sum_{n=1}^{L}\left(1/|h_n|^2\right)}, \quad \forall k. \end{cases}$$ (4.12)

Consequently, the mean BER of a single-block LP-OFDM system using a QPSK constellation is given by

$$Pb = \frac{1}{2} erfc\left(\sqrt{\frac{L\tilde{E}}{2N_0} \frac{1}{\sum_{n=1}^{L}\left(1/|h_n|^2\right)}}\right).$$ (4.13)

The mean BER can also be written as a function of $E_b / N_0$, as follows

$$Pb = \frac{1}{2} erfc \left( \sqrt{\frac{LE_b}{N_0} \frac{1}{\sum_{n=1}^{L} \left( 1/ \mid h_n \mid^2 \right)}} \right), \qquad (4.14)$$

with $E_b = \tilde{E}/2$ the bit energy of the single-block LP-OFDM system using a QPSK constellation.

### 4.2.2 Multiple-block system

After having presented the simple case of a single-block LP-OFDM system, we move to the study of a general multiple-block LP-OFDM system using a single QPSK constellation. Let $B$ be the number of blocks, each having a different code length $L_b$. The mean BER of a multiple-block LP-OFDM system is given by

$$Pb = \frac{\sum_{b=1}^{B} \left( R_b Pb_b \right)}{\sum_{b=1}^{B} R_b}, \qquad (4.15)$$

where $Pb_b$ is the BER for block $b$ given from (4.13) by

$$Pb_b = \frac{1}{2} erfc \left( \sqrt{\frac{L_b \tilde{E}}{2N_0} \frac{1}{\sum_{n=1}^{L_b} \left( 1/ \mid h_{n,b} \mid^2 \right)}} \right), \qquad (4.16)$$

and $R_b$ the number of bits in block $b$, given in the case of a unique constellation order by

$$R_b = R_{c,b} L_b, \qquad (4.17)$$

with $R_{c,b}$ the number of bits allocated to code $c$ within block $b$. In the case of a QPSK constellation, $R_{c,b} = 2, \forall c, \forall b$. The MBM problem can then be written as

$$\begin{cases} \min_{B} \dfrac{1}{N} \sum_{b=1}^{B} \left( L_b \, Pb_b \right), \\[2em] \text{with} \quad \sum_{b=1}^{B} L_b = N. \end{cases} \qquad (4.18)$$

Finding the optimal number $B$ of blocks and their optimal lengths $L_b$ that minimize the system mean BER leads to solving a complex combinational optimization problem that can not be reduced to an equivalent convex problem. Thus, no analytical solution exists and the

optimal solution can only be obtained through exhaustive search. Consequently, in this study, we propose a suboptimal solution that reduces the system mean BER considerably.

### 4.2.2.1 Case of a 2-subcarrier system

In order to better understand the effect of adding a spreading component to the OFDM system, we first consider a simplified system composed of only $N = 2$ subcarriers. Two possible system configurations can be studied:

- A 1-block system ($B = 1$) where the two subcarriers are linked with the same spreading code of length $L = 2$.
- A 2-block system ($B = 2$) where the two subcarriers are kept separated as in an OFDM system, and thus $L = 1$.

The mean BER of the 1-block system is given by

$$Pb_{B=1} = \frac{1}{2} erfc\left(\sqrt{\frac{N\tilde{E}}{2N_0} \frac{1}{1/|h_1|^2 + 1/|h_2|^2}}\right), \tag{4.19}$$

with $h_1$ and $h_2$ the frequency responses for the two subcarriers. Similarly, the mean BER of the 2-block system is given by

$$Pb_{B=2} = \frac{1}{4} erfc\left(\sqrt{\frac{N\tilde{E}}{4N_0}|h_1|^2}\right) + \frac{1}{4} erfc\left(\sqrt{\frac{N\tilde{E}}{4N_0}|h_2|^2}\right). \tag{4.20}$$

If $h_1$ is the frequency response with the smallest amplitude ($|h_1| \leq |h_2|$), then let $x$ and $y$ be two real numbers such that

$$\begin{cases} x = \dfrac{N\tilde{E}}{2N_0}|h_1|^2, \\ y = |h_1|^2 / |h_2|^2, \qquad \text{with} \quad 0 < y \leq 1. \end{cases} \tag{4.21}$$

Finding the best system configuration that reduces the mean BER is equivalent to studying the sign of the difference between $Pb_{B=1}$ and $Pb_{B=2}$, which can be expressed as

$$f(x, y) = Pb_{B=1} - Pb_{B=2} = \frac{1}{2} erfc\left(\sqrt{\frac{x}{1+y}}\right) - \frac{1}{4} erfc\left(\sqrt{\frac{x}{2}}\right) - \frac{1}{4} erfc\left(\sqrt{\frac{x}{2y}}\right). \tag{4.22}$$

For $0 < y \leq 1$, the sign of $f(x, y)$ depends on the value of $x$, and equivalently, on the value of $E_b / N_0$. Solving (4.22), we find

- If $x < 0.9846$, i.e. $E_b / N_0 < 0.4923 / |h_1|^2$, then $f(x, y) > 0$. Thus, the two subcarriers should be kept separated ($B = 2$).

- If $x > 2.9850$, i.e. $E_b / N_0 > 1.4925 / |h_1|^2$, then $f(x, y) < 0$. Thus, the two subcarriers should be put in a single block ($B = 1$).

- If $0.9846 \leq x \leq 2.9850$, i.e. $0.4923 / |h_1|^2 \leq E_b / N_0 \leq 1.4925 / |h_1|^2$, the sign of $f(x, y)$ depends on the ratio $y$ as follows

  - If $y \geq y_{limit}$, then $f(x, y) \geq 0$. Thus, two blocks should be used ($B = 2$).

  - If $y \leq y_{limit}$, then $f(x, y) \leq 0$. Thus, one single block should be used ($B = 1$),

  where $y_{limit}$ is the solution of the equation $f(x, y) = 0$. Using curve-fitting techniques, $y_{limit}$ can be approximated by

$$y_{limit} \approx \exp\left(\frac{x - 1.2137}{2.7172}\right) - 0.9191. \tag{4.23}$$

Equivalently, for a given ratio $y = |h_1|^2 / |h_2|^2$, the value of $E_b / N_0$ that leads to $f(x, y) = 0$ is approximated by

$$E_b / N_{0\,limit} \approx \frac{1}{2|h_1|^2}\left[2.7172 \log(y + 0.9191) + 1.2137\right]. \tag{4.24}$$

Consequently, when $E_b / N_0 \leq E_b / N_{0\,limit}$, the mean BER of a 2-block system is lower than the mean BER of a 1-block system, and thus the optimal code length is $L = 1$. When $E_b / N_0 \geq E_b / N_{0\,limit}$, the mean BER of a 1-block system is lower than the mean BER of a 2-block system, and thus the optimal code length is $L = 2$. We conclude that the spreading component can be advantageously used for high $E_b / N_0$ values, whereas for low $E_b / N_0$ values the OFDM system might provide lower mean BER.

### 4.2.2.2    2-block system with a unique code length

Now we consider two blocks having the same code length *L*. The objective is to know if the two blocks should be merged into one single LP-OFDM block of length $2L$ or kept separated, in order to minimize the system mean BER. The mean BERs of the 1-block and 2-block systems are given by

$$Pb_{B=1} = \frac{1}{2} erfc\left(\sqrt{\frac{N\tilde{E}}{2N_0} \frac{1}{\sum_{n=1}^{L}\left(1/|h_{1,n}|^2\right) + \sum_{n=1}^{L}\left(1/|h_{2,n}|^2\right)}}\right), \tag{4.25}$$

$$Pb_{B=2} = \frac{1}{4} erfc\left(\sqrt{\frac{N\tilde{E}}{4N_0} \frac{1}{\sum_{n=1}^{L}\left(1/|h_{1,n}|^2\right)}}\right) + \frac{1}{4} erfc\left(\sqrt{\frac{N\tilde{E}}{4N_0} \frac{1}{\sum_{n=1}^{L}\left(1/|h_{2,n}|^2\right)}}\right), \quad (4.26)$$

with $N$ the total number of subcarriers in the system, and $h_{1,n}$ and $h_{2,n}$ the $L$ frequency responses for each block. Let $H_1$ and $H_2$ be two real positive numbers such that

$$\begin{cases} \dfrac{1}{|H_1|^2} = \displaystyle\sum_{n=1}^{L}\left(1/|h_{1,n}|^2\right), \\[4mm] \dfrac{1}{|H_2|^2} = \displaystyle\sum_{n=1}^{L}\left(1/|h_{2,n}|^2\right). \end{cases} \quad (4.27)$$

If we consider $|H_1| \leq |H_2|$, then let $x$ and $y$ be two real numbers such that

$$\begin{cases} x = \dfrac{N\tilde{E}}{2N_0}|H_1|^2, \\[4mm] y = |H_1|^2 / |H_2|^2, \qquad \text{with} \quad 0 < y \leq 1. \end{cases} \quad (4.28)$$

The problem can be solved in the same way as in the 2-subcarrier system study. We find that the $E_b / N_0$ limit is given by

$$\begin{cases} x_{limit} \approx 2.7172 \log\left(y + 0.9191\right) + 1.2137, \\[4mm] E_b / N_{0_{limit}} \approx \dfrac{\sum_{n=1}^{L}\left(1/|h_{1,n}|^2\right)}{N}\left[2.7172 \log\left(y + 0.9191\right) + 1.2137\right]. \end{cases} \quad (4.29)$$

Consequently, when $E_b / N_0 \leq E_b / N_{0_{limit}}$, the two blocks should be kept separated to reduce the system mean BER, and when $E_b / N_0 \geq E_b / N_{0_{limit}}$, the two blocks should be merged into a single block of length $2L = N$.

### 4.2.2.3   3-block system with a unique code length

Now we consider three blocks having the same code length $L$. The objective is to know if the three blocks should be merged into one single LP-OFDM block of length $3L$ or kept separated, in order to minimize the system mean BER. The mean BERs of the 1-block and 3-block systems are given by

$$Pb_{B=1} = \frac{1}{2} erfc\left(\sqrt{\frac{N\tilde{E}}{2N_0} \frac{1}{\sum_{n=1}^{L}\left(1/|h_{1,n}|^2\right) + \sum_{n=1}^{L}\left(1/|h_{2,n}|^2\right) + \sum_{n=1}^{L}\left(1/|h_{3,n}|^2\right)}}\right), \quad (4.30)$$

$$Pb_{B=3} = \frac{1}{6} erfc\sqrt{\frac{N\tilde{E}/6N_0}{\sqrt{\sum_{n=1}^{L}\left(1/|h_{1,n}|^2\right)}}} + \frac{1}{6} erfc\left(\sqrt{\frac{N\tilde{E}/6N_0}{\sqrt{\sum_{n=1}^{L}\left(1/|h_{2,n}|^2\right)}}}\right) + \frac{1}{6} erfc\left(\sqrt{\frac{N\tilde{E}/6N_0}{\sqrt{\sum_{n=1}^{L}\left(1/|h_{3,n}|^2\right)}}}\right), \quad (4.31)$$

with $N$ the total number of subcarriers, and $h_{1,n}$, $h_{2,n}$ and $h_{3,n}$ the $L$ frequency responses of each block. Let $H_1$, $H_2$ and $H_3$ be three real positive numbers such that

$$\begin{cases} \dfrac{1}{|H_1|^2} = \sum_{n=1}^{L}\dfrac{1}{|h_{1,n}|^2}, \\[2mm] \dfrac{1}{|H_2|^2} = \sum_{n=1}^{L}\dfrac{1}{|h_{2,n}|^2}, \\[2mm] \dfrac{1}{|H_3|^2} = \sum_{n=1}^{L}\dfrac{1}{|h_{3,n}|^2}. \end{cases} \qquad (4.32)$$

If we consider $|H_1|\le|H_2|$ and $|H_2|\le|H_3|$, then let $x$, $y$ and $z$ be three real numbers such that

$$\begin{cases} x = \dfrac{N\tilde{E}}{2N_0}|H_1|^2, \\[2mm] y = |H_1|^2/|H_2|^2, & \text{with} \quad 0 < y \le 1, \\[2mm] z = |H_2|^2/|H_3|^2, & \text{with} \quad 0 < z \le 1. \end{cases} \qquad (4.33)$$

Finding the best system configuration that reduces the system mean BER is equivalent to studying the sign of the difference $Pb_{B=1} - Pb_{B=3}$, which can be expressed as

$$f(x,y,z) = \frac{1}{2} erfc\left(\sqrt{\frac{x}{1+y+yz}}\right) - \frac{1}{6} erfc\left(\sqrt{\frac{x}{3}}\right) - \frac{1}{6} erfc\left(\sqrt{\frac{x}{3y}}\right) - \frac{1}{6} erfc\left(\sqrt{\frac{x}{3yz}}\right). \quad (4.34)$$

For $0 < y \le 1$, the sign of $f(x,y,z)$ depends on the value of $x$, and equivalently, on the value of $E_b/N_0$ as follows

- If $x < 1.174$, i.e. $E_b/N_0 < 1.174 \sum_{n=1}^{L}\left(1/|h_{1,n}|^2\right)/N$, the three blocks should be kept separated.
- If $x > 4.5$, i.e. $E_b/N_0 > 4.5 \sum_{n=1}^{L}\left(1/|h_{1,n}|^2\right)/N$, the three blocks should be merged into one single block.
- If $1.174 \le x \le 4.5$, the sign of $f(x,y,z)$ depends on the ratio $y$ as follows

- If $y < 0.3$, $x_{limit}$ follows a straight line function given by

$$\begin{cases} x_{limit} \approx a\,z + b \\ a = \exp\left[(y - 0.0772)/0.3780\right] - 0.8161 \\ b = 0.2549\log(y + 0.0756) + 1.8205 \end{cases} \tag{4.35}$$

- If $0.3 \le y \le 0.6$, $x_{limit}$ follows a logarithmic curve as a function of $z$ given by

$$\begin{cases} x_{limit} \approx a\log(z + b) + c \\ a = 5.883\,y^2 - 1.231\,y + 1.353 \\ b = 6.55\,y^2 - 6.552\,y + 2.524 \\ c = -11.3\,y^2 + 11.2\,y - 1.052 \end{cases} \tag{4.36}$$

- If $0.6 < y \le 1$, $x_{limit}$ follows a logarithmic curve as a function of $z$ given by

$$\begin{cases} x_{limit} \approx a\log(z + b) + c \\ a = -17.95\,y^2 + 30.635\,y - 9.187 \\ b = -6.083\,y^2 + 9.387\,y - 2.491 \\ c = 22.75\,y^2 - 34.355\,y + 14.023 \end{cases} \tag{4.37}$$

Consequently, for a given $y$ value and a given $z$ value, $x_{limit}$ is derived from (4.35), (4.36) or (4.37). Then, if $x \ge x_{limit}$ the three blocks should be merged into a single block of length $3L = N$ in order to reduce the system mean BER, and if $x < x_{limit}$ these blocks should be kept separated.

### 4.2.3   Proposed algorithm

Taking into account the results obtained in the 2-block and 3-block system studies, we propose a new suboptimal allocation algorithm that reduces the mean BER of the LP-OFDM system under a PSD constraint, a target throughput and a single QPSK constellation. This algorithm finds the suboptimal number of blocks and their corresponding code lengths that minimize the system mean BER for a given channel response. This algorithm can be implemented at the receiver side, and then the suboptimal code length configuration can be sent to the transmitter at the beginning of each frame by a simple feedback. Thus, the same code length configuration can be maintained for the whole frame, thanks to the UWB channel response that varies slowly in time and that can be considered as quasi-static during one frame.

As we will see in the global system study in Chapter 5, Walsh-Hadamard orthogonal spreading codes are used for the proposed LP-OFDM system to limit the self-interference (SI). Only Sylvester constructions of Hadamard matrices are chosen and a unique spreading code length is used to simplify the LP-OFDM system. Thus, compared to the WiMedia system, the number of data subcarriers in each OFDM symbol is reduced from 100 to 96. However, in this section we consider variable block lengths in order to minimize the system mean BER. The set of code lengths that can be used is $S_L = \{96, 32, 16, 8, 4, 2, 1\}$. All these lengths are extracted from Sylvester constructions, except the length of 96 which is related to Paley construction and which is considered here to study the case of a single-block LP-OFDM system using $N = 96$ subcarriers. The proposed algorithm, presented in Figure 4.2, starts by considering one single-block system of length $L = 96$. Then, it studies the effect of the next possible code length in $S_L$, which is $L = 32$. Based on Section 4.2.2.3, it finds whether the single block of length $L = 96$ should be divided into three blocks of length $L = 32$ each, or it should be kept as one block to reduce the system mean BER. If $L = 96$ is the optimal solution, then the algorithm ends. Otherwise, it moves to the next possible code length ($L = 16$) and finds which of the three new blocks should be divided into two blocks of length $L = 16$ each, based on the study in Section 4.2.2.2. The algorithm ends if none of the blocks should be divided. The same procedure continues until $L = 1$.

### 4.2.4   Optimal subcarriers distribution

In the proposed mean BER minimization algorithm, the channel responses of the different subcarriers were randomly distributed between the different blocks without any particular arrangement. These channel responses could be judiciously distributed in order to further reduce the system mean BER. However, this distribution might increase the algorithm complexity significantly.

Let us for example study the case of a 2-block system using a unique code length *L* as in Section 4.2.2.2. For a given set of $N = 2L$ channel responses, the idea is to know how the channel responses, and equivalently the subcarriers, should be distributed between the two blocks in order to minimize the mean BER. We first consider that the subcarriers are distributed between the two blocks in such a way that the mean BER of the two blocks is the same. Then, we study the effect of interchanging some subcarriers between the two blocks on the final system mean BER.

From (4.26), the subcarriers of two blocks having equal BER should respect

**1. Initialization**

Set $S_L = \{96, 32, 16, 8, 4, 2, 1\}$, $L_{opt} = [\ ]$.

**2. Comparing 1-block and 3-block configurations**

$N = S_L(1) = 96$, $L = S_L(2) = 32$,

Compute $x$, $y$ and $z$ from (4.33),

Compute $x_{limit}$ from (4.35), (4.36) or (4.37),

If $x \geq x_{limit}$

$L_{opt} = [96]$,

Algorithm ends,

else

$L_{opt} = [32, 32, 32]$,

end.

**3. Comparing 1-block and 2-block configurations**

For $i = 2$ to $6$,

$L_{new} = [\ ]$,

$N = S_L(i)$, $L = S_L(i+1)$,

For $block = 1$ to $length(L_{opt})$,

If $L_{opt}(block) = N$,

Compute $x$ and $y$ from (4.28),

Compute $x_{limit}$ from (4.29),

If $x \geq x_{limit}$,

$L_{new} = [L_{new}, N]$,

else

$L_{new} = [L_{new}, N/2, N/2]$,

end

else

$L_{new} = [L_{new}, L_{opt}(block)]$,

end

end

$L_{opt} = L_{new}$,

end.

**4. Output**

Return $L_{opt}$.

Figure 4.2: Mean BER minimization algorithm with variable code length for LP-OFDM systems, under a PSD constraint, a given target throughput and a single QPSK constellation.

$$\sum_{n=1}^{L} \frac{1}{\left|h_{a,n}\right|^2} = \sum_{n=1}^{L} \frac{1}{\left|h_{b,n}\right|^2}, \tag{4.38}$$

where $h_{a,n}$ and $h_{b,n}$ are the channel responses of the first and second block subcarriers, respectively. The resulting system mean BER, which will be a reference for the sequel, can be written as

$$Pb_{ref} = \frac{1}{2} erfc\left(\sqrt{\frac{N\tilde{E}}{4N_0} \frac{1}{\sum_{n=1}^{L}\left(1/\left|h_{a,n}\right|^2\right)}}\right). \tag{4.39}$$

Let $\{h'_{a,m}\}$ and $\{h'_{b,m}\}$ the sets channel responses we want to interchange between the two blocks, with $m = 1\cdots L'$. The resulting system mean BER after subcarriers interchanging is given by

$$\left\{ \begin{aligned} &Pb' = \frac{1}{4} erfc\left(\sqrt{\frac{N\tilde{E}}{4N_0} \frac{1}{\sum_{n=1}^{L}\left(1/\left|h_{a,n}\right|^2\right)+d}}\right) + \frac{1}{4} erfc\left(\sqrt{\frac{N\tilde{E}}{4N_0} \frac{1}{\sum_{n=1}^{L}\left(1/\left|h_{b,n}\right|^2\right)-d}}\right), \\ &\text{with} \quad d = \sum_{m=1}^{L'}\left(1/\left|h'_{b,m}\right|^2\right) - \sum_{m=1}^{L'}\left(1/\left|h'_{a,m}\right|^2\right). \end{aligned} \right. \tag{4.40}$$

Let $x$, $y$ and $\alpha$ be three real numbers such that

$$\left\{ \begin{aligned} &x = \frac{N\tilde{E}}{2N_0} \frac{1}{\sum_{n=1}^{L}\left(1/\left|h_{a,n}\right|^2\right)} = \frac{N\tilde{E}}{\alpha N_0}, \\ &y = \frac{d}{\sum_{n=1}^{L}\left(1/\left|h_{a,n}\right|^2\right)} = \frac{2d}{\alpha}, \quad \text{with} \quad 0 < y < 1, \\ &\alpha = \sum_{n=1}^{2L}\left(1/\left|h_n\right|^2\right), \end{aligned} \right. \tag{4.41}$$

where $\{h_n\}$ is the set of all the system frequency responses. To understand the effect of this subcarriers interchanging on the final system mean BER, we study the BER difference $Pb_{ref} - Pb'$ which is equal to

$$f(x,y) = \frac{1}{2} erfc\left(\sqrt{\frac{x}{2}}\right) - \frac{1}{4} erfc\left(\sqrt{\frac{x}{2(1+y)}}\right) - \frac{1}{4} erfc\left(\sqrt{\frac{x}{2(1-y)}}\right). \tag{4.42}$$

Solving this equation, we find that

- If $x \geq 3$, then $f(x, y) < 0, \forall y$, i.e. $Pb_{ref} < Pb', \forall y$. Thus, the optimal configuration that minimizes the system mean BER is to have two blocks with equal BER. Consequently, the subcarriers should be distributed between the two blocks such that

$$\sum_{n=1}^{L} \frac{1}{|h_{1,n}|^2} = \sum_{n=1}^{L} \frac{1}{|h_{2,n}|^2}, \tag{4.43}$$

where $h_{1,n}$ and $h_{2,n}$ are the channel responses of the first and second block subcarriers, respectively.

- If $x < 3$, $f(x, y)$ is maximized, and consequently $Pb'$ is minimized, for a given value of $x$, when $y$ is equal to

$$y \approx 0.362 \log(3.2615 - x) + 0.5856. \tag{4.44}$$

Since we have that $2d = \alpha y$, the optimal subcarriers distribution that minimizes the system mean BER respects the following equation

$$\sum_{n=1}^{L} \frac{1}{|h_{1,n}|^2} - \sum_{n=1}^{L} \frac{1}{|h_{2,n}|^2} \approx \alpha \left[ 0.362 \log\left( 3.2615 - \frac{N\tilde{E}}{\alpha N_0} \right) + 0.5856 \right]. \tag{4.45}$$

The MBM algorithm in Section 4.2.3 can be easily modified in order to take into account the optimal subcarriers distribution. In fact, before every comparison between 1-block and 2-block configurations, the 2-block scheme is first optimized by efficiently distributing the subcarriers between the two blocks as proposed in (4.43) and (4.45).

### 4.2.5  Simulation results

After having described the different mean BER minimization strategies that can be carried out on the LP-OFDM system with variable code length, using a single QPSK constellation order and for a target throughput, we present the simulations performed on the first three bands (3.1–4.7 GHz) of the MB-OFDM solution using the UWB channel model CM1. The transmitted PSD is $\tilde{E} = -41.3$ dBm/MHz and the noise density is $N_0 = -114$ dBm/MHz. In addition, the OFDM symbol of the LP-OFDM system consists of $N = 96$ data subcarriers. Consequently, the target throughput is $R = 192$ bit/symbol. Note that in this section, the channel coding is not taken into account.

In Figure 4.3, the system mean BER is plotted as a function of $E_b/N_0$ for different LP-OFDM system configurations with constant and variable spreading code lengths. At low $E_b/N_0$ values, the LP-OFDM system with a constant code length of $L=1$, which is equivalent to a classical OFDM system, has lower mean BER than LP-OFDM systems with $L=16$ and $L=96$. On the other hand, at high $E_b/N_0$ values, the LP-OFDM system with $L=96$ has the lowest mean BER. Thus, we conclude that increasing $E_b/N_0$ leads to increasing the spreading code length of the LP-OFDM system in order to reduce the system mean BER.

When the proposed MBM algorithm with variable code length is applied to the LP-OFDM system, the mean BER is reduced compared to LP-OFDM systems with constant code length, as we can see from Figure 4.3. Note that in this figure, the subcarriers are randomly distributed on the different blocks. At $E_b/N_0$ values lower than $5\,\mathrm{dB}$, the dynamic LP-OFDM system performance converges to the performance of an OFDM system ($L=1$). At $E_b/N_0$ values higher than $22\,\mathrm{dB}$, the optimal code length that minimizes the mean BER is $L=96$, and consequently the dynamic LP-OFDM system performance converges to the performance of a LP-OFDM system using a single block. At medium $E_b/N_0$ values, the dynamic LP-OFDM system outperforms the different LP-OFDM con-
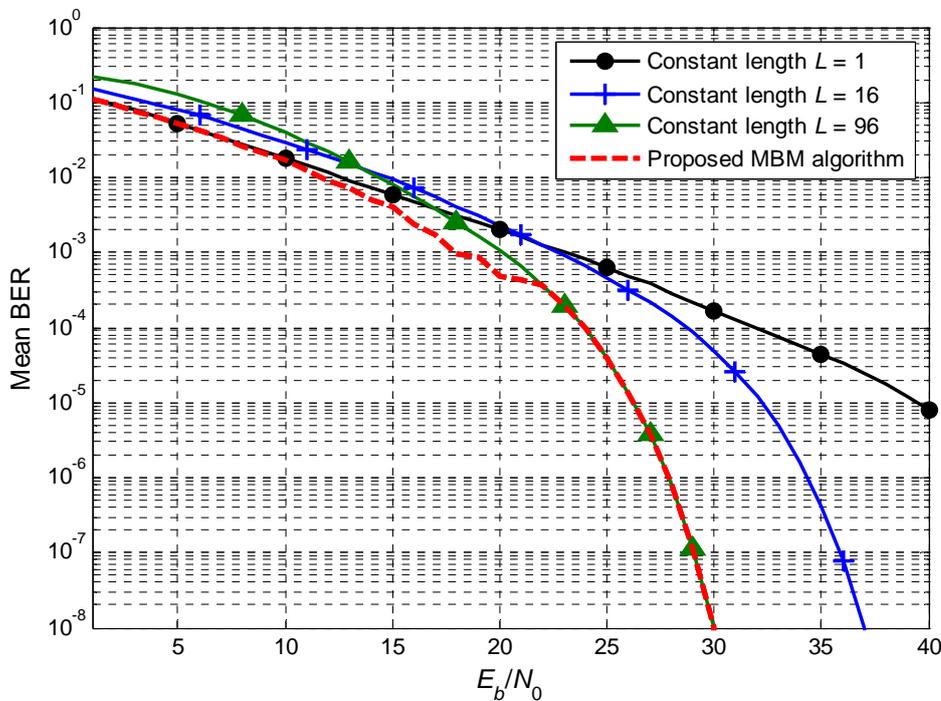


Figure 4.3: Performance of the mean BER minimization algorithm with variable code length compared to the performance of LP-OFDM systems with constant code length.

figurations with constant code length. In addition, at a BER level of $10^{-5}$, the proposed algorithm offers an $E_b / N_0$ gain of 6 dB compared to a LP-OFDM system with $L = 16$ and a 13 dB gain compared to an OFDM system ($L = 1$). Similarly, at a BER level of $10^{-1}$, it offers a 4 dB gain compared to a LP-OFDM system with $L = 16$. Hence, we conclude that the proposed algorithm can be efficiently applied to the LP-OFDM system to improve its performance in terms of mean BER.

Figure 4.4 presents an example of the suboptimal code length configuration provided by the MBM algorithm for a given channel realization at $E_b / N_0 = 8 \, \text{dB}$. This algorithm can be implemented at the receiver side, and then the output can be sent to the transmitter as a vector, equal to $L_{opt} = [32, 16, 1, 1, 1, 1, 4, 8, 8, 1, 1, 2, 4, 8, 4, 2, 1, 1]$ in this example, at the beginning of the frame by a simple feedback.

Figure 4.5 presents the performance of the proposed MBM algorithm with random and optimal subcarriers distribution. As we can see, optimizing the subcarriers distribution as described in Section 4.2.4 reduces the mean BER of the LP-OFDM system. However, this system improvement is not very important ($E_b / N_0$ gain less than 0.2 dB). This is due to the fact that the proposed dynamic code length optimization provides a very good exploitation of the available frequency diversity, and thus the remaining frequency diversity that can be exploited by the optimal subcarriers distribution is very small. Consequently, a random subcarriers distribution can be sufficient to reduce the mean BER significantly without increasing the system complexity considerably.

## 4.3   Variable constellation orders

In order to further improve the system performance, we move away from the MB-OFDM proposal and we consider variable constellations (BPSK, QPSK, 8-QAM and 16-QAM). Here, knowledge of CSI is assumed at the transmitter. We first study the case of mean BER minimization of an OFDM system for a given target throughput, and then we move to the case of a LP-OFDM system.

### 4.3.1   OFDM system

The throughput of an OFDM system in bit per symbol in the case of variable SNR gap per subcarrier can be derived from (3.11) as

$$R_{OFDM} = \sum_{n=1}^{N} R_n = \sum_{n=1}^{N} \log_2 \left( 1 + \frac{1}{\Gamma_n} |h_n|^2 \frac{E_n}{N_0} \right), \tag{4.46}$$
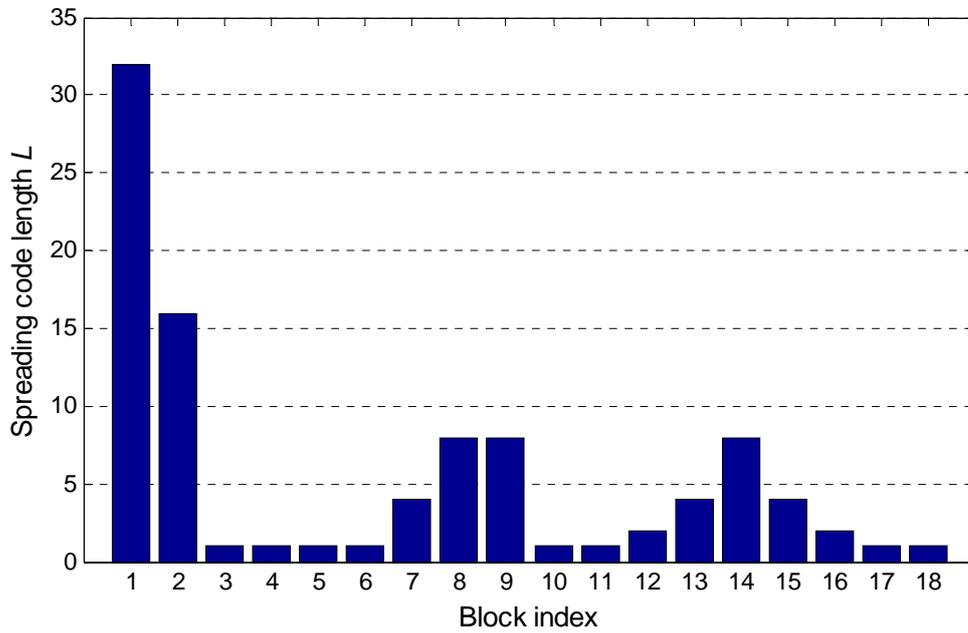
Figure 4.4: An example of the suboptimal code length configuration provided by the mean BER minimization algorithm for a given channel realization at $E_b / N_0 = 8$ dB .
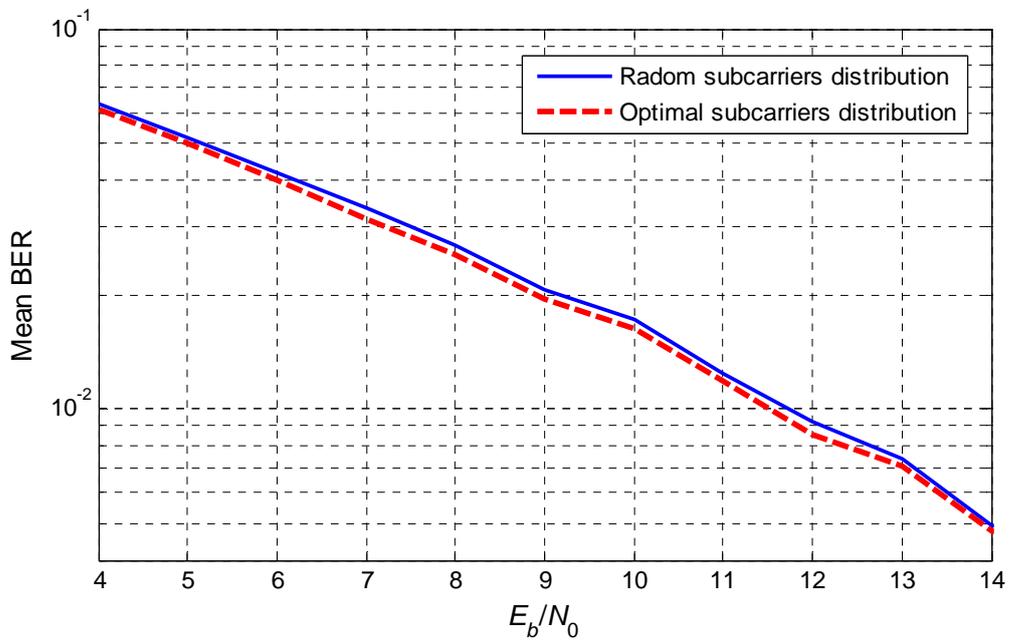


Figure 4.5: Effect of the optimal subcarriers distribution on the proposed mean BER minimization algorithm.

where $N$ is the number of data subcarriers and $\Gamma_n$ the variable SNR gap relative to the QAM constellation order of subcarrier $n$. The MBM problem can be written as

$$
\begin{cases}
\min \dfrac{\sum_{n=1}^{N}\left(R_n Pb_n\right)}{\sum_{n=1}^{N} R_n}, \\[2mm]
\text{subject to} \quad E_n \le \tilde{E}, \quad \forall n, \\[2mm]
\text{and} \quad \displaystyle\sum_{n=1}^{N} R_n = \tilde{R},
\end{cases}
\tag{4.47}
$$

where $\tilde{E}$ is the PSD limit for each subcarrier and $\tilde{R}$ the target throughput. The BER for subcarrier $n$ can be expressed from [86] and (4.46) as

$$
Pb_n \approx \frac{1}{R_n} 2\,erfc\left( \sqrt{\frac{3}{2}\,|\,h_n\,|^2\,\frac{E_n}{N_0}\,\frac{1}{2^{R_n}-1}} \right).
\tag{4.48}
$$

It is clear that to minimize the mean BER, the total available energy on each subcarrier should be used, thus $E_n = \tilde{E}, \forall n$. The optimization problem can be solved using Lagrange multipliers in (4.47) as follows

$$
L\left(R_n, \lambda\right) = \sum_{n=1}^{N} 2\,erfc\left( \sqrt{\frac{\alpha_n}{2^{R_n}-1}} \right) + \lambda\left( \tilde{R} - \sum_{n=1}^{N} R_n \right),
\tag{4.49}
$$

with
$$
\alpha_n = \frac{3}{2}\,|\,h_n\,|^2\,\frac{\tilde{E}}{N_0}.
\tag{4.50}
$$

After differentiating with respect to $R_n$ and considering the approximation $2^{R_n} - 1 \approx 2^{R_n}$, the Lagrange multiplier becomes

$$
\lambda = 2\ln 2 \sqrt{\frac{\alpha_n}{\pi 2^{R_n}}}\, e^{-\alpha_n/2^{R_n}}.
\tag{4.51}
$$

Equation (4.51) can be solved using the Lambert W function [110]. Thus, the real bit and power allocation solution can be written as

$$
\begin{cases}
R_n = \dfrac{\tilde{R}}{N} + \log_2\left(|h_n|^2\right) - \dfrac{1}{N}\sum_{n=1}^{N} \log_2\left(|h_n|^2\right), \quad \forall n, \\[4mm]
E_n = \tilde{E}_n, \quad \forall n.
\end{cases}
\tag{4.52}
$$

---

**1. Initialization**

Set $\bar{R}_n = 0, \forall n$.

**2. While** $\sum_{n=1}^{N} \bar{R}_n < \tilde{R}$

$$\hat{n} = \arg\left[\min_{n,\ \bar{R}_n < R_{\max QAM}} \left[\left(R_n + 1\right) Pb_n\left(R_n + 1\right)\right]\right] = \arg\left[\max_{n,\ \bar{R}_n < R_{\max QAM}} \left(\frac{|h_n|^2}{2^{R_n+1} - 1}\right)\right],$$

$\bar{R}_{\hat{n}} = \bar{R}_{\hat{n}} + 1$.

**3. Output**

Return $\bar{R}_1 \cdots \bar{R}_N$.

---
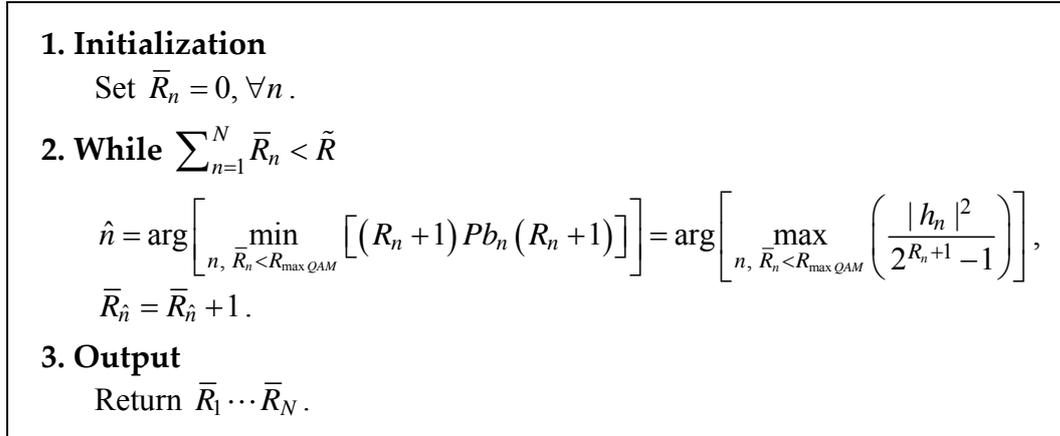
Figure 4.6: Mean BER minimization algorithm with variable constellation orders for OFDM systems.

It is interesting to note here that this result is the same as the one obtained in the case of margin maximization of OFDM systems for a given target throughput and a fixed SER for each subcarrier, discussed in Section 3.2.3. Thus, we conclude that maximizing the margin of OFDM systems equivalently minimizes their mean BER.

Since the number of bits allocated to each subcarrier has to be integer, discrete greedy methods that incrementally allocate these bits to minimize the mean BER can be used. In this study, the proposed MBM algorithm is presented in Figure 4.6. This algorithm starts by considering zero bits on each subcarrier. Bits are then allocated to the subcarriers with the lowest SER until the target throughput is reached, while not exceeding the maximum allowed constellation order $R_{\max QAM}$ in the system.

### 4.3.2  LP-OFDM system

In this section, we propose a new resource allocation study that minimizes the mean BER of a LP-OFDM system for a given target throughput using variable constellation orders. This study is carried out by first considering a simple single-block LP-OFDM system, and then moving to the case of a general multiple-block LP-OFDM system.

#### 4.3.2.1  Single-block system

The MBM problem in the case of a single-block LP-OFDM system can be written as

$$
\begin{cases}
\min \dfrac{\sum_{k=1}^{K}\left(R_k Pb_k\right)}{\sum_{k=1}^{K} R_k}, \\[4mm]
\text{subject to} \quad \sum_{k=1}^{K} E_k \le \tilde{E} \\[4mm]
\text{and} \quad \sum_{k=1}^{K} R_k = \tilde{R},
\end{cases}
\tag{4.53}
$$

where $\tilde{E}$ is the PSD limit of the single block and $\tilde{R}$ the system target throughput. The BER for code $k$ can be expressed from [86] and (4.4) as

$$
Pb_k \approx \frac{1}{R_k}\, 2\,erfc\left( \sqrt{\frac{3}{2}\,\frac{L^2}{\sum_{n=1}^{L}\left(1/|h_n|^2\right)}\,\frac{E_k}{N_0}\,\frac{1}{2^{R_k}-1}} \right).
\tag{4.54}
$$

The optimization problem can be solved using Lagrange multipliers in (4.53) as follows

$$
L\left(E_k, R_k, \lambda, \mu\right) = \sum_{k=1}^{K} 2\,erfc\left( \sqrt{\frac{\alpha\,E_k}{2^{R_k}-1}} \right) + \lambda\left( \tilde{E} - \sum_{k=1}^{K} E_k \right) + \mu\left( \tilde{R} - \sum_{k=1}^{K} R_k \right),
\tag{4.55}
$$

with
$$
\alpha = \frac{3}{2}\,\frac{L^2}{\sum_{n=1}^{L}\left(1/|h_n|^2\right)}\,\frac{1}{N_0}.
\tag{4.56}
$$

After differentiating with respect to $E_k$ and $R_k$, and considering the approximation $2^{R_k}-1 \approx 2^{R_k}$, the Lagrange multipliers become

$$
\begin{cases}
\lambda = -2\sqrt{\dfrac{\alpha}{\pi\,E_k\,2^{R_k}}}\; e^{-\alpha E_k/2^{R_k}}, \\[5mm]
\mu = 2\ln 2\sqrt{\dfrac{\alpha\,E_k}{\pi\,2^{R_k}}}\; e^{-\alpha E_k/2^{R_k}}.
\end{cases}
\tag{4.57}
$$

Solving (4.57), we find

$$
\begin{cases}
E_k = \dfrac{\tilde{E}}{K}, \quad \forall k, \\[5mm]
R_k = \dfrac{\tilde{R}}{K}, \quad \forall k.
\end{cases}
\tag{4.58}
$$

Thus, the energy and the real bits should be uniformly distributed on the different codes. The only remaining parameter to be optimized to minimize the mean BER is the number $K$ of codes. Consequently, the MBM problem is reduced to

$$\begin{cases} \min_K K \, erfc\left( \sqrt{\dfrac{\alpha \tilde{E}}{K\left(2^{\tilde{R}/K} -1\right)}} \right), \\[4mm] \text{with} \quad 1 \le K \le L. \end{cases} \tag{4.59}$$

Since this problem can not be solved analytically, curve-fitting techniques are used. We find that the optimal number of codes that should be used in the single block to minimize the mean BER can be approximated by

$$K^* \approx \text{Round}\left[ \frac{2}{3} \frac{\alpha \tilde{E}}{2^{\tilde{R}} -1} e^{\left(\tilde{R}-0.415\right)/1.4427-1} \right]. \tag{4.60}$$

In the case of integer bit optimization, similarly to the scenario in Section 3.3.3.1, the optimal bits distribution for a given number $K^*$ of codes would be to allocate $\lfloor \tilde{R} / K^* \rfloor +1$ bits to $m$ codes and $\lfloor \tilde{R} / K^* \rfloor$ bits to the remaining $K^* - m$ codes. Since we have a target throughput $\tilde{R}$, $m$ should respect the equation $m\left(\lfloor \tilde{R} / K^* \rfloor +1\right)+\left(K^* -m\right)\lfloor \tilde{R} / K^* \rfloor = \tilde{R}$. Thus, we find

$$m = \tilde{R} - K^* \lfloor \tilde{R} / K^* \rfloor. \tag{4.61}$$

Consequently, the integer bit allocation solution for a single-block system is given by

$$\begin{cases} \overline{R}_k = \lfloor \tilde{R} / K^* \rfloor +1, & \forall k \in [1:m], \\[2mm] \overline{R}_k = \lfloor \tilde{R} / K^* \rfloor, & \forall k \in [m+1:K^*]. \end{cases} \tag{4.62}$$

### 4.3.2.2   Multiple-block system

After having study the single-block case, we move to a multiple-block LP-OFDM system study. Let $B$ be the number of blocks, all having the same length $L$. The MBM problem can be written as

$$
\begin{cases}
\min \dfrac{\sum_{b=1}^{B}\left(R_b\, Pb_b\right)}{\sum_{b=1}^{B} R_b}, \\[4mm]
\text{subject to} \quad \displaystyle\sum_{k=1}^{K_b} E_{k,b} \le \tilde{E}, \quad \forall b, \\[4mm]
\text{and} \quad \displaystyle\sum_{b=1}^{B} R_b = \tilde{R},
\end{cases}
\tag{4.63}
$$

where $R_b$ and $K_b$ are the number of bits and codes in block $b$, respectively, $Pb_b$ the BER for block $b$, $\tilde{E}$ the PSD limit of each block, and $\tilde{R}$ the system target throughput. Taking into account the result presented in (4.58) for a given block, the MBM problem can be re-defined as

$$
\min \sum_{b=1}^{B} K_b\, erfc\left(\sqrt{\frac{\alpha_b\, \tilde{E}}{K_b\left(2^{R_b/K_b}-1\right)}}\right),
\tag{4.64}
$$

where $\alpha_b$ is given by

$$
\alpha_b = \frac{3}{2}\, \frac{L^2}{\sum_{n=1}^{L}\left(1/\mid h_{n,b}\mid^2\right)}\, \frac{1}{N_0}.
\tag{4.65}
$$

Supposing that $K_b \approx L$, which is the case in most of the times, and using Lagrange multipliers, we find

$$
R_b = \frac{\tilde{R}}{B} - \log_2\left(\sum_{n=1}^{L}\frac{1}{\left|h_{n,b}\right|^2}\right) + \frac{1}{B}\sum_{b=1}^{B}\log_2\left(\sum_{n=1}^{L}\frac{1}{\left|h_{n,b}\right|^2}\right), \quad \forall b.
\tag{4.66}
$$

Equation (4.66) gives the optimal real number of bits per block that minimizes the system mean BER. Since the number of bits allocated to each block has to be integer, a discrete incremental algorithm can be used to find the optimal integer number $\bar{R}_b$ of bits per block. Then, each block can be individually optimized as in the single-block study. Thus, we find

$$
\begin{cases}
\overline{R}_{k,b} = \left\lfloor \overline{R}_b / K_b^* \right\rfloor + 1, \qquad \forall b, \ \forall k \in \left[ 1 : m_b \right], \\[2ex]
\overline{R}_{k,b} = \left\lfloor \overline{R}_b / K_b^* \right\rfloor, \qquad\quad \forall b, \ \forall k \in \left[ m_b + 1 : K_b^* \right], \\[2ex]
\text{with} \quad m_b = \overline{R}_b - K_b^* \left\lfloor \overline{R}_b / K_b^* \right\rfloor, \\[2ex]
K_b^* \approx \text{Round} \left[ \dfrac{2}{3} \dfrac{\alpha_b \, \tilde{E}}{2^{\overline{R}_b} - 1} e^{\left( \overline{R}_b - 0.415 \right)/1.4427 - 1} \right], \\[2ex]
\overline{R}_b \ \text{given by the greedy algorithm.}
\end{cases}
\tag{4.67}
$$

### 4.3.2.3   Proposed algorithm

The algorithm we propose in this study to minimize the mean BER of the LP-OFDM system is given in Figure 4.7. This algorithm starts by considering zero bits for each block. The first step consists in finding the optimal number $\overline{R}_b$ of bits that should be allocated to each block $b$. Thus, bits are incrementally allocated to the codes that are within the blocks whose noise margin is the maximum, and that have the smallest number of allocated bits, until the target system throughput $\tilde{R}$ is reached. The second step consists in finding the optimal number $\overline{R}_{c,b}$ of bits that should be allocated to each code in order to reach the block throughput $\overline{R}_b$, as given in (4.67). Note that the algorithm takes into account the maximum constellation order $R_{\max QAM}$. In fact, when the number of bits allocated to a given code exceeds $R_{\max QAM}$, the number $K_b^*$ of codes in the corresponding block is incremented, which relatively reduces the constellation orders of these codes since the same $\overline{R}_b$ bits is now distributed on a larger number of codes.

### 4.3.3   Simulation results

In this section, we present the results of simulations performed on the first MB-OFDM band using the UWB channel model CM1. The transmitted PSD is $\tilde{E} = -41.3$ dBm/MHz and the noise density is $N_0 = -114$ dBm/MHz. In addition, the OFDM symbol of the LP-OFDM system consists of $N = 96$ data subcarriers, and the code length is the same for all the blocks, equal to $L = 16$. Note that in this section, the channel coding is not taken into account.

Figure 4.8 presents the resulting mean BER of different OFDM and LP-OFDM configurations for a system target throughput $R = 192$ bit/symbol, with fixed and variable constellation orders. If we consider a unique QPSK constellation order, the performance of the OFDM system in terms of mean BER is slightly better than the performance of the LP-OFDM system at low SNR levels. However, at high SNR levels, the LP-OFDM system

**1. Initialization**
  Set $\bar{R}_b = 0, \forall b$.

**2. Find** $\bar{R}_b$ **for** $b = 1 \cdots B$
  While $\sum_{b=1}^{B} \bar{R}_b < \tilde{R}$
  $\hat{b} = \arg\max_{b} \left\{ 1 / \left[ \sum_{n=1}^{L} \left( 1/|h_{n,b}|^2 \right) \sum_{k=1}^{L} \left( 2^{R_{k,b}+1} - 1 \right) \right] \right\}$,
  $\hat{k} = \arg\min_{k} \left( R_{k,\hat{b}} \right)$,
  $\bar{R}_{\hat{k},\hat{b}} = \bar{R}_{\hat{k},\hat{b}} + 1$,
  $\bar{R}_b = \sum_{k} \bar{R}_{k,b}, \forall b$.

**3. Blocks optimization**
  Compute $K_b^*$ from (4.67),
  $K_b^* \left( K_b^* < 1 \right) = 1$ and $K_b^* \left( K_b^* > L \right) = L$,
  While $\left\lfloor \bar{R}_b / K_b^* \right\rfloor + 1 > R_{\max QAM}$ and $K_b^* < L$
  $K_b^* = K_b^* + 1$,
  Find $\bar{R}_{k,b}$ from (4.67).

**4. Output**
  Return $\bar{R}_{k,b}, \forall k, \forall b$.
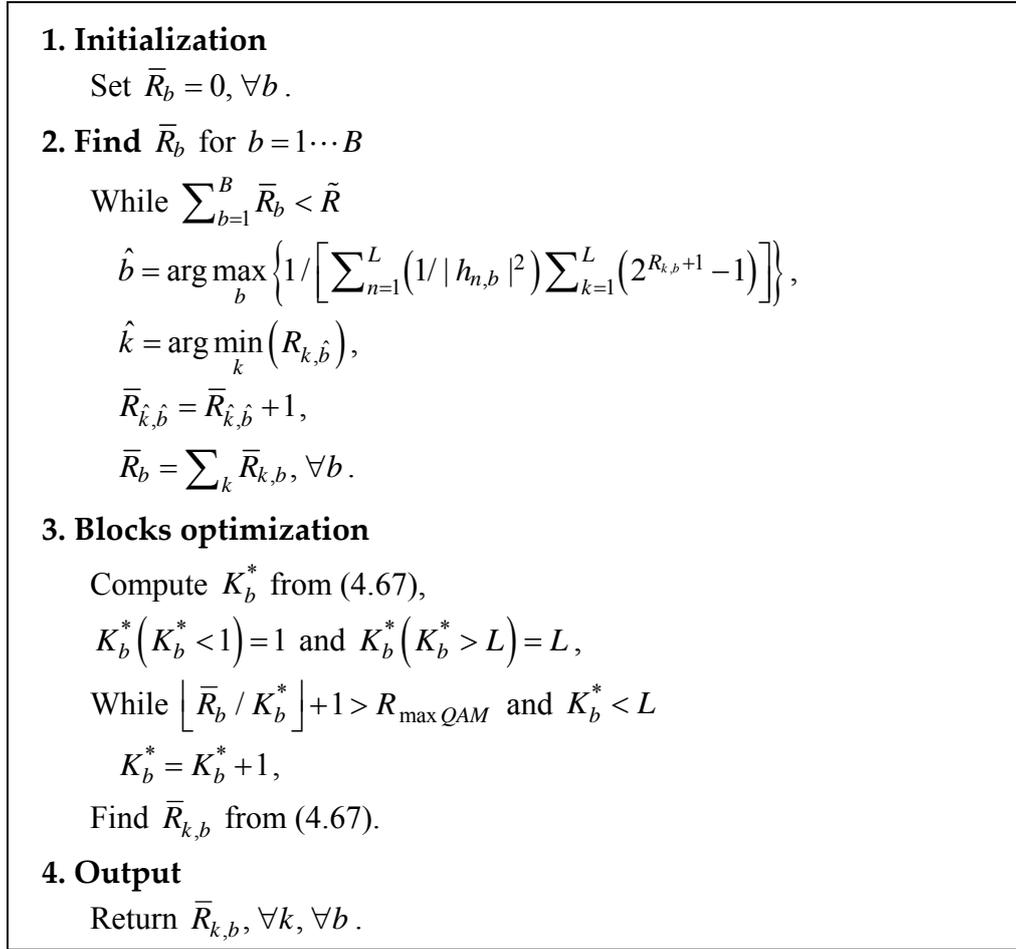
Figure 4.7: Mean BER minimization algorithm with variable constellation orders for LP-OFDM systems using a constant spreading code length.

outperforms the OFDM system. For instance, at a mean BER level of $10^{-3}$, the LP-OFDM system provides a 1 dB gain compared to the OFDM system. On the other hand, when the MBM algorithm with variable constellation orders is applied to the LP-OFDM system, the mean BER is reduced considerably. For very low SNR values, the LP-OFDM system using the MBM algorithm outperforms the LP-OFDM system with fixed constellation order. Note that in this figure, the constellations are limited to 16-QAM. If higher constellation orders were used, the mean BER could be further reduced. For high SNR values, the mean BER is minimized significantly with the MBM algorithm. For instance, at a mean BER level of $10^{-3}$, the MBM algorithm provides a 6 dB gain compared to the LP-OFDM system with fixed constellation and a 7 dB gain compared to the OFDM system.

In Figure 4.8, the MBM algorithm performance is also compared to the performance of the margin maximization algorithm presented in Section 3.3.3.2. At low SNR levels, the MBM algorithm outperforms the MM algorithm. This is due to the MBM algorithm flexibility brought by the dynamic number $K_b^*$ of codes that can be reduced when the SNR reaches critical low values, contrarily to the MM algorithm whose number of codes is fixed and equal to $L$. On the other hand, at high SNR levels, we notice that the performance of both algorithms is similar. This was expected since at these SNR levels the optimal number $K_b^*$ of codes is equal to its maximum possible value $L$. Consequently, the MBM algorithm provides exactly the same result as with the MM algorithm.

Figure 4.9 presents another comparison between MBM and MM algorithms for different system target throughputs, at a SNR level of 11 dB. We notice that the mean BER of the LP-OFDM system using the MBM algorithm is always lower than the mean BER with the MM algorithm, for the different target throughputs. Compared to the LP-OFDM with fixed throughput, the MBM reduces the mean BER considerably, especially for low target throughputs. For instance, a LP-OFDM using a single 2-QAM constellation ($R = 96$ bit/symbol) provides a mean BER of about $10^{-1}$, whereas a LP-OFDM employing the MBM algorithm provides a mean BER of about $7 \times 10^{-3}$.

## 4.4   Conclusion

In this chapter, we have proposed a new resource allocation approach that focuses on the system mean BER instead of the subcarriers and codes SER. This study, whose main objective was to minimize the system mean BER for a given target throughput, was carried out in two scenarios. The first scenario considered a fixed constellation order where the mean BER of the LP-OFDM system is minimized by optimizing the variable code lengths configuration. Simulation results showed that the proposed MBM algorithm in this scenario reduces the mean BER significantly at the different SNR levels, and that the resulting LP-OFDM system with variable code length outperforms the LP-OFDM systems using a unique code length for their different blocks. Note that since the UWB channel response varies slowly in time and can be considered as quasi-static during one frame, the algorithm implementation complexity is reduced. In fact, this algorithm can be implemented at the receiver side, and then the algorithm output can be sent to the transmitter at the beginning of each frame by a simple feedback.
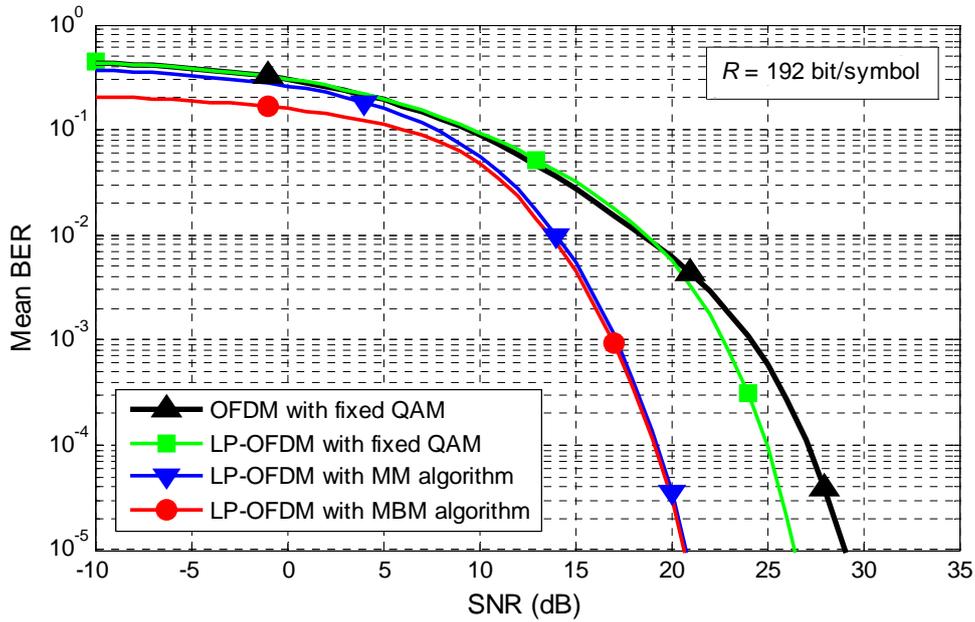
Figure 4.8: Performance of the mean BER minimization algorithm with variable constellation orders, for a given system target throughput $R = 192$ bit/symbol.
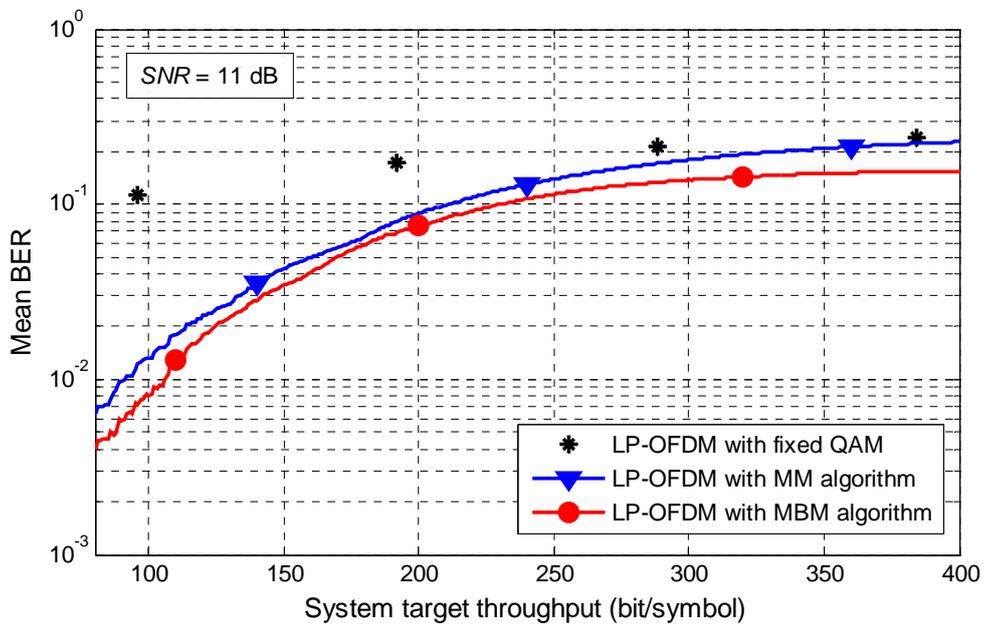


Figure 4.9: Performance comparison between the mean BER minimization algorithm and the margin maximization algorithm with variable constellation orders for different system target throughputs, at a SNR level of 11 dB.

The second scenario considered variable constellation orders with a constant code length. Different resource allocation studies that find the optimal power and bit distribution that minimizes the mean BER of OFDM and LP-OFDM systems were proposed. Simulation results show that the MBM algorithm proposed for LP-OFDM systems reduces the mean BER significantly, compared to the LP-OFDM systems using a fixed constellation order. In addition, this algorithm is very flexible since it dynamically selects the optimal number of codes that should be used in each block.

Finally, we should note that the analytical study carried out in this chapter helped us to better understand the effect of linear precoding on multicarrier systems. Starting from the simple case of two subcarriers, we derived the boundaries than define whether a simple OFDM system or a LP-OFDM system offers better performance in terms of mean BER. Although this study highlighted the intrinsic characteristics of the precoding function without taking the channel coding gain into account, the analytical results found in this chapter will be verified in the global system study carried out in Chapter 5. In addition, this global study will show the effect of combining spreading and channel coding to well exploit the channel diversity.

# Chapter 5

# Global MIMO LP-OFDM UWB system optimization

AFTER having analytically studied the linear precoding scheme in the previous chapters and presented its advantages when combined with an OFDM modulation, we consider here a global UWB system study that takes into account the different functions of the transmission chain. This chapter is divided into two parts. The first part discusses the performance of the proposed LP-OFDM system in a single-input single-output (SISO) context. After a discussion on the main parameterization strategies that improve the system performance, the spreading code length is optimized through system simulations, and the resulting solutions verify the analytical results obtained in Chapter 4. In addition, simulation results of the SISO LP-OFDM system using the optimal code length show the advantage of combining the LP component with the OFDM scheme of the MB-OFDM solution.

The second part of the chapter is dedicated to the study of MIMO techniques in UWB applications. After a general overview on MIMO technology, we describe a new realistic MIMO UWB channel model developed at IETR, which will be used in our study. Then, we propose to add an Alamouti space-time scheme to the LP-OFDM system. Thanks to its orthogonal properties, this scheme requires a very simple maximum likelihood (ML) decoder, resulting in low cost receivers. The objective of this study is first to improve the system range while maintaining a QPSK constellation [111], and then to provide very high data rates through a joint combination of MIMO with a 16-QAM constellation [112].

## 5.1 SISO LP-OFDM system

### 5.1.1 System configuration

A global study of the LP-OFDM UWB system is carried out in this section, under a SISO context. In this study, the different blocks of the transmission chain, listed in Figure 5.1,
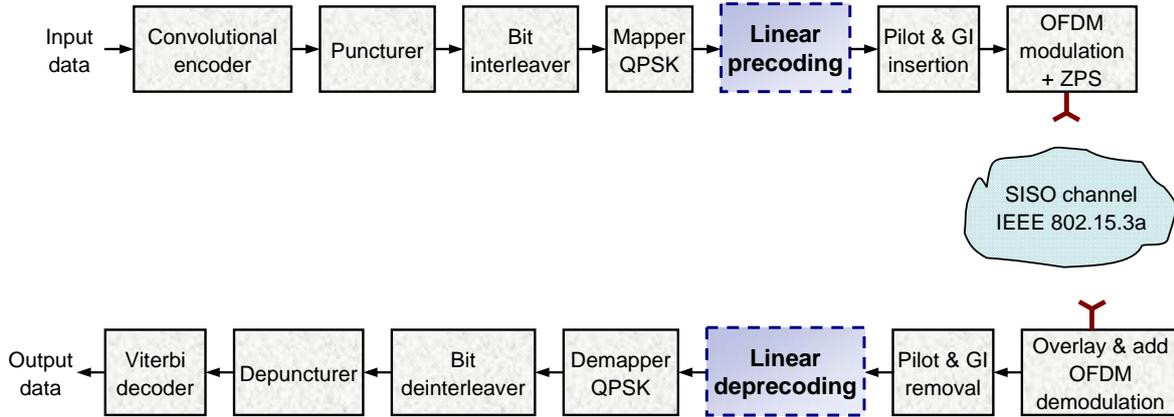
Figure 5.1: Simplified SISO LP-OFDM UWB transmission system.

are taken into account. As we can see from Figure 5.1, the main difference between the LP-OFDM and MB-OFDM systems is the simple addition of the linear precoding block. Although the LP component can be easily implemented using a simple matrix, some parameter modifications have to be carried out on other blocks of the transmission chain in order to optimize the system performance and benefit well from the addition of the LP component. The system parameters that are different from the MB-OFDM ones are described in the sequel.

The proposed LP function consists of Walsh-Hadamard orthogonal spreading codes that are used to limit the SI in the LP-OFDM system. In this system study, a unique spreading code length is used for all blocks of the LP-OFDM scheme in order not to significantly increase the complexity of the system compared to the MB-OFDM system. Thus, the algorithm presented in Section 4.2.3, which minimizes the mean BER with variable code lengths, is not applied here. In addition, only Sylvester constructions of Hadamard matrices are considered. In order to use these Sylvester schemes and have many possible code lengths, we reduce the number $N$ of data subcarriers in each OFDM symbol to 96. Note that $N$ was initially equal to 100 in the MB-OFDM system. An additional code length $L = 96$ can be considered, using Paley construction, to study the case of a single-block LP-OFDM system. The resulting set of possible spreading code lengths is then given by $S_L = \{96, 32, 16, 8, 4, 2, 1\}$. Note that the remaining 4 subcarriers can be grouped into an additional block of length $L = 4$ in order to use 100 data subcarriers as in the MB-OFDM system. However, since we are only considering a single code length for the whole system, this approach will not be studied here. Thus, the 4 subcarriers are set to zero, which gives a total number of 10 null tones.

Table 5.1: OFDM parameters of the LP-OFDM system.

| Parameter | Value |
|---|---|
| Number of data subcarriers ($N$) | 96 |
| IFFT / FFT size ($N_{FFT}$) | 128 |
| Sampling frequency ($f_s$) | 528 MHz |
| Subcarrier frequency spacing ($\Delta_f$) | 4.125 MHz |
| IFFT / FFT period ($T_{FFT}$) | 242.42 ns |
| Number of samples in ZPS ($N_{ZPS}$) | 37 |
| ZPS duration ($T_{ZPS}$) | 70.08 ns |
| Symbol interval ($T_s$) | 312.5 ns |

The same convolutional encoder as in the MB-OFDM system, using the industry-standard rate $\overline{r} = 1/3$ code, with generator polynomials $g_0 = 133_8$, $g_1 = 165_8$ and $g_2 = 171_8$, is considered. Additional coding rates, derived from the mother rate $\overline{r} = 1/3$ code by employing a puncturing procedure, are proposed in Section 5.1.2.1 after the optimization of the spreading code length.

Except for the number of data subcarriers, the OFDM parameters of the LP-OFDM system, listed in Table 5.1, are chosen the same as the OFDM parameters of the MB-OFDM system. In addition, in the SISO context, we only consider a QPSK constellation to have comparable constellation complexity with the MB-OFDM system. Besides, the same TFC technique as the one of the MB-OFDM system, described in Section 2.2.1.5, is applied on the LP-OFDM system to provide frequency hopping between the users from a band to another at the end of every OFDM symbol, and thus to benefit from an additional frequency diversity. Furthermore, a MMSE detection is used in this system study since it offers better performance than the ZF technique, especially at low SNR values.

### 5.1.1.1 Subcarriers distribution

In the analytical study in Chapter 3 and Chapter 4, we have discussed the effect of subcarriers distribution on the system performance. For instance, in Chapter 3, we showed that the optimal solution for the subcarriers distribution in the bit loading algorithms would be to sort the system subcarriers according to the amplitude of their frequency responses, before distributing them on the different LP-OFDM blocks. Besides, in the mean BER minimization study in Section 4.2, we demonstrated that the subcarriers distribution between

two given blocks should respect a certain condition, given by (4.43) and (4.45), in order to minimize the system mean BER.

In LP-OFDM systems, two different frequency assignment approaches can actually be considered to split up the subcarriers into the spreading blocks associated to the precoded symbols [113]. The first approach, so-called *standard block interleaving scheme*, consists in interleaving the subcarriers assigned to each spreading block so that the corresponding chips are regularly distributed across the whole bandwidth. Consequently, maximum frequency diversity is made available at the receiver. The second scheme, so-called *adjacent subcarrier scheme*, gathers the chips of one spread symbol from neighboring subcarriers. In contrast to the first scheme, the *adjacent subcarrier scheme* provides a weaker exploitation of the available frequency diversity. However, the correlation between channel coefficients of adjacent subcarriers is more important, and consequently the channel variance is smaller. It is proven in [114] that the SI variance is proportional to the channel variance over a specific subset of subcarriers. Thus, using adjacent subcarriers reduces the SI.

Consequently, the *adjacent subcarrier scheme* will be chosen in the sequel in order to limit the SI. In this case, the frequency diversity is jointly exploited by the spreading component, which is carried out in the frequency direction, and the channel coding combined with bit interleaving.

### 5.1.1.2   Bit interleaving

As in the WiMedia solution, the bit interleaving process is performed in three distinct stages: *Symbol interleaving*, *Intra-symbol tone interleaving* and *Intra-symbol cyclic shifts*. The symbol interleaver is the same as in WiMedia, given in (2.13).

The output $a_S[i]$ of the symbol interleaver is then permuted using a block intra-symbol interleaver of size $N_{Tint} \times 16$, with $N_{Tint} = N_{CBPS}/16$ and $N_{CBPS}$ the number of coded bits per OFDM symbol. The tone interleaver output $a_T[i]$, with $i = 0, \ldots, N_{CBPS} - 1$, is given by

$$a_T[i] = a_S \left[ \left\lfloor \frac{i}{N_{Tint}} \right\rfloor + 6 \times \mathrm{mod}(i, N_{Tint}) \right]. \tag{5.1}$$

The sequence $a_T[i]$ is then passed through an intra-cyclic shifter whose output is the same as in (2.15), but with a shift factor $N_{cyc}$ given by

$$N_{cyc} = 2K + 1, \tag{5.2}$$

where $K$ is the number of used spreading codes in a LP-OFDM block. Thus, intra-cyclic shifter of the LP-OFDM system varies dynamically with the number of used codes in order to get a better exploitation of the frequency diversity.

### 5.1.2   Simulation results

In this section, in a first step, we find the optimal spreading code length that minimizes the system BER, and consequently improves the system performance, by carrying out simulations on the global LP-OFDM system. Besides, we compare the results to the analytical ones obtained in previous chapters. In a second step, taking these results into account, we present the performance of the LP-OFDM system for different system configurations, and we compare it to the performance of the WiMedia system.

#### 5.1.2.1   Spreading code length optimization

In Chapter 4, we have analytically studied the effect of the code length $L$ on the system mean BER while only taking into account the LP and OFDM components. In this section, we present the effect of $L$ in a global system environment taking into account the different components of the transmission chain, including the channel coding. The different LP-OFDM system parameters are selected as described in Section 5.1.1. Note that the number $K$ of used codes is considered equal to $L$. The system simulations are performed on the first three MB-OFDM bands using the IEEE 802.15.3a channel model CM1, and under a SISO context. Frames of 150 OFDM symbols are used, each frame being transmitted on a different channel realization, from a total of 100 available realizations.

Figure 5.2 (a) presents $E_b / N_0$ for different code length values at different BER operating points, when no channel coding is used in the system. Besides, Figure 5.2 (b) depicts the optimal values of $L$ that minimize the BER of the system presented in Figure 5.2 (a) as a function of $E_b / N_0$. We notice that when $E_b / N_0$ increases, the optimal value of $L$ in-



| (a)   $E_b / N_0$ variation | (b)   Optimal code length |
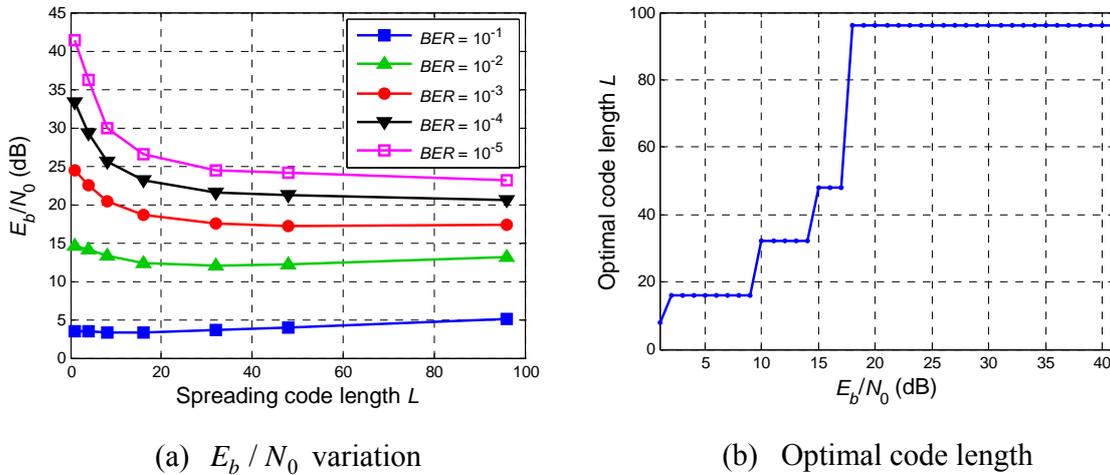
Figure 5.2: Spreading code length optimization in a LP-OFDM system without channel coding.

creases, which verifies the analytical results obtained in Chapter 4. In addition, for high values of $E_b/N_0$, i.e. $E_b/N_0 > 17$ db or $BER < 10^{-3}$, the optimal code length value is $L = 96$. Thus, a single LP-OFDM block should be used to minimize the system BER.

Figure 5.3 (a) presents $E_b/N_0$ as a function of $L$ at different BER operating points, when a channel coding rate $r = 3/4$ is used in the system. We notice that the optimal value of $L$ that minimizes $E_b/N_0$ is reduced compared to the one in a LP-OFDM system without channel coding. For example, at $BER = 10^{-3}$, the optimal code length with $r = 3/4$ is $L = 32$, whereas it was equal to 96 without channel coding, as can be seen in Figure 5.2 (a). This is due to the fact that when a channel coding is used, the system benefits from the frequency diversity recovered by this coding, and consequently less frequency diversity



(a)   $E_b/N_0$ variation with $r = 3/4$          (b)   Optimal code length with $r = 3/4$

(c)   $E_b/N_0$ variation $r = 1/2$                (d)   Optimal code length with $r = 1/2$

Figure 5.3: Spreading code length optimization for different channel coding rates in a global LP-OFDM system.

than in the system without coding must be exploited by the linear precoding scheme. Thus, less spreading is required to minimize the system BER and the optimal spreading code length is reduced. In addition, when the channel coding rate is reduced to $r = 1/2$, as depicted i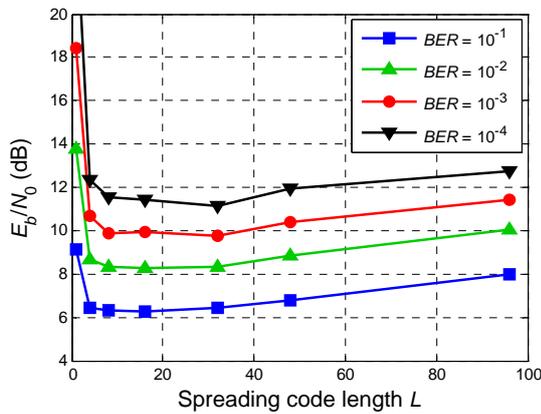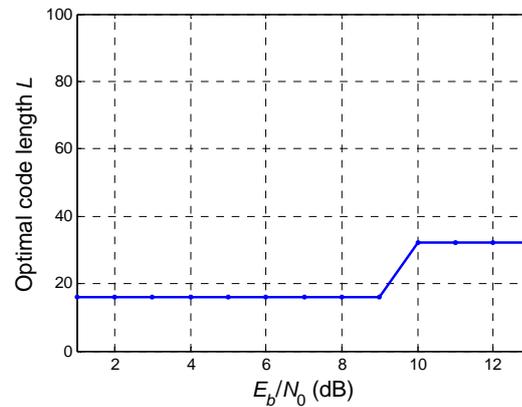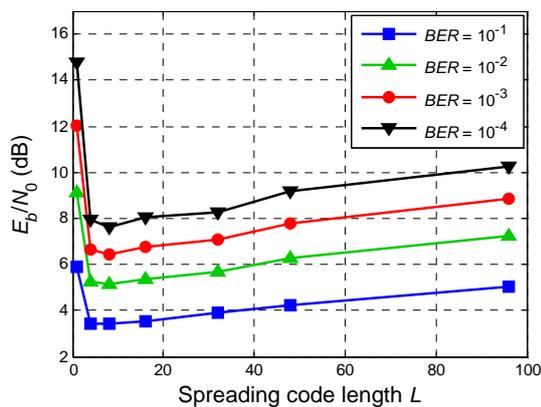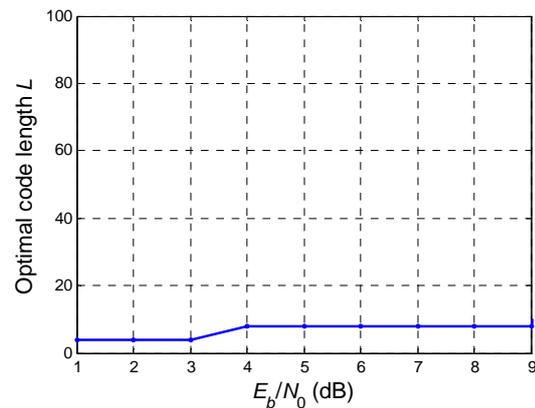n Figure 5.3 (c) and Figure 5.3 (d), the optimal code length is decreased more and the average optimal code length is $L = 8$.

Consequently, we conclude that increasing the channel coding rate or the value of $E_b / N_0$ leads to increasing the optimal spreading code length that minimizes the system BER. In the sequel, for the sake of simplicity, we use a unique code length for the different LP-OFDM configurations. The chosen code length is $L = 16$, since it seems to be a good compromise and gives good performance for the different channel coding rates that will be considered. As the number of data subcarriers is $N = 96$, the resulting LP-OFDM system is composed of 6 blocks of 16 subcarriers each. Note that a normalization factor of $1 / \sqrt{L}$, presented in (2.12), is added before the Hadamard matrix at the transmitter and at the receiver to compensate for the energy provided by the spreading process.

As mentioned in Chapter 3, the number $K$ of used codes in a given LP-OFDM block is not necessarily equal to $L$. Thus, one significant advantage of the LP-OFDM system is that it provides a wide range of data rates due to the high flexibility brought by the joint assignment of the number of used spreading codes and the rate of the channel convolutional coding. For simulation comparison, eight $r$ and $K$ combinations, out of a very large number of possible combinations, are selected in order to obtain data rate levels that are close to the ones defined by the WiMedia solution (see Table 2.1).Thus, the proposed LP-OFDM data rates are listed in Table 5.2.

Table 5.2: LP-OFDM system data rates.

| Data rate (Mb/s) | Constellation | Coding rate $r$ | Number $K$ of codes |
|:---:|:---:|:---:|:---:|
| 51.2 | QPSK | 1/3 | 4 |
| 76.7 | QPSK | 1/3 | 6 |
| 115.1 | QPSK | 1/3 | 9 |
| 153.6 | QPSK | 1/3 | 12 |
| 192 | QPSK | 1/2 | 10 |
| 307 | QPSK | 1/2 | 16 |
| 409 | QPSK | 2/3 | 16 |
| 460 | QPSK | 3/4 | 16 |

From Table 5.2, the low data rates are obtained using a number $K$ of codes lower than $L$, which can be selected from a set of $L$ available spreading sequences. In the presence of multipath channels, the orthogonality between spreading sequences is lost and not completely restored by the MMSE detection. Thus, the $K$ spreading codes should be judiciously selected to reduce the SI in the LP-OFDM system. In this study, we use an optimized spreading codes assignment, proposed in [115], which minimizes the largest degradation among any two symbols.

### 5.1.2.2    System Simulations with $L = 16$

After having described the different parameters of the proposed LP-OFDM scheme, we present the LP-OFDM system performance and we compare it to the performance of the WiMedia system. Note that the suboptimal spreading code length $L = 16$, the optimized spreading codes assignment for $K < L$, and the *adjacent subcarrier scheme* are used here. The system simulations are performed on the first three MB-OFDM bands using the IEEE 802.15.3a channel model CM1, and under a SISO context. Frames of 150 OFDM symbols are used, each frame being transmitted on a different channel realization.

In Figure 5.4, the system BER is presented as a function of $E_b / N_0$, while considering the ideal case of perfect channel estimation. The performance of the LP-OFDM system is presented for the different data rates proposed in Table 5.2. By comparing Figure 5.4 and Figure 2.9, we notice that for a given $E_b / N_0$ value, the BER of the LP-OFDM system at a given data rate is always lower than the BER of the WiMedia system at a close data rate. For example at $E_b / N_0 = 12$ dB, the WiMedia system with a data rate of 480 Mb/s provides a BER of $2.3 \times 10^{-4}$ whereas the LP-OFDM system with a data rate of 460 Mb/s offers a BER of only $4.8 \times 10^{-5}$. This data rate difference is due to the number of data subcarriers which is equal to 100 in the WiMedia system and to 96 in the LP-OFDM system.

For a better comparison between the WiMedia and LP-OFDM systems, Figure 5.5 gives for both systems the required $E_b / N_0$ that provides a BER of $10^{-4}$ at the output of the Viterbi decoder, at different data rates. The LP-OFDM system outperforms the WiMedia system for all the data rates, as it was expected from the analytical studies. The LP gain of the global LP-OFDM system is around 1dB, which is lower than the LP gain obtained in the analytical study. This is due to the fact that the channel coding component that is added to the global system exploits a part of the available frequency diversity, which squeezes the LP gain considerably. We conclude that the proposed LP-OFDM system provides better performance than the OFDM system, and a wider range of possible data rates due to the high flexibility brought by the joint assignment of the number of used codes and the selected coding rates.
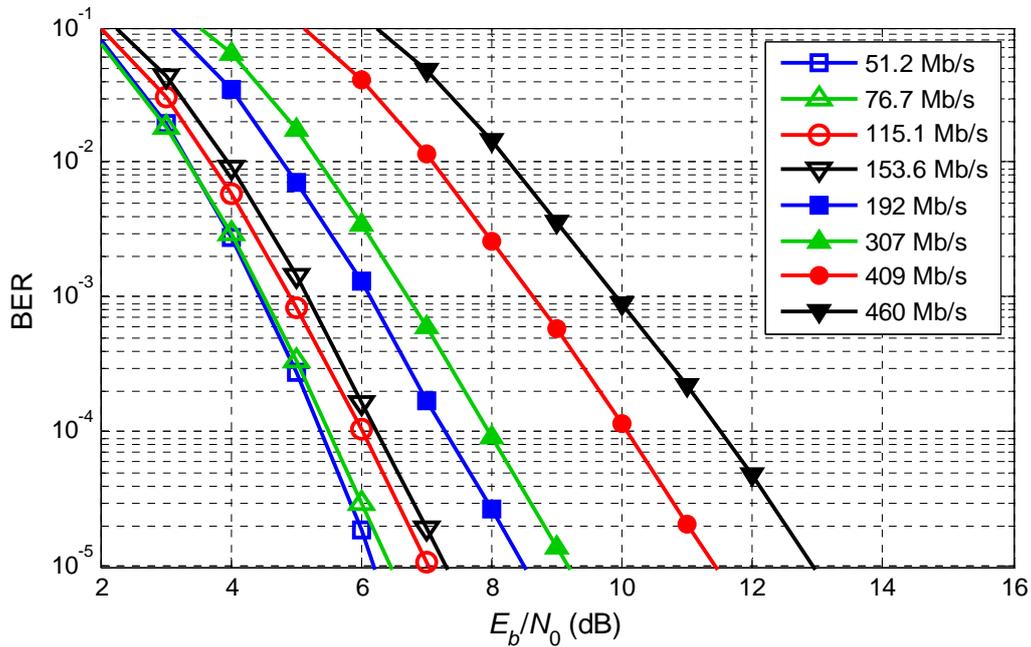
Figure 5.4: LP-OFDM system performance on bands 1, 2 and 3, using channel model CM1 and considering a TFC frequency hopping between the three bands.
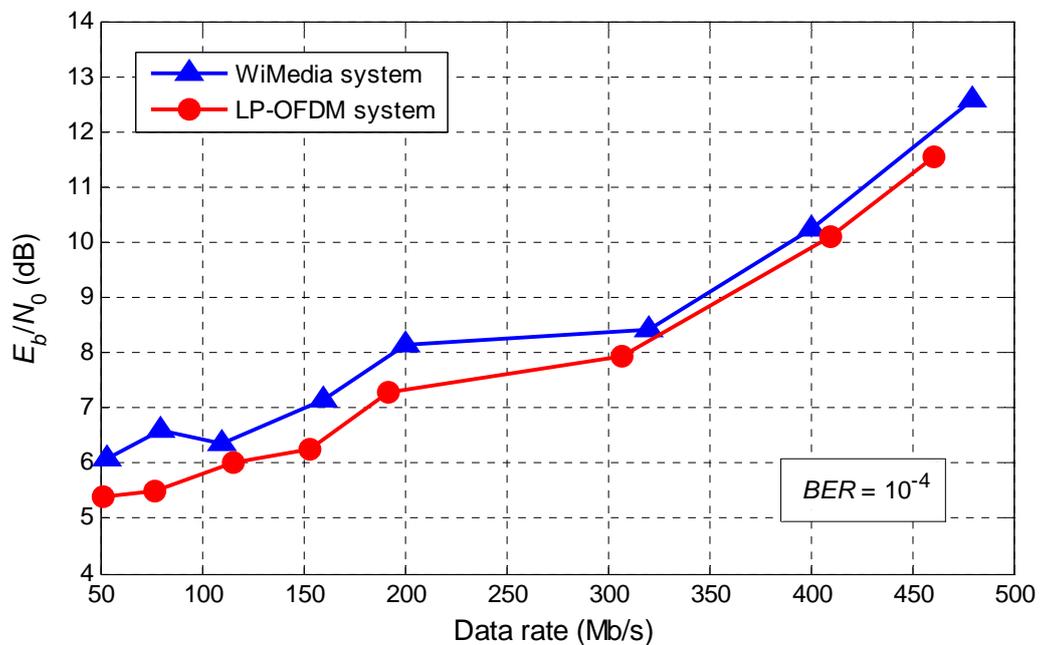


Figure 5.5: Required $E_b / N_0$ to obtain $BER = 10^{-4}$ at the output of the Viterbi decoder, for the different WiMedia and LP-OFDM data rates.

## 5.2   Brief overview on MIMO technology

The demands for capacity driven by Internet and multimedia applications in next generation wireless communications have been rapidly increasing worldwide. As the available radio spectrum is limited, higher data rates can be achieved only by designing more efficient signaling techniques. Recent research in information theory has shown that MIMO techniques provide large gains in capacity of communication over wireless channels [86]. In radio communications, MIMO is defined as the use of multiple antennas at both the transmitter and receiver to improve the communication performance. Thus, through the use of a new spatial dimension, MIMO technology offers significant increases in data throughput and link range without additional bandwidth or transmit power. Today, MIMO is used or planned to be used in several communications standards including the IEEE 802.11n, the IEEE 802.16e, and the 3GPP LTE standard.

MIMO can be sub-divided into two main categories. The first one requires the knowledge of the CSI at the transmitter. It can be seen as a generalized beamforming to support multi-layer transmission in MIMO radio systems [116], [117]. Conventional beamforming considers linear single-layer precoding so that the same signal is emitted from each of the transmit antennas with appropriate weighting such that the signal power is maximized at the receiver output. When the receiver has multiple antennas, the single-layer beamforming can not simultaneously maximize the signal level at all of the receive antennas and so precoding is used for multi-layer beamforming in order to maximize the throughput performance of a multiple receive antenna system. In MIMO precoding, the multiple streams of the signals are emitted from the transmit antennas with independent and appropriate weighting per each antenna such that the link throughput is maximized at the receiver output.

The second category of MIMO techniques requires the knowledge of the CSI only at the receiver side. This category is also divided into two main techniques: spatial multiplexing and spatial diversity. Spatial multiplexing is used when we want to increase the system throughput, and spatial diversity is considered when we want to improve the link reliability.

### 5.2.1   Spatial multiplexing

The use of multiple antennas results in increasing the capacity of MIMO channels [118]. Therefore, one may transmit at a higher throughput, compared to SISO channels, for a given probability of error. The capacity analysis in [118] shows that when the number of transmit and receive antennas is the same, the capacity grows at least linearly with the number of antennas.

One approach to achieve the higher possible throughput is spatial multiplexing. In spatial multiplexing, a high rate signal is split into $A_t$ lower rate streams, using a serial-to-parallel converter, and each stream is transmitted from a different transmit antenna in the same frequency channel. As a result, the throughput is $A_t$ symbols per MIMO channel with $A_t$ transmit antennas. This increase in throughput will generally come at the cost of a lower diversity gain compared to spatial diversity technique. Therefore, spatial multiplexing is a better choice for high rate systems operating at relatively high SNR while spatial diversity is more appropriate for transmitting at relatively low rates and low SNR.

Different methods can then be used to recover the $A_t$ lower rate streams at the receiver. The first methods are based on detection techniques. The optimal technique is the maximum likelihood (ML) detection. However, this technique has some practical limitations since its complexity increases exponentially with the number $A_t$ of transmit antennas. Thus, other suboptimal receivers with lower complexity, such as ZF and MMSE, are generally preferred.

An alternative to the ZF and MMSE receivers is the layered space-time (LST) architecture, proposed by Foschini [119], which can attain a tight lower bound on the MIMO channel capacity. This architecture allows processing of multidimensional signals in the space domain by 1-D processing steps, where 1-D refers to one dimension in space. The method relies on powerful signal processing techniques at the receiver and conventional 1-D channel codes. In the originally proposed architecture, $A_t$ information streams are transmitted simultaneously, in the same frequency band, using $A_t$ transmit antennas. The receiver uses $A_r = A_t$ antennas to separate and detect the $A_t$ transmitted signals. The separation process involves a combination of interference suppression and interference cancellation. The separated signals are then decoded by using conventional decoding algorithms developed for (1-D)-component codes, leading to much lower complexity compared to maximum likelihood decoding. Besides, the complexity of the LST receivers grows linearly with the data rate.

There are a number of various LST architectures, depending on whether error control coding is used or not, and on the way the modulated symbols are assigned to transmit antennas. A well-known practical architecture is the uncoded LST structure, known as vertical Bell Laboratories layered space-time (VBLAST) scheme [120].

## 5.2.2 Spatial diversity

The second category of MIMO schemes not requiring CSI at the transmitter is the spatial diversity technique that improves the signal robustness instead of the system throughput. An effective and practical way to approaching the capacity of MIMO wireless channels is

to employ space-time coding. Coding is performed in both spatial and temporal domains to introduce correlation between signals transmitted from various antennas at various time periods. The spatial-temporal correlation is used to exploit the MIMO channel fading and minimize transmission errors at the receiver. Space-time coding can achieve transmit diversity and power gain over spatially uncoded systems without sacrificing the bandwidth, through an efficient exploitation of multipath effects. There are various approaches in coding structures, including space-time trellis codes (STTC) and space-time block codes (STBC). In the sequel, we briefly present the STTC scheme and then we describe the STBC technique which will be used in the proposed MIMO LP-OFDM system.

### 5.2.2.1 Space-time Treillis codes

Trellis-coded modulation (TCM) combines modulation and coding to achieve higher coding gains [121]. It provides significant coding gain and a better performance for a given bandwidth compared to uncoded modulation schemes. STTCs can be seen as TCM schemes for MIMO channels, which combine modulation and trellis coding to transmit information over multiple transmit antennas and MIMO channels. Introduced for the first time by Tarokh *et al.* [122], the STTC technique was widely discussed and explored in the literature as it can simultaneously offer a substantial coding gain, spectral efficiency, and diversity improvement on flat fading channels. More information on STTC design and performance can be found in [118].

### 5.2.2.2 Space-time block codes

STBC schemes have attracted considerable interest in MIMO communications due to their low complexity and high flexibility. Contrarily to STTCs, STBCs do not provide any coding gain. The Alamouti scheme is historically the first STBC to provide full transmit diversity for systems with two transmit antennas [123]. It was then generalized to an arbitrary number $A_t$ of transmit antennas by applying the theory of orthogonal designs. A major characteristic of the Alamouti scheme is that the transmit sequences from the two transmit antennas are orthogonal. Thus, the Alamouti scheme belongs to the so-called orthogonal STBC (OSTBC) family, where the different transmit sequences are orthogonal, allowing a very simple ML decoding algorithm, based on linear processing of the received signals [124].

In general, a STBC is defined by a $A_t \times p$ transmission matrix $X$, where $p$ is the number of time periods for transmission of one block of coded symbols. At each encoding operation, a block of $sm$ information bits are mapped into the signal constellation to select $s$ modulated signals $x_1, \cdots, x_s$, where the signal constellation consists of $2^m$ points. The $s$

modulated signals are encoded by a space-time block encoder to generate $A_t$ parallel signal sequences of length $p$, transmitted through $A_t$ transmit antennas simultaneously in $p$ time periods. Thus, there are $p$ space-time symbols transmitted from each antenna for each block of $s$ input symbols. The rate of the STBC is defined as

$$r_{STBC} = s / p .\tag{5.3}$$

The spectral efficiency of the STBC is given by

$$\eta = \frac{r_b}{W} = \frac{sm}{p} \quad \text{bit/s/Hz} ,\tag{5.4}$$

where $r_b$ and $W$ are the bit rate and the signal bandwidth, respectively.

When the number $A_t$ of transmit antennas is larger than two, there does not exist any OSTBC that provides full transmit diversity while maintaining the orthogonality between the transmit sequences. Thus, some non-orthogonal codes, known as *perfect codes*, which provide a full transmit diversity while offering a code rate $r_{STBC} = A_t$, can be used. The most famous example of *perfect codes* is the Golden code, with $A_t = 2$ [125]. However, these space-time schemes require a high complexity decoder which increases the receiver cost. Consequently, they are not practical for UWB applications.

In this section, we describe the Alamouti scheme since it will be used in the final MIMO LP-OFDM system. In the Alamouti space-time encoder, each group of $m = \log_2 (M)$ information bits is first modulated with a *M*-ary constellation. Then, a block of two modulated symbols $x_1$ and $x_2$ is taken in every encoding operation and mapped to the transmit antennas according to the code matrix $X$ given by

$$X = \begin{bmatrix} x_1 & -x_2^* \\ x_2 & x_1^* \end{bmatrix},\tag{5.5}$$

where $x_1^*$ denotes the complex conjugate of $x_1$. The encoder outputs are transmitted in two consecutive transmission periods from two transmit antennas. During the first period, signals $x_1$ and $x_2$ are transmitted simultaneously from the first and second antennas, respectively, and during the second period, signals $x_1$ and $x_2$ are transmitted from the first and second antennas. Note that the transmit sequences from the two transmit antennas are orthogonal.

Let us now assume that two receive antennas are used at the receiver. The received Alamouti signals at the receive antenna $a_r$ over two consecutive symbol periods, denoted by $r_1^{a_r}$ and $r_2^{a_r}$ for time $t$ and $t+T$ , respectively, can be expressed as

$$\begin{cases} r_1^{a_r} = h_{1a_r} x_1 + h_{2a_r} x_2 + n_1^{a_r}, \\ r_2^{a_r} = -h_{1a_r} x_2^* + h_{2a_r} x_1^* + n_2^{a_r}, \end{cases} \tag{5.6}$$

where $h_{a_t a_r}$ is the fading coefficient for the path from transmit antenna $a_t$ to receive antenna $a_r$, with $a_t = \{1, 2\}$ and $a_r = \{1, 2\}$, and $n_1^{a_r}$ and $n_2^{a_r}$ are the noise signals for receive antenna $a_r$ at time $t$ and $t + T$, respectively.

The receiver constructs two decision statistics based on the linear combination of the received signals. The decision statistics, denoted by $\tilde{x}_1$ and $\tilde{x}_2$, are given by

$$\begin{cases} \tilde{x}_1 = \sum_{a_r=1}^{2} \left( h_{1a_r}^* r_1^{a_r} + h_{2a_r} r_2^{a_r *} \right) = \sum_{a_t=1}^{2} \sum_{a_r=1}^{2} \left| h_{a_t a_r} \right|^2 x_1 + \sum_{a_r=1}^{2} \left( h_{1a_r}^* n_1^{a_r} + h_{2a_r} n_2^{a_r *} \right), \\ \tilde{x}_2 = \sum_{a_r=1}^{2} \left( h_{2a_r}^* r_1^{a_r} - h_{1a_r} r_2^{a_r *} \right) = \sum_{a_t=1}^{2} \sum_{a_r=1}^{2} \left| h_{a_t a_r} \right|^2 x_2 + \sum_{a_r=1}^{2} \left( h_{2a_r}^* n_1^{a_r} + h_{1a_r} n_2^{a_r *} \right). \end{cases} \tag{5.7}$$

The Alamouti scheme can achieve a full diversity of $A_t \times A_r = 2$, due to the orthogonality between the sequences coming from the two transmit antennas. However, it does not provide any coding gain relative to the uncoded modulation scheme.

### 5.2.3   MIMO technology in UWB communications

The idea of employing MIMO technology in UWB systems to enhance the systems data rates and transmission ranges has gained considerable interest recently. In conventional RF technology, MIMO has been well known for its effectiveness of improving the system performance in fading environments. Most UWB applications are in rich scattering indoor environment, which provides an ideal transmission scenario for MIMO techniques. In addition, the high center frequency of UWB radio relaxes the requirements on the spacing between antenna array elements. Furthermore, MIMO techniques can be a possible solution for overcoming the very low UWB transmission levels, resulting in enhanced data rates and communication ranges. MIMO-UWB systems benefit from SNR improvements, higher channel capacities and better interference rejection [126], [127]. Consequently, the combination of UWB and MIMO technology can be seen as a cost efficient method to achieve the very high data rate requirement for future short range wireless applications.

However, given the important multipath diversity of the UWB channels, one may wonder whether the MIMO technique would provide significant additional spatial diversity or not. In fact, the UWB signals are not very sensitive to deep notches that can occur in any part of the spectrum due to the very large UWB frequency band. The answer to that will be

found when studying the capacity of the MIMO channel for different UWB bandwidths in Section 5.3.

To this date, UWB-MIMO technology has been well documented for the traditional single-band UWB system. Two main approaches were considered: the overall diversity enhancement with no data rate improvement [128], [129], and the spatial multiplexing resulting in enhanced data rates with no transmit diversity gain [130], [131]. On the other hand, research for MIMO MB-OFDM UWB systems is less explored, thus offering limited resources in handling the benefits and challenges of UWB-MIMO communications. Some works on MIMO MB-OFDM systems can be found in [132]–[134]. Most of these works propose to use space-time codes as well as space-time-frequency codes based on Alamouti schemes, to obtain a diversity gain.

## 5.3 New realistic MIMO UWB channel model

In this section, we describe a new realistic channel model for indoor MIMO UWB applications, developed at IETR by Dr. Louis-Marie Aubert and Prof. Bernard Uguen within an external research contract with France Télécom R&D [135]. This channel model with be used for the simulations of the proposed MIMO LP-OFDM system.

In channel modeling techniques, a modeling approach with correlation matrices is generally simple since it requires only a power delay profile and two correlation matrices. In the case of UWB channels, whose bandwidth is very large, the channel model requires a time partitioning into very narrow taps, each tap containing only a very small number of channel paths. Consequently, Rayleigh model can not be directly applied to the UWB case, and MIMO channel matrix can not be derived from a Gaussian matrix. In order to solve this problem, the UWB channel can be partitioned into sub-channels of bandwidth equal to the channel coherence bandwidth, which leads to larger taps with a larger number of channel paths. Each MIMO sub-channel can then be obtained from a Gaussian matrix. However, reconstructing the global MIMO UWB channel from the different sub-channels is very difficult since correlation between the sub-channels might occur.

Due to the difficulty of the correlation matrices approach in the UWB context, the proposed channel model considers a geometric statistic channel (GSC) approach, similar to the one adopted by the spatial channel model of 3GPP/3GPP2 [136]. In the 3GPP/3GPP2 approach, a MIMO channel response can be obtained from a SISO impulse response, the angle of departure (AoD) and angle of arrival (AoA) statistics, and the antennas geometry at the transmitter and the receiver. Similarly, in the MIMO UWB model, we select the SISO impulse response from the SISO-UWB channel model adopted by IEEE 802.15.3a

(see Section 1.7). Then, the spatial component is chosen based on the IEEE 802.11n model [137], where AoD and AoA of the different clusters follow a uniform distribution, and the AoD and AoA of the intra-clusters paths follow a Laplace distribution.

The capacity of the frequency selective MIMO UWB channel is expressed in b/s/Hz as

$$C = \frac{1}{W} \int_{-W/2}^{W/2} \log_2 \det\left( I + \frac{SNR}{A_t} H_f H_f^H \right) df \,, \tag{5.8}$$

where $W$ is the channel bandwidth and $H_f$ the frequency domain MIMO matrix of size $A_r \times A_t$, with $A_t$ and $A_r$ the number of transmit and receive antennas, respectively. After singular value decomposition (SVD) of $H_f$, this capacity can be written in b/s/Hz as

$$C = \frac{1}{W} \sum_{a=1}^{\min(A_t, A_r)} \int_{-W/2}^{W/2} \log_2\left( I + \frac{SNR}{A_t} \lambda_a^2(f) \right) df \,, \tag{5.9}$$

where the real numbers $\lambda_a^2(f)$, with $a = 1, \cdots, \min(A_t, A_r)$, are the eigenvalues of $H_f H_f^H$.

Figure 5.6 depicts the capacity of the proposed GSC channel for different SNR levels and channel bandwidths, with $A_t = A_r = 2$ and an antennas spacing of $d = 5\,\text{cm}$ at the transmitter and at the receiver. As expected, when the bandwidth is very large, the diversity order exploited in the frequency domain is very high, and the additional gain due to
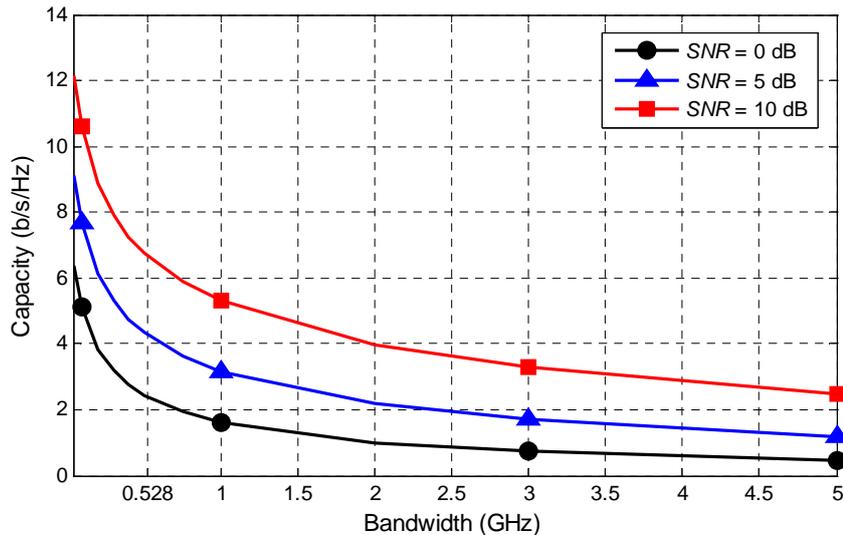


Figure 5.6: Capacity of the proposed MIMO UWB channel model with two transmit and two receive antennas, and an antennas spacing of $d = 5\,\text{cm}$.

exploitation of the spatial diversity is lower. As we can see, in the case of a channel bandwidth of $W = 528\,\text{MHz}$, equivalent to the bandwidth of one MB-OFDM band, the MIMO channel offers a considerable capacity that is much higher than the capacity limit obtained at very high channel bandwidths ($W > 4\,\text{GHz}$). This shows that the MIMO technique can provide considerable spatial diversity gain with the 528 MHz bandwidth we are using, even if the multipath diversity of the UWB channels is important. Consequently, MIMO technology can be efficiently exploited for MB-OFDM UWB applications.

A typical channel realization of the proposed GSC model, with $A_t = A_r = 2$ and $d = 1\,\text{cm}$, is presented in Figure 5.7, in the frequency and time domains. Note that $h_{a_t a_r}$ represents the channel response between transmit antenna $a_t$ and receive antenna $a_r$.

## 5.4 MIMO LP-OFDM system

### 5.4.1 System configuration

Based on the previous MIMO channel capacity study showing that the spatial diversity of UWB systems can be efficiently exploited, and in order to further improve the performance of the LP-OFDM system, we propose to add a low complexity MIMO scheme. We have chosen the well-known Alamouti scheme with two transmit and two receive antennas, which can be very efficient in an UWB context since it provides full spatial diversity gain, with no ISI and with low complexity ML receivers. The different blocks of the resulting MIMO LP-OFDM transmission system are depicted in Figure 5.8.

We have chosen a STBC scheme, since it offers important flexibility in the systems combining multicarrier and spread spectrum techniques, and low additional complexity. For instance, the good performance of the combination of Alamouti codes with a MC-CDMA waveform is presented in [138], for frequency selective and non-selective channels. In addition, combining STBC with a channel coding provides a considerable coding gain for the system. Thus, a system using STBC with MC-SS techniques offers maximum diversity order in the space, frequency and time directions.

One of the main reasons behind the choice of the Alamouti scheme is the orthogonality of its transmit sequences which allows a very simple ML decoding algorithm, based on linear processing of the received signals, resulting in low cost receivers. The number of transmit and receive antennas is limited to two in order not to significantly increase the complexity. Other non-orthogonal STBC schemes providing full transmit diversity, like the Golden code for example, could have been considered. However, the absence of orthogonality leads to high complexity decoders, and thus to expensive receivers, which is not practical for UWB applications which require very low cost and small size UWB devices.

(a)  Channel response $h_{11}$



(b)   Channel response $h_{12}$



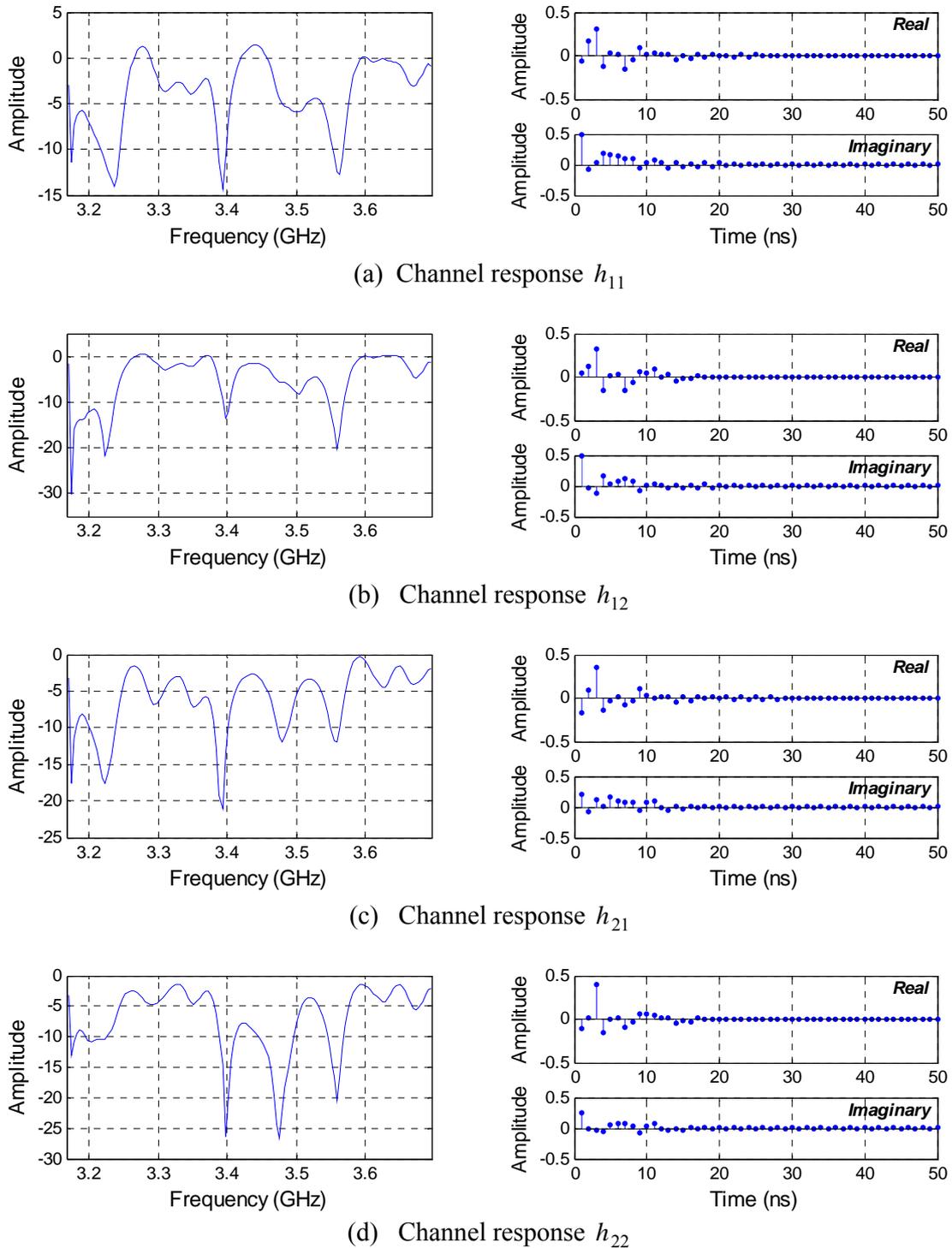(c)  Channel response $h_{21}$



(d)  Channel response $h_{22}$

Figure 5.7: A typical channel realization of the proposed MIMO UWB channel model, with two transmit and two receive antennas, and an antennas spacing of $d = 1\,\mathrm{cm}$, presented in the frequency and time domains.
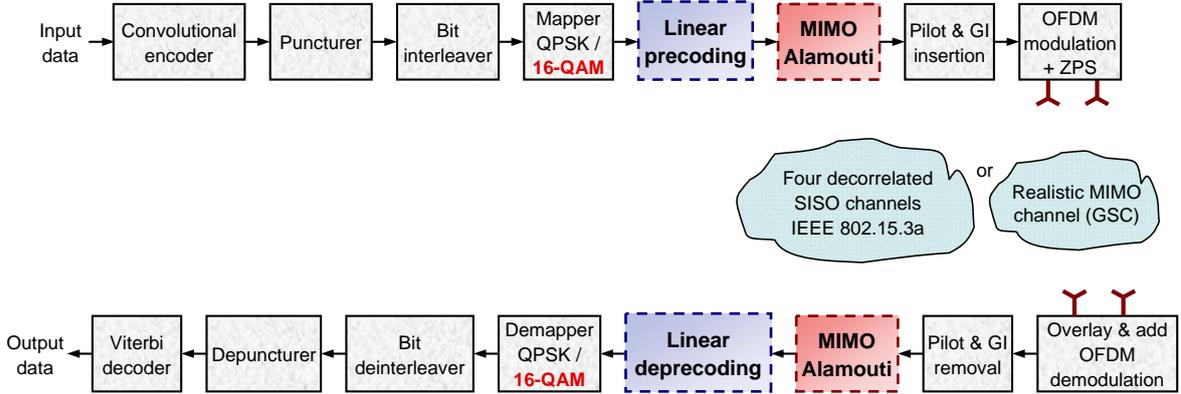
Figure 5.8: Simplified MIMO LP-OFDM UWB transmission system.

The spacing $d$ between the two transmit antennas and between the two receive antennas strongly depends on the characteristics of the propagation channel. In order to obtain enough decorrelation between the signals of the different antennas, we study different antennas spacings $d$. An antennas spacing of $d = 5$ cm at the transmitter and the receiver sides, equivalent to $0.66\lambda$, with $\lambda$ the wavelength of the center frequency, seems to be a good solution offering a considerable diversity gain, as we will see in the simulation results in Section 5.4.3.

On the other hand, the multi-user access is performed using TFC sequences. However, contrarily to the WiMedia system, the frequency hopping from a MB-OFDM band to another occurs at the end of each two consecutive OFDM symbols, since in the Alamouti scheme a block of two modulated symbols $x_1$ and $x_2$ are taken in every encoding operation and mapped to the transmit antennas.

### 5.4.2 Data rate enhancement with extension to 16-QAM constellation

In the proposed MIMO LP-OFDM system, two possible constellations are considered: the QPSK and the 16-QAM. In a first step, we consider a single QPSK constellation, same as in the SISO LP-OFDM system. In this case, the objective of adding the Alamouti scheme is to improve the system robustness, and consequently the system range, without any data rate enhancement. The main system parameters and the proposed data rates are the same as in the SISO LP-OFDM system.

In a second step, in order to improve the UWB system throughput, an additional 16-QAM constellation is considered. Four very high data rates from 614 Mb/s to around 1 Gb/s are thus proposed, listed in Table 5.3. The number $K$ of used codes is equal to the code length $L = 16$ for all these data rates. In this extension to a 16-QAM constellation,

Table 5.3: Extended LP-OFDM system data rates, using a 16-QAM constellation.

| Data rate (Mb/s) | Constellation | Coding rate $r$ | Number $K$ of codes |
|:---:|:---:|:---:|:---:|
| 614 | 16-QAM | 1/2 | 16 |
| 819 | 16-QAM | 2/3 | 16 |
| 921 | 16-QAM | 3/4 | 16 |
| 983 | 16-QAM | 4/5 | 16 |

one or two additional bits could be needed for the analog-to-digital conversion of the UWB receiver in order to reduce the quantification noise. Hence, the radio-frequency front-end complexity of the receiver is not significantly increased compared to the WiMedia solution.

The extension to a 16-QAM constellation requires some system parameters modifications. In fact, when a 16-QAM constellation is used, the information is carried by the phase as well as the amplitude of the symbol. Since the MMSE technique modifies the amplitude of the received signal, a normalization factor $\rho$ has to be applied before the demapper to normalize the symbols arriving at the demodulator after having undergone amplitude distortions. Taking into account the MIMO and LP characteristics of the system, $\rho$ is given for each LP-OFDM block by

$$\rho_b = L \left/ \sum_{n=1}^{L} \frac{\sum_{a_t=1}^{A_t} \sum_{a_r=1}^{A_r} \left| h_{a_t a_r, n, b} \right|^2}{\sum_{a_t=1}^{A_t} \sum_{a_r=1}^{A_r} \left| h_{a_t a_r, n, b} \right|^2 + \dfrac{1}{SNR_{a_r, n, b}}} \right. , \qquad (5.10)$$

where $h_{a_t a_r, n, b}$ is the channel response for the $n^{\text{th}}$ subcarrier of block $b$ between transmit antenna $a_t$ and receive antenna $a_r$, and $SNR_{a_r, n, b}$ is the signal-to-noise ratio for subcarrier $n$ of block $b$, at the receive antenna $a_r$.

At the receiver, the received 16-QAM signals are first demodulated by a soft-output demapper and deinterleaved, and then passed to a standard binary soft-input Viterbi decoder [139]. The idea is to demap the received signal into soft bits which have the same sign as the one provided by a hard detector and whose absolute value indicates the reliability of the decision.

Let $y(n,b) = y_I(n,b) + j\, y_Q(n,b)$ denote the output of the equalizer corresponding to subcarrier $n$ of block $b$, with $I$ and $Q$ representing the in-phase and quadrature components, respectively. The log-likelihood ratio (LLR) for the decision of the in-phase bits $b_{I,m}(n,b)$

and quadrature bits $b_{Q,m}(n,b)$ of the 16-QAM constellation, with $m = \{1, 2\}$, in the case of a MIMO LP-OFDM system, can be derived from the LLR approximation of a SISO OFDM system given in [140], as follows

$$\begin{cases} LRR\big(b_{I,m}(n,b)\big) \equiv \dfrac{\sum_{a_t=1}^{A_t}\sum_{a_r=1}^{A_r}\sum_{n=1}^{L}\big|h_{a_t a_r,n,b}\big|^2}{A_t A_r L}\, D_{I,m}(n,b), \\[4mm] LRR\big(b_{Q,m}(n,b)\big) \equiv \dfrac{\sum_{a_t=1}^{A_t}\sum_{a_r=1}^{A_r}\sum_{n=1}^{L}\big|h_{a_t a_r,n,b}\big|^2}{A_t A_r L}\, D_{Q,m}(n,b), \end{cases} \tag{5.11}$$

where $D_{I,m}(n,b)$ and $D_{Q,m}(n,b)$ are given for the normalized mapping levels $\{\pm 1, \pm 3\}$ we are using by

$$D_{I,1}(n,b) = \begin{cases} y_I(n,b), & |y_I(n,b)| \leq 2, \\ 2\big(y_I(n,b)-1\big), & y_I(n,b) > 2, \\ 2\big(y_I(n,b)+1\big), & y_I(n,b) < -2, \end{cases} \tag{5.12}$$

$$D_{I,2}(n,b) = -\big|y_I(n,b)\big| + 2, \tag{5.13}$$

$$D_{Q,1}(n,b) = \begin{cases} y_Q(n,b), & |y_Q(n,b)| \leq 2, \\ 2\big(y_Q(n,b)-1\big), & y_Q(n,b) > 2, \\ 2\big(y_Q(n,b)+1\big), & y_Q(n,b) < -2, \end{cases} \tag{5.14}$$

$$D_{Q,2}(n,b) = -\big|y_Q(n,b)\big| + 2. \tag{5.15}$$

Note also that in the case of a 16-QAM constellation, a mapping normalization factor $\rho_{mapper} = 1/\sqrt{10}$ is applied before the mapper and a normalization factor of $1/\rho_{mapper}$ is applied before the demapper, whereas in the case of a QPSK constellation, $\rho_{mapper}$ is equal to $1/\sqrt{2}$.

### 5.4.3 Simulation results

After having described the proposed MIMO LP-OFDM system based on an Alamouti scheme with two transmit and two receive antennas, we present in this section the results of the system simulations performed on the first three MB-OFDM bands. The new realistic MIMO GSC model is used for the MIMO system simulations. In addition, results of sys-

tem simulations carried out on four fully decorrelated SISO channels IEEE 802.15.3a are also presented as reference, as presented in Figure 5.8. As in the SISO system simulations, frames of 150 OFDM symbols are used, each frame being transmitted on a different channel realization, from a total of 100 available realizations. Note that for the different results presented in the sequel, the power gain provided by the use of two receive antennas is not taken into account. If it was considered, all the BER curves of the MIMO system performance would be shifted 3 dB to the left.

### 5.4.3.1   Range improvement

In this section, we present the simulation results of the LP-OFDM system using a MIMO scheme with a QPSK constellation to improve the system range at low and medium data rates, listed in Table 5.2.

In Figure 5.9, the WiMedia system performance at the highest and lowest possible data rates of 480 and 53.3 Mb/s, respectively, is presented as reference. The LP-OFDM system using a QPSK constellation and a TFC technique, with data rates close to these two WiMedia data rates, i.e. the medium data rate of 460 Mb/s and the low data rate of 51.2 Mb/s, is given for comparison. We can see that the LP component of the SISO LP-OFDM system offers around 1.1 dB gain at medium data rate, and around 0.6 dB at low data rate for a BER level of $10^{-4}$. In addition, the simulation results of the MIMO LP-OFDM system using the proposed realistic GSC model are presented for spacing values of $d = 1\,\text{cm}$ and $d = 5\,\text{cm}$ between the two transmit antennas and between the two receive antennas. These two antennas spacings are equivalent to $d \approx 0.13\lambda$ and $d \approx 0.66\lambda$, respectively, where $\lambda$ is the wavelength of the center frequency $f = 3.96\,\text{GHz}$ of the first three MB-OFDM bands. In this figure, we notice that at $BER = 10^{-4}$ with $d = 1\,\text{cm}$, the MIMO scheme offers an additional gain of 3.5 dB at medium data rate, resulting in a total MIMO LP-OFDM gain of 4.6 dB compared to the WiMedia system. When the antennas spacing is increased to $d = 5\,\text{cm}$, more spatial diversity is obtained, and thus, the system performance converges to the performance of a MIMO LP-OFDM system using four fully decorrelated SISO channels IEEE 802.15.3a. Consequently, with $d = 5\,\text{cm}$, which is a very practical antennas spacing, a total MIMO LP-OFDM gain of 5.2 dB is obtained compared with the WiMedia system.

Since the objective of combining MIMO and LP techniques at low and medium data rates, i.e. when a QPSK constellation is used, is to improve the UWB system robustness, and consequently to improve the system range, we present the system simulation results in terms of the system range. From [43], the ratio $E_b / N_0$ can be written as a function of the system range *D* as follows

$$\frac{E_b}{N_0} = E + 10\log_{10}(W) + G_t + G_r - 10\,\alpha\log_{10}\left(\frac{4\pi f'D}{c}\right) - 10\log_{10}(R) - (-174 + F) - I. \quad (5.16)$$

In (5.16), $E$ represents the transmit power density equal to $E = -41.3\,\text{dBm/MHz}$, and $W$ the useful bandwidth of the transmitted signal. In this analysis, isotropic antennas at the transmitter and receiver are assumed, thus the transmit and receive antennas gains are equal to $G_t = G_r = 0\,\text{dBi}$. In the path loss expression, we assume that the path loss exponent is equal to $\alpha = 2$ and that $c = 3\times10^8$ m/s, and we consider the geometric center frequency of the waveform $f' = \sqrt{f_{\min}\,f_{\max}} \approx 3882\,\text{MHz}$, where $f_{\min}$ and $f_{\max}$ are the -10 dB edges of the waveform spectrum. Besides, $R$ represents the system transmission rate in b/s, and $F$ the noise figure at the receive antenna side. In this study, we choose $F = 6.6\,\text{dB}$, which is derived from the practical noise figure analysis in [20], where the primary sources for noise are the LNA, mixer and preselect filter. Losses due to front-end filtering, ADC degradation, channel estimation, clock frequency mismatch, carrier-offset recovery and so forth, are included in the implementation loss component $I$, assumed equal to $I = 2.5\,\text{dB}$ [20].

Figure 5.10 gives the data rates as a function of the system range $D$ for different system configurations, considering only a QPSK constellation. $D$ can be derived from (5.16) for a given value of $E_b / N_0$. We notice that the MIMO LP-OFDM system with $d = 5\,\text{cm}$ has a very close range to the one of a MIMO LP-OFDM system using four fully decorrelated SISO channels IEEE 802.15.3a. This means that an antennas spacing of 5 cm is enough to benefit well from the spatial diversity and improve the system range. In addition, the MIMO LP-OFDM system with $d = 5\,\text{cm}$ has a range that is approximately 2 meters larger than the WiMedia system range, for any data rate, and approximately 1.5 meters larger than the range of the SISO LP-OFDM system.

### 5.4.3.2 Data rate enhancement

In this section, we present the simulation results of the MIMO LP-OFDM system offering very high data rates going up to around 1 Gb/s, listed in Table 5.3, through the combination of an Alamouti scheme with a 16-QAM constellation.

We notice from Figure 5.11 that, for all these very high data rates, the performance of the MIMO LP-OFDM system in terms of BER is better than the performance of the WiMedia system with a data rate of 480 Mb/s. This shows the advantage of combining MIMO with LP techniques and using higher constellation orders to increase the system data rate while maintaining or even improving the system performance in terms of BER, at the expense of a small complexity increase.
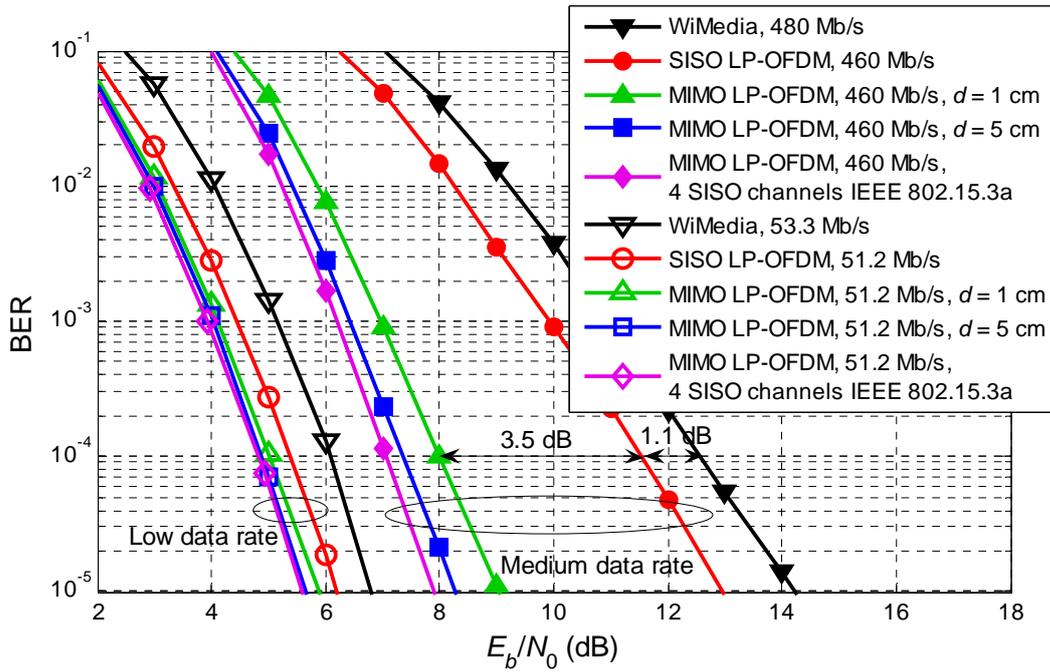
Figure 5.9: Performance of the SISO and MIMO LP-OFDM systems using a QPSK constellation, at low and medium data rates and for different antennas spacings *d*.
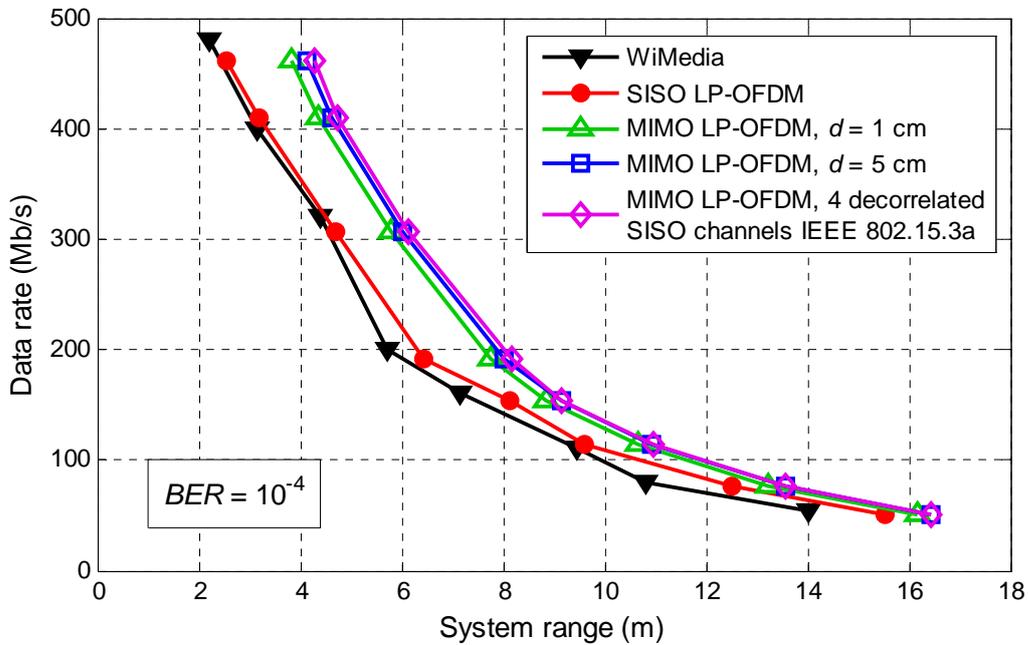


Figure 5.10: Range improvement of the MIMO LP-OFDM system using a QPSK constellation, at low and medium data rates and for different antennas spacings *d*.

In Figure 5.11, if we compare the curves of the MIMO LP-OFDM system at 983 Mb/s and the WiMedia system at 480 Mb/s, we notice that the MIMO LP-OFDM system, whose data rate is twice the one of the WiMedia system, has even better performance in terms of BER. This result shows the advantage of using the proposed system in applications targeting gigabit data rates.

Figure 5.12 presents the simulation results of the MIMO LP-OFDM system for all the proposed data rates, listed in Table 5.2 and Table 5.3. The required $E_b / N_0$ that provides a BER of $10^{-4}$ is given for the different system configurations and the gain offered by the use of TFC technique is evaluated. Here also, the results show the advantage of combining a low complexity Alamouti scheme with LP-OFDM technique in UWB applications. At the medium data rate of 460 Mb/s, a MIMO LP-OFDM system with $d = 5$ cm has a considerable gain of 5.2 dB compared to the WiMedia system at 480 Mb/s, as shown previously. In addition, a MIMO LP-OFDM system with $d = 1$ cm and without TFC has a gain of 2.7 dB, and when a TFC technique is applied, an additional gain of 1.8 dB is obtained. Besides, we notice that with $d = 5$ cm, the TFC gain is only around 0.1 dB. This is due to the fact that for $d = 5$ cm, the MIMO and LP-OFDM components fully benefit from the total available diversity. On the other hand, at very high data rates, we notice the advantage of applying the TFC technique whose gain increases significantly. In fact, at the highest data rate of 983 Mb/s, the TFC gain is equal to 3.9 dB with $d = 1$ cm, and 1.3 dB with $d = 5$ cm. In addition, at this data rate, the MIMO LP-OFDM system with $d = 5$ cm and using TFC sequences is even 0.6 dB better than the WiMedia system which is providing only half of this data rate.

In conclusion, the proposed MIMO LP-OFDM system can be used to provide a data rate of 460 Mb/s with a gain of 5.2 dB compared to the WiMedia system, or to double the WiMedia maximum data rate and provide a data rate of around 1 Gb/s with slight performance improvement. Note that all these results are obtained with a practical antennas spacing of $d = 5$ cm and a low complexity ML receivers.

Besides, these simulation results have shown that the combination of Alamouti space-time schemes with LP schemes improves the system performance significantly, while not increasing the complexity of the receiver, thanks to the orthogonality properties of the Alamouti scheme. Finally, these results also prove that the MIMO technology can be advantageously exploited for UWB applications using frequency bands of 528 MHz.
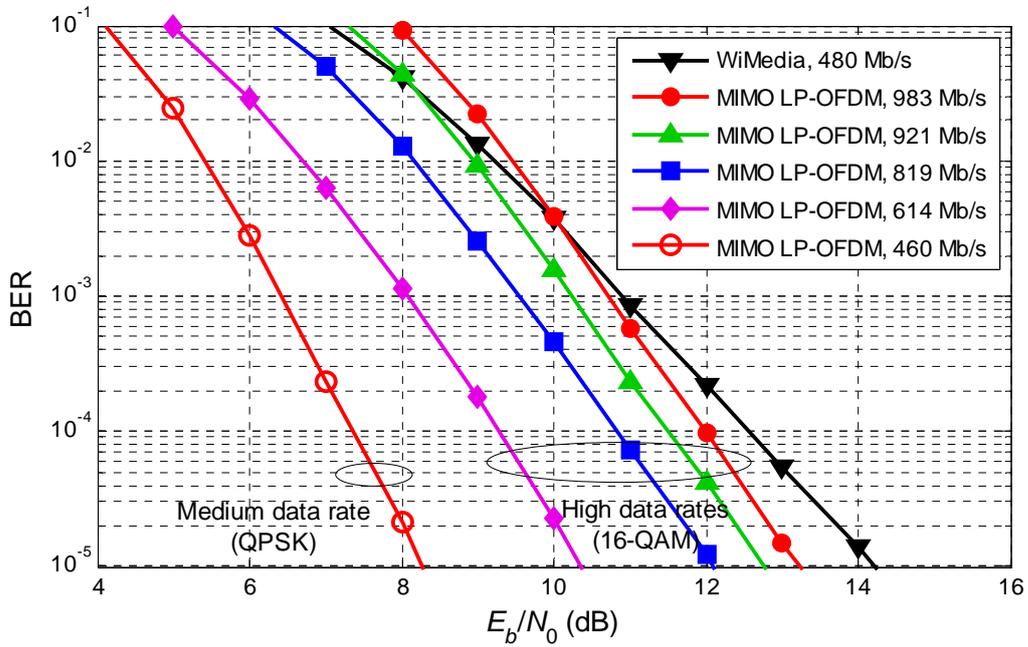
Figure 5.11: Performance of the MIMO LP-OFDM system using a 16-QAM constellation and an antennas spacing of $d = 5\,\mathrm{cm}$, for different very high data rates.
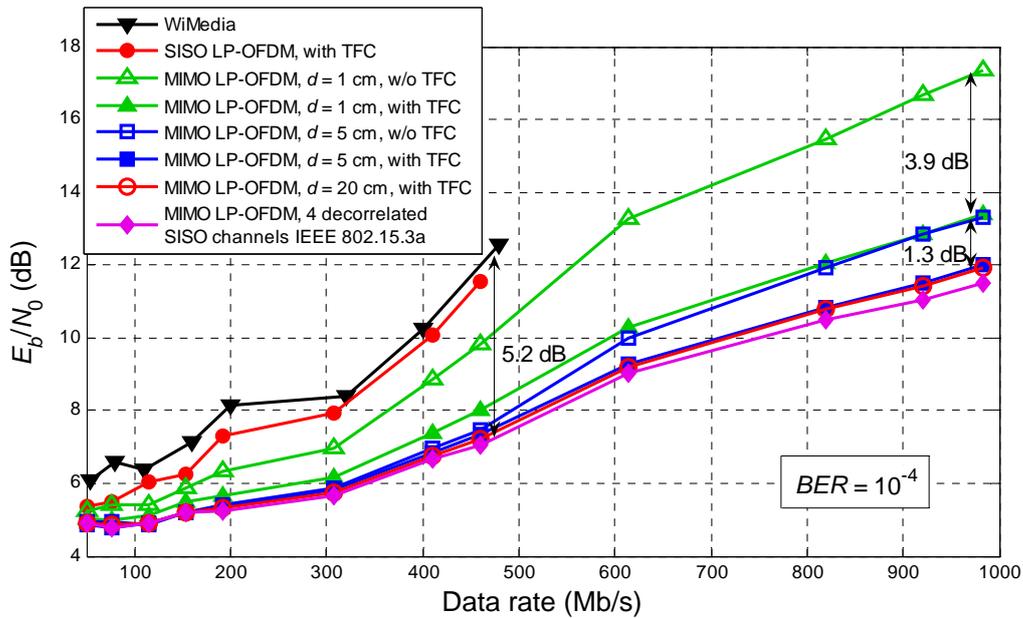


Figure 5.12: Performance of the SISO and MIMO LP-OFDM systems with and without TFC, for the all proposed data rates, at $BER = 10^{-4}$.

## 5.5    Conclusion

In this chapter, we have studied the global UWB system taking into account the different functions of the transmission chain. First, we presented the optimal parameters that improve the performance of the proposed LP-OFDM system, in a SISO context. One significant advantage of the LP-OFDM system is that it provides a wide range of data rates due to the high flexibility brought by the joint assignment of the number of used codes and the coding rate. The system simulation results for different spreading code lengths verify the analytical results, obtained in Chapter 4, regarding the effect of the code length on the system performance. In addition, we showed that the benefits of the spreading and channel coding functions on the channel diversity exploitation are complementary and depend on each other. Besides, the global SISO LP-OFDM system study has brought comparable simulation results, showing the advantage of adding a linear precoding component to the OFDM scheme, which leads to a high flexibility and to a gain of around 1 dB compared with the WiMedia system.

In the second part of the chapter, we studied the addition of an Alamouti space-time coding scheme to the LP-OFDM system, to benefit from the available spatial diversity. This Alamouti scheme, which provides full spatial diversity gain with low complexity ML receivers, is very efficient for UWB applications since they require very low cost and small size UWB devices. The objective of the MIMO addition is first to improve the system range, while maintaining a single QPSK constellation, and then to provide very high data rates through a joint combination of MIMO with a 16-QAM constellation. For low and medium data rates (from 51.2 to 460 Mb/s), the proposed MIMO LP-OFDM system outperforms the WiMedia system in terms of system robustness, and consequently in terms of system range. For instance, the MIMO LP-OFDM system provides a data rate of 460 Mb/s with a gain of 5.2 dB compared to the WiMedia system. On the other hand, one outstanding result is that the MIMO LP-OFDM system offers a data rate of around 1 Gb/s, which is twice the maximum data rate provided by the WiMedia system, with even slight BER performance improvement. Note that these results are obtained with a practical MIMO antennas spacing of only 5 cm. In conclusion, the proposed MIMO LP-OFDM system can be advantageously exploited for high data rate UWB applications.

# Conclusion and perspectives

T HIS thesis has proposed a new very high data rate UWB system based on the combination of OFDM, linear precoding, MIMO schemes and resource allocation principles.

In the first part of the thesis, mainly Chapter 1 and Chapter 2, we have started with a general overview on the emerging UWB technology, focusing on the advantages of this technology, which make it a potential candidate for future wireless communications. Then, we have listed the wide application areas of UWB, which can be divided into high data rate and low data rate communications. Since this thesis focuses on the high data rate WPAN applications, we described the two main modulation schemes considered for WPAN environment: the MB-OFDM and IR-UWB techniques. The MB-OFDM approach, based on the combination of OFDM with a multibanding technique, was chosen as the starting point of our studies as it is the most promising candidate for high data rate WPAN applications, due to its numerous advantages over IR-UWB and its wide support by the standardization and industrial groups.

On the other hand, we presented the principles of the main transmission techniques we are dealing with in this thesis, mainly the OFDM and linear precoding schemes. Besides, we described the MB-OFDM system and discussed its advantages in UWB communications, as well as its limitations notably in terms of system range and robustness, and in terms of multiple access between users. Then, we described the proposed new LP-OFDM UWB scheme, based on the combination of linear precoding techniques with the OFDM waveform, whose objective is to reduce the MB-OFDM limitations and improve the total system performance.

The second part of the thesis, mainly Chapter 3 and Chapter 4, was dedicated to the analytical study of the LP-OFDM system, and particularly, to the study of the LP component. In the first chapter, we considered a classical target SER approach and we presented the main adaptive resource allocation strategies that can be carried out on multicarrier systems. Then, a new optimization study of LP-OFDM systems was carried out. This study offers a wide variety of scenarios that can be chosen depending on the desired system complexity. In fact, a novel low complexity optimization algorithm that maximizes the LP-OFDM system range when a single QPSK constellation is used, as in the MB-OFDM

system, was proposed. Additional algorithms that maximize either the system range or the throughput were also proposed in the case where variable constellation orders are allowed. Furthermore, a new system optimization study based on a dynamic TFC allocation was considered. The numerical results of simulations carried out on the different adaptive and non-adaptive systems showed that the LP-OFDM system outperforms the MB-OFDM system in terms of throughput and range. This is due to the spreading gain provided by the linear precoding component, and to the efficiency of the proposed algorithms. Note that some of the proposed algorithms require the knowledge of the CSI at the transmitter side and others just need a small information vector to be sent from the receiver to the transmitter. One of the main advantages of applying resource allocation principles for indoor UWB communications is that the UWB channel response varies slowly in time and can be considered as quasi-static during one frame. Consequently, the CSI can be sent by a simple feedback to the transmitter at the beginning of each frame, which does not significantly increase the implementation complexity of the proposed allocation algorithms.

On the other hand, in Chapter 4, we proposed a novel resource allocation approach that focuses on the system mean BER instead of the subcarriers and codes SER. This approach facilitates the error rate conversion between network layers, since the error rate limit imposed by the upper layers is in terms of BER and not SER. The main objective of this study was to minimize the system mean BER for a given target throughput. This study also offers a wide variety of scenarios that can be chosen depending on the desired system complexity. Thus, the first proposed new algorithm minimizes the LP-OFDM system mean BER under a single QPSK constellation order, by optimizing the variable spreading code lengths configuration. Simulation results showed that this algorithm reduces the mean BER significantly at the different SNR levels, and that the resulting adaptive LP-OFDM system with variable code length outperforms the LP-OFDM systems using a unique code length. In addition, new resource allocation algorithms which find the optimal power and bit distribution that minimizes the mean BER of OFDM and LP-OFDM systems when variable constellation orders are allowed, were also proposed. Simulation results showed that the resulting adaptive LP-OFDM system reduces the mean BER significantly, compared to the LP-OFDM systems using a fixed constellation order.

The last part of the thesis, i.e. Chapter 5, was dedicated to the global system study, taking into account the different functions of the transmission chain. In a SISO context, the different parameters of the proposed LP-OFDM system were first optimized to improve the system range in terms of BER. One significant advantage of the LP-OFDM system is that it provides a wide range of data rates due to the high flexibility brought by the joint assignment of the used spreading codes number and the channel coding rate. The global sys-

tem study brought comparable simulation results, showing the advantage of adding a linear precoding component to the MB-OFDM solution, in terms of performance and flexibility, which verifies the analytical results obtained in the previous chapters. On the other hand, a MIMO component was added to the LP-OFDM system, first to improve the system robustness while considering a QPSK constellation, and then to reach higher data rates with good robustness, while considering a higher constellation order of 16-QAM. A new geometric statistic MIMO channel model, developed at IETR, was used for the MIMO UWB system simulations. Simulation results show that the proposed MIMO LP-OFDM system outperforms the WiMedia system in terms of robustness at low and medium data rates. In addition, when a 16-QAM constellation is combined with a MIMO scheme, the resulting MIMO LP-OFDM system offers a 1 Gb/s data rate with even better BER performance than the WiMedia system, which can provide at maximum only half of this data rate.

In conclusion, the different results show the advantage of combining linear precoding and MIMO schemes with OFDM, and using dynamic resource allocation algorithms to improve the performance of UWB systems. Thus, the proposed MIMO LP-OFDM system can be efficiently exploited for high data rate UWB applications at reasonable additional complexity of the receivers.

The theoretical and practical results of this thesis work led to contributions to the European FP7 OMEGA project [1], and to an external research contract with Orange Labs RESA/WIN/CREM (France Télécom R&D). This work has also led to two published journal papers and seven published international conference papers. Furthermore, one additional journal paper and two international conference papers are under process.

## Perspectives

There are a variety of fruitful areas for future research on UWB communications and related topics. We present in what follows some of interesting research directions that need to be further investigated.

Concerning the **analytical study** of Chapter 3 and Chapter 4, the intrinsic characteristics and capabilities of the precoding function were highlighted and different resource allocation algorithms were developed without taking into account the channel coding. The global system study verified the analytical study results and showed the effect of combining spreading and channel coding to well exploit the channel diversity. Thus, a smart approach, with some increased analytical complexity, would be to modify the proposed allocation algorithms to accommodate the coding gains relative to the channel coding schemes. This approach has been considered in [105] in the case of linear precoded discrete multi-tone modulation for power line communication. In fact, the SNR gap value for a given

target SER or BER can be modified to carry the desired margin of the system as well as the coding gain of the channel coding scheme.

Besides, the resource allocation principles with a mean BER approach are new in wireless communications and more investigation is required. In fact, only few papers in the literature have considered a BER approach, where only discrete greedy-type methods were used. Thus, finding new numerical methods that solve the allocation problems, such as the method we have proposed for mean BER minimization study, would be very useful to improve the system performance while not significantly increasing the algorithms complexity. One example that could be analytically investigated is the LP-OFDM rate maximization problem under a target mean BER, which can be seen as a complementary study to the greedy-type method we have proposed in [106].

In addition, interesting analytical studies can also be carried out on the MIMO LP-OFDM scheme. In fact, considering a partial or perfect knowledge of the CSI at the transmitter, different resource allocation algorithms that maximize the margin or throughput of the MIMO LP-OFDM system can be derived. In addition, dynamic MIMO configurations that select the optimal MIMO scheme which increases the diversity or complexity gain for a given channel condition, can be proposed.

Concerning the **global LP-OFDM system study**, additional enhancements can be carried out to further improve the system performance. For instance, the use of low-density parity-check (LDPC) codes or turbo codes instead of the convolutional codes proposed by the MB-OFDM solution could be investigated. LDPC and turbo codes could significantly reduce the mean BER of the system at the cost of a low increase of the complexity. On the other hand, in this thesis we have only used the well-known orthogonal Alamouti scheme since it provides a high diversity gain at low complexity. If higher complexity systems are allowed, other MIMO schemes, such as the Golden code, could also be investigated to further improve the performance in terms of diversity and multiplexing gains.

Furthermore, in the global LP-OFDM system study, we did not consider CSI knowledge at the transmitter side, and thus the allocation algorithms were not implemented. An interesting future work would be to implement and test these algorithms in the final LP-OFDM system. Besides, these algorithms could be combined within enhanced cross-layer mechanisms in order to improve the system performance, while respecting the QoS requirements and constraints provided by the MAC layer [104]. Thus, dynamic cross-layer spectrum allocation for high data rate multiband UWB systems could be developed without notably increasing the system complexity.

# Bibliography

[1] ICT FP7 OMEGA project. Available: http://www.ict-omega.eu.

[2] T. W. Barrett, "History of ultra wideband (UWB) radar & communications: pioneers and innovators," in *Proc. Progress in Electromagnetics Symposium (PIERS'00)*, USA, July 2000.

[3] H. F. Harmuth, "Application of Walsh functions in communications," *IEEE Spectrum*, pp. 82–91, Nov. 1969.

[4] J. D. Taylor, Ed., *Introduction to Ultra-Wideband Radar Systems*. Boca Raton, FL: CRC Press,1995.

[5] G. F. Ross, "Transmission and reception system for generating and receiving base-band duration pulse signals for short base-band pulse communication system," *U.S. Patent* 3 728 632, April 17, 1973.

[6] C. L. Bennett and G. F. Ross, "Time-domain electromagnetics and its applications," *Proc. of IEEE*, vol. 66, no. 3, pp. 299–318, 1978.

[7] H. F. Harmuth, *Nonsinusoidal Waves for Radar and Radio Communication*. Academic Press, New York, NY, USA, 1981.

[8] Federal Communications Commission (FCC), "Revision of part 15 of the commission's rules regarding ultra-wideband transmission systems," *First report and order*, ET Docket 98–153, FCC 02–48, Feb. 14, 2002.

[9] C. Shannon, "A mathematical theory of communication," *The Bell System Technical Journal 27*, pp. 379–423, 623–656, July, Oct. 1948.

[10] I. Oppermann, M. Hamalainen and J. Iinatti, *UWB Theory and Applications*. John Wiley & Sons, 2004.

[11] J. F. M. Gerrits and J. R. Farserotu, "Wavelet generation circuit for UWB impulse radio applications," *Electronics Letters*, vol. 38, no. 25, pp. 1737–1738, Dec. 2002.

[12] Time Domain Corporation, "Comments of Time Domain Corporation, Docket 98–154. In the Matter of Revision of Part 15 of the FCC's Rules Regarding Ultra wide-band Transmission Systems," 1998.

[13] K. Ohno and T. Ikegami, "Interference mitigation study for UWB radio using template waveform processing," *IEEE Transactions on Microwave Theory and Techniques*, vol. 54, pp. 1782–1792, June 2006.

[14] M. Hamalainen, J. Saloranta, J-P. Makela, I. Oppermann and T. Pantana, "Ultra wideband signal impact on IEEE 802.11b and Bluetooth performances," in *Proc. IEEE International Symposium on Personal, Indoor and Mobile Radio Communications (PIMRC'03)*, vol. 1, pp. 280–284, China, Sept. 2003.

[15] J. P. Van't Hof and D. D. Stancil, "Ultra-wideband high data rate short range wireless links," in *Proc. IEEE Vehicular Technology Conference (VTC'02 Spring)*, vol. 1, pp. 85–89, USA, May 2002.

[16] K. Sarfaraz, A. Ghorashi, M. Ghavami and H. Aghvami, "Performance of Wi-Max receiver in presence of DS-UWB system," *Electronics Letters*, vol. 41, pp. 1388–1390, Dec. 2005.

[17] CEPT ECC, "ECC decision of 24 March 2006 on the harmonised conditions for devices using ultra-wideband (UWB) technology in bands below 10.6 GHz," ECC/DEC/(06)04, March 2006.

[18] "Commission decision of 21 February 2007 on allowing the use of the radio spectrum for equipment using ultra-wideband technology in harmonised manner in the community," 2007/131/EC, Feb. 2007.

[19] WiMedia Alliance. Available: http://www.wimedia.org.

[20] R. Aiello and A. Batra, *Ultra Wideband Systems: Technologies and Applications*. Communications Engineering Series, Newnes, 2006.

[21] Standard ECMA-368, "High rate ultra wideband PHY and MAC standard," 1st edition, Dec. 2005, 2nd edition, Dec. 2007.

[22] Standard ECMA-369, "MAC-PHY interface for ECMA-368," 1st edition, Dec. 2005, 2nd edition, Dec. 2007.

[23] IEEE 802.15 WPAN Low Rate Alternative PHY Task Group 4a (TG4a). Available: http://www.ieee802.org/15/pub/TG4a.html.

[24] IEEE 802.15 WPAN Millimeter Wave Alternative PHY Task Group 3c (TG3c). Available: http://www.ieee802.org/15/pub/TG3c.html.

[25] R. J. Fontana and S. Gunderson, "Ultra-wideband precision asset location system," in *Proc. IEEE Conference on Ultra Wideband Systems and Technologies (UWBST'02)*, USA, May 2002.

[26] E. M. Staderini, "UWB radar in medicine," *IEEE Aerospace and Electronic Systems Magazine*, vol. 17, pp. 13–18, Jan. 2002.

[27] R. A. Scholtz, "Multiple access with time-hopping impulse modulation," in *Proc. Military Communications Conference (MILCOM'93)*, vol. 2, pp. 447–450, USA, Oct. 1993.

[28] X. Shen, M. Guizani, R. C. Qiu and T. Le-Ngoc, *Ultra-Wideband Wireless Communications and Networks*. John Wiley & Sons, 2006.

[29] J. G. Proakis and M. Salehi, *Communication System Engineering*. Prentice-Hall, Englewood Cliffs, NJ, USA, 1994.

[30] M. Ghavami, L. B. Michael and R. Kohno, "Hermite Function Based Orthogonal Pulses for UWB Communication," in *Proc. International Symposium on Wireless Personal Multimedia Communications (WPMC'01)*, Denmark, pp. 437–440, Sept. 2001.

[31] J. T. Conroy, J. L. LoCicero and D. R. Ucci, "Communication techniques using monopulse waveforms," in *Proc. IEEE Military Communications Conference (MILCOM'99)*, vol. 2, pp. 1181–1185, USA, Oct. 1999.

[32] M. Z. Win and R. A. Scholtz, "Comparisons of analog and digital impulse radio for wireless multiple-access communications," in *Proc. IEEE International Conference on Communications (ICC'97)*, vol. 1, pp. 91–95, Canada, June 1997.

[33] M-G. Di Benedetto, T. Kaiser, A. Molisch, I. Oppermann, C. Politano and D. Porcino, *UWB Communication Systems: A Comprehensive Overview*. Series on Signal Processing and Communications, EURASIP, 2006.

[34] V. S. Somayazulu, J. R. Foerster and S. Roy, "Design challenges for very high data rate UWB systems," in *Proc. Asilomar Conference on Systems, Signals and Computers*, vol. 1, no. 3–6, pp. 717–721, USA, Nov. 2002.

[35] A. Batra *et al.*, "TI Physical layer proposal for IEEE 802.15 task group 3a," *IEEE P802.15-03/142r2-TG3a*, March 2003.

[36] A. Batra, J. Balakrishnan, R. Aiello, J. R. Foerster and A. Dabak, "Design of multiband OFDM system for realistic UWB channel environments," *IEEE Transactions on Microwave Theory and Techniques*, vol. 52, no. 9, pp. 2123–2138, Sept. 2004.

[37] D. Cassioli, M. Z. Win and A. F. Molisch, "The ultra-wide bandwidth indoor channel: from statistical model to simulations," *IEEE Journal on Selected Areas in Communications*, vol. 20, no. 6, pp. 1247–1257, Aug. 2002.

[38] M. Z. Win and R. A. Scholtz, "On the robustness of ultra-wide bandwidth signals in dense multipath environments," *IEEE Communications Letters*, vol. 2, no. 2, pp. 51–53, Feb. 1998.

[39] R. J-M. Cramer, R. A. Scholtz and M. Z. Win, "Evaluation of an ultra-wideband propagation channel," *IEEE Transactions on Antennas and Propagation*, vol. 50, no. 5, pp. 561–570, May 2002.

[40] M. Z. Win and R. A. Scholtz, "Characterization of ultra-wide bandwidth wireless indoor channels: a communication theoretic view," *IEEE Journal on Selected Areas in Communications*, vol. 20, no. 9, pp. 1613–1627, Dec. 2002.

[41] J. R. Foerster, "The effects of multipath interference on the performance of UWB systems in an indoor wireless channel," in *Proc. IEEE Vehicular Technology Conference (VTC'01 Spring)*, vol. 2, pp. 1176–1180, Greece, May 2001.

[42] A. F. Molisch, J. R. Foerster and M. Pendergrass, "Channel models for ultra wideband personal area networks," *IEEE Transactions on Wireless Communications*, vol. 10, no. 6, pp. 14–21, Dec. 2003.

[43] J. R. Foerster, "Channel modeling sub-committee report final," *IEEE 802.15-02/490r1-SG3a, IEEE P802.15 Working Group for Wireless Personal Area Networks (WPANs)*, Feb. 2003.

[44] A. Saleh and R. Valenzuela, "A statistical model for indoor multipath propagation," *IEEE Journal on Selected Areas in Communications*, vol. 5, no. 2, pp. 128–137, Feb. 1987.

[45] M. L. Doelz, E. T. Heald and D. L. Martin, "Binary data transmission techniques for linear systems," in *Proc. IRE*, vol. 45, pp. 656–661, May 1957.

[46] R. W. Chang and R. A Gibby, "A theoretical study of performance of an orthogonal multiplexing data transmission scheme," *IEEE Transactions on Communication Technology*, vol. 16, pp. 529–540, Aug. 1968.

[47] B. Le Floch, M. Alard and C. Berrou, "Coded orthogonal frequency division multiplex," *Proc. of the IEEE*, vol. 83, no. 6, pp. 982–996, June 1995.

[48] R. L. Pickholtz, D. L. Schilling and L. B. Milstein, "Theory of spread-spectrum communications – a tutorial," *IEEE Transactions on Communications*, vol. 30, no. 5, pp. 855–884, May 1982.

[49] TIA/EIA/IS-95, "Mobile station-base station compatibility standard for dual-mode wideband spread spectrum cellular system," *TIA*, July 1993.

[50] ETSI UMTS (TR 101 112), "Universal mobile telecommunications system (UMTS)," Sophia Antipolis, France, 1998.

[51] R. C. Dixon, *Spread Spectrum Systems*. John Wiley & Sons, 2nd edition, 1986.

[52] R. S. Stankovic, "Some remarks on terminology in spectral techniques for logic design: Walsh transform and Hadamard matrices," *IEEE Transactions on Computer-Aided Design of Integrated Circuits and Systems*, vol. 17, no. 11, pp. 1211–1214, Nov. 1998.

[53] M. J. E. Golay, "Complementary series," *IRE Transactions on Information Theory*, vol. 7, no. 2, pp. 82–87, April 1961.

[54] R. Gold, "Optimal binary sequences for spread spectrum multiplexing," *IEEE Transactions on Information Theory*, vol. 13, no. 2, pp. 619–621, Oct. 1967.

[55] R. Prasad, *Universal Wireless Personal Communications*. Artech House, 1998.

[56] D. C. Chu, "Polyphase codes with good periodic correlation properties," *IEEE Transactions on Information Theory*, vol. 18, pp. 531–532, July 1972.

[57] K. Fazel and L. Papke, "On the performance of convolutionally-coded CDMA/OFDM for mobile communication system," in *Proc. IEEE International Symposium on Personal, Indoor and Mobile Radio Communications (PIMRC'93)*, pp. 468–472, Japan, Sept. 1993.

[58] N. Yee, J. P. Linnartz and G. Fettweis, "Multi-carrier CDMA in indoor wireless radio networks," in *Proc. IEEE International Symposium on Personal, Indoor and Mobile Radio Communications (PIMRC'93)*, pp. 109–113, Japan, Sept. 1993.

[59] L. Vandendorpe, "Multitone direct sequence CDMA system in an indoor wireless environment," in *Proc. IEEE First Symposium of Communications and Vehicular Technology*, Delft, The Netherlands, pp. 4.1.1–4.1.8, Oct. 1993.

[60] A. Chouly, A. Brajal and S. Jourdan, "Orthogonal multicarrier techniques applied to direct sequence spread spectrum CDMA systems," in *Proc. IEEE Global Communications Conference (GLOBECOM'93)*, pp. 1723–1728, USA, Nov. 1993.

[61] V. DaSilva and E. S. Sousa, "Performance of orthogonal CDMA codes for quasi-synchronous communication systems," in *Proc. IEEE International Conference on Universal Personal Communications (ICUPC'93)*, pp. 995–999, Ottawa, Canada, Oct. 1993.

[62] K. Fazel and S. Kaiser, *Multi-Carrier and Spread Spectrum Systems*. John Wiley & Sons, 2003.

[63] S. Kaiser, *Multi-Carrier CDMA Mobile Radio Systems – Analysis and Optimization of Detection, Decoding, and Channel Estimation*. Ph.D. thesis, Dusseldorf: VDI-Verlag, Fortschritt-Berichte VDI, series 10, no. 531, 1998.

[64] S. Kaiser and K. Fazel, "A flexible spread spectrum multi-carrier multiple-access system for multi-media applications," in *Proc. IEEE International Symposium on Personal, Indoor and Mobile Communications (PIMRC'97)*, pp. 100–104, Finland, Sept. 1997.

[65] A. Batra *et al.*, "Multiband OFDM physical layer proposal for IEEE 802.15 task group 3a," *IEEE P802.15-04/0493r1-TG3a*, Sept. 2004.

[66] B. Muquet, Z. Wang, G. B. Giannakis, M. D. Courville and P.Duhamel, "Cyclic prefixing or zero padding for wireless multicarrier transmissions?" *IEEE Transactions on Communications*, vol. 50, no. 12, pp. 2136–2148, Dec. 2002.

[67] L. Maret and I. Siaud, "Ultra-wideband MBOA PHY layer performance analysis and enhanced issues (IST-MAGNET project," in *Proc. European Conference on Propagation and Systems (ECPS'05)*, France, March 2005.

[68] M. Schmidt and F. Jondral, "Ultra wideband transmission based on MC-CDMA," in *Proc. IEEE Global Communications Conference (GLOBECOM'03)*, vol. 2, pp. 749–753, USA, Dec. 2003.

[69] Y-B. Park *et al.*, "Performance of UWB DS-CDMA/OFDM/MC-CDMA system," in *Proc. IEEE International Midwest Symposium on Circuits and Systems (MWSCAS'04)*, vol. 1, pp. 37–40, Japan, July 2004.

[70] J. Wang and L. Milstein, "Multicarrier CDMA overlay for ultra-wideband communications," *IEEE Transactions on Communications*, vol. 52, no. 10, pp. 1664–1669, Oct. 2004.

[71] W. Tung and J. Wang, "MMSE receiver for multicarrier CDMA overlay in ultra-wide-band communications," *IEEE Transactions on Vehicular Technology*, vol. 54, no. 2, pp. 603–614, March 2005.

[72] K. Ohno and T. Ikegami, "An interference avoidance technique for coexistence of pulse based UWB and MC-CDMA," in *Proc. IEEE International Conference on Ultra-Wideband (ICUWB'07)*, pp. 899–904, Singapore, Sept. 2007.

[73] C. Zhang, X. Lin and M. Hatori, "Novel two dimensional complementary sequences in ultra wideband wireless communications," in *Proc. IEEE Conference on Ultra Wideband Systems and Technologies (UWBST'02)*, pp. 398–402, USA, Nov. 2003.

[74] L-L. Yang, "Time-hopping multicarrier code-division multiple access," *IEEE Transactions on Vehicular Technology*, vol. 56, no. 2, pp. 731–741, March 2007.

[75] P. Tu, X. Huang and E. Dutkiewicz, "A Novel Approach of Spreading Spectrum in OFDM Systems," in *Proc. International Symposium on Communications and Information Technologies (ISCIT'06)*, pp. 487–491, Thailand, Oct. 2006.

[76] A. Stephan, E. Guéguen, M. Crussière, J-Y. Baudais and J-F. Hélard, "Optimization of linear precoded OFDM for high-data-rate UWB systems," *EURASIP Journal on Wireless Communications and Networking*, vol. 2008, Article ID 317257, 2008.

[77] Z. Wang and G. B. Giannakis, "Linearly precoded or coded OFDM against Wireless channel fades?" in *Proc. IEEE Workshop on Signal Processing Advances in Wireless Communications (SPAWC'01)*, pp. 267–270, Taiwan, March 2001.

[78] S. Ohno and G. B. Giannakis, "Optimal training and redundant precoding for block transmissions with application to wireless OFDM," *IEEE Transactions on Communications*, vol. 50, no. 12, pp. 2113–2123, Dec. 2002.

[79] D. Mottier and D. Castelain, "Spreading sequence allocation procedure for MC-CDMA transmission systems," in *Proc. IEEE Vehicular Technology Conference (VTC'00 Fall)*, vol. 3, pp. 1270–1275, USA, Sept. 2000.

[80] A. Stephan, J-Y. Baudais and J-F. Hélard, "Resource allocation for multicarrier CDMA systems in ultra-wideband communications," in *Proc. IEEE International Telecommunications Symposium (ITS'06)*, pp. 135–140, Brazil, Sept. 2006.

[81] D. Tse and P. Viswanath, "On the capacity region of the vector Gaussian broadcast channel," in *Proc. IEEE International Symposium on Information Theory (ISIT'03)*, p. 342, June 2003.

[82] N. Jindal, S. Vishwanath and A. Goldsmith, "On the duality of Gaussian multiple-access and broadcast channels," *IEEE Transactions on Information Theory*, vol. 50, no. 5, pp. 768–783, May 2004.

[83] D. Tse, "Optimal power allocation over parallel gaussian broadcast channels," in *Proc. IEEE International Symposium on Information Theory (ISIT'97)*, p. 27, Ulm, Germany, 1997.

[84] R. S. Cheng and S. Verdu, "Gaussian multiaccess channels with ISI: Capacity region and multiuser water-filling," *IEEE Transactions on Information Theory*, vol. 39, no. 3, pp. 773–785, May 1993.

[85] J. M. Cioffi, "A multicarrier primer," *ANSI T1E1.4/91–157 Committee Contribution*, Nov. 1991.

[86] J. G. Proakis, *Digital Communications*. McGraw-Hill, 4th edition, 2001.

[87] D. Hughes-Hartogs, "Ensemble modem structure for imperfect transmission media," *U.S. Patents* 4 679 227, July 1987, 4 731 816, March 1988 and 4 833 796, May 1989.

[88] P. S. Chow, J. M. Cioffi and J. A. C. Bingham, "Practical discrete multitone transceiver loading algorithm for data transmission over spectrally shaped channels," *IEEE Transactions on Communications*, vol. 43, pp. 773–775, 1995.

[89] A. Leke and J. M. Cioffi, "A maximum rate loading algorithm for discrete multitone modulation systems," in *Proc. IEEE Global Communications Conference (GLOBECOM'97)*, vol. 3, pp. 1514–1518, USA, Nov. 1997.

[90] R. F. H. Fischer and J. B. Huber, "A new loading algorithm for discrete multitone transmission," in *Proc. IEEE Global Communications Conference (GLOBECOM '96)*, vol. 1, pp. 724–728, London, U.K., 1996.

[91] B. S. Krongold, K. Ramchandran and D. L. Jones, "Computationally efficient optimal power allocation algorithms for multicarrier communication systems," *IEEE Transactions on Communications*, vol. 48, no. 1, pp. 23–27, 2000.

[92] Z. Xu and L. Liu, "Power allocation for multi-band OFDM UWB communication networks," in *Proc. IEEE Vehicular Technology Conference (VTC'04 Fall)*, vol. 1, pp. 368–372, USA, Sept. 2004.

[93] W. Pam Siriwongpairat, Zhu Han and K. J. Ray Liu, "Power Controlled Channel Allocation for Multiuser Multiband UWB," *IEEE Transactions on Wireless Communications*, vol. 6, no. 2, pp. 583–592, Feb. 2007.

[94] J. Wang, G. Zhu and J. Jin, "Optimal power allocation for space-time coded OFDM UWB systems," in *Proc. International Conference on Wireless Communications, Networking and Mobile Computing (WCNM'05)*, vol. 1, pp. 189–192, China, Sept. 2005.

[95] F. Cuomo, C. Martello, A. Baiocchi and F. Capriotti, "Radio resource sharing for ad hoc networking with UWB," *IEEE Journal on Selected Areas in Communications*, vol. 20, no. 9, pp. 1722–1732, Dec. 2002.

[96] H. Xu and A. Ganz, "A radio resource control method in UWB MAC protocol design," in *Proc. IEEE Military Communications Conference (MILCOM'03)*, vol. 2, pp. 886–891, USA, Oct. 2003.

[97] G. Giancola, L. De Nardis, M.-G. Di Benedetto and E. Dubuis, "Dynamic resource allocation in time-varying ultra wide band channels," in *Proc. IEEE International Conference on Communications (ICC'04)*, vol. 6, pp. 3581–3585, France, June 2004.

[98] M. Crussière, *Etude et optimisation de communications à haut-débit sur lignes d'énergie : exploitation de la combinaison OFDM/CDMA*. Ph.D. Thesis, France, Nov. 2005.

[99] A. Stephan, J-Y. Baudais and J-F. Hélard, "Adaptive multi-carrier spread-spectrum with dynamic time-frequency codes for UWB applications," in *Proc. IEEE Workshop on Multi-Carrier Spread Spectrum (MC-SS'07)*, pp. 197–206, Germany, May 2007.

[100] M. Crussière, J-Y. Baudais and J-F. Hélard, "Adaptive linear precoded DMT as an efficient resource allocation scheme for power-line communications," in *Proc. IEEE Global Communications Conference* (*GLOBECOM'06*), pp. 1–5, USA, Dec. 2006.

[101] A. Stephan, J-Y. Baudais and J-F. Hélard, "Efficient allocation algorithms for multicarrier spread-spectrum schemes in UWB applications," in *Proc. IEEE International Conference on Ultra-Wideband (ICUWB'07)*, pp. 551–555, Singapore, Sept. 2007.

[102] M. Crussière, J-Y. Baudais and J-F. Hélard, "Adaptive spread spectrum multicarrier multiple access over wirelines," *IEEE Journal on Selected Areas in Communications, Special Issue on Power Line Communications*, vol. 24, no. 7, pp. 1377–1388, July 2006.

[103] A. Stephan, J-Y. Baudais and J-F. Hélard, "Adaptive spread spectrum multicarrier multiple-access for UWB systems," in *Proc. IEEE Vehicular Technology Conference (VTC'07 Spring)*, pp. 2926–2930, Dublin, Ireland, April 2007.

[104] A. Khalil, A. Stephan, M. Crussière and J-F. Hélard, "Multi-user cross-layer allocation design for LP-OFDM high data rate UWB systems," in *Proc. IEEE International Symposium on Wireless Communication Systems (ISWCS'08)*, pp. 6–10, Iceland, Oct. 2008.

[105] F-S. Muhammad, J-Y. Baudais, J-F. Hélard and Matthieu Crussière, "A coded bit-loading linear precoded discrete multitone solution for power line communication," in *Proc. IEEE Workshop on Signal Processing Advances in Wireless Communications (SPAWC'08)*, pp. 555–559, Brazil, July 2008.

[106] F-S. Muhammad, A. Stephan, J-Y. Baudais and J-F. Hélard, "Mean BER minimization loading algorithm for linear precoded OFDM," submitted to *IEEE Sarnoff Symposium (Sarnoff'09)*, Princeton, USA, March, April 2009.

[107] A. M. Wyglinski, F. Labeau and P. Kabal, "Bit loading with BER-constraint for multicarrier systems," *IEEE Transactions on Wireless Communications*, vol. 4, no. 4, pp. 1383–1387, July 2005.

[108] Y. George and O. Amrani, "Bit loading algorithms for OFDM," in *Proc. IEEE International Symposium on Information Theory (ISIT'04)*, p. 388, USA, July 2004.

[109]  T. N. Zogakis, J. T. Aslanis and J. M. Cioffi, "A coded and shaped discrete multi-tone system," *IEEE Transactions on Communications*, vol. 43, no. 12, pp. 2941–2949, Dec. 1995.

[110]  J. H. Lambert, "Observations variae in mathesin puram," *Acta Helvitica, physico-mathematico-anatomico-botanico-medica*, vol. 3, pp. 128–168, 1758.

[111]  A. Stephan, J-Y. Baudais and J-F. Hélard, "Range improvement of UWB systems using adaptive multicarrier spread-spectrum and MIMO techniques," *European Transactions on Telecommunications (ETT), Special Issue on Multi-Carrier Spread Spectrum*, vol. 19, no. 5, pp. 589–599, 2008.

[112]  A. Stephan, J-F. Hélard and B. Uguen, "MIMO UWB systems based on linear precoded OFDM for home gigabit applications," in *Proc. IEEE Global Communications Conference (GLOBECOM'08)*, pp. 1–6, USA, Dec. 2008.

[113]  E. Guéguen, M. Crussière and J-F. Hélard, "An OFDM-CDMA scheme for high data rate UWB applications," in *Proc. IEEE International Conference on Ultra-Wideband (ICUWB'07)*, pp. 551–555, Singapore, Sept. 2007.

[114]  L. Cariou and J-F. Helard, "A simple and efficient channel estimation for MIMO OFDM code division multiplexing uplink systems," in *Proc. IEEE Workshop on Signal Processing Advances in Wireless Communications (SPAWC'05)*, pp. 176–180, USA, June 2005.

[115]  D. Mottier and D. Castelain, "A spreading sequence allocation procedure for MC-CDMA transmission systems," in *Proc. IEEE Vehicular Technology Conference (VTC'00 Fall)*, vol. 3, pp. 1270–1275, USA, Sept. 2000.

[116]  J. Litva and T. K.-Y. Lo, *Digital Beamforming in Wireless Communications*. Artech House Publishers, 1996.

[117]  T. Kaiser *et al.*, *Smart Antennas—State of the Art*. Series on Signal Processing and Communications, EURASIP, 2005.

[118]  H. Jafarkhani, *Space-Time Coding: Theory and Practice*. Cambridge University Press, 2005.

[119]  G. J. Foschini, "Layered space-time architecture for wireless communication in a fading environment when using multi-element antennas," *Bell Labs Technical Journal*, pp. 41–59, Autumn 1996.

[120] G. D. Golden, G. J. Foschini, R. A. Valenzuela and P. W. Wolniansky, "Detection algorithm and initial laboratory results using the V-BLAST space-time communication architecture," *Electronics Letters*, vol. 35, no. 1, pp. 14–15, Jan. 1999.

[121] E. Biglieri, D. Divsalar, P. J. McLane and M. K. Simon, *Introduction to Trellis Coded Modulation with Applications*. Prentice Hall, 1992.

[122] V. Tarokh, N. Seshadri and A. R. Calderbank, "Space-time codes for high data rate wireless communication: performance criterion and code construction," *IEEE Transactions on Information Theory*, vol. 44, no. 2, pp. 744–765, March 1998.

[123] S. M. Alamouti, "A simple transmit diversity technique for wireless communications," *IEEE Journal on Selected Areas in Communications*, vol. 16, no. 8, pp. 1451–1458, Oct. 1998.

[124] V. Tarokh, H. Jafarkhani and A. R. Calderbank, "Space-time block codes from orthogonal designs," *IEEE Transactions on Information Theory*, vol. 45, no. 5, pp. 1456–1467, July 1999.

[125] J-C. Belfiore, G. Rekaya and E. Viterbo, "The Golden code: a 2×2 full-rate space-time code with nonvanishing determinant," *IEEE Transactions on Information Theory*, vol. 51, no. 4, pp. 1432–1436, April 2005.

[126] H. Zhang and T. Gulliver, "Performance and capacity of PAM and PPM UWB systems with multiple receive antennas," in *Proc. IEEE Pacific Rim Conference on Communications, Computers and signal Processing (PACRIM'03)*, vol. 2, pp. 740–743, Canada, Aug. 2003.

[127] C. Tsung-Hui, C. Yu-Jung, P. Chun-Hsien, L. Yu-Hang and C. Chong-Yung, "Space time MSINR-SRAKE receiver with finger assignment strategies in UWB multipath channels," in *Proc. IEEE International Conference on Ultra-Wideband (ICUWB'05)*, pp. 242–247, Switzerland, Sept. 2005.

[128] L. Yang and G. B. Giannakis, "Space-time coding for impulse radio," in *Proc. IEEE Conference on UWB Systems and Technologies*, pp. 235–239, USA, May 2002.

[129] W. Siriwongpairat, M. Olfat and K. J. R. Liu, "On the performance evaluation of TH and DS UWB MIMO systems," in *Proc. IEEE Wireless Communications and Networking Conference (WCNC'04)*, vol. 3, pp. 1800–1805, March 2004.

[130] M. Weisenhorn and W. Hirt, "Performance of binary antipodal signaling over the indoor UWB MIMO channel," in *Proc. IEEE International Conference on Communications (ICC'03)*, vol. 4, pp. 2872–2878, May 2003.

[131] L. Zhiwei, B. Premkumar, and A. S. Madhukumar, "MMSE detection for high data rate UWB MIMO systems," in *Proc. IEEE Vehicular Technology Conference (VTC'04 Fall)*, vol. 2, pp. 1463–1467, Sept. 2004.

[132] W. P. Siriwongpairat, W. Su, M. Olfat and K. J. R. Liu, "Multiband-OFDM MIMO coding framework for UWB communication systems," *IEEE Transactions on Signal Processing*, vol. 54, no. 1, pp. 214–224, Jan. 2006.

[133] E. Dimitrov and T. Kaiser, "Advanced MIMO VHDR MB-OFDM approaches," in *Proc. IEEE International Conference on Ultra-Wideband (ICUWB'08)*, vol. 3, pp. 51–54, Germany, Sept. 2008.

[134] J. Yang, A. Seyedi, D. Birru and D. Wang, "Design and Performance of Multi-Band OFDM UWB System with Multiple Antennas," in *Proc. IEEE International Symposium on Personal, Indoor and Mobile Radio Communications (PIMRC'07)*, Greece, Sept. 2007.

[135] L-M. Aubert and B. Uguen, "Modélisation du canal MIMO-UWB," *Technical report, External research contract, France Télécom R&D*, 2005.

[136] "Spatial channel model for multiple input multiple output (MIMO) simulations," *3GPP, TR 25.996 V6.1.0*, Sept. 2003.

[137] V. Ercerg *et al.*, "TGn channel models," *IEEE 802.11-03/940r4*, May 2004.

[138] J-M. Auffray, J-Y. Baudais and J-F. Hélard, "STBC MC-CDMA systems: comparison of MMSE single-user and multiple-user detection schemes over Rayleigh and MIMO METRA channels," *European Transactions on Telecommunications (ETT), Special Issue on Multi-Carrier Spread Spectrum*, vol. 15, no. 3, pp. 275–281, May 2004.

[139] M. Speth, A. Senst and H. Meyr, "Low complexity space-frequency MLSE for multi-user COFDM," in *Proc. IEEE Global Communications Conference (GLOBECOM'99)*, pp. 2395–2399, Brazil, Dec. 1999.

[140] F. Tosato and P. Bisaglia, "Simplified soft-output demapper for binary interleaved COFDM with application to HIPERLAN/2," in *Proc. IEEE International Conference on Communications (ICC'02)*, vol. 2, pp. 664–668, USA, Aug. 2002.